Northumbria Research Link

Citation: Culham, Stacey (2013) Polymetallic triplet emitters. Doctoral thesis, Northumbria University.

This version was downloaded from Northumbria Research Link: http://nrl.northumbria.ac.uk/id/eprint/36124/

Northumbria University has developed Northumbria Research Link (NRL) to enable users to access the University's research output. Copyright © and moral rights for items on NRL are retained by the individual author(s) and/or other copyright owners. Single copies of full items can be reproduced, displayed or performed, and given to third parties in any format or medium for personal research or study, educational, or not-for-profit purposes without prior permission or charge, provided the authors, title and full bibliographic details are given, as well as a hyperlink and/or URL to the original metadata page. The content must not be changed in any way. Full items must not be sold commercially in any format or medium without formal permission of the copyright holder. The full policy is available online: http://nrl.northumbria.ac.uk/policies.html

Northumbria University NEWCASTLE

University Library

Polymetallic Triplet Emitters

Stacey Culham

Ph.D. Chemistry

2013

Polymetallic Triplet Emitters

Stacey Culham BSc

A thesis submitted in partial fulfilment of the requirements of Northumbria University for the degree of Doctor of Philosophy

Research undertaken in the Faculty of Health and Life Sciences

September 2013

Abstract

This work is concerned with the synthesis and property investigation of a relatively new class of cyclometallated Ir(III) and Pt(II) complexes in which two metal centres are coordinated to a common heterocycle resulting in a rigid polymetallic assembly. Highly luminescent materials which can emit and absorb in a red region of the spectrum were targeted.

There are three main parts of the thesis. The first part investigates how luminescent properties of the diplatinum systems are affected by the bridging ligand. A series of novel mono- and dinuclear Pt(II) complexes has been prepared and their luminescent and redox properties investigated. The main observation is that the introduction of the second metal centre leads to a substantial red-shift in absorption and emission.

In the second part the role of changing the ligand substituents in a cyclometallated complex has been investigated to determine the extent to which luminescence is affected by the nature of the substituents. A series of mono- and dinuclear Pt(II) complexes have been prepared using substituted pyrazine bridging ligands. It was found that electron donating substituents such as –OMe in the benzene cyclometallating ring cause a red-shift, while electron withdrawing substituents such as –F cause a blue-shift in emission.

The final part of the work describes the synthesis of cyclometallated homometallic bis Ir(III) complexes. A series of bis- Ir(III) complexes have been prepared using a terdentate cyclometallating N^C^N coordinating 1,3-di(2-pyridyl)benzene derivative as an auxiliary ligand. It was found that the nature of the bridging ligand determines the overall stability of the complex. Pyrimidine-linked systems were found to be the most stable, while pyrazine analogues readily photodecompose/isomerise. Pyridazine-linked systems lead to ionic complexes where one chloride ligand is shared by two Iridium metal centres.

Contents

List of Figures

List of Schemes

Acknowledgments

I would like to thank Dr. Valery Kozhevnikov and Dr. Marcus Durrant for their valuable guidance, encouragement and advice throughout the project. In addition, I would extend my appreciations to Northumbria University for the funding and resources for the project. Special considerations go to all of the technical staff here at Northumbria University who have given an enormous amount of support. In particular, I would extend my gratitude to Gordon Forrest for his assistance through my time here. I would also like to thank Gareth from Durham University for carrying out luminescent measurements for my work and for taking the time to show me how the measurements are carried out.

My thanks go to my fellow researchers and friends from Northumbria University with particular appreciations to Adam, Michael, Dave, Shaun and Ari for their friendship and help throughout. I wish you all the best for the future and hope that we can continue to keep in touch.

My appreciations go to my friends who have been supportive throughout the process. A special thanks to Jodie who has been behind me with support and encouragement through what has been a challenging time for both my academic and personal life over the past 7 years, and more recently to Wijee who has kept me laughing, sane and motivated during the writing of my thesis.

Finally, I would like to express thanks to my family who have encouraged me every step of the way through the last 7 years. Particularly to my parents, Jimmy and Maureen, I would not have been able to do this without you, thank you.

Declaration

I declare that the work contained in this thesis has not been submitted for any other award and that it is all my own work. I also confirm that this work fully acknowledges opinions, ideas and contributions from the work of others. This work was done in collaboration with Northumbria University.

Name: Stacey Culham

Signature:

Date:

Abbreviations

Acac	acetylacetone
Aq	aqueous
Bpy	2,2'-bipyridine
Bpb	1,4-bis(pyridine-2-yl)benzene
Bzppy	bis(2-phenyl-5-benzoyl-pyridine)
Bzq	benzo(h)quinoline
BDBP	1,3-bis(3,4-dibutoxyphenyl)propane-1,3-dionate-o,o
DMSO	dimethylsulfoxide
DPM	dipivaloylmethane
LC	ligand centred
MLCT	metal to ligand charge transfer
Mpm	multiphoton microscopy
N^C	a bidentate ligand coordinating *via* one N and one C atom
N^C^N	a terdentate ligand coordinating *via* one N, one C and by one N atom
OLED	organic light emitting diode
Pbq-g	2-phenylbenzo[g]quinolone
Pbt	2-phenylbenzothiazole
Peg	polyethylene glycol
Phq	7-phenylquinoline
Piq	1-phenyl-isoquinoline
Ppy	2-phenylpyridine
TD-DFT	time-dependant density functional theory
Terpy	terpyridine
Trem	time-resolved emission imaging microscopy

Chapter 1: Introduction

1 Introduction

Phosphorescent red and near-infrared emitters are desired for a variety of applications. For example they can be used in organic light-emitting diodes (OLEDs), which are emerging as the leading technology for a new generation of flat screen display technologies. To be able to have this technology, highly efficient red (~650-700 nm), green (~500-550 nm) and blue (~450-470 nm) emitting compounds are required. Currently the red emitters have not been able to match up to the performance of the green emitters. This is mainly due to the energy gap law, in that luminescence quantum yields have a tendency to decrease as the emission wavelength increases[1]. Red emitters are also of interest in the development of luminescent sensors and probes for bioimaging[2]. In this wavelength range (650-950 nm), there is good tissue penetration and low autofluoresence. In addition IR or NIR wavelengths can pass through tissue without causing any cellular damage[3].

Initially, the development of luminescent metal complexes has been focused on ruthenium(II) complexes as they often absorb and emit in the red region due to the MLCT excited state. More recently, cyclometallated platinum(II) and iridium(III) complexes are becoming more popular as they have somewhat superior photoluminescent properties [4]. For example the quantum yield in solution of the best performing ruthenium(II) complexes is 4%, while many cyclometallated iridium(III) analogues emitting in the same region have quantum yields of 10-20%[5].

Cyclometallated complexes are organometallic compounds. They are cyclometallated when a metal is covalently bound to a carbon atom of a polydentate ligand. The remaining bonds come from coordinate bonds from heteroatoms such as nitrogen in the ligand[6].

The following literature review first describes the synthesis of the main classes of highly luminescent cyclometallated Ir(III) and Pt(II) complexes. The review then goes on to describe in detail the photophysical properties of these complexes and the strategies employed to design red and infrared emitters. The review is concluded by discussing the application of red emitters in organic light emitting diodes and in bioimaging.

1.1 Synthesis of cyclometallated complexes

1.1.1 Synthesis of Pt(II) acac complexes

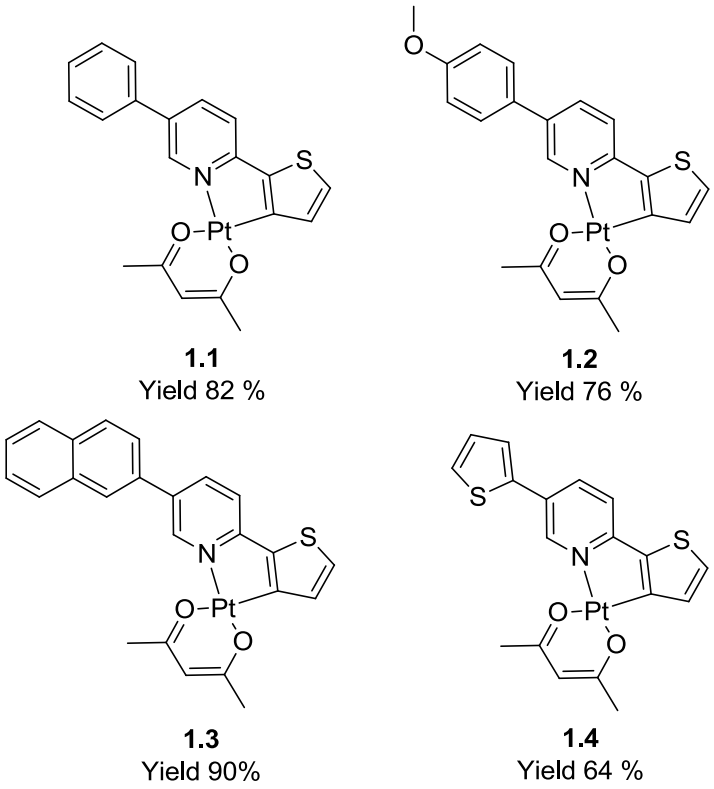

Figure 1.1 Examples of Pt(II) acac complexes

There have been several methods used to synthesise the Pt(II) complexes (examples of some Pt(II) complexes are shown in Figure 1.1[7]), one of which is to heat the pro-ligand with potassium tetrachloroplatinate in 2-ethoxyethanol and water for 16 hours at 80°C. The chloride-bridged product is then heated with acetylacetone and sodium chloride for 16 hours at 100°C to give the product[8] (Scheme 1.1).

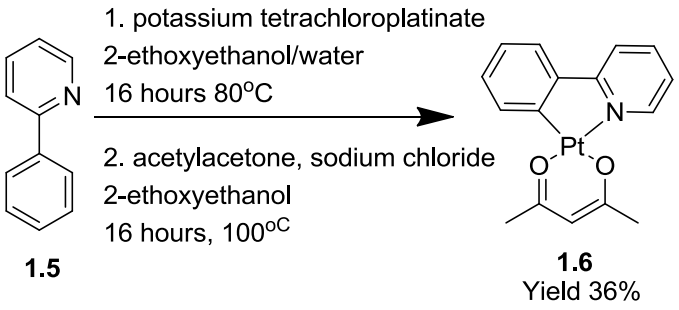

Scheme 1.1 Synthesis of Pt(ppy)(acac)

Another method is to add the pro-ligand to a suspension of potassium tetrachloroplatinate in acetic acid. The reaction mixture is stirred for 3-5 days at 80°C to give the chlorobridged dimer. This dimer is then refluxed with acetylacetone and sodium carbonate in 2-ethoxyethanol for 12 hours to give the product (**1.6**) with a yield of 36 %[9]. A similar method is to heat the pro-ligand and potassium tetrachloroplatinate(II) in acetic acid at 70°C for 24 hours. The resulting precipitate is then added to dimethylsulfoxide and refluxed for 10 minutes, precipitating [Pt(L)Cl(dmso)] (**1.8**). This is then stirred with sodium acetylacetonate monohydrate and acetone at 50°C for 12 hours to give the final product (**1.6**)[7] (Scheme 1.2).

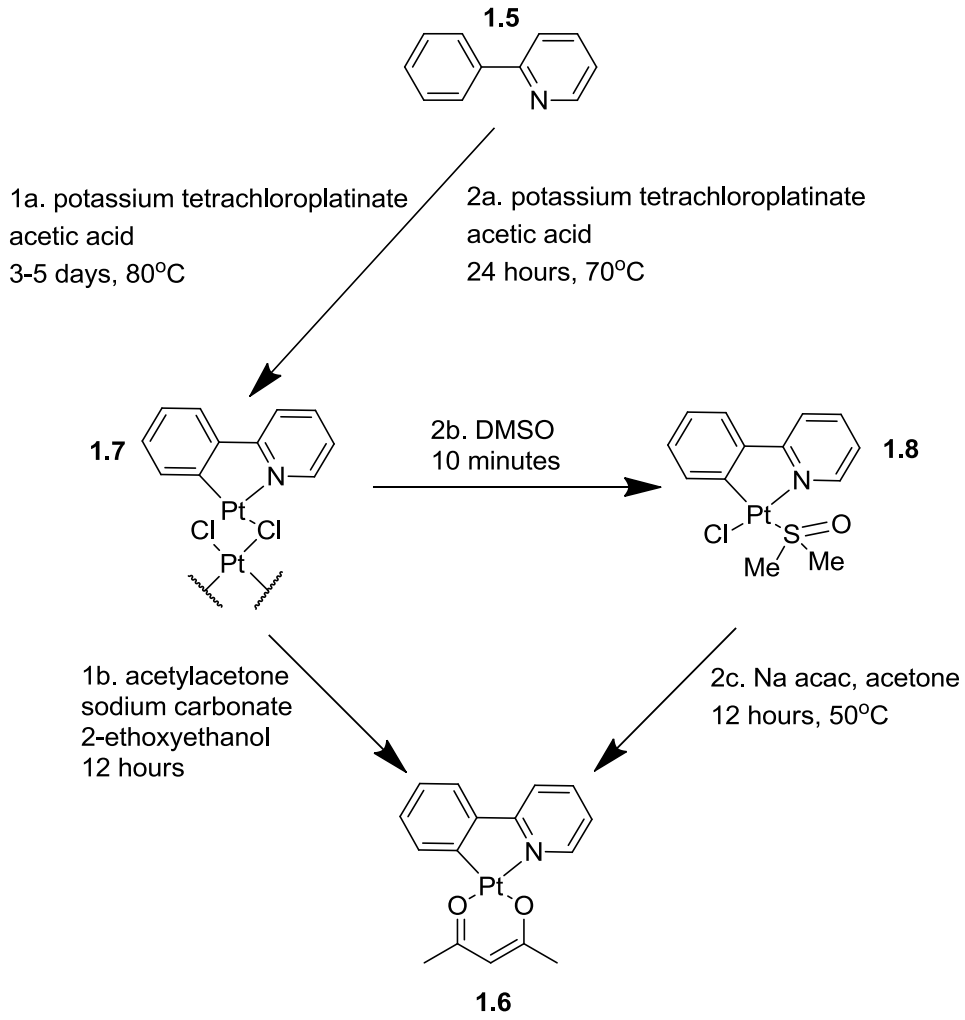

Scheme 1.2 Similar routes to achieving synthesis of Pt(II) complexes

An alternative method is to add a solution of platinum(II)chloride in benzonitrile to a solution of the pro-ligand (**1.5**) dissolved in diphenyl ether. The solution is stirred at 190°C for 10 minutes then cooled, and acetone is added. Acac and triethylamine are then added and stirred for 30 mins. Hexane is added to precipitate the product (**1.6**) giving a yield of 65 % (Scheme 1.3) [10].

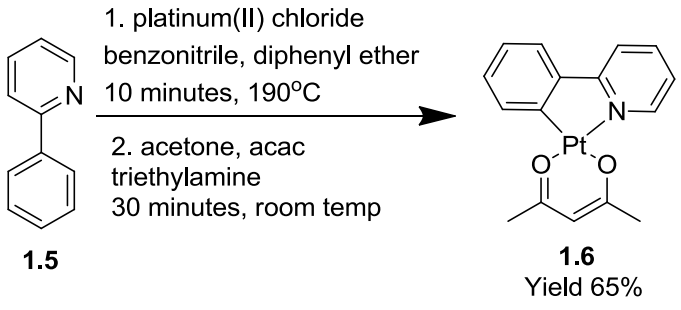

Scheme 1.3 Alternative synthesis of Pt(II) acac complexes

1.1.2 Synthesis of Ir(III) acac complexes

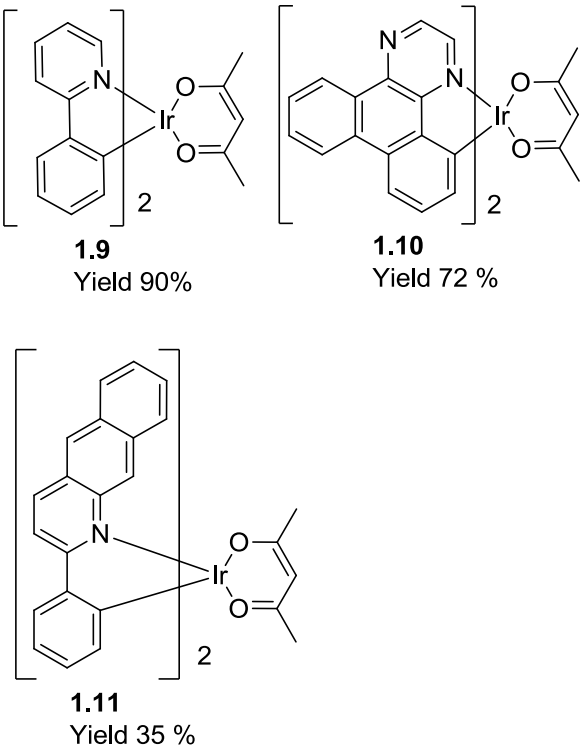

Figure 1.2 Examples of Ir(II) acac complexes

Figure 1.2 shows some examples of Ir(III) acac complexes[1,11,12]. The first report of the synthesis of an iridium chloride-bridged complex was by Nonoyama in 1974[13]. A solution of $Na_3[IrCl_6]$, 2-methoxyethanol and the pro-ligand (**1.12**) was stirred at room temperature for 8 hours then refluxed for a further 24 hours to give the chloride-bridged product (**1.13**) (Scheme 1.4).

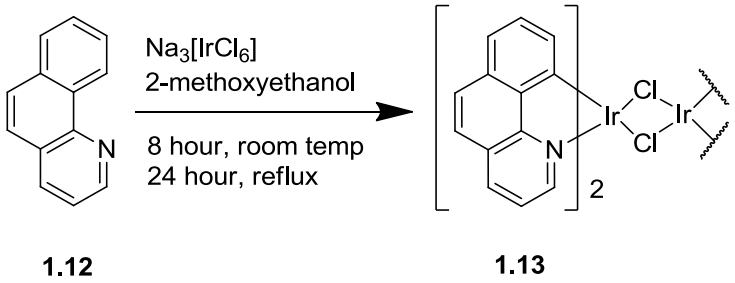

Scheme 1.4 First reported synthesis of Ir(II) complex

More recent reports have described refluxing $IrCl_3.nH_2O$ with the pro-ligand in 2-methoxyethanol for 48 hours. On cooling, water is added to precipitate the chloride-bridged dimer[14]. At present the most common method is to reflux $IrCl_3.nH_2O$ with the pro-

ligand (**1.14**) in a mixture of 2-ethoxyethanol and water (3:1) for 24 hours. This gives the chloride-bridged dimer (**1.15**) which is then refluxed with acetylacetone and sodium carbonate in 2-ethoxyethanol for 12 hours to give the desired product (**1.16**) giving a yield of 45 % (Scheme 1.5) [15]. In my own work sodium acetylacetonate was used rather than acetylacetone and sodium carbonate as it was readily available.

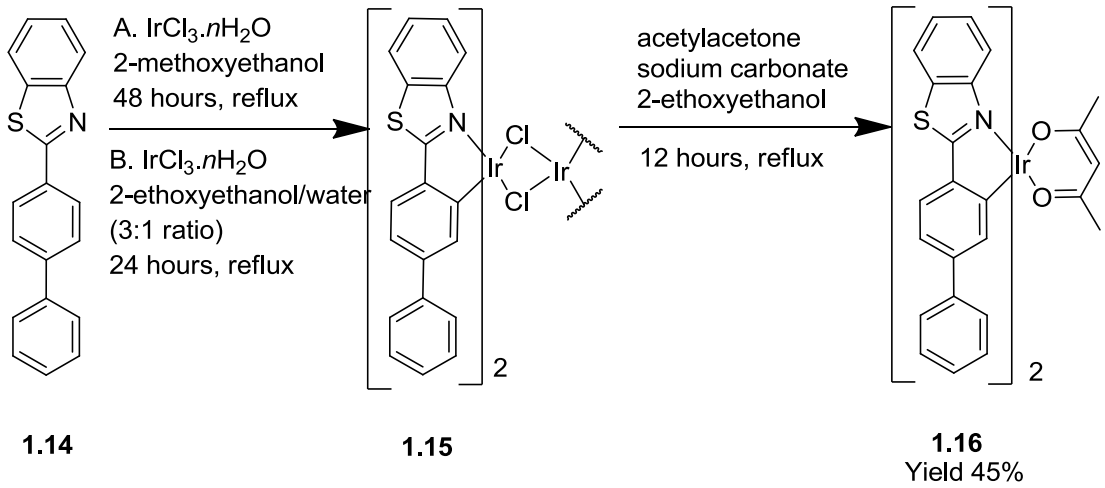

Scheme 1.5 Two routes to synthesis of Ir(III)(acac) complexes

1.1.3 Synthesis of triscyclometallated Ir(III) complexes

One of the simplest Ir(III) cyclometallated complexes is $[Ir(ppy)_3]$, the synthesis of which was first reported by Watts and co-workers in 1985[16,17].

Scheme 1.6 shows the complex which is synthesised by refluxing iridium trichloride hydrate and 2-phenylpyridine (**1.5**) in a mixture of 2-ethoxyethanol and water (3:1 ratio). The yellow precipitate is then washed with ethanol and acetone. The solvent is evaporated from these washings to give a yellow solid which is, after purification, $[Ir(ppy)_3]$ in a 10% yield (**1.17**) (synthesis A of Scheme 1.6). However, the main product from this synthesis is **1.18** which, after purification, gives a 72% yield.

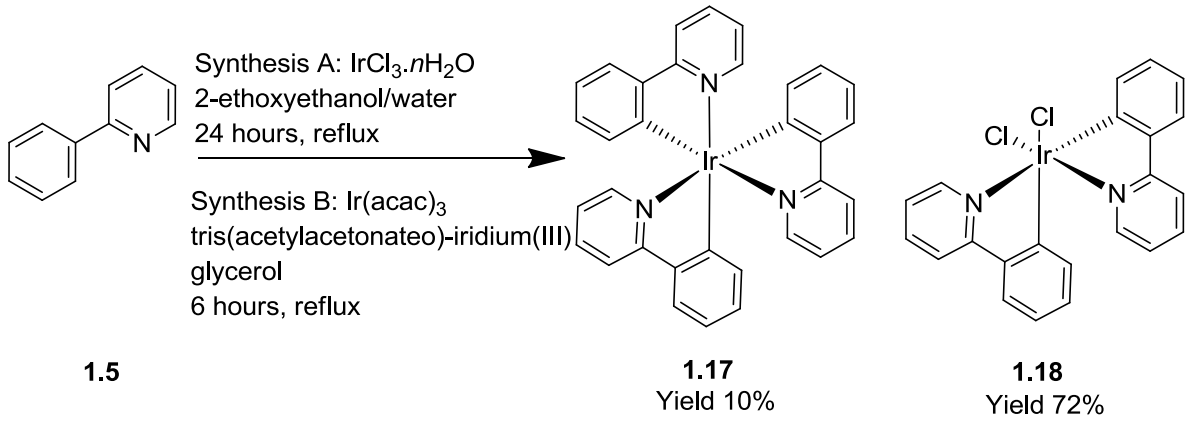

Scheme 1.6 Synthesis of $[Ir(ppy)_3]$

An alternative method is to dissolve tris(acetylacetonateo)-iridium(III), $Ir(acac)_3$ and the pro-ligand (**1.5**) in glycerol and reflux for 6 hours. 1M aqueous hydrochloric acid is then added to precipitate the product (**1.17**),[18,19] giving a yield of 45% (synthesis B of Scheme 1.6).

1.1.4 Synthesis of N^C^N Pt(II) complexes

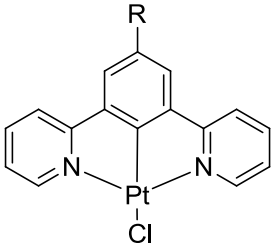

1.19
R = CH_3, Yield 40 %
R = H, Yield 78 %

Figure 1.3 Example of a N^C^N Pt(II) complex

An example of a N^C^N Pt(II) complex is shown in Figure 1.3[20]. An aqueous solution of potassium tetrachloroplatinate is added to a solution of the pro-ligand (**1.20**) in acetonitrile and the mixture is refluxed for 3 days to give the product (**1.19**)[21] (synthesis A of Scheme 1.7). Another method is to reflux a mixture of the ligand (**1.20**) and potassium tetrachloroplatinate in acetic acid for 3 days the resulting precipitate is the product (**1.19**)[22] (synthesis B of Scheme 1.7).

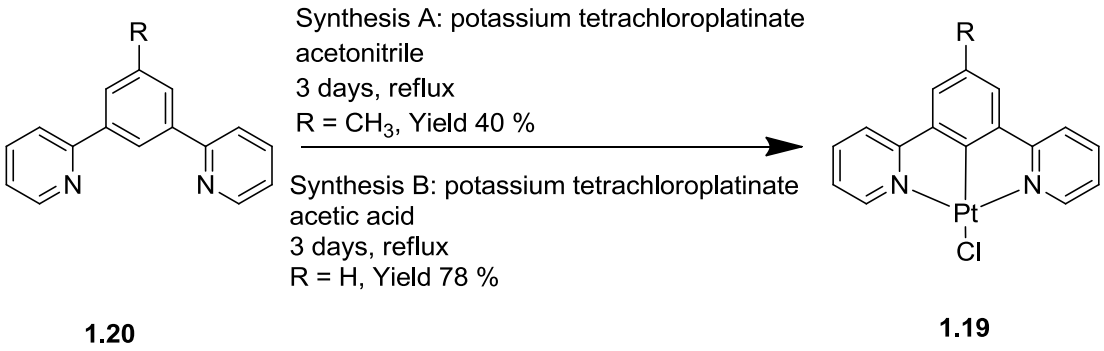

Scheme 1.7 Two routes to synthesis of an N^C^N Pt(II) complex

1.1.5 Synthesis of N^C^N Ir(III)

Scheme 1.8 shows an N^C^N Ir(III) complex[23]. The synthesis of N^C^N Ir(III) complexes are very similar to that of Ir(III) acac complexes in that the pro-ligand (**1.21**) is reacted with $IrCl_3.3H_2O$ in a mixture of 2-ethoxyethanol and water (in a 3:1 ratio) to give the product (**1.22**) in a yield of 77 %[24,23] (Scheme 1.8). However unlike the synthesis of Ir(III) acac complexes, no further reactions are required.

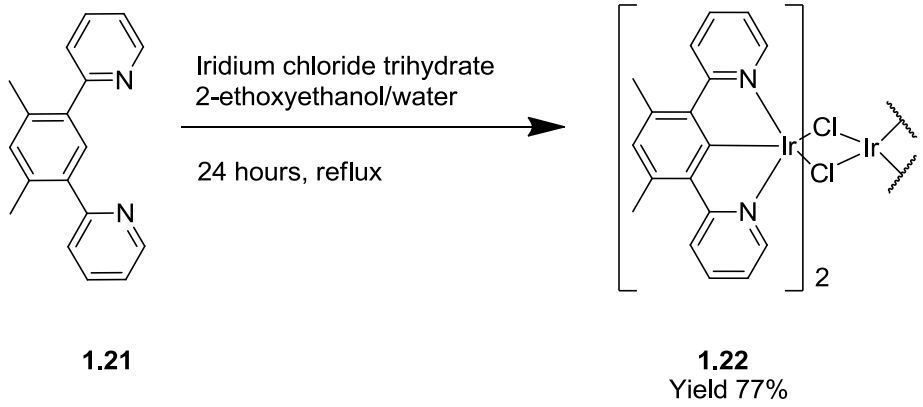

Scheme 1.8 Synthesis of an N^C^N Ir(III) complex

1.2 Photophysical properties of cyclometallated complexes

Iridium complexes used in electroluminescent devices are generally octahedral with a 3+ oxidation state[11]. Iridium(III) polyimine complexes are luminescent, and the emissive state is dependent on the energy of the highest lying metal-centred orbital. This in turn is determined by the number of anionic or cyclometallating donor atoms. If there are no anionic or cyclometallating ligands bound to iridium(III), then emission occurs from the

ligand centred (LC) states. For example $[Ir(bpy)_3]^{3+}$ shows a highly structured emission at 77 K with λem ~ 440 nm and a lifetime of ~80 μs[25]. Iridium bis-terpyridine complexes are also luminescent at room temperature. $[Ir(terpy)_2]^{3+}$ shows an emission spectrum that is highly structured with λem at 458 nm for the highest energy peak[26]. Emission is from an LC state but it is also likely to be mixed with metal-to-ligand charge transfer (MLCT) states. The interplay between LC and MLCT emissive states is one reason for the investigation of such Iridium complexes as luminescent sensors.

1.3 Strategies to achieve red shift

1.3.1 Substitution in the cyclometallating and auxiliary ligands

The HOMO and LUMO orbitals can be influenced by electron donating or withdrawing substituents. Modifications to the ligands by adding substituents allow the emission energy to be tuned over a wide range. This is mainly due to the HOMO and LUMO being localised on different parts of the molecule[27]. A recent study looked at a series of Ir(III) complexes based on aryl(6-arylpyridin-3-yl)methanone ligands[28] (Figure 1.4).

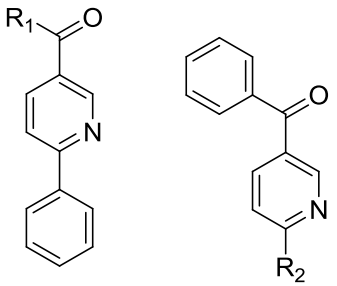

1.23 621 nm **1.24** 668 nm

Figure 1.4 The Ir(III) complexes were based on aryl(6-arylpyridin-3-yl)methanone ligands

The authors incorporated 1-napthyl, 2-napthyl and fluorenyl groups into the ligand in this way, tuning of the emission was achieved. Compared to $(Bzppy)_2Ir(acac)$ (**1.25**, Figure 1.5) which showed an emission of 619 nm, the complexes showed an emission in the range of 621-668 nm giving a shift further into the red region.

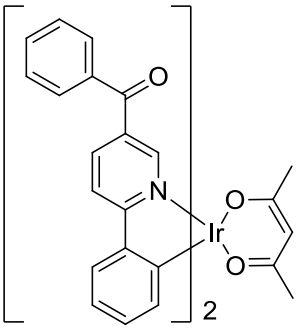

1.25
619 nm

Figure 1.5 (bis(2-phenyl-5-benzoyl- pyridine)Ir(acetylacetonate) or [(Bzppy)2Ir(acac)]

Another paper[29] showed that fluorinated analogues of a ligand can reduce triplet-triplet annihilation processes and also the sublimation temperature of these complexes is decreased, making them more desirable for applications such as OLEDs. Introducing bulky groups can decrease the self-quenching of emitters at high doping levels. Using fluorine ligands yields crystallisation-resistant materials that can be incorporated into single layer OLEDs, while expanding the π-conjugation of C^N ligands can result in enhanced device performance.

Solutions of $Ir(ppy)_2(acac)$ exhibit green photoluminescence (λmax = 516 nm). Tuning of this emission can be achieved by substitution of 2-phenylpyridine with other C^N binding ligands, from 512 nm to 612 nm[30]. Changing the acac ligand results in a relatively minor shift. A study of an $Ir(pbt)_2(acac)$ complex reported on the effects of modifications to the phenyl ring of the ligand[31]. Laskar and Chen showed that fluorination at the 4-position of the complex results in a blue-shift of 16 nm, while fluorination at the 3-position of the complex results in a small red-shift and a tripling of photoluminescence quantum yield relative to the parent compound.

When an electron donating group is introduced to the phenyl moiety of ppy, then the emission wavelength of the Ir(III)-ppy complex will be red shifted. Recently, a series of Ir(III) complexes based on the 5-acetyl-2-phenylpyridine ligand was reported[32]. Lee and co-workers found that all structures exhibited efficient red electroluminescence. These

results suggest that complexes made from this ligand have excellent properties suitable for orange-red emitting materials for OLEDs. The same group also noted that the position of an electron donating group on the ring can also affect the luminescence[33]. Figure 1.6 shows an iridium complex with a methyl group on the phenyl ring either para to the pyridine ring (complex **1.26**) or ortho to the pyridine ring (complex **1.27**). It was found that **1.27** was red-shifted by ~14 nm compared to **1.26**. It is thought that putting the methyl ortho to the pyridine ring causes a steric effect in the phenyl and pyridine rings. The phenyl groups are then no longer planar with the central metal and the pyridine ring. This gives a larger distorted angle and the energy gap in **1.27** becomes smaller compared to that of **1.26** after splitting from the ligand-iridium complex.

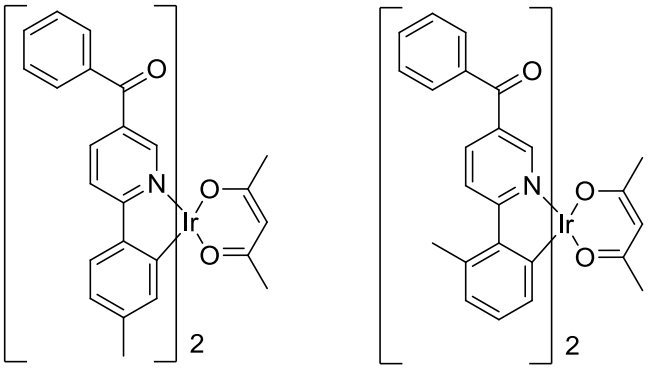

1.26
618 nm

1.27
632 nm

Figure 1.6 The position of the electron donating group can also affect emission

Red emitters can be achieved by adding electron-donating groups to the phenyl moiety and electron-withdrawing groups onto the pyridyl moiety of a metal complex. The addition of electron-donating groups to the phenyl moiety leads to destabilisation of the HOMO, whereas the addition of electron-withdrawing groups to the pyridyl moiety reduces the energy of the LUMO, since it is generally localised on the π-orbitals of the pyridyl groups[15]. However, one group has reported iridium complexes containing electron withdrawing groups on the phenyl moieties. Three of these complexes (Figure 1.7) show bathochromic shifts compared to the parent complex $[Ir(ppy)_2(acac)]$ (**1.9**)[34].

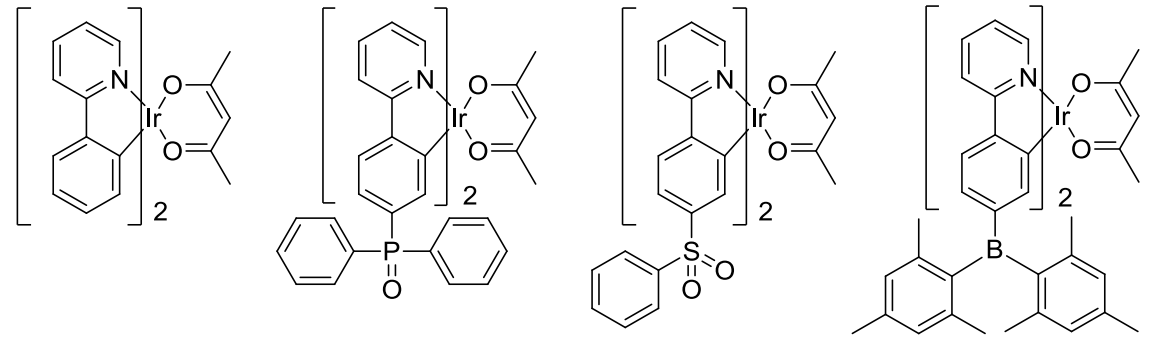

Figure 1.7 The addition of electron withdrawing groups to the phenyl moiety of a complex can cause a red shift in emission

Time-dependent density functional theory (TD-DFT) calculations showed that for the LUMOs there were large differences in the complexes. The pyridyl ring π-orbitals contribute 63% to the LUMOs of **1.28**, which is typical for Ir complexes. However, the contribution for **1.29** was 44% and for **1.30** 35%. The π-orbitals of the pyridyl moiety are no longer the only contributor to the LUMO of **1.30**; It is also distributed over the boron atom and the mesityl groups. Therefore, for **1.30**, the MLCT will be transferring electron density to the $B(Mes)_2$ moiety rather than onto the pyridyl moiety which is typical of other iridium complexes. The $B(Mes)_2$ moiety will tend to stabilise the MLCT states strongly due to the "empty" p_π orbital. This low energy MLCT state of **1.30** is responsible for the intense red phosphorescence.

1.3.2 Increase in conjugation

There are many examples of how extending the conjugation and, therefore, the π-system achieves a bathochromic (or red) shift in the wavelength (Figure.1.8). A simple example shows how changing the pyridine of the ligand 2-phenylpyridine (ppy) to isoquinoline (piq), causes a bathochromic shift of ~100 nm. Switching to isoquinoline lowers the LUMO of the complex, inducing the red shift[35].

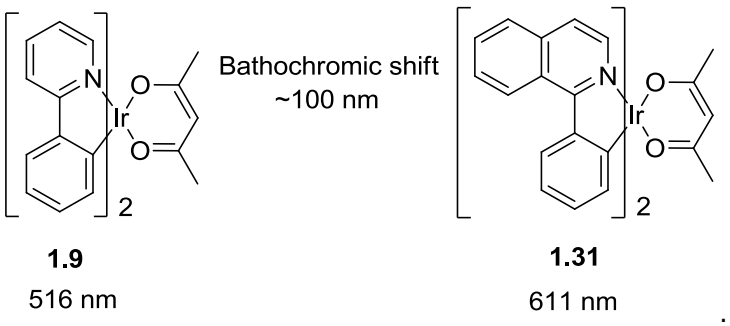

Figure.1.8 The addition of a phenyl ring can induce a red shift in emission

These types of complexes are desirable as they are easy to synthesise, are thermally stable, and have good solubility in common organic solvents. It is not enough for a complex to be a good emitter with high quantum yields; solubility is also important for use in OLED devices as the complexes can then be readily employed onto a substrate without the need for vacuum deposition methods which are expensive and inefficient. More examples of red emitters are shown in Figure 1.9. Once again the conjugated system of these complexes gave emissions in the red region. These complexes are synthesised by stirring a mixture of the ligand and iridium trichloride hydrate in ethoxyethanol at 120°C for 24 hours. The resulting precipitate is then filtered off and stirred with acac and sodium carbonate in 2-ethoxyethanol at 90°C for 12 hours. The precipitate is then filtered off.[36,11]

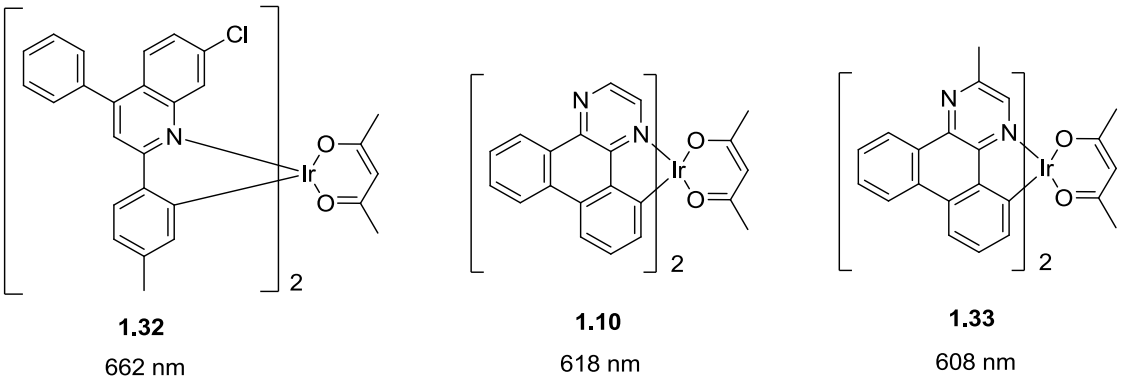

Figure 1.9 Examples of red emitters

As conjugation is increased, emissions can be achieved that reach into the far red and even NIR of the spectrum. Although, as will be discussed later, this does have limitations in that there is a point where the effect of conjugation breaks down and has a detrimental effect on emission. Examples using dendrimers have achieved emissions as long as 693 nm (Figure 1.10)[5]. Dendrimers have a central, light-emitting core with an interior branched structure and an exterior surface containing functional groups, in this case, to

provide solubility. Potential advantages over other conjugated complexes include improved solubilty by using appropriate surface groups, also the intermolecular interactions can be fine-tuned by the type and level of dendrons used.

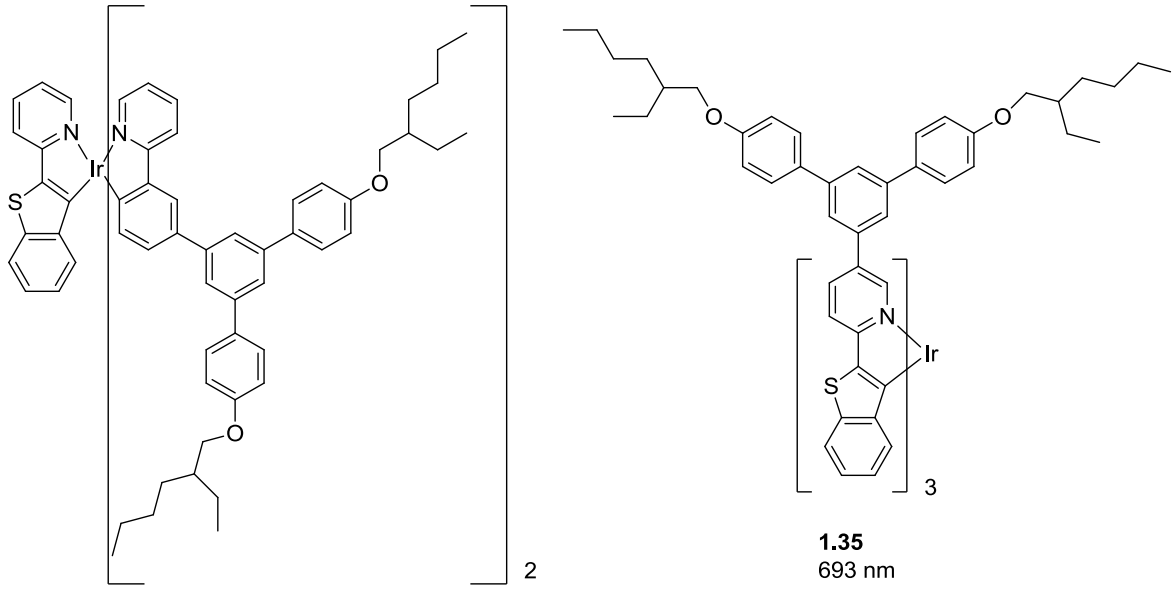

Figure 1.10 First generation dendrons

It is also possible, by modification of the quinoline portion of a compound, to further enhance the red shift towards and into the NIR region of the spectrum (Figure 1.11). Extension of the π-electron delocalisation of the aromatic ligand leads to a shortened energy gap between the ground and lowest excited states[1].

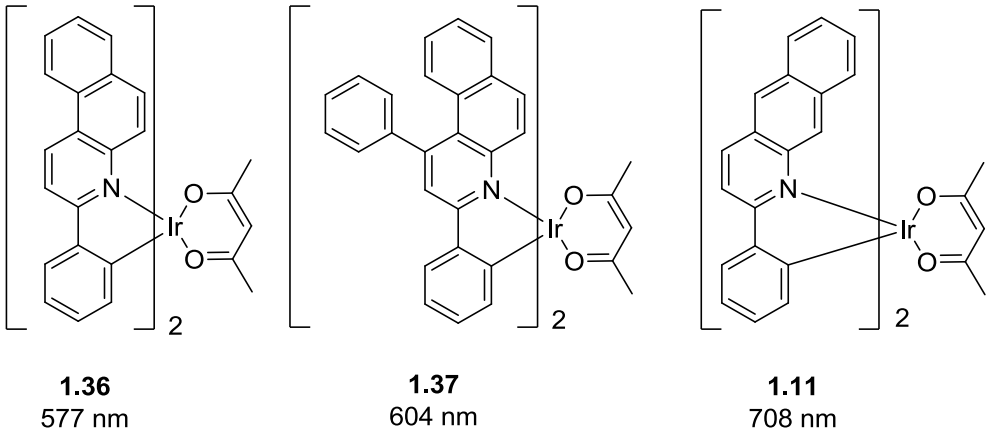

Figure 1.11 Modification of the quinoline portion gives a NIR emission

The positioning of additional phenyl rings on either the phenyl or pyridyl moieties of the ligand can also influence the wavelength of emission for a complex. The complex shown

in Figure.1.8, **1.38** gives an emission at 618 nm. If the position of the additional ring is moved (**1.39**) then there is a slight hypsochromic shift and emission is 597 nm[37](Figure 1.12).

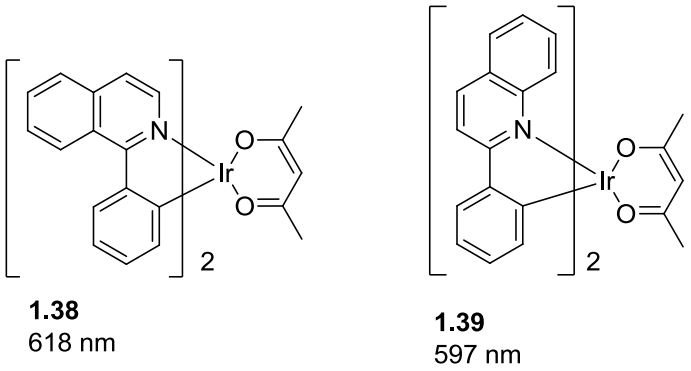

1.38
618 nm

1.39
597 nm

Figure 1.12 The position of the additional ring affects the emission

The same can also be said when adding an additional ring onto the phenyl moiety of the complex. A further increase of the conjugation gives an even greater red shift, but again just how much is dependent on the position of the ring[38]. Figure 1.13 shows how the addition and position of an additional ring to the phenyl moiety can give a red shift of up to 60 nm.

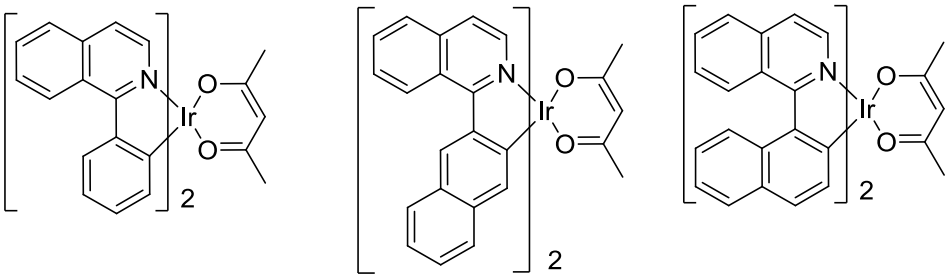

1.38
618 nm

1.40
633 nm

1.41
680 nm

Figure 1.13 Addition and position of an additional ring gives a bathochromic shift

A red shift can also be achieved by incorporating an additional nitrogen into the pyridyl ring. For example, changing the pyridyl moiety to pyrazine can achieve a red shift of 60-80 nm. This is mainly due to a lowering of the LUMO of the pyrazine derived ligand[39]. In the example shown in Figure 1.14[39], the complexes are NIR emitters giving emissions of 775 and 855 nm.

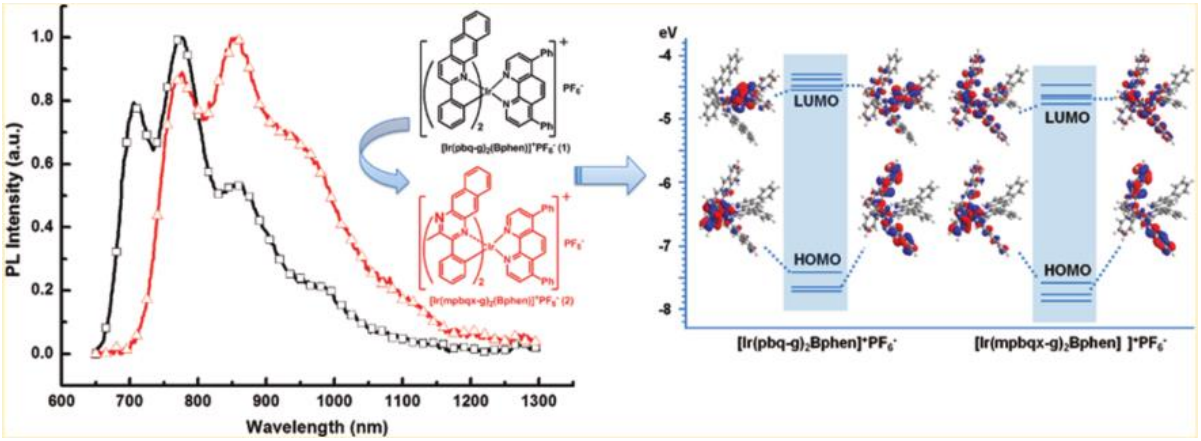

Figure 1.14 NIR emitters are more red shifted with the addition of an extra nitrogen into the complex

As already stated, an increase of the conjugation of the ligand can increase the wavelength of emissions, but where the increase in conjugation on the ligand occurs is also a contributing factor. Figure 1.15 shows copolymers based on carbazole-*alt*-fluorene as a main chain with an iridium complex as a side group. The side groups differ only in the position of the additional phenyl ring. The shortest wavelength has the phenyl ring attached to the phenyl moiety of the ligand (**1.42**)[40].

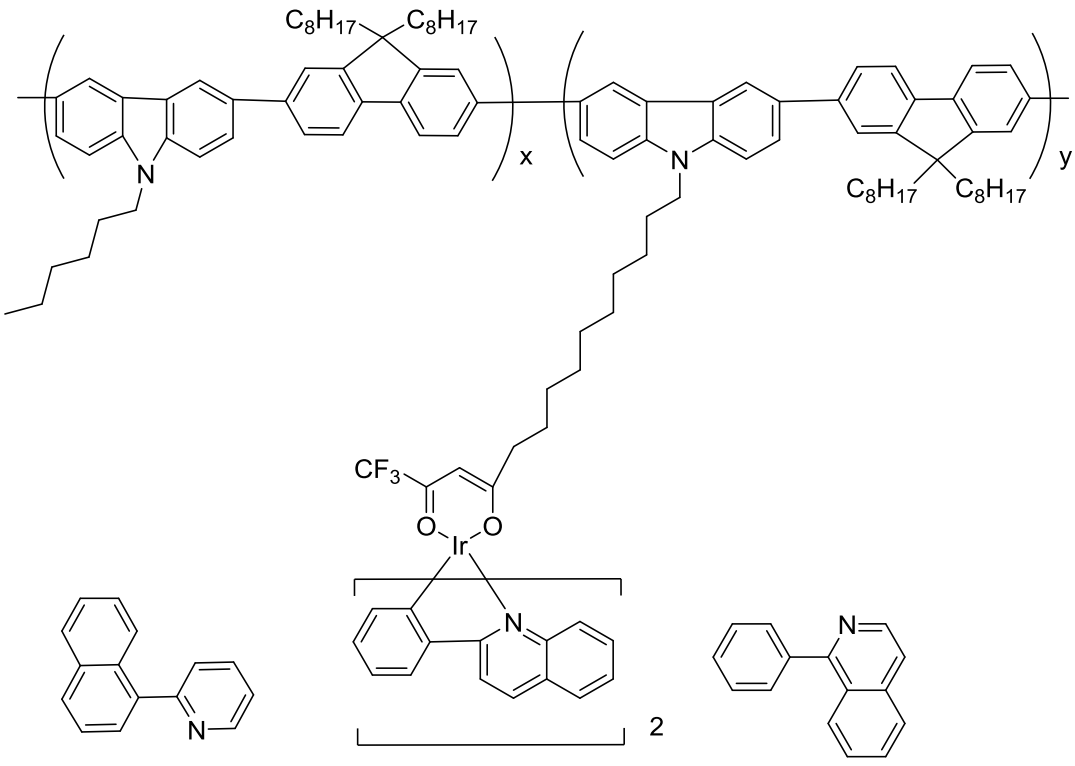

1.42
415 nm

1.43
580 nm

1.44
610 nm

Figure 1.15 The position of the extra phenyl ring can also effect emission

Figure 1.16 shows how replacement of a methyl group at the pyridyl moiety by nitrogen gives a pyrazine moiety. The electronegative nitrogen causes a significantly decreased LUMO. The energy gap of this complex is then reduced since the HOMO of the complex, which is mainly located at the phenyl moiety of the complex and is electron rich, remains unchanged. Attachment of an extra aromatic ring to the pyrazine moiety increases the π-conjugation of the complex, therefore reducing the energy gap further. In this way tuning of the complexes to emit in the red region can be achieved[14].

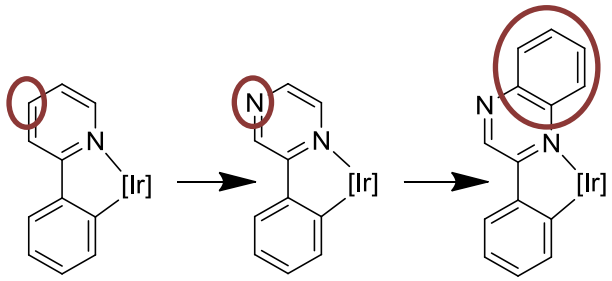

1.45 **1.46** **1.47**

Figure 1.16 Ligand tuning to achieve a red shift in emission

There does come a point when increasing the conjugation of a complex starts to have a detrimental effect on the emission. A recent study reports on the synthesis of a series of oligothienylpyridines as both platinum(II) and iridium(III) complexes with increasingly conjugated systems[41]. Figure 1.17 shows some of the complexes synthesised with both **1.49** and **1.52** emitting far into the red/NIR region. The addition of a thiophene ring, therefore increasing the conjugation further, leads to a blue shift in emission. This blue shift is due to the decrease in the participation of the metal d orbitals if there is too much conjugation and the HOMO decreases. This leads to an increasing energy gap which also reduces the rate of intersystem crossing. As a consequence, fluorescence is also observed and the intensity of the phosphorescence decreases.

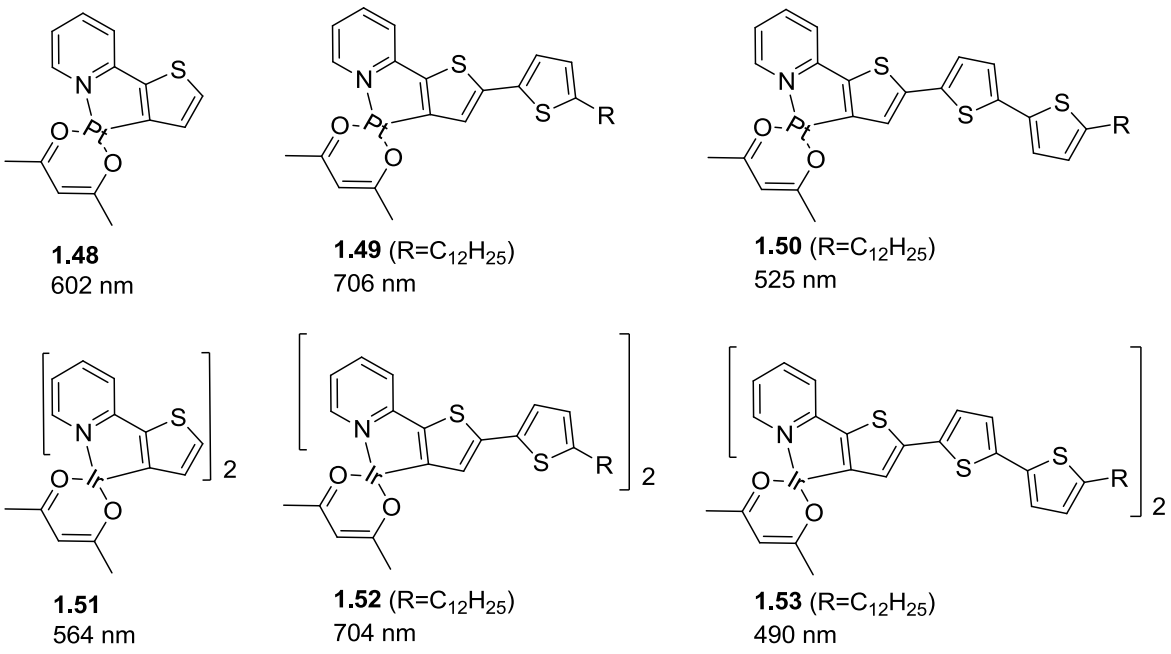

Figure 1.17 Increasing conjugation too much causes a hypsochromic shift in emission

1.3.3 Excimers of NCN Ir(III)

Complexes with two bidentate N^C ligands are usually synthesised by a reaction that introduces both N^C ligands at the same time to the metal ion, followed by the addition of an auxiliary ligand. This means that two differently substituted cyclometallated ligands cannot be investigated by this method. However, by using one terdentate cyclometallating ligand, one bidentate cyclometallating ligand and a monodentate cyclometallating ligand, the effects on emission of substitution in two different cyclometallated ligands can be investigated. Brulatti and co-workers investigated a series of Ir(III) complexes based on 1,3-di(2-pyridyl)benzene[23]. Figure 1.18 shows two Ir(III) complexes from the study which both emit in the red region of the spectrum. Addition of fluorine groups onto the ppy ligand (**1.55**) results in a blue shift of 21 nm. The electron-withdrawing fluorine atoms decrease the delocalised electron density in the aromatic ring.

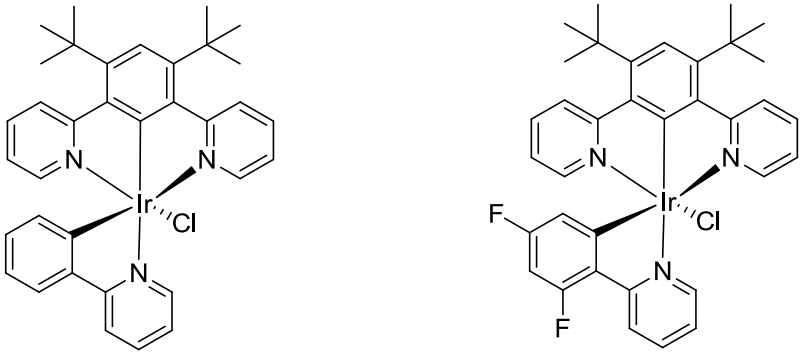

1.54
593 nm

1.55
572 nm

Figure 1.18 N^C^N coordinated complexes. Fine tuning can be achieved through substitution on the bidentate cyclometallating ligand.

The TD-DFT data for these complexes show that the terdentate cyclometallating ligand contributes to both the HOMO and the LUMO, whereas the bidentate cyclometallating ligand shows very little role in the LUMO. Compared to tris-bidentate Ir(III) complexes, these complexes give a wider diversity of substitution and so give further opportunities to manipulate their emissive properties.

In order to achieve the desired coordination mode, Wilkinson and co-workers[24] describe how the addition of methyl substituents into the ligand at the C4 and C6 positions can avoid competitive cyclometalation and the desired complex can be achieved. They describe a number of iridium complexes, not all of which have good emissive properties.

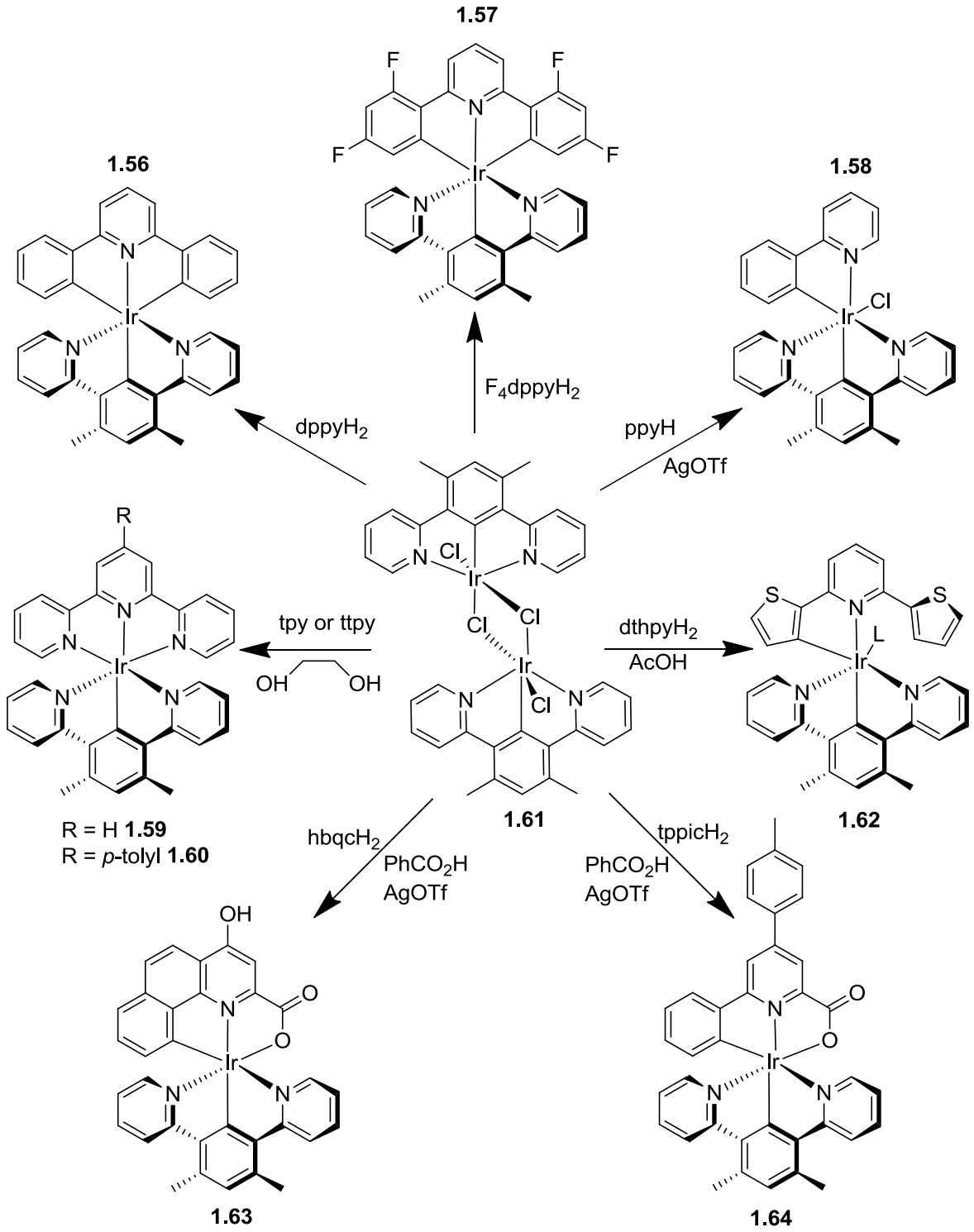

Figure 1.19 Structures of the Iridium complexes containing the N^C^N bound ligand dpyx

Figure 1.19 shows the Iridium complexes described, with complexes **1.59** and **1.60** being very weakly emissive at room temperature. It was also noted that they were a pale yellow colour compared to the other complexes which were a strong orange colour. Complex **1.58** was shown to be very strongly emissive.

Figure 1.20[42] shows some of the complexes synthesised by Obara and co-workers with the general formula [Ir(N^C^N)(ppy)X][42]. They give another example of how tuning of the monodentate and/or bidentate ligands can affect the emission. Fluorination of the complexes causes a slight blue-shift in emission of 9 nm in compound **1.65** compared to compound **1.66**. The blue-shift is greater between compound **1.67** and 1 with a shift of 15 nm.

Compound **1.68** is more red-shifted than compound **1.66** by 29 nm as cyanide is a much stronger electron withdrawing group than chlorine. Comparing all four complexes, the monodentate ligand has a bigger effect on the luminescent properties than the bidentate ligand, in this case.

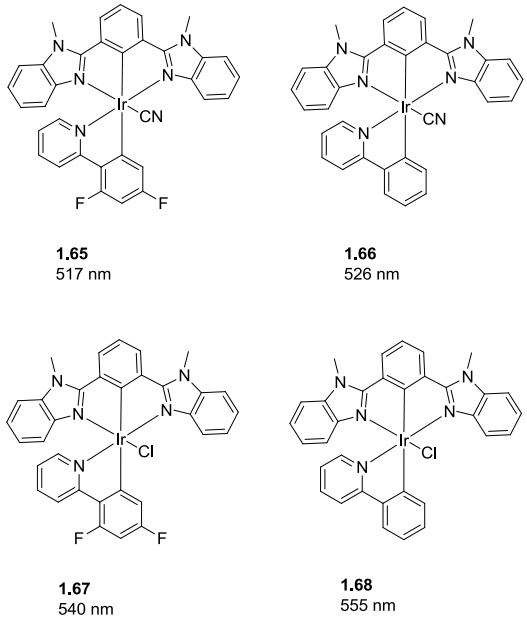

1.65
517 nm

1.66
526 nm

1.67
540 nm

1.68
555 nm

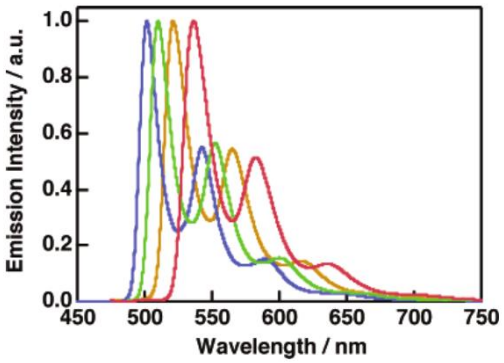

Emission spectra of Ir complexes **1.65** (blue), **1.66** (green), **1.67** (orange) and **1.68** (red) in CH_2Cl_2-toluene (1:1 v/v) at 77 K

Figure 1.20 Mixed-ligand Ir complexes [Ir(N^C^N)(ppy)X] and their emission spectra

1.3.4 Polymetallic assemblies

Most reports so far have involved complexes synthesised using platinum(II) or iridium(III) as the only metal present in the complex. Recently, complexes have been synthesised using both platinum(II) and iridium(III) in the same complex[43].

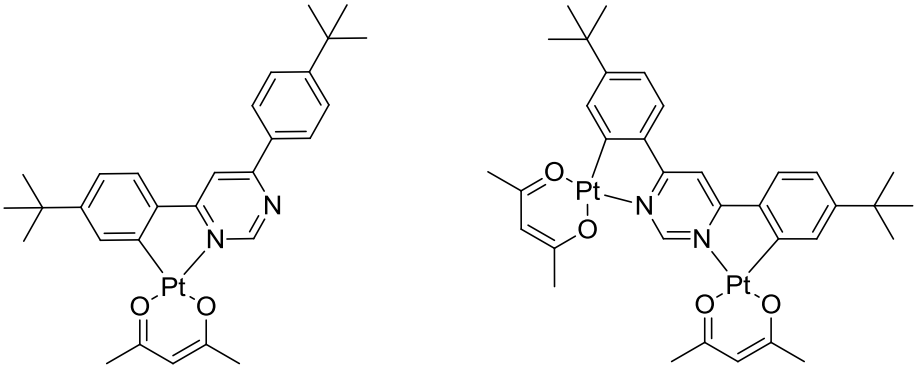

1.69
399 nm

1.70
530 nm

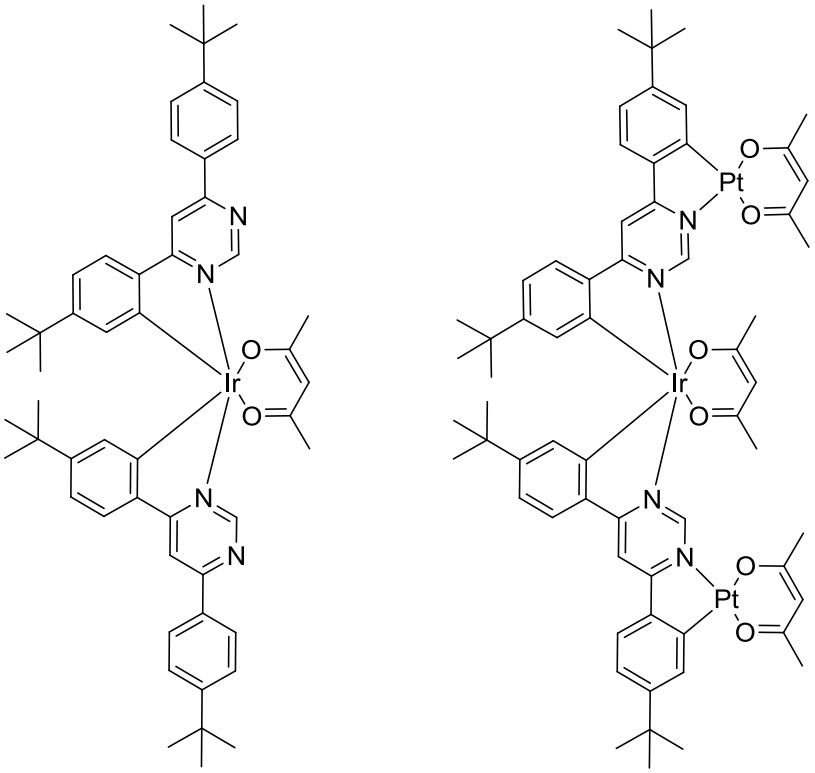

1.71
513 nm

1.72
568 nm

Figure 1.21 Platinum(II), iridium(III) and polymetallic complexes

Figure 1.21 shows the complexes synthesised for this work. The introduction of the additional metal was found to lead to a red shift in absorption and emission. Figure 1.22[43] shows the UV-visible absorption spectra of the complexes. It was concluded that the multimetallic complexes behave very differently to their monometallic counterparts. This is mostly due to the conjugation of the LUMO across the entire aromatic ligand. The pyrimidine acts as a bridge of communication. The metallic units do not retain their separate identities, which are found to be the case with many other multimetallic systems. For instance, it can be seen that the absorption and emission of an iridium(III) complex can be greatly red shifted with the addition of platinum(II) ions.

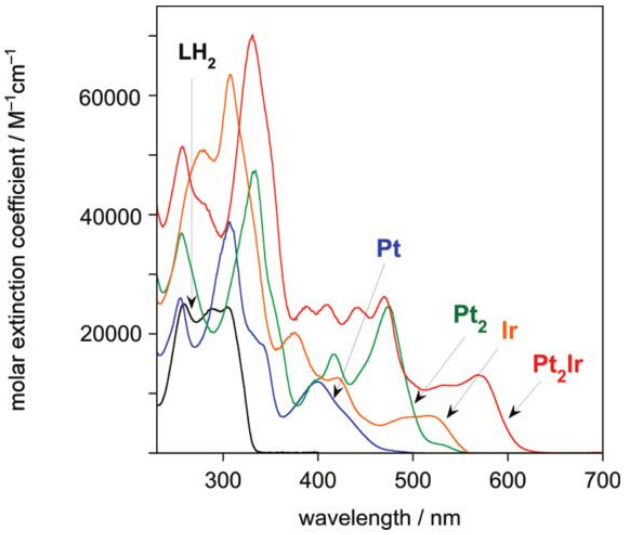

Figure 1.22 UV-visible absorption spectra of the metal complexes in CH_2Cl_2 solution at 298 K

1.3.5 Auxiliary ligand

It is important for applications such as OLEDs and cell imaging that the metal complex has a good solubility. This can be achieved by including bulky groups on the ligand. When they are introduced to the auxiliary ligand then solubilty can be increased without affecting the luminescence of the complex. Figure 1.23 shows an iridium complex synthesised using three different auxiliary ligands – 1,3-bis(3,4-dibutoxyphenyl)propane-1,3-dionate-o,o (bdbp, **1.73**), dipivaloylmethanate (dpm, **1.74**), acetylacetonate (acac, **1.75**). They all emit at the same wavelength, showing that, in this case, the auxiliary ligand does not affect luminescence. It was found that **1.73** had an increase in quantum yield compared to **1.74** and **1.75**[44]. Replacing acac and dpm with bdbp does enhance the phosphorescence quantum efficiency of these systems.

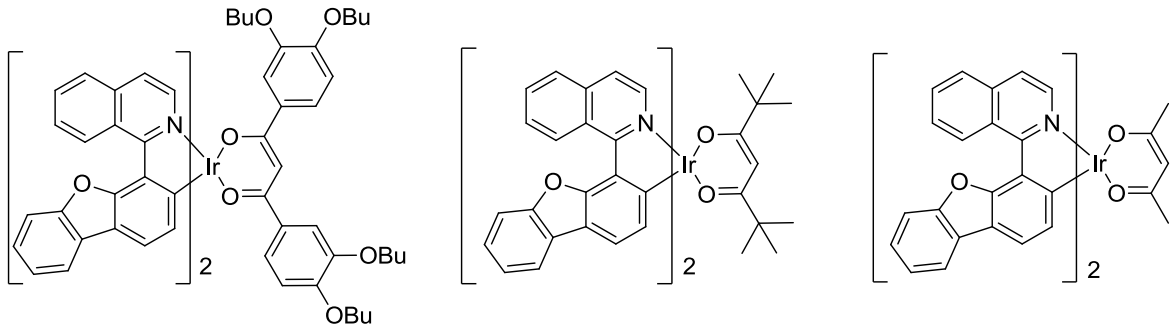

1.73
640 nm

1.74
639 nm

1.75
640 nm

Figure 1.23 Complexes showing that luminescence is not affected by the auxiliary ligand

1.4 Organometallic Complexes and Cell Imaging

1.4.1 Cells

The Cell is the fundamental building block of all living organisms. It is the simplest collection of matter that can live. There are two types of cell; prokaryotic or eukaryotic. Prokaryotic cells are those without membrane-bound nuclei and are only found in bacteria or archaea. Eukaryotic cells are those with membrane-bound nuclei and are found in animals, plants, fungi and protists. Eukaryotic cells are generally larger and more complex. They contain membrane-bound organelles, which are lacking in prokaryotic cells. Organelles have a specialised structural or functional role within the cell, such as the nucleus, lysosome or mitochondria.

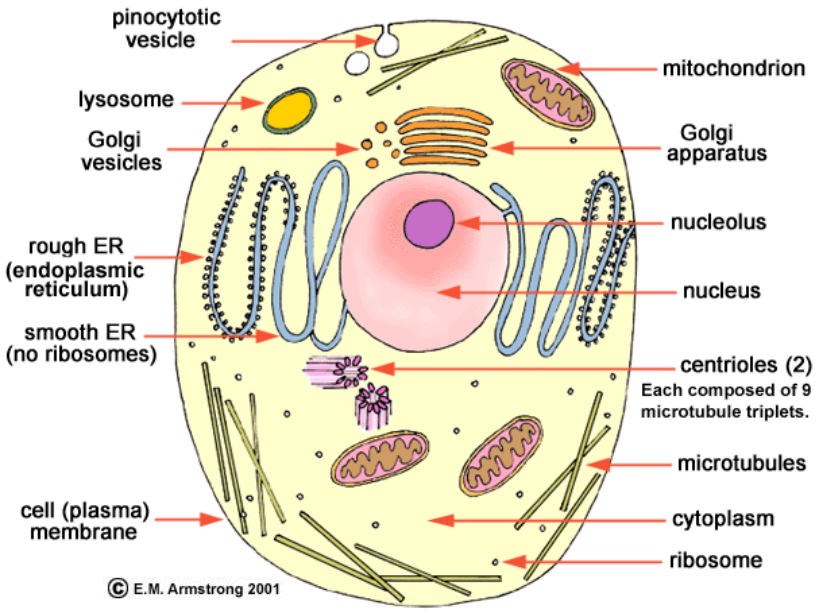

Figure 1.24 Figure of an animal cell taken from http://waynesword.palomar.edu/lmexer1a.htm

Most cells are between 1 and 100 µm in diameter so to understand how a cell functions, cell biologists need microscopes to be able to view them. There are various techniques in light microscopy used to view a cell, such as brightfield or phase-contrast. Brightfield passes light directly through either a stained or unstained specimen but this technique has little contrast. Amplifying variations in density in a specimen using phase-contrast can be

useful for examining living, unpigmented cells. If specific molecules within the cell are to be studied then fluorescent cell imaging is a very important tool[45].

1.4.2 Cell Imaging

The application and use of phosphorescent heavy-metal complexes as bioimaging probes is a relatively new research field that is showing rapid development[46]. To date there are few studies that involve organometallics. These complexes, which contain one or more metal-carbon bonds, have a number of properties required to make a useful fluorophore for applications in cell imaging.

Fluorescent cell imaging is important for diagnostics and biomedical research. This method involves excitation of the cell sample and detection of the emitted light. This detection is usually done by confocal microscopy[2]. Confocal microscopy is a very powerful technique as it eliminates interference from reflected/diffracted light. It allows filtering by depth of field which allows 'slices' of a sample to be recorded separately. These images can then be combined to build up a 3D image of the sample[46]. Confocal microscopy has a much greater sensitivity than normal microscopy as only emitted light is observed rather than the reflected or transmitted light.

Cell imaging uses fluorescence to highlight the important structures within the cell. Some parts of a cell are already fluorescent, however the non-fluorescent areas of the cell can also be observed with the application of a commercially available fluorescent dye[47]. Each dye is targeted to a different part of the cell and emits at different wavelengths. By applying more than one dye to a cell, confocal microscopy can be used to collect images of the different areas of the cell, which can then be brought together as one 3D image highlighting all of the important areas of the cell.

When using these dyes, there is a need to differentiate between the autofluorescence (natural emission of light by biological structures) of the biological species and the fluorescence derived from the dye. It can be difficult to distinguish clearly between the

areas that have accumulated the dye and those that are showing autofluoresence. There are two techniques that can be used to combat this problem, namely co-localisation and z-scans. Co-localisation is the technique of applying two dyes simultaneously, one of which will be suspected of targeting a certain part of the cell. The second dye will have different emission properties but be well known to target the part of the cell in question. The images from the two dyes are then overlaid and can then be measured. From this the specificity of the new dye for its desired target can be determined. Confocal microscopy is then used to acquire images, which represent slices through the depth of the cell (the z-dimension). Z-scans are used to ensure that the new dye has penetrated the interior of the cell rather than just associating with the surface (Figure 1.25[48]).

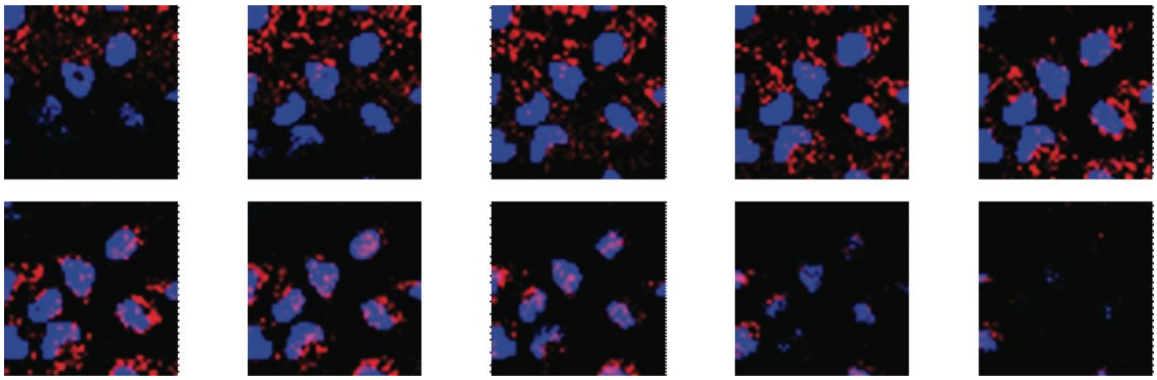

Figure 1.25 Confocal fluorescence Z-section live cell images of AuNP-2 (20 μM) with Hela cells showing luminescence in three dimensions. Shown is the image obtained with cells costained with nuclear stain DAPI (blue) and AuNP-2 (red). Scanning from left to right.

There are several characteristics required of a successful fluorophore to be used in cell imaging. The optimal excitation wavelength for a fluorophore should be in the deep red or near-infrared range (650-950 nm). In this range there is both good tissue penetration and low autofluoresence. In addition IR or NIR wavelengths can pass through tissue without causing any cellular damage. Fluorescent brightness is another consideration. The brighter the emission from the compound, the less excitation intensity is needed[3].

The desired photophysical characteristics for a fluorophore are -

-excitation and emission at non-damaging wavelengths

-large Stokes shift

-resistant to photobleaching

If there is a large enough difference in wavelength between the two modes of fluorescence then autofluorescence can be filtered out. This is highly likely if the fluorophore has a large Stokes shift. The Stokes shift is the difference in wavelength between the absorbed and emitted light. Typically, the Stokes shift involved in autofluoresence is small[2]. Photobleaching is the photochemical degradation of fluorophores. Most organic fluorophores suffer from photobleaching in long-term observation[49].

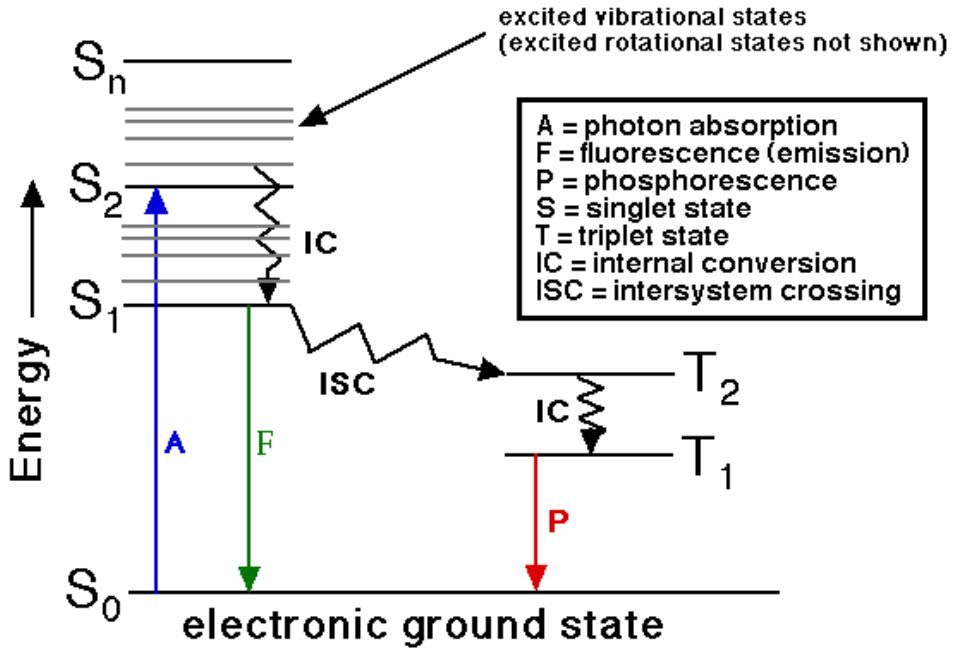

Figure 1.26 Jablonski diagram taken from http://www.files.chem.vt.edu/chem-ed/quantum/jablonsk.html

Heavy metal complexes can have the stability and photophysical properties required of a cell imaging agent. These triplet emitters tend to have a large Stokes shift. They also have long luminescence lifetimes due to the forbidden nature of the emission from triplet states. The presence of heavy atoms facilitates inter-system crossing by spin-orbit coupling[50]. Figure 1.26 shows a Jablonski diagram which illustrates the molecular electronic and vibrational energy levels. Fluorescent complexes are excited to the singlet state and quickly relax back down to ground state. Phosphorescent complexes are excited to singlet state and can then undergo intersystem crossing and become a triplet state. Return to the ground state is forbidden.

The long luminescent lifetimes make these complexes suitable for use in time-resolved emission imaging microscopy (TREM). This technique uses time-scales from hundreds of nanoseconds to microseconds and allows for time-gated experiments that can distinguish the target fluorescence from short-lived autofluorescence[51]. Images are obtained using a time-gated camera at different time delays after the excitation pulse (Figure 1.27).

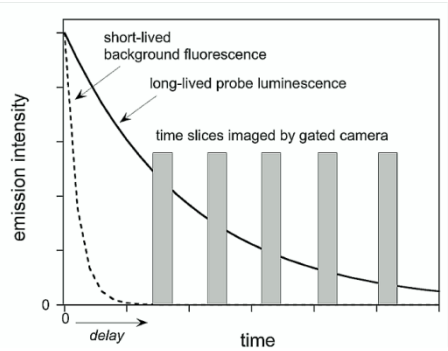

Figure 1.27 Diagrammatic illustration of the concept of time gating to eliminate short-lived background fluorescence and of time slicing to monitor the temporal decay of emission and obtain quantitative data.

For example, images of cells pre-treated with a Pt(II) complex in the presence of fluorescein dianion (whose emission serves as a model of short-lived background fluorescence) were taken. Figure 1.28[51] shows that the image on the left, taken immediately after the excitation pulse, is dominated by the fluorescein emission. However, when the camera was activated after a delay of 10 ns, the cells could be visualised using the long-lived emission from the Pt(II) complex[51].

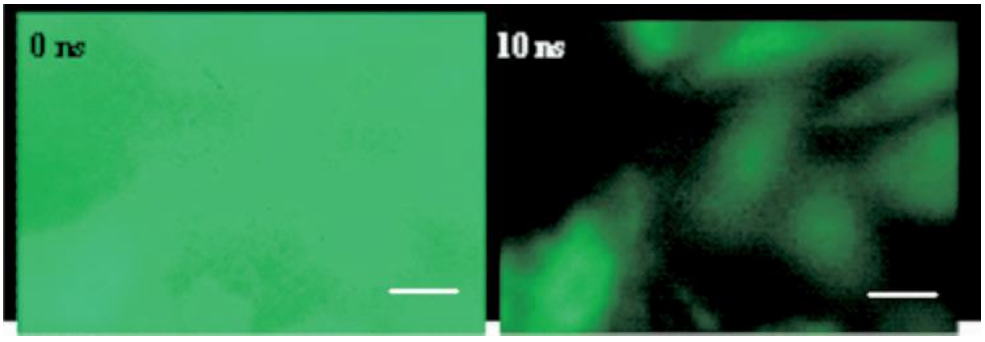

Figure 1.28 Time-gated cellular imaging: live CHO cells preincubated with [PtL1Cl], imaged in the presence of solution of fluorescein in 1M NaOH. The images were taken at 0 ns (Left) and at 10 ns (Right) delays after the 355-nm laser pulse. (Scale bar: 10 μm.)

Multiphoton microscopy (MPM) is a form of laser-scanning microscopy that is proving useful for imaging thick tissue and live animals[52]. Two-photon excitation uses two photons of equal energy from the same laser. The photons interact with a molecule and produce an excitation, which is the equivalent to the absorption of a single photon but has twice the energy.

In addition to above-mentioned photophysical characteristics, to be useful in cell imaging a fluorophore must ideally be:

-able to enter cells

-able to localise in desired compartments

-non-toxic and stable

To be a successful imaging agent, it is important to have a good balance of lipophilicity and solubility. Cell membranes are composed of lipids and so highly polar species can be poorly uptaken by cells. On the other hand, the medium in which the cells are incubated is an aqueous buffer, so it is important to have sufficient solubility to be available for uptake by cells. Localisation is a useful property to be able to target a specific area inside the cell (Figure 1.29[46]). This could be controlled by either a chemical reaction with a species present within the organelle or by matching charges, polarity and lipophilicity with the target. It is also desirable to have a compound which has low toxicity during the experiment so kinetic inertness is important[2].

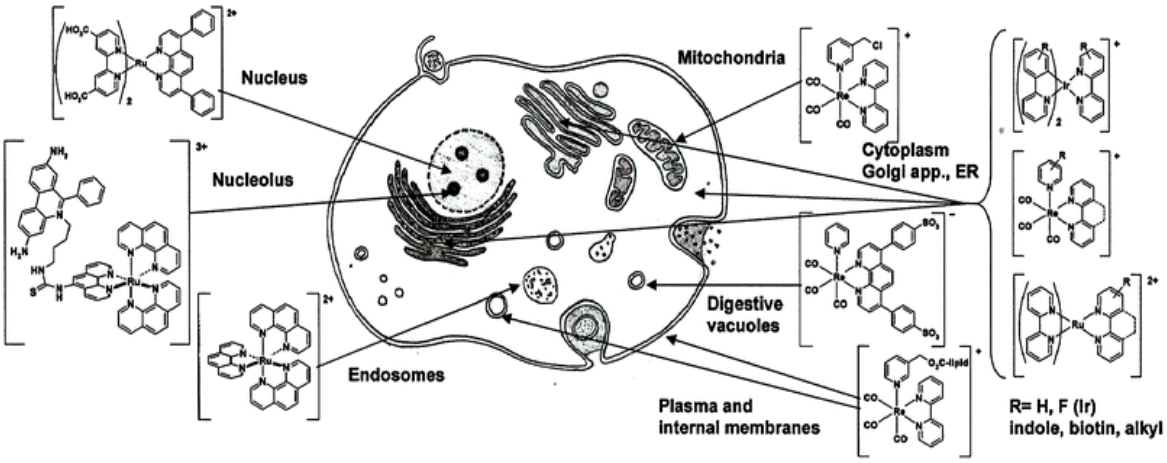

Figure 1.29 Localisation of the d^6 species in cells

The charge of a species is important for cellular uptake. Cells have a negative surface charge so heavy-metal complexes with a positive charge can easily interact with and enter living cells. There are many examples of Ir(III) and Ru(II) complexes with a positive charge that can enter living cells[53].

A suitable hydrophobicity can also help heavy metal complexes to enter living cells. One example[54] shows the cellular uptake of iridium complexes. The cellular uptake efficiencies increase with the enhancement of the lipophilicity. Ideally, such molecules are amphipathic; part of the molecule needs to be hydrophilic for solubility in water and part of it needs to be lipophilic for cell permeation. Excess lipophilicity can reduce the efficiency of cellular uptake. Lipophilicity can be enhanced by lengthening the alkyl chains and conjugated skeleton[55].

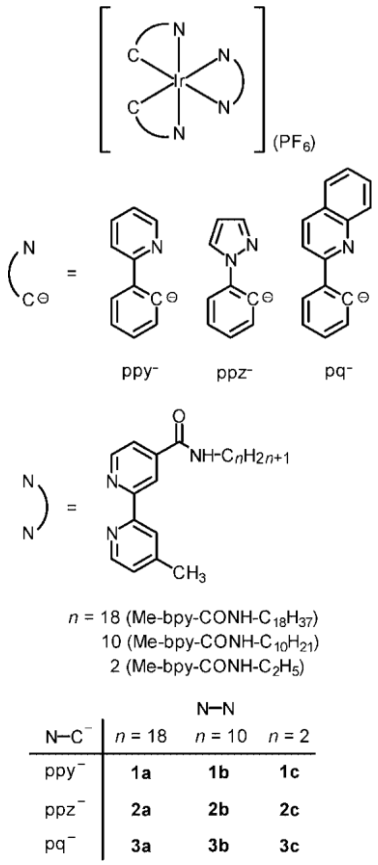

Complex	log $P_{o/w}$
1a	8.79
1b	4.42
1c	0.44
2a	6.52
2b	3.94
2c	-0.34
3a	9.89
3b	5.34
3c	2.01

Figure 1.30 Structures used by Lo & Lau (2008). The table of log P values show a correlation between alkyl chain length and lipophilicity

Figure 1.30 shows that lengthening the alkyl chain in a series of complexes can substantially enhance their lipophilicity, shown by the larger log *P* values of the C18 complexes compared to the C2 complexes.

1.4.3 Cyclometallated platinum(II) complexes in bioimaging

There are very few examples of cyclometallated platinum(II) complexes being used in cell imaging. Most work to date has involved iridium(III) complexes. Platinum(II) complexes are found to have useful properties, and some of them can be used for protein staining. This is of particular importance in biochemistry as common methods such as Bradford, bicinchoninic acid and Lowry assays are hampered by the interfering agents found in the sample preparation buffers. They also need large sample volumes, have limited range and exhibit responses which are affected by the structure of proteins, the amino acid sequence and the isoelectric point[56].

Reports suggest[57] that Pt complexes can be used to act as luminescent probes. When incubated with HeLa cells, it was found that the [Pt(C^N^N)Cl] complex shown in Figure 1.31 had luminescent signals with different intensities localised in different compartments of the HeLa cells. This platinum complex was mostly distributed inside the cytoplasm. Functionalisation of the cyclometalating ligand with pendant moieties of different bioactivities and functionalities can be achieved, and with these pendants, a series of biolabelling and biosensing probes for different sub-cellular targets can be developed[56].

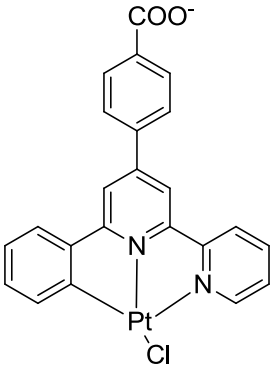

1.76

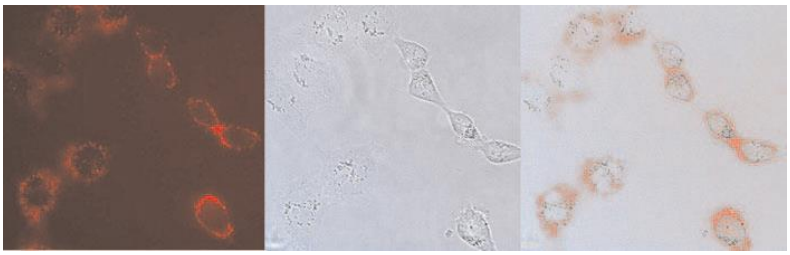

Figure 1.31 Structure of platinum complex and images showing luminescence (left), brightfield (middle) and overlaid (right) HeLa cells with the Pt complex.

Platinum(II) complexes have been shown to be capable of 2-photon excitation[58]. The platinum(II) complex shown in Figure 1.32 has multiphoton luminescence, fast bioaccumulation in live cells and relatively low cytotoxicity.

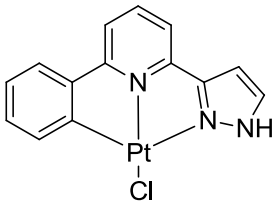

1.77

Figure 1.32 Chemical structure of platinum (II) complex capable of 2-photon excitation

In a later paper, Lam and co-workers added a cationic triphenylphosphonium pendant linked together by a C-5 methylene spacer (**1.78,** Figure 1.33). This Pt(II) complex has an affinity for nuclear or nucleolar proteins within the organelle. They demonstrated that functionalization of the cyclometallating ligand with different moieties can be achieved; thus, a range of compounds can be generated with differing sub-cellular targets[59].

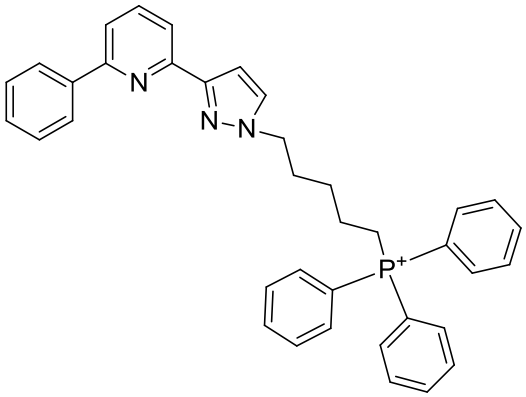

1.78

Figure 1.33 Cationic triphenylphosphonium pendant linked together by a C-5 methylene spacer

1.4.4 Cyclometallated iridium(III) complexes in bioimaging

There are many examples of cyclometallated iridium(III) complexes exhibiting intense and long-lived emission in the visible region. This enables them to function as luminescent sensors[60]. For example Huang and co-workers reported on the synthesis of an iridium(III) complex that can be used as a sensor for homocysteine[61]. It's thought that the aldehyde group of the iridium (III) complex reacts with the amino group of the homocysteine (Figure 1.34). When homocysteine is added to the complex, a colour change from orange to yellow is observed. The emission colour also changes from deep red to green. This property is unique to homocysteine over other amino acids.

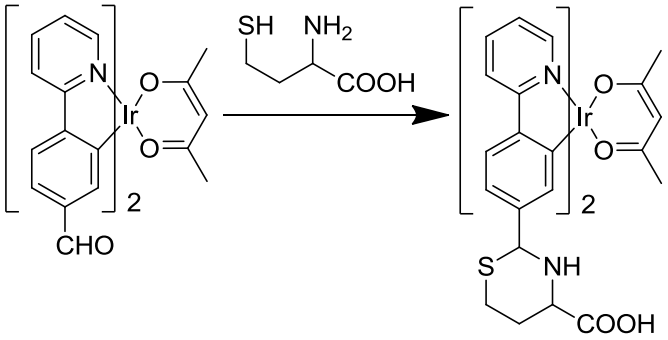

1.79 **1.80**

Figure 1.34 Possible reaction of the iridium (III) complex with homocysteine

Complexes of the general formula $[Ir(ppy_2(N\hat{}N)]^+$ are attractive for cell imaging purposes as they are monocationic, which assists with membrane potential-driven uptake[2]. One of the first reports of iridium complexes in cell imaging came from Yu and co-workers. They demonstrated that fluorinated cyclometallates (Figure 1.35) were efficiently taken up by HeLa cells and localised in the cytoplasm[62]. HeLa cells are human cervical cancer cells. They were initially taken from a woman named Henrietta Lacks in 1951 and have been continuously cultured in the lab since. There are lots of different strains of HeLa cells now used for furthering research in understanding cancer, HIV/AIDS and cells in general[63].

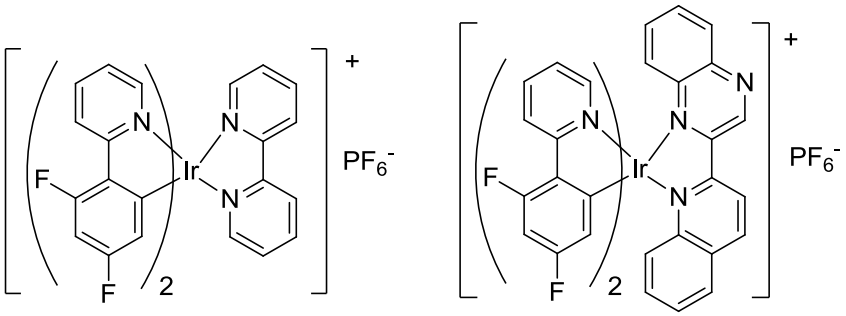

1.81 **1.82**

Figure 1.35 Chemical structures of iridium(II) complexes reported by Yu and co-workers

Yu and co-workers suggested that the fluorinated units are essential for increased lipophilicity and, therefore, assisting with cellular uptake. However, subsequent studies have suggested that iridium cyclometallates themselves are of high enough lipophilicity to ensure efficient cellular uptake. There tends to be non-specific localisation throughout the cytoplasm[2], but there are some examples of complexes being more localised. Zhang and co-workers reported an iridium complex (Figure 1.36) that has an extended conjugated aromatic system suitable for DNA intercalation. Figure 1.36 shows fluorescence laser-scanning confocal microscopy images of fixed MDCK cells treated successively with fibrillarin antibody, Alexa 633 antirabbit IgG antibody, and **1.83**. It shows nucleolar localisation[64].

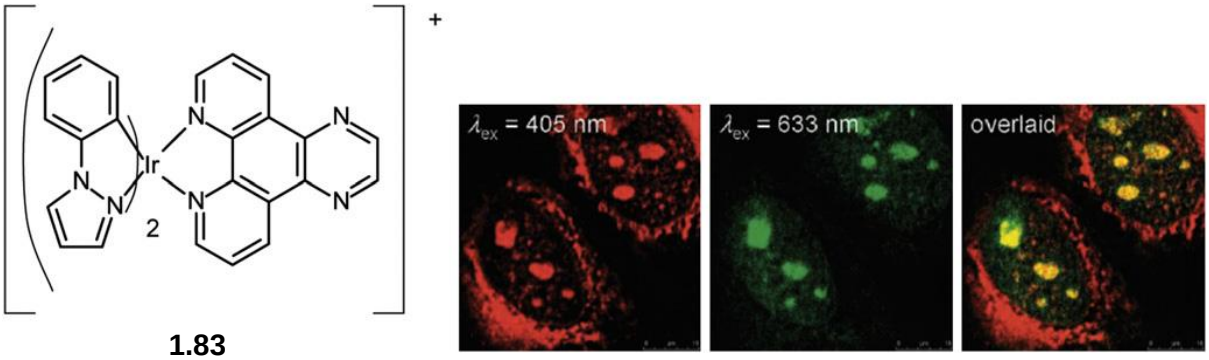

1.83

Figure 1.36 Molecular structure of a DNA-intercalating complex and its cell imaging application

Complexes with a high lipophilicity also have a tendency to be highly cytotoxic. The cytotoxicity of the complex is related to its cellular uptake efficiency if the cytotoxicity originates from binding to organelles. To decrease the cytotoxicity, Lo and co-workers[65] introduced protective groups to the complex to supress non-specific interactions with the extracellular matrix. Their complexes included protective poly(ethylene glycol) (PEG) pendants in the ligands (Figure 1.37) which gave them a very low cytotoxicity, improved their water solubility and gave them a high cellular uptake efficiency.

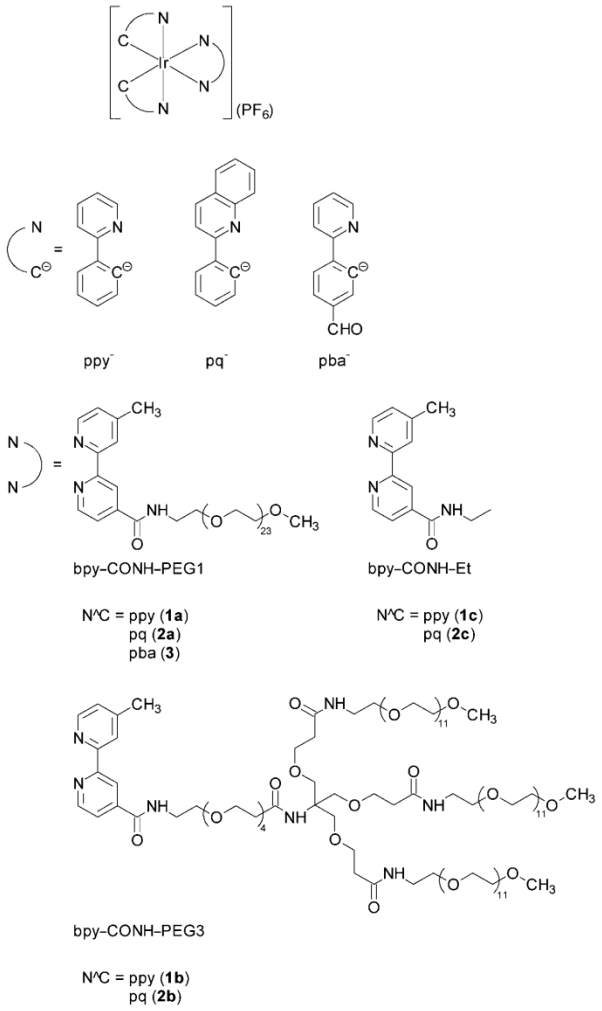

Figure 1.37 Iridium complexes with protective groups

Iridium cyclometallates show long luminescence lifetimes, making them ideal candidates for time-gated experiments. Williams and co-workers have described a pH-responsive probe (Figure 1.38) with a long lifetime that is dependent upon its protonation state. It was used to image a cell that had also been co-stained with the nuclear-selective dye Hoescht 33342. Initially the images were dominated by the Hoescht 33342, however, a short delay of 10 ns showed the stain to be completely excluded from the images. Clear images of the iridium-derived luminescence could be observed[66].

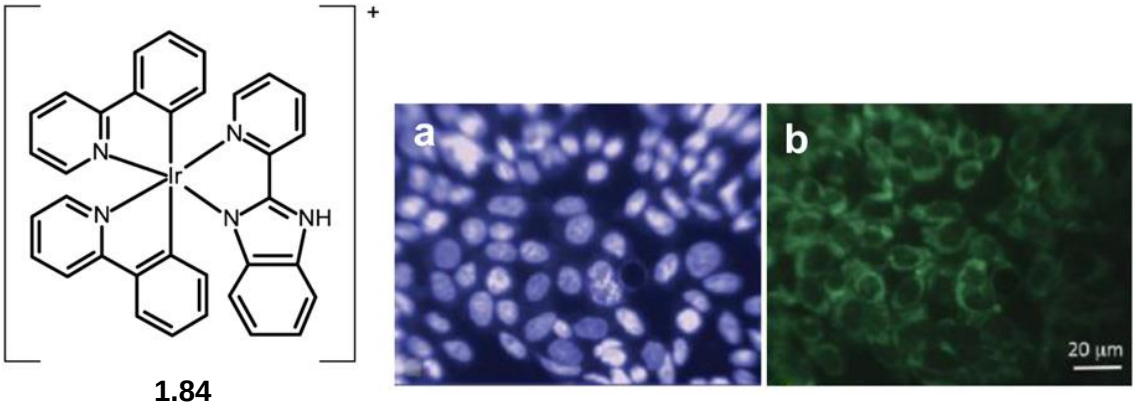

1.84

Figure 1.38 Molecular structure of complex and cell imaging. Image a shows no time-gate. Image b shows 10 ns delay.

The size of metal complexes can affect their cellular uptake properties. Lo and co-workers synthesised a series of dendritic Ir(III) complexes[67] (Figure 1.39). Compared to the monomeric complexes, the dendritic complexes showed lower cellular uptake efficiencies. This is due to their much larger size and higher cationic charge. Cells loaded with the dentritic complexes displayed Golgi staining, as well as localization in the perinuclear regions.

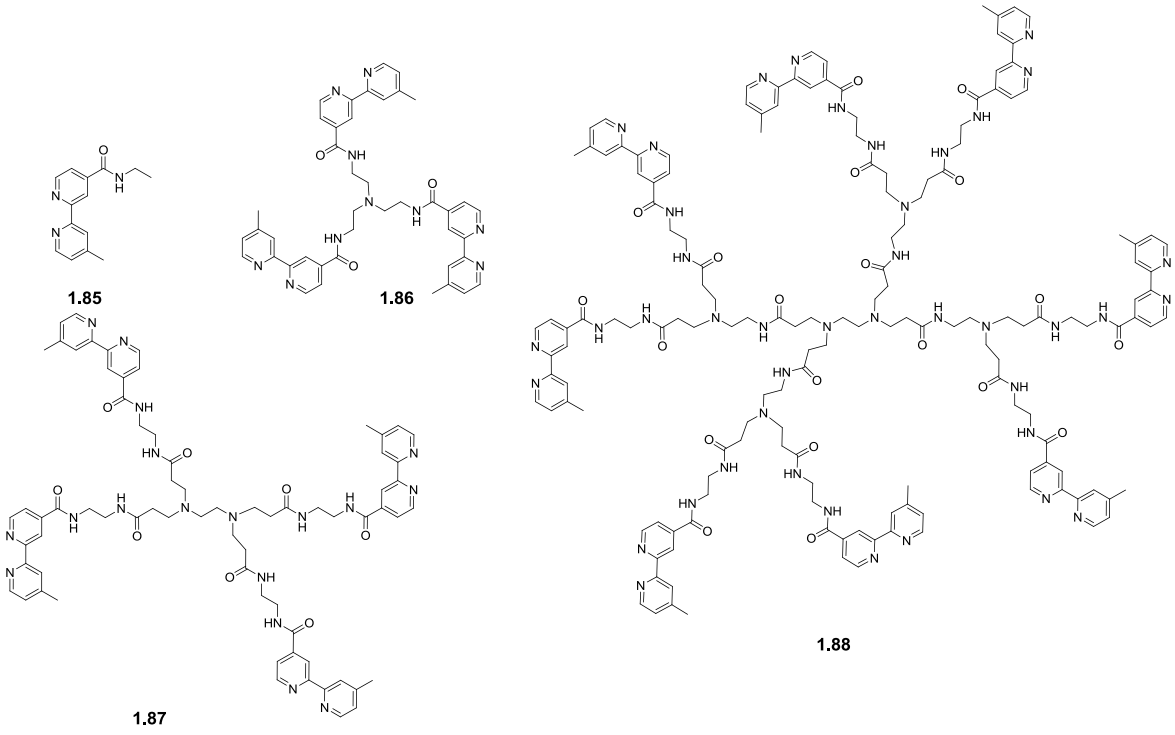

1.85 1.86 1.87 1.88

Figure 1.39 Structures of polypyridine ligands

A recent publication has described metal complexes with a dual function as a luminescence pH-sensor and a pH-dependent photosensitizer. Photosensitizers are used to generate $^1O_2$ which is used as a treatment for various tumours[68].

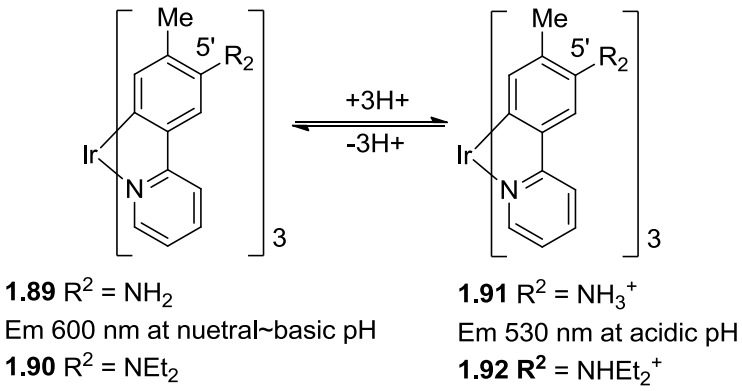

1.89 $R^2 = NH_2$
Em 600 nm at nuetral~basic pH
1.90 $R^2 = NEt_2$

1.91 $R^2 = NH_3^+$
Em 530 nm at acidic pH
1.92 $\mathbf{R^2} = NHEt_2^+$

Figure 1.40 Ir Complexes

Figure 1.40 shows Ir complexes with either NH_2 or Net_2 attached[68]. It was reported that the emission colour in aqueous solution of compound **1.89** is dependent on the pH of the solution[69]. In neutral/basic conditions, compound **1.89** gives a red-coloured emission at ~600 nm, but under acidic conditions (**1.90**) gives a green emission at ~530 nm. Its electron-donating NH_2 group becomes an electron-withdrawing $(NH_3)^+$ group when protonated. Conversely, the introduction of electron-donating groups results in a significant red shift when compared to the parent complex.

1.4.5 Outlook

Heavy-metal complexes are attractive for bioimaging purposes. The complexes show good cell uptake behaviour, allowing them to be tracked using luminescence microscopy. They have highly tuneable physiochemical properties, resulting from easy functionalization of the ligands and the choice of metal ion. Their use as bioimaging probes is still a very new area of research but is starting to attract more attention.

1.5 Organometallic Complexes and Organic Light Emitting Diodes

Organic light emitting diodes (OLEDs) are emerging as the leading technology for the new generation of flat screen display technologies. They have a major advantage over LCDs in that no backlighting is required, which makes them thinner, lighter and more efficient. To enable this technology, highly efficient red (~650-700 nm), green (~500-550 nm) and blue (~450-470 nm) emitting compounds are required. OLEDs generate light by electroluminescence (EL) from excited-state organic molecules. They consist of a multilayered arrangement of thin organic films sandwiched between two electrodes. There are three layers: the electron-transporting layer (ETL), emitting layer (EML) and a hole-transporting layer (HTL). Usually, indium tin-oxide (ITO) is used as the anode and a low work function metal alloy (e.g. Mg, Al, Ca) is used as the cathode. Electrons are injected from the cathode and holes are injected from the anode. The two carriers approach each other in the emitting layer of the OLED (Figure 1.41[70]). Excited states may be formed if both charges arrive on a single molecule or a pair of closely spaced molecules. Their radiative decay produces electroluminescence light (EL). Hence the importance in optimising the luminescent properties of metal complexes[70].

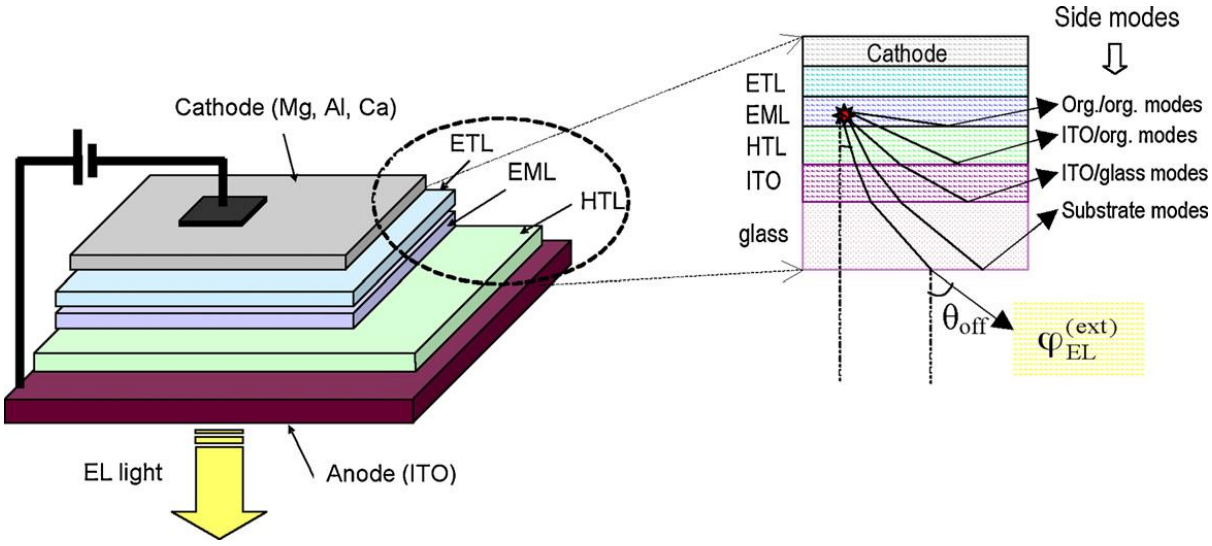

Figure 1.41 Three-layer OLED and the radiative modes generated within the device structure

Platinum(II) and iridium(III) are the metals most studied in this field as they have high spin-orbit coupling constants but can form discrete, kinetically inert, charge-neutral coordination complexes with aromatic ligands. Studies have shown that through ligand design the excited state energies and, therefore, colour can be controlled[71]. Colour tuning is important as the manufacture of a full colour display requires the use of emitters with all three primary colours[29]. There is also a great demand that they give a bright colour, such as orange-red or light blue, for multiple colour display purposes[11].

When red phosphorescent materials are used in OLEDs, then triplet-triplet annihilation almost always occurs. A way to avoid this is by using a host-guest doped emitter system. Doped OLEDs are more difficult to adapt to practical applications than non-doped OLEDs. It is, therefore, desirable to design non-doped compounds with high brightness and efficiency[72].

There is still a lot more work to be done to make OLED's a commercial reality. There are many challenges to overcome, such as developing a synthesis that can be used for low-cost manufacturing.

Chapter 2: Highly luminescent dinuclear platinum(II) complexes incorporating bis-cyclometallating pyrazine-based ligands

2 Highly luminescent dinuclear platinum(II) complexes incorporating bis-cyclometallating pyrazine-based ligands

The aim of this part of the project was to look at the role of the bridging ligand in determining the photophysical properties of diplatinum(II) complexes. In order to achieve this goal, a series of mono and dinuclear platinum(II) complexes incorporating a variety of ligands have been prepared and their photophysical properties investigated.

2.1 Synthesis

The complexes consist of a potentially bridging cyclometallating ligand coordinated to one or two Pt(II) atoms. The metals are coordinated to the same heterocycle (diazine) to give a rigid structure. 1,3-Diketonates are used as auxiliary ligands to give an overall neutral molecule. The synthesis of these complexes is similar to one reported for monometallic complexes of phenylpyridine[8,73]. In the first step, a dichloro-bridged derivative is prepared by reacting the ligand with potassium tetrachloroplatinate. In all cases these dichloro-bridged derivatives are highly insoluble compounds and were not characterised. In the second step the auxiliary ligand is introduced.

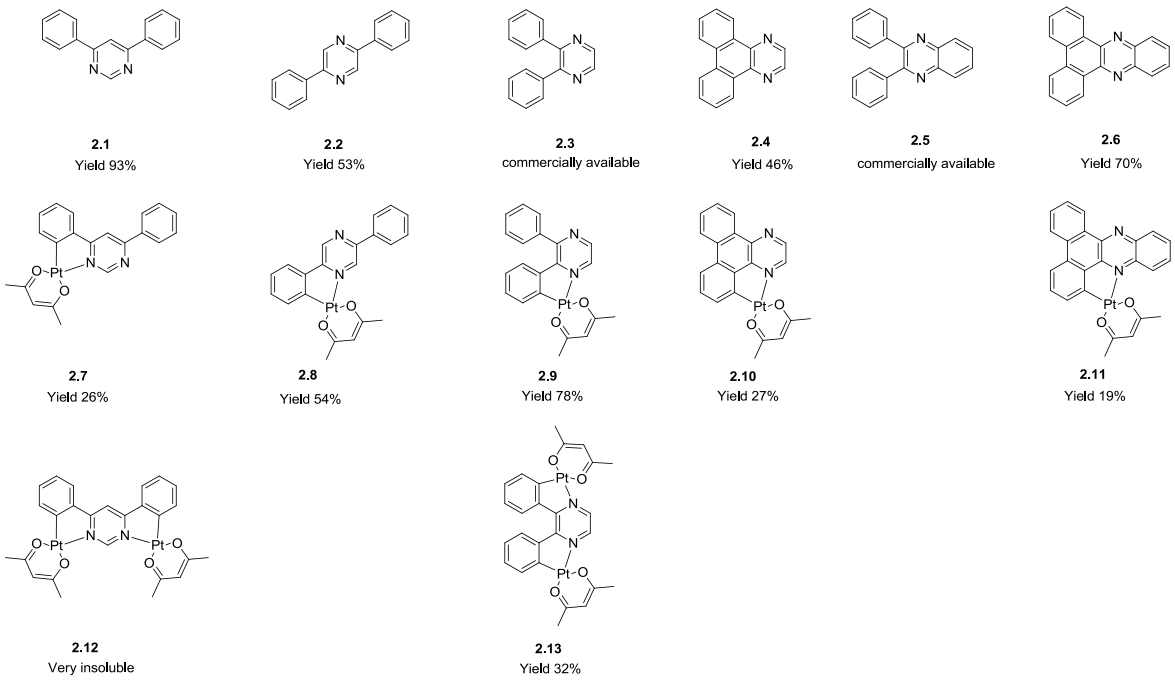

Figure 2.1 Structures of the proligands and corresponding mono- and di-nuclear platinum(II) complexes

Attempts to synthesise the series using acetylacetonate (acac) as the auxiliary ligand were initially investigated (Figure 2.1), but problems with solubility meant that synthesis of the whole series, particularly with **2.5** and **2.6**, and also of the di-nuclear complexes was difficult. Of the di-nuclear complexes, only **2.12** and **2.13** were successfully synthesised but **2.12** was very insoluble. Given the difficulties, a switch was made to dipivaloylmethane (dpm). Dpm allows the complexes to retain good solubility without the need for *tert*-butyl groups in the cyclometallating ligands. Figure 2.2 shows the series of Pt(II) complexes successfully synthesised using dpm as the auxiliary ligand.

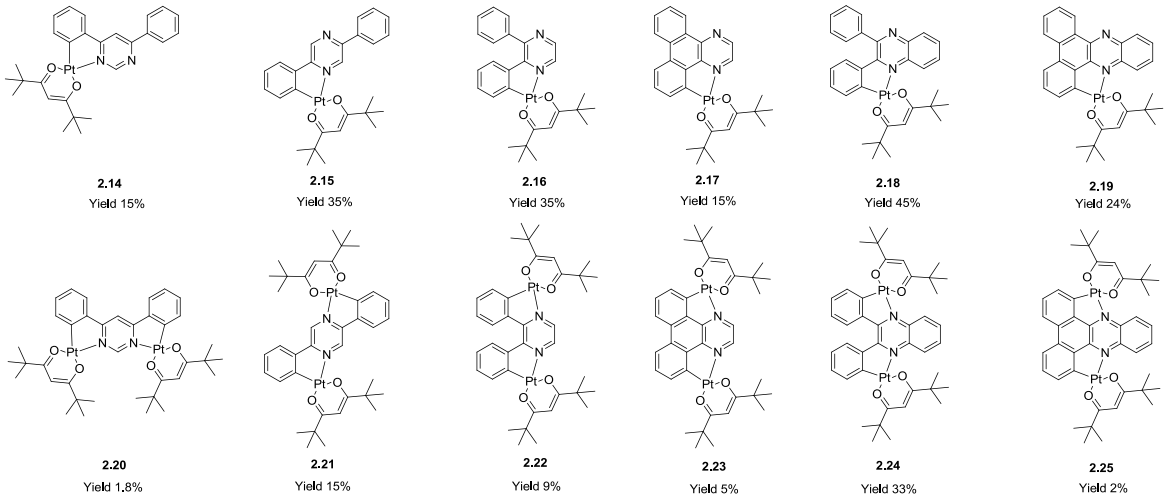

Figure 2.2 Structures of the mono-nuclear platinum(II) complexes and dinuclear platinum(II) complexes

2.1.1 Proligand Synthesis

Pro-ligand **2.1** is derived from 4,6-diphenylpyrimidine. It was used in order to provide a comparison to work published previously[43], which reports on the synthesis of mono- and di-Pt(II) complexes containing *tert*-butyl groups on the phenyl moieties of the ligand. The remaining ligands (**2.2-2.6**) are derived from a diphenylpyrazine core. They are all cyclometallated either once or twice. The compounds based on **2.1**, **2.2** and **2.3** are all isomers of each other so comparisons can be made on the influence of changing from pyrimidine to pyrazine (**2.1** to **2.2** or **2.3**) and also of changes in the position of the substituents in the pyrazine ring. In **2.2** the phenyl rings are at the 2,5 positions and in **2.3** at the 2,3 positions. Increased conjugation can be investigated through **2.3-2.6** as additional C-C bonds are introduced and the pyrazine is replaced by quinoxaline.

2,3-Diphenylpyrazine (**2.3**) and 2,3-diphenylquinoxaline (**2.5**) are commercially available, and so were not synthesised. **2.1** and **2.2** (Scheme 2.1) were synthesised by Suzuki coupling using commercially available 4,6-dichloropyrimidine or 2,5-dibromopyrazine (**2.26**) and phenylboronic acid (**2.27**). The reactions were carried out by stirring at 95°C the deairated mixture of 1 equivalent of 4,6-dichloropyrimidine or 2,5-dibromopyrazine, 2.6 equivalents of phenylboronic acid, 5 equivalents of 2M aqueous K_2CO_3, 6 mol% of tetrakis(triphenylphosphine) palladium(0) as a catalyst, and 1,4-dioxane as a solvent.

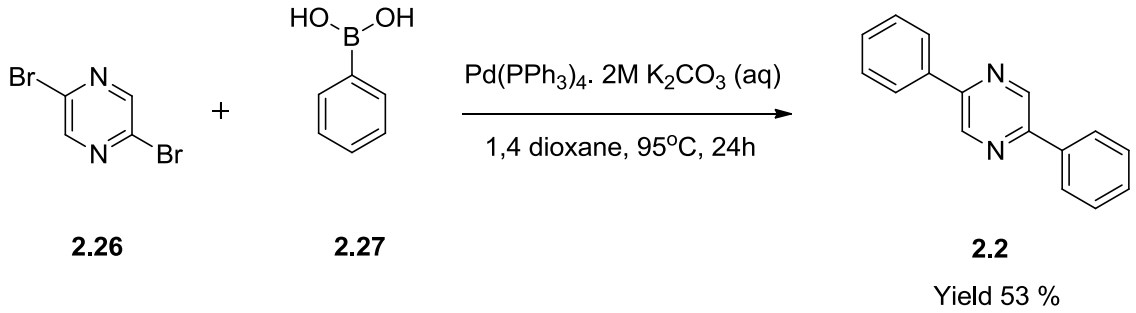

2.26 **2.27** **2.2**

Yield 53 %

Scheme 2.1 Synthesis of 2.2 using the Suzuki cross-coupling reaction

2.4 (Scheme 2.2) and **2.6** were synthesised by following literature procedures[74,75]. Conditions for the condensation reactions included refluxing 1 equivalent of 9,10-phenanthenequinone (**2.28**) and ethylenediamine (**2.29**) (1.3 eq.) or *o*-phenylenediamine (1 eq.) in ethanol, followed by the addition of an acid and further reflux under nitrogen.

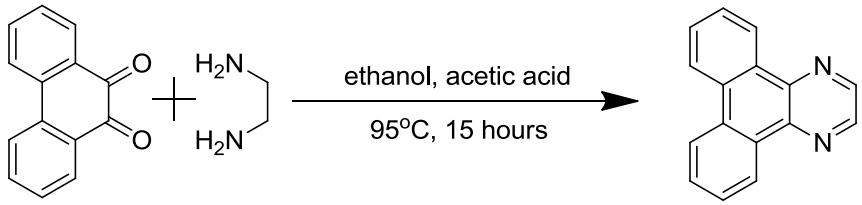

2.28 **2.29** **2.4**

Yield 46 %

Scheme 2.2 Synthesis of 2.4 by a condensation reaction

2.1.2 Platinum(II) Complex Synthesis

The monometallic Pt(II) complexes with acac as the auxiliary ligand (**2.7-2.11**), were obtained by heating at reflux a mixture of the proligand and one equivalent of K_2PtCl_4 in acetic acid for up to 2 days. The resulting dichloro-bridged intermediates were then reacted with sodium acetylacetonate to give, after purification by column chromatography, the mono-platinum complexes. The synthesis of complex **2.9** is given in Scheme 2.3.

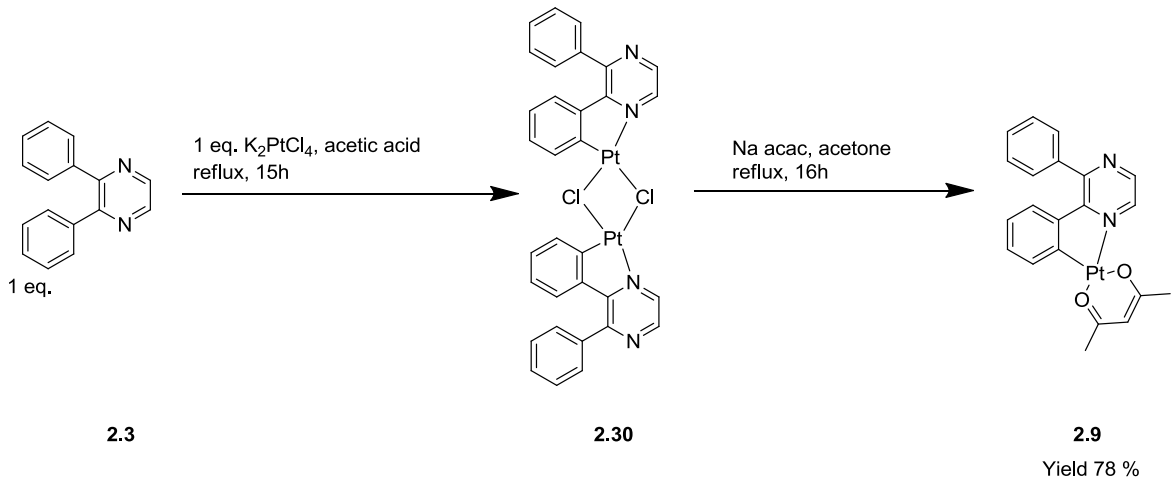

Scheme 2.3 Synthesis of complex 2.9

The monometallic Pt(II) complexes with dpm as the auxiliary ligand, were obtained by heating at reflux a mixture of the proligand and one equivalent of K_2PtCl_4 in acetic acid for up to 3 days. The resulting dichloro-bridged intermediates were then reacted with dipivaloylmethane in the presence of base to give, after purification by column chromatography, the mono-platinum complexes in a low to moderate yield. The formation of a small amount of the corresponding di-platinum complex was also observed in each case. The synthesis of complex **2.15** is shown in Scheme 2.4.

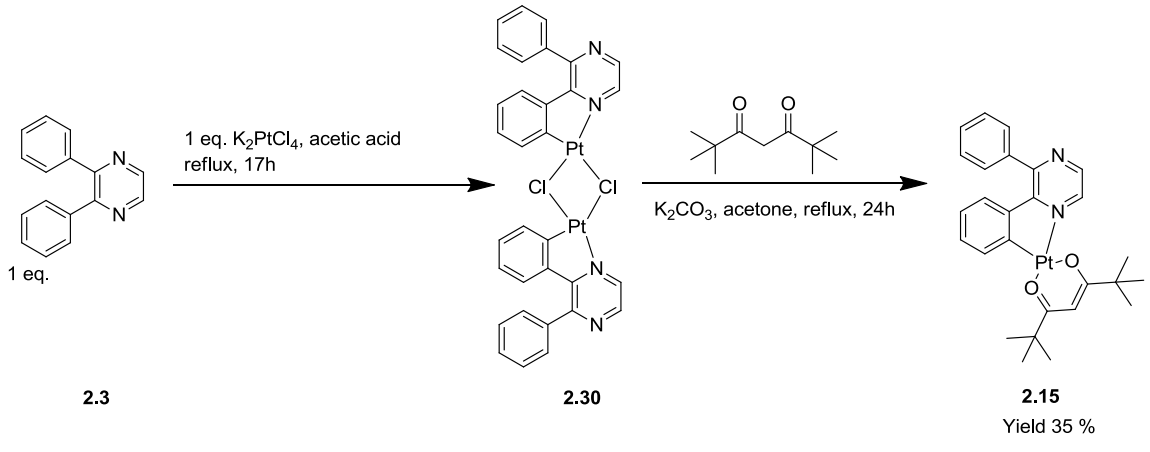

Scheme 2.4 Synthesis of complex 2.15

The dinuclear platinum(II) complexes were synthesised either by reaction of the mono-Pt complex with one equivalent of K_2PtCl_4 or by reacting the proligand with two equivalents of K_2PtCl_4. Under these conditions, it was found that, although the dinuclear complex was the main product, the corresponding mono-platinum complex was still present in the mixture. In general, it was more convenient to prepare the two complexes together in a 'one pot' synthesis by reaction of 1 equivalent of the proligand with 2 equivalents of K_2PtCl_4 (Scheme 2.5).

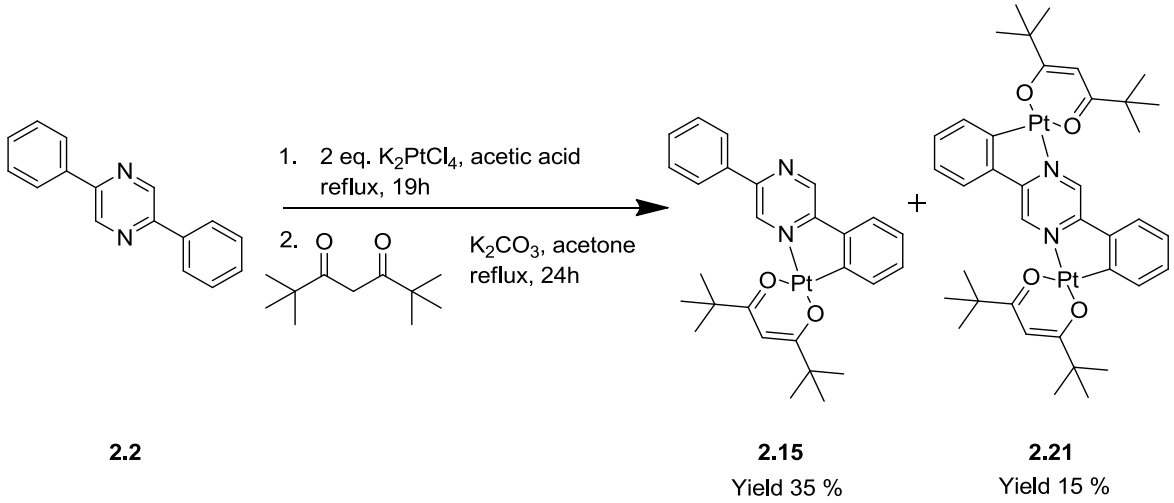

Scheme 2.5 One pot synthesis of 2.15 and 2.21

After introduction of the dpm ancillary ligand under conventional conditions, the mono- and dinuclear platinum complexes are readily separated by column chromatography (typically on silica gel eluting with dichloromethane) to give both products in one procedure.

2.1.2.1 Yields

The yields of the platinum complexes are low. For the mono-Pt dpm complexes, yields were found to be ~15-45% and the di-Pt dpm complexes yields at ~1-33%. An alternative synthesis was tried using **2.1** with acac as the auxiliary ligand. The phase transfer synthesis was carried out by adding potassium tetrachloroplatinate to a solution of tetrabutylammonium bromide (**2.31**) in DCM. This was added to a solution of **2.1** in ethoxyethanol and heated at 100°C. The solution was purged with nitrogen to remove the DCM and then left stirring overnight. The precipitate was then filtered off and treated with acac in the usual way to give **2.7** (Scheme 2.6).

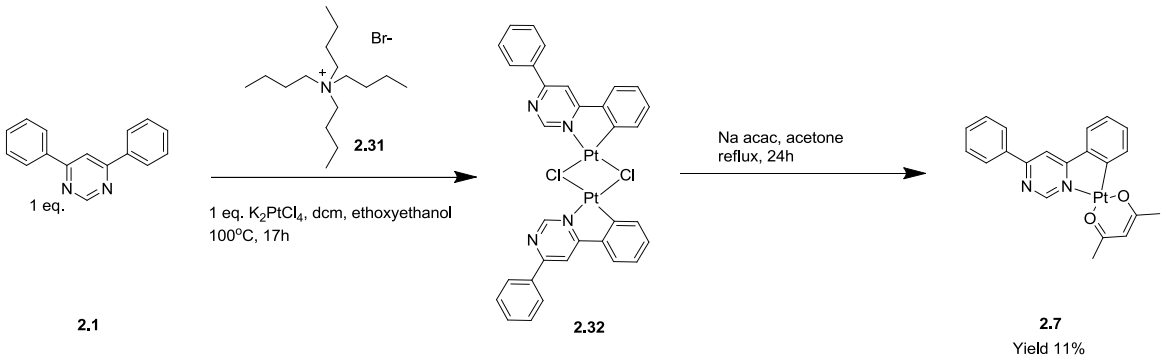

Scheme 2.6 Synthesis of 2.7 by phase transfer

Complex **2.7** has also been synthesised in the usual way with acac as the auxiliary ligand. The yield was 26%. Using the alternative phase transfer method gave a lower yield of 11%, so was not investigated further. It is unclear as to the reason why the yields are so poor. However, the first stage of the synthesis gives a yield of 90% for the dimer (or 43% using the alternative synthesis) so it seems that a lot of material is lost whilst attaching the auxiliary ligand.

2.1.2.2 Alternative synthesis

As mentioned previously, initial attempts at synthesis of the compounds were made using acac as the auxiliary ligand. This proved difficult as the products turned out to be black insoluble compounds, making purification very difficult. Several attempts were made to synthesise the di-Pt complexes with acac but with no success. Firstly, a change of solvent from acetone to ethoxyethanol was made in order to be able to raise the reaction temperature; this resulted in the same black insoluble compound. Purification by column chromatography only recovered the starting material, when either the ligand had been reacted with 2 equivalents of platinum or when the mono-Pt complex reacted with 1 equivalent of platinum, and a lot of the black material was left stuck on the column. Attempts were also made to break the di-Cl bridged complex by refluxing in dimethylsulfoxide before then going on to add the acac to the complex. This method of synthesis has been used successfully[43] for **2.1**. However, through the ^{1}H-NMR spectra of the crude product it did look as if a mixture of mono-Pt and di-Pt complexes were present. The Di-Pt complex was too insoluble to be purified. Once again, purification by column chromatography just recovered the mono-Pt complex. A switch in the acac salt was also made from sodium acetylacetonate to lithium acetylacetonate (purchased from Sigma Aldrich). A synthesis was carried out to make complex **2.7** as this had already been successfully synthesised using Na (acac) and so the same conditions were followed. The results were very poor with a very messy ^{1}H-NMR spectrum. Further purification would have been needed to try to recover the product which was not needed when using Na (acac). It was decided not to pursue this route any further as it was then thought that using dpm would be a better option to improve on the solubility of the complexes.

A recent paper[73] describes a one-pot synthesis of cyclometallated platinum(II) β-diketonates carried out at ambient temperature. The starting material $[PtMe_2(SMe_2)]_2$ was stirred at room temperature in THF along with 2 equivalents of the proligand (**2.33**) for 1 hour. CF_3SO_3H was then added followed by 2 equivalents of Na acac and left stirring at room temp for 1.5 hours to give the pure product (**2.34**) in 87% yield (Scheme 2.7[73]).

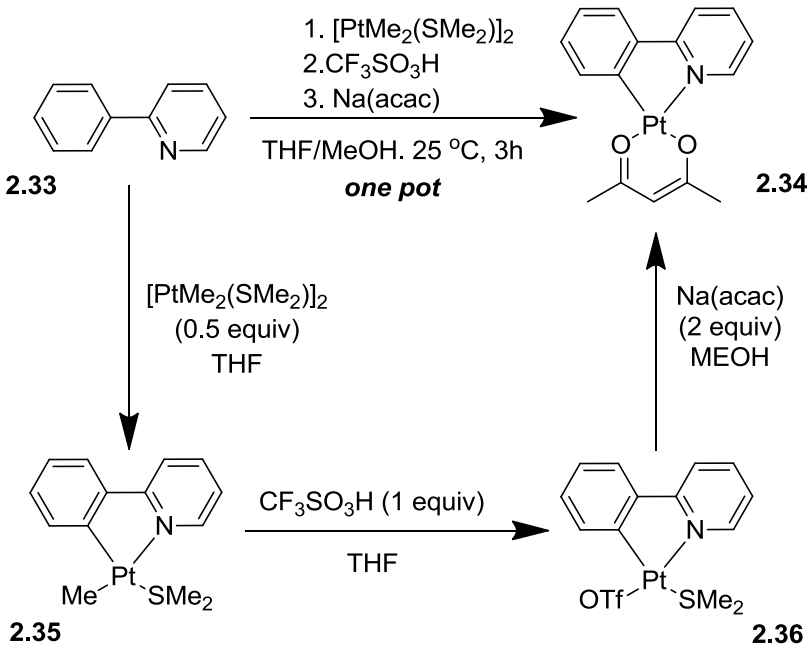

Scheme 2.7 One pot, room temperature synthesis of cyclometallated Pt(II) β-diketonates

The one-pot synthesis was first attempted with **2.3** using the same conditions as shown in Scheme 2.7 but using TFA rather than CF_3SO_3H. The ^{1}H-NMR spectrum of the crude product, showed that the reaction had not gone to completion. More acac was added along with K_2CO_3 and acetone and the mixture was refluxed for 4 hours. This time the ^{1}H-NMR spectrum showed that the reaction had gone to completion and that there was a mixture of mono- and di-Pt complexes. Similar reactions were attempted with ligands **2.1** and **2.4** – **2.6**, but again these were unsuccessful at room temperature. Most of these reactions gave an oily black solid that was insoluble in DCM and so could not be purified.

2.2 The role of the auxiliary ligand

As mentioned previously, initial, attempts at synthesising the series of complexes were made using acac as the auxiliary ligand. Problems with solubility led us to a switch to using dpm. The introduction of the *tert*-butyl groups gave a much improved solubility and, hence, the complete series could be synthesised.

It has been reported that in general, the auxiliary ligand does not significantly affect the photophysical properties of a complex [Pt(C^N)(X^Y)][76,6]. In order to check that the same could be said of these complexes, the UV spectra were compared using **2.3**. Both the acac and dpm complexes have been synthesised using **2.3** (Scheme 2.8).

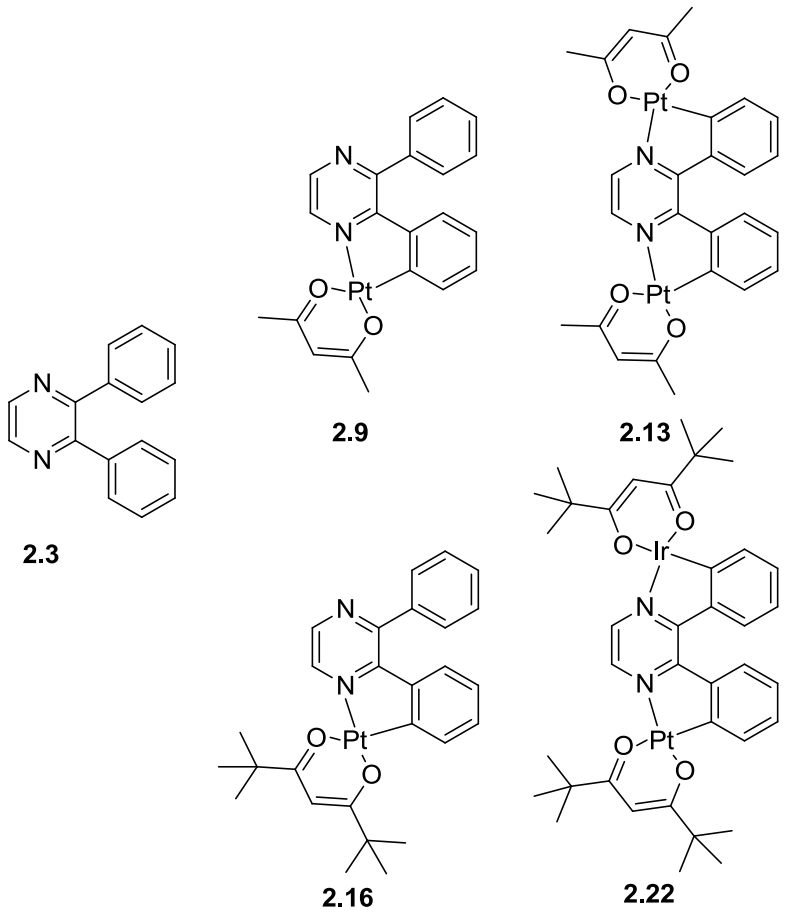

Scheme 2.8 2,3-diphenylpyrazine(2.3) and its mono- and di-Pt derivatives with acac and dpm auxiliary ligand

Chart 2.1 shows the UV-vis absorption spectra for **2.9** and **2.16**. Both complexes absorb at a very similar wavelength (392 nm for acac and 398 nm for dpm). Chart 2.2 also shows very little difference in absorption for the di-Pt complexes. **2.22** is slightly more red-shifted than **2.13** (443 nm for acac and 450 nm for dpm). The solubility of the complex is certainly improved for the DPM auxiliary ligand.

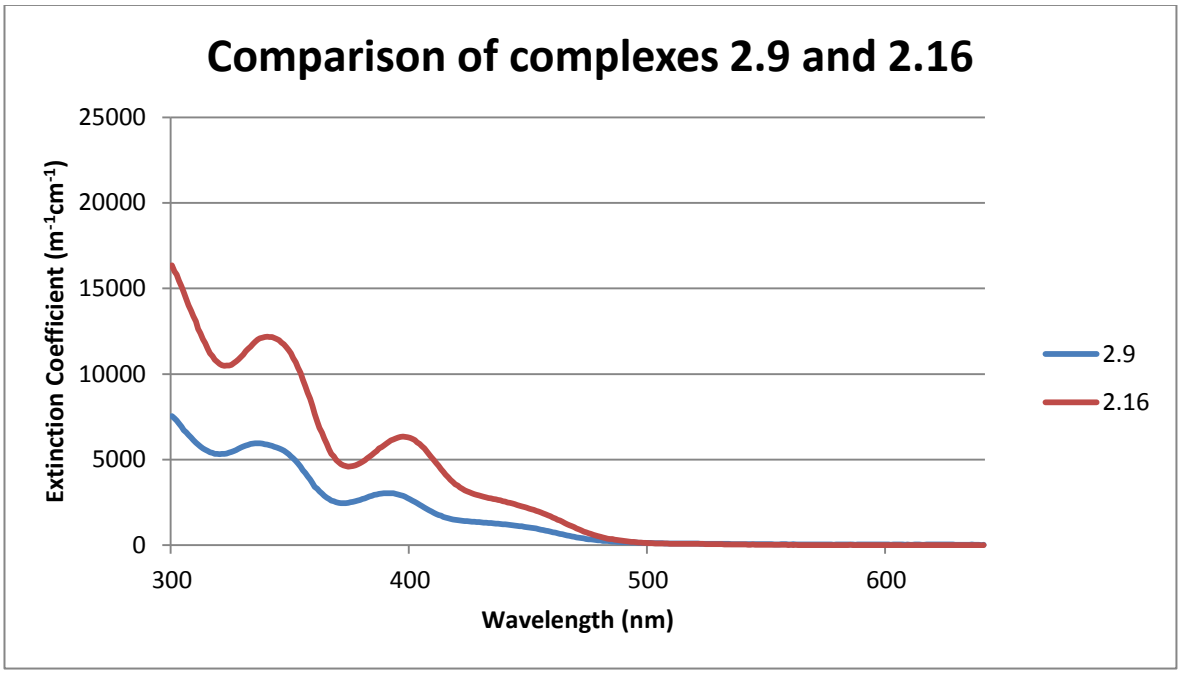

Chart 2.1 UV spectra for mono-Pt

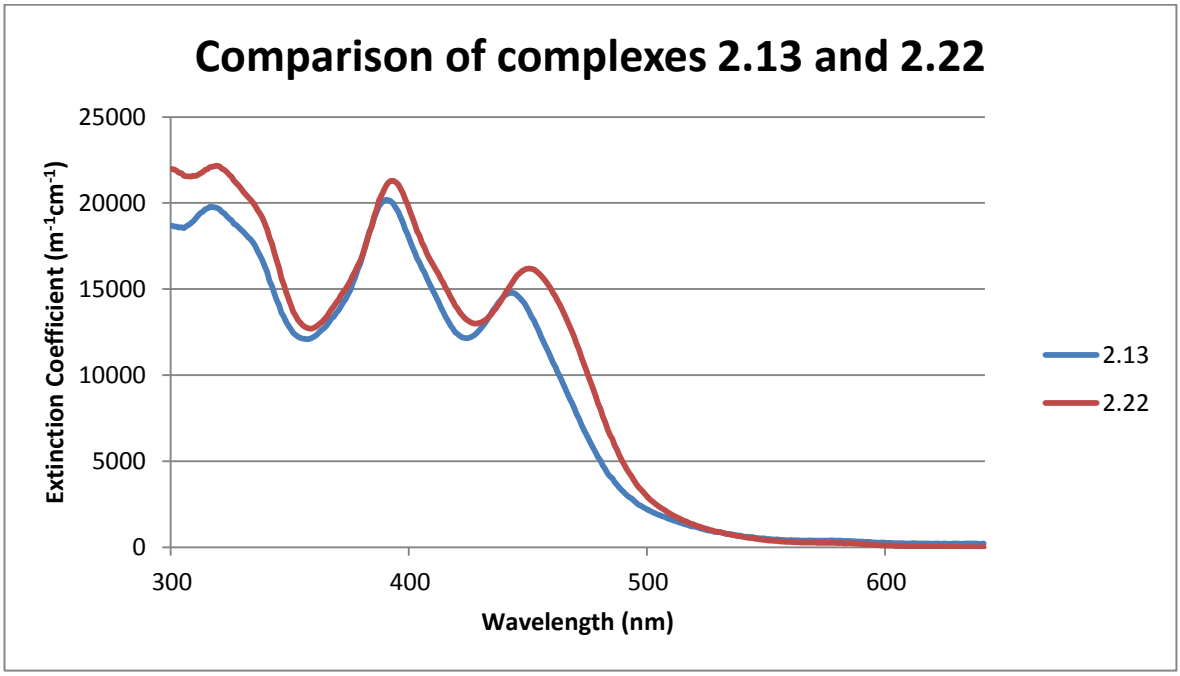

Chart 2.2 UV spectra for di-Pt

2.3 Absorption Spectroscopy

2.3.1 Acetylacetone (acac)

Complexes **2.1**, **2.2**, **2.3**, **2.4** and **2.6** were synthesised as mono-Pt complexes with acac co-ligands, and their absorption data is shown in Table 2.1 and the spectra shown in Chart 2.3. Also **2.12** and **2.13** were synthesised but **2.12** was too insoluble to get UV measurements. Chart 2.4 shows the spectra comparing the mono- and di-platinum complexes for **2.3** with acac as the auxiliary ligand. Comparisons can be made with the complexes of dpm as the auxiliary ligand (see Table 2.2 later in this chapter) and the wavelengths are very similar for both acac and dpm.

Table 2.1 UV-visible absorption data for the complexes with acac as the auxiliary ligand

Complex	λ_{max} / nm (ε / $M^{-1}cm^{-1}$)
2.7	301 (8476), 337 (8785), 392 (4490)
2.8	336 (11370), 359 (9615), 393 (4014), 434 (3364)
2.9	337 (8785), 392 (4490), 440 (1808)
2.13	317 (22833), 390 (23414), 443 (17114), 573 (565)
2.10	340 (9152), 402 (5848), 459 (1625)
2.11	280 (41231), 400 (11431), 454 (8062), 510 (4971)

The absorptions are progressively more red-shifted through the series of ligands, with **2.11** being the most red-shifted. The formation of the C-C bond is likely to give a planar structure for **2.10** but not for **2.9**. Also there could be some steric crowding of C-H bonds within **2.9**, meaning less of a red-shift than **2.10**.

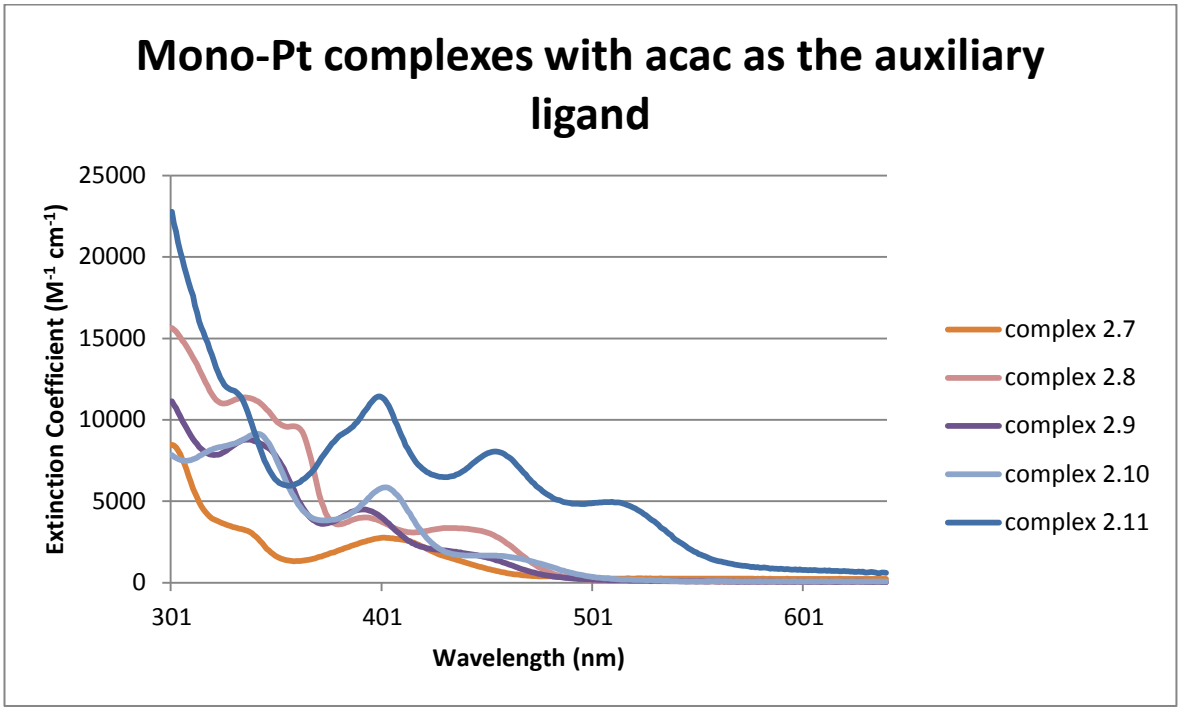

Chart 2.3 UV data for complexes 2.7, 2.8, 2.9, 2.10 and 2.11

As mentioned previously, the only di-Pt complex with an acac co-ligand to be successfully synthesised and characterised by UV was **2.13**. Chart 2.4 shows the UV data for both **2.9** and **2.13**. The di-Pt complex (573 nm) is much more red shifted compared to the mono-Pt complex (440 nm). Returning to the mono-Pt complexes, **2.11** has a much higher extinction coefficient compared to the others and is also the most red-shifted. This is also true of the dpm complexes which will be discussed later on in this chapter. Both the acac and the dpm complexes gave very similar UV results with **2.9** giving an absorption at 449 nm and **2.13** giving an absorption at 572 nm.

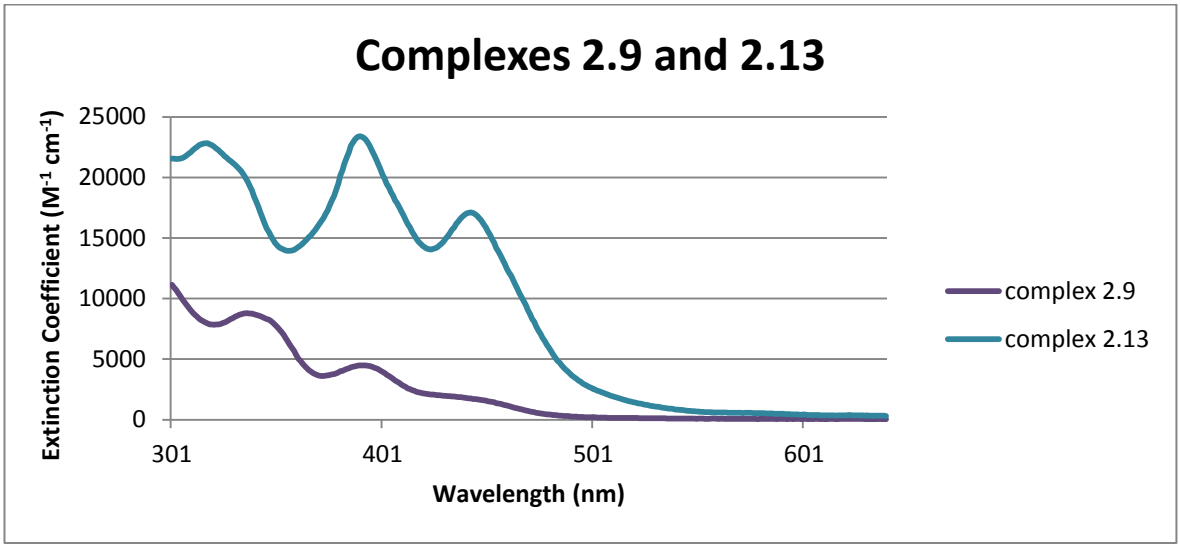

Chart 2.4 UV data for complexes 2.9 and 2.13

2.3.2 Dipivaloylmethane (dpm)

The absorption data for all 12 dpm complexes are compiled in Table 2.2, and spectra are shown in Chart 2.5 and Chart 2.6. The measurements for the dpm complexes were carried out by Dr J.A.G. Williams of Durham University. The mononuclear complexes display absorption spectra that are quite typical of platinum(II) complexes with N^C-cyclometallating, aryl-heterocyclic ligands, such as Pt(ppy)(acac) and related derivatives. There are intense bands in the UV region, < 350 nm, with extinction coefficients ε in the range 10 000 – 30 000 $M^{-1}cm^{-1}$, corresponding to $^{1}\pi$–π^* transitions associated with the ligands. Somewhat weaker bands, ε < 10 000 $M^{-1}cm^{-1}$, in the visible region (390 – 500 nm) have no counterparts in the spectra of the free proligands. Based on the conclusions of previous studies[8,77,78,79], and on the results of time-dependent density functional theory calculations for the dpm series of complexes(discussed later in this chapter), at least some of these bands can be attributed to charge-transfer transitions from the aryl–metal unit to the heterocyclic ring, reflecting the predominant localisation of the frontier orbitals on these two different parts of the molecule.

The dinuclear complexes **2.20, 2.21** and **2.22** display very different spectra from their corresponding mononuclear analogues **2.14, 2.15** and **2.16**. For the complexes of **2.1** and **2.2**, the set of lower energy bands in the visible region are substantially red-shifted in the dinuclear compared to the mononuclear complexes (lowest-energy band shifts by around 4000 cm^{-1}), and there is a large increase in the extinction coefficients of most of the bands. The visible-region bands in **2.22**, on the other hand, are scarcely shifted compared to **2.16**, although there is again a very large increase in the extinction coefficients. The red-shift in the complexes of **2.20** and **2.21** is likely to be associated with the extension of conjugation that would be expected to accompany the introduction of the second metal ion. In the case of **2.22**, on the other hand, it seems likely that steric crowding of the C–H bonds of the pendent phenyl groups is occurring, which would account for the lack of red shift.

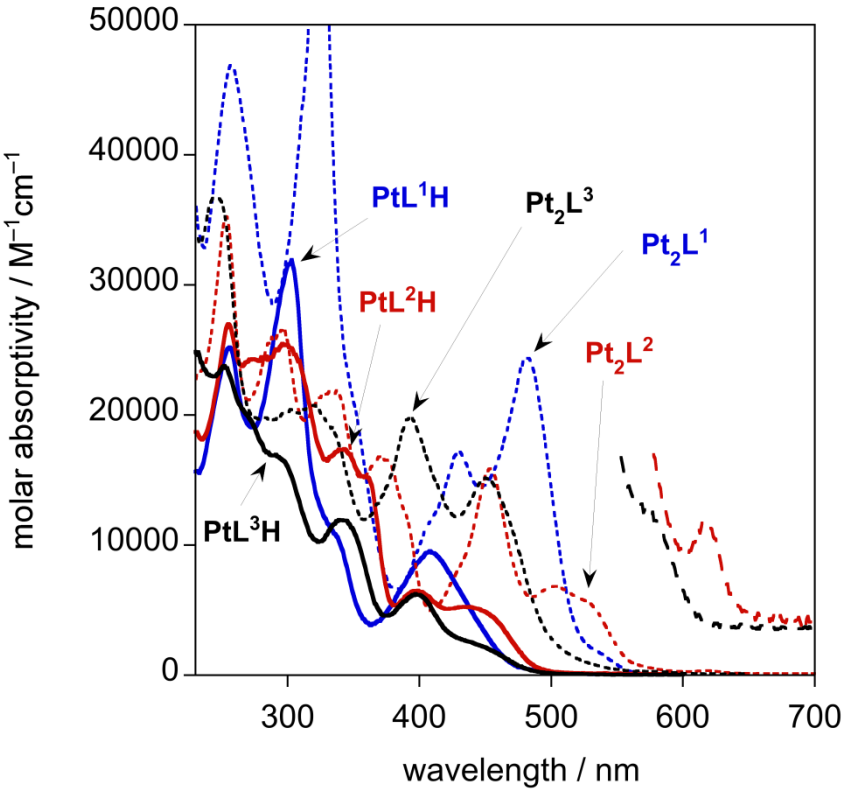

Chart 2.5 UV-visible absorption spectra of 2.14, 2.15 and 2.16 (blue, red, and black solid lines respectively) and of 2.20, 2.21 and 2.22 (blue, red, and black short-dashed lines respectively) in CH_2Cl_2 solution at 298 K. The low-energy region of the spectra of 2.21 and 2.22 is shown on an arbitrarily expanded scale (red and black long-dashed lines respectively).

The absorption spectra of all the other complexes (**2.17, 2.18, 2.19, 2.23, 2.24** and **2.25)** are shown in Chart 2.6, together with those of **2.16** and **2.22** again as a point of

comparison. Considering first the mononuclear complexes, it can be seen that all four display spectra that are quite similar to one another in form, but the visible-region bands move progressively further to the red. The displacement is small on going from **2.16** to **2.17** (~700 cm^{-1}), but nevertheless the trend would be consistent with the planarization of the structure that becomes possible upon fusing the aromatic rings and loss of the sterically unfavourable interaction between the C–H bonds on the two rings mentioned above. A much larger red-shift accompanies the change from the pyrazine unit of **2.16** to the quinoxaline of **2.18** (around 1800 cm^{-1} for the lowest-energy band, and around 2600 cm^{-1} for the next lowest). Again, it is clear that the introduction of the second metal ion leads to a red-shift in the visible region bands, and to a large increase in the molar absorptivity of these bands.

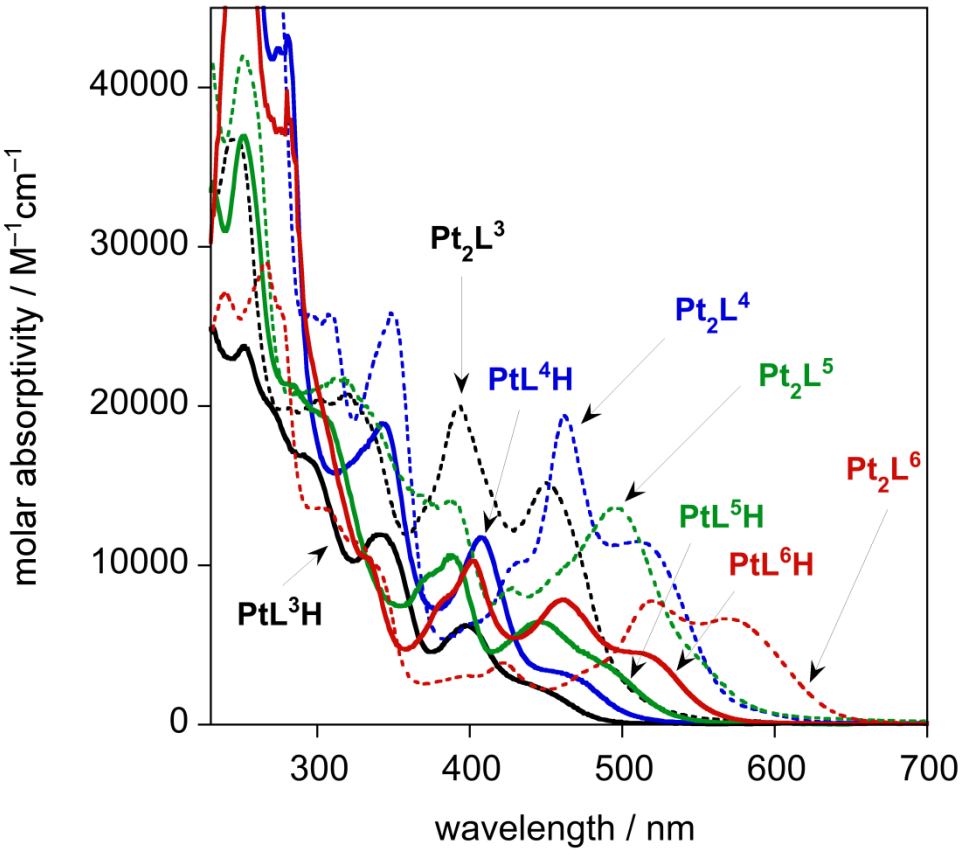

Chart 2.6 UV-visible absorption spectra of 2.16, 2.17, 2.18 and 2.19 (black, blue, green, and red solid lines respectively) and of 2.23, 2.24 and 2.25 (correspondingly coloured dashed lines) in CH_2Cl_2 solution at 298 K.

Table 2.2 UV-visible absorption data for the complexes with dpm as the auxiliary ligand

Complex	λ_{max} / nm (ε / $M^{-1}cm^{-1}$)
2.14	256 (25200), 301 (31600), 338sh (10600), 408 (9550)
2.20	257 (47000), 326 (63200), 430 (17100), 481 (24300), 532sh (1990)
2.15	254 (26800), 299 (25400), 342 (17300), 398 (6430), 435 (5240)
2.21	253 (35300), 296 (26500), 333 (21900), 372 (16600), 453 (15900), 503 (6830), 618 (346)
2.16	252 (23800), 292 (16900), 340 (11900), 398 (6170), 449 (2170)
2.22	245 (36700), 301 (20300), 319 (20700), 390 (19600), 451 (15200), 572 (310)
2.17	251 (66000), 278 (42100), 344 (18900), 407 (11800), 463 (3190)
2.23	258 (59300), 295 (25900), 308 (25700), 350 (25800), 428 (10100), 462 (19400), 509 (11500)
2.18	252 (40000), 294 (20000), 373sh (9380), 388 (10600), 445 (6470), 488sh (3790)
2.24	251 (42000), 313 (21600), 387 (14200), 428 (8610), 496 (1360)
2.19	251 (52300), 282 (38000), 383sh (7870), 401 (10300), 463 (7790), 511 (4520)
2.25	266 (29000), 301sh (13600), 324sh (11500), 396 (3070), 422 (3890), 476sh (3350), 519 (7780), 569 (6690)

2.4 Photoluminescent Properties

All twelve dpm complexes are luminescent in degassed solution at room temperature, most of them intensely so. The emission data for the compounds are compiled in Table 2.3, and the spectra are shown in Chart 2.7 and Chart 2.8. The trends in emission maxima are mostly quite similar to those observed in the absorption spectra. In particular, it may be immediately seen that, for a given ligand, the spectrum of the binuclear complex is significantly red-shifted compared to that of the corresponding mononuclear complex. The shift is in the range 1600 – 1900 cm^{-1} for the five pairs of pyrazine-based complexes (based on the emission maxima), and 1270 cm^{-1} for the pyrimidine pair (**2.14** and **2.20**).

Amongst the three isomeric complexes **2.14 – 2.16**, the pyrimidine complex **2.14** emits at a higher energy (λ_{max} = 520 mm), while the two pyrazine complexes emit in a similar region to one another, with **2.15** displaying a more structured profile. Meanwhile, the trend amongst the four complexes **2.16 – 2.19** is similar to that in absorption, except that **2.18** emits at marginally lower energy than **2.19** – the opposite of the trend in absorption – and its spectrum is markedly broader.

Two instances of a reversal in the relative order of emission energies versus absorption energies are observed amongst the binuclear complexes. Thus, **2.22** emits at significantly lower energy than **2.20**, contrary to the absorption being significantly lower in energy for the latter. The second instance is the pair of complexes **2.24** and **2.25**, where the emission of the former has a slightly longer λ_{max}, despite having an absorption maximum at a higher energy. Excited-state reorganisation at room temperature can be anticipated for **2.24** similar to that proposed for **2.22**, given the expected sterically unfavourable interactions in the ground state. At 77 K, the emission spectra show otherwise similar trends as at room temperature but the spectra become more vibrationally resolved. The observed vibrational spacing is around 1200 – 1400 cm^{-1}, as typically expected for coupling to aromatic ring vibrations.

Table 2.3 Emission data for the dpm complexes in degassed CH_2Cl_2 at 298 K except where stated otherwise

Complex	λ_{max} / nm	Φ_{lum} [(a)]	τ / ns [(b)]	k_Q^{SQ} [(c)] / 10^7 $M^{-1}s^{-1}$	k_r [(d)] / 10^4 s^{-1}	Σk_{nr} [(d)] / 10^4 s^{-1}	k_Q^{O2} [(e)] / 10^8 $M^{-1}s^{-1}$	ΔE^{A-E} [(f)] / cm^{-1}	Emission at 77 K [(g)]	
									λ_{max} / nm	τ / μs
2.14	521	0.25	1600 [460]	87	16	47	7.0	5320	501, 527, 573sh	6.4
2.20	558, 594	0.36	1100 [670]	[(h)]	33	58	2.6	2870	539, 582, 630	4.3
2.15	565, 608	0.30	8900 [840]	71	3.4	7.9	4.9	5290	554, 603, 654	11
2.21	628, 685, 753	0.41	3200 [680]	[(h)]	13	18	5.3	3960	617, 676, 742	3.4
2.16	554, 578	0.43	7700 [850]	210	5.6	7.4	4.8	4220	536, 576, 618	11
2.22	612	0.37	4000 [750]	3.5	9.3	16	4.9	5830	586, 634, 693	6.1
2.17	568	0.15	2600 [510]	270	5.8	33	7.2	3990	528, 566, 615	11
2.23	628	0.20	1800 [650]	27	11	44	4.5	3720	601, 654, 716	7.0
2.18	668	0.14	3700 [700]	15	3.8	23	5.3	5520	625, 677, 747sh	5.7
2.24	749	0.025[(i)]	910 [490]	[(h)]	2.7[(i)]	110	4.3	6810	694, 760	3.5
2.19	639, 686	0.13	3800 [700]	180	3.4	23	5.3	3920	617, 676, 746	1.3
2.25	728, 799	0.027[(i)]	2000 [580]	[(h)]	1.4[(i)]	49	5.6	3840	712, 793	1.5

(a) Measured using $[Ru(bpy)_3]Cl_2$ as the standard. *(b)* Values in air-equilibrated solution in parenthesis. *(c)* Self-quenching rate constant, estimated from a plot of τ^{-1} versus concentration. *(d)* k_r and Σk_{nr} are the radiative and non-radiative decay rate constants, estimated from the quantum yield and lifetime assuming that the emissive state is formed with unitary efficiency. *(e)* Bimolecular rate constant for quenching by O_2, estimated from the luminescence lifetimes in degassed and air-equilibrated solutions, and taking $[O_2]$ = 2.2 mM in CH_2Cl_2 at p = 1 atm air and T = 298 K. *(f)* The difference between the energy of the lowest-energy (singlet) absorption band and the emission band, using the λ_{max} values. *(g)* In diethyl ether / isopentane / ethanol (2:2:1 v/v). *(h)* The change in lifetime with concentration was too small to estimate a self-quenching rate constant, being scarcely larger than the uncertainty on the measurements. *(i)* The quantum yields of these two complexes will be underestimated, owing to a significant part of the emission falling out of the range of detection of our equipment. Radiative rate constants will be underestimated as a result.

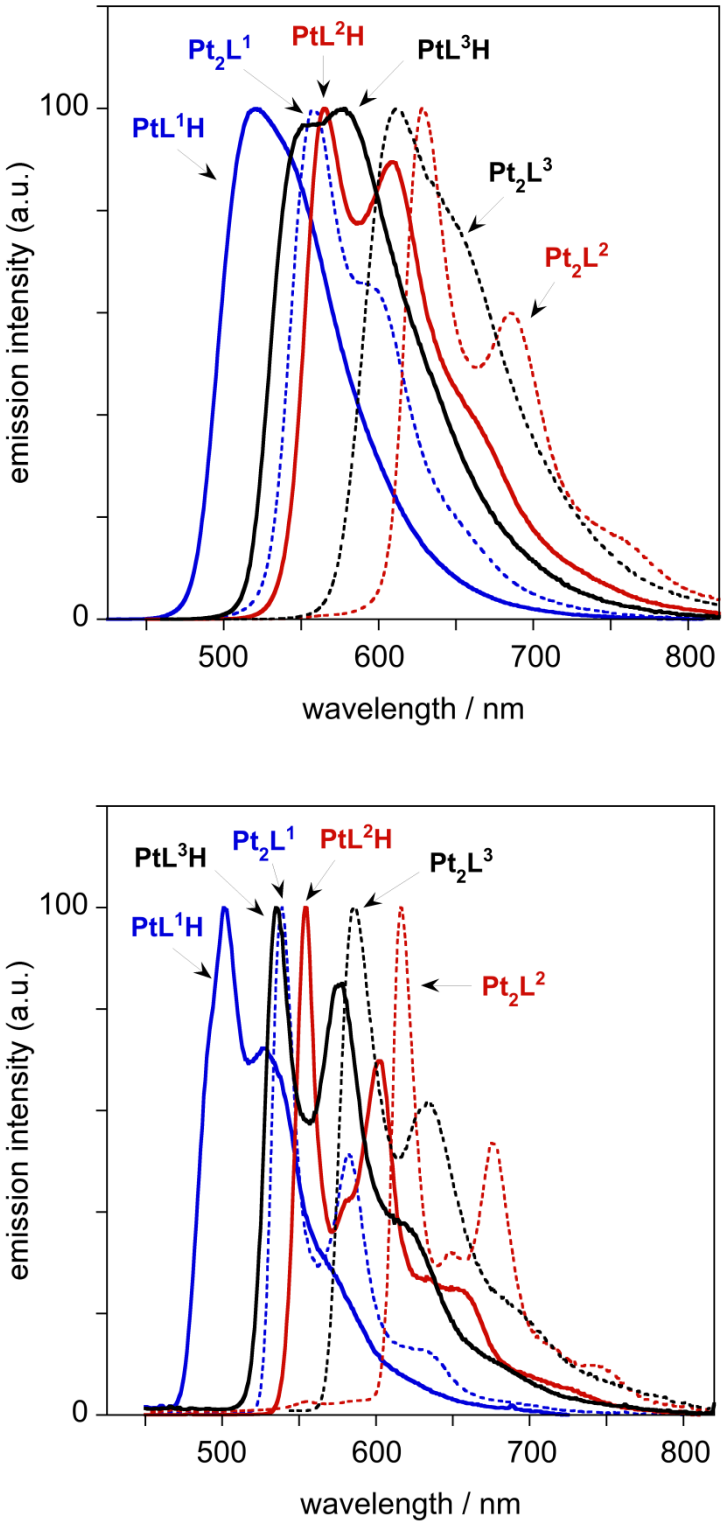

Chart 2.7 Top: Normalized emission spectra of 2.14 – 2.16 (blue, red, and black solid lines respectively, legend as in Figure 2) and of 2.20 – 2.22 (blue, red, and black short-dashed lines respectively) in CH_2Cl_2 solution at 298 K. Bottom: Corresponding spectra in an EPA glass at 77 K (EPA = diethyl ether / isopentane / ethanol, 2:2:1 v/v).

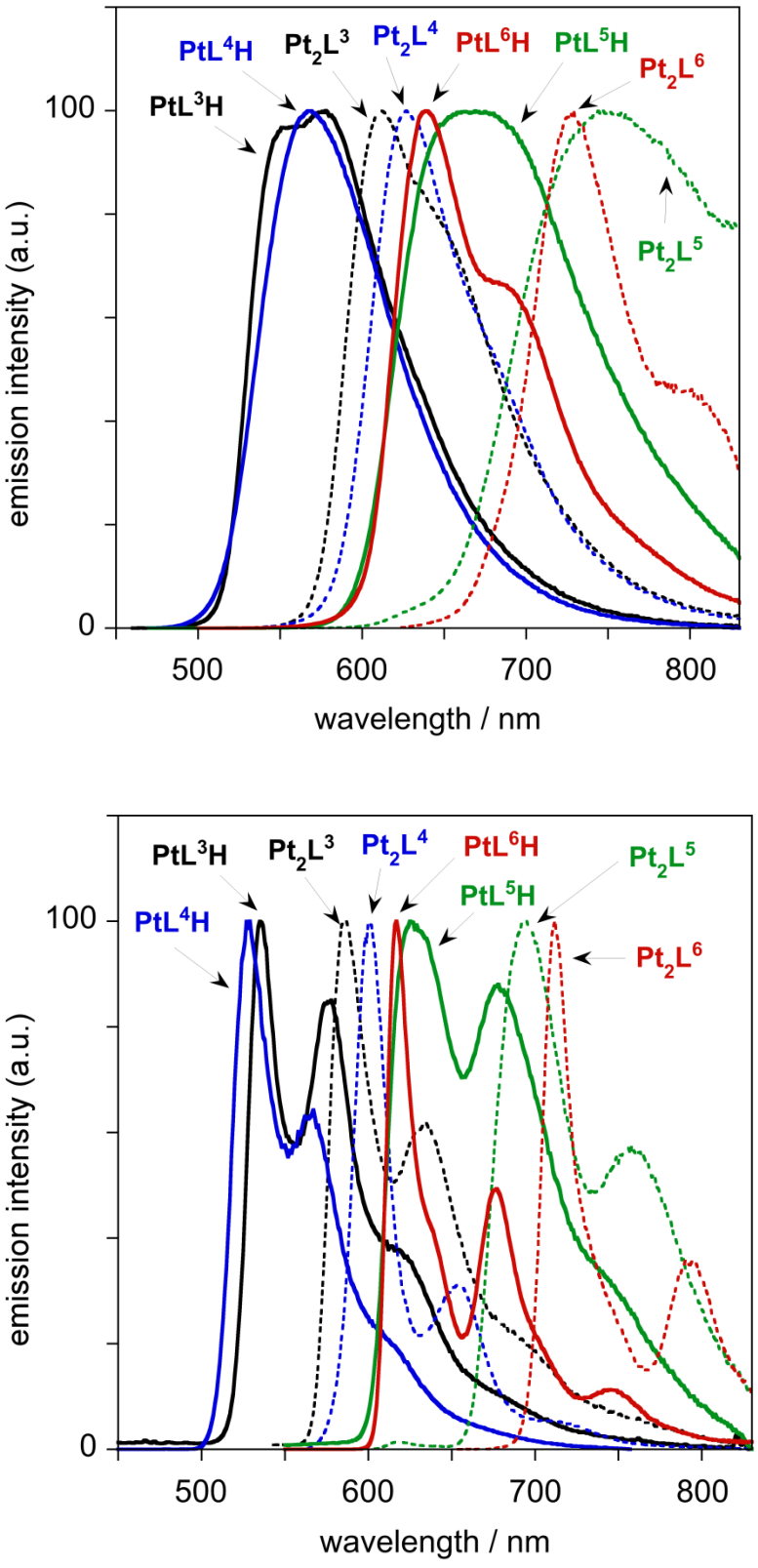

Chart 2.8 Top: Normalized emission spectra of 2.16 – 2.19 (black, blue, green, and red solid lines respectively) and of 2.22 – 2.25 (correspondingly coloured dashed lines) in CH_2Cl_2 solution at 298 K. Bottom: Corresponding spectra in an EPA glass at 77 K.

The photoluminescence quantum yields, Φ_{lum}, are high for many of the complexes (Table 2.3), falling off to < 0.1 only for the most red-emitting complexes, where much of the emission lies in the near infra-red. Binuclear complexes such as **2.21** and **2.22** are particularly striking in that they have quantum yields of around 0.40 at a λ_{max} that matches well with those of the standard red emitters in RGB displays (e.g. Eu^{3+} phosphors emit at around 617 nm). Indeed, these complexes are brighter than many of the widely-investigated iridium(III) complexes of phenylisoquinoline and benzothienylpyridine ligands[80,18,81], which emit in a similar region, and are competitive with quinoxaline-based iridium(III) complexes[11,14].

The luminescence lifetimes are of the order of a few microseconds in degassed solution and, for each pair, the lifetime of the binuclear complex is shorter than that of its mononuclear analogue. By estimating the radiative, k_r, and non-radiative, Σk_{nr}, decay rate constants from the quantum yield and lifetime data (Table 2.3), it can be seen that the introduction of the second metal ion facilitates the radiative decay process by a factor of around 2. Apparently, the emissive transition becomes more allowed in the binuclear complex. Whilst it might be tempting to attribute this effect to additional spin-orbit coupling associated with the second heavy metal ion, it should be noted that the molar absorptivities of the lowest-energy spin-allowed absorption bands are also increased by around two-fold in the binuclear complexes compared to their mononuclear analogues (Table 2.2).

2.5 Time-dependent density functional theory (TD-DFT) calculations

Density functional theory calculations have been carried out by Dr Marcus Durrant on all of the compounds shown in Figure 2.2. In order to facilitate the calculations, acac was used rather than dpm. As discussed in the previous section, changing from dpm to acac has very little influence on the photophysical properties of these complexes. All calculations were performed with Gaussian09W, using the B3LYP functional[82] and 6-31+G(d) basis set for all atoms except Pt, for which the LanL2DZ basis set was employed[83]. After full geometry optimization, the visible spectra were calculated by TD-DFT, both in vacuum and in dichloromethane solution using the polarized continuum model for the solvent[84].

In addition to the spectroscopic analysis, the DFT calculations provide a measure of the relative ground-state stabilities of the mononuclear and dinuclear complexes of a given ligand. For each ligand, the energy changes have been calculated for the hypothetical reactions [1] and [2], generating both the mono and dinuclear complexes (Ln denotes the proligands):

$$LnH_2 + Pt(acac)_2 \rightarrow Pt(acac)LnH + acacH \quad [1]$$

$$Pt(acac)LnH + Pt(acac)_2 \rightarrow \{Pt(acac)\}_2Ln + acacH \quad [2]$$

The energy changes (ΔE) associated with these reactions are shown in Table 2.4.

Table 2.4 Calculated gas-phase energy changes for reactions [1] and [2] generating the mono or dinuclear complex.

Species Ln n =	Reaction [1] → Pt(acac)LnH ΔE / kJ mol^{-1}	Reaction [2] →{Pt(acac)}$_2$Ln ΔE / kJ mol^{-1}
2.1	– 13.4	– 42.0
2.2	– 10.3	– 46.7
2.3	– 4.2	– 32.8
2.4	– 6.5	– 33.0
2.5	+ 25.8	– 12.4
2.6	+ 14.9	– 23.6

As the data shows, the introduction of the second Pt center is always energetically more favourable than the first, indicating a synergy in the binding. The stabilities of the complexes can be linked to steric effects. The least sterically hindered ligands **2.1** and **2.2** give the most stable complexes, whilst **2.5** and **2.6** are the least stable. Their instability could be explained by the close contacts between the O atoms of the acac ligands and the CH groups of the extra ring (Figure 2.3). The closest CH---O contacts are 2.68Å for **2.24** and 2.37Å for **2.25** (Table 2.5). The fused ring systems **2.4** and **2.6** are a little better than their *ortho*-diphenyl analogues **2.3** and **2.5** respectively in terms of stability.

Table 2.5 Closest contact between the O atom of the acac ligand and the CH group of the ring

Species $Pt_2Ln(acac)$ n =	Closest CH---O contact (Å)
2.1	3.88
2.2	3.86
2.3	3.52
2.4	3.71
2.5	2.68
2.6	2.37

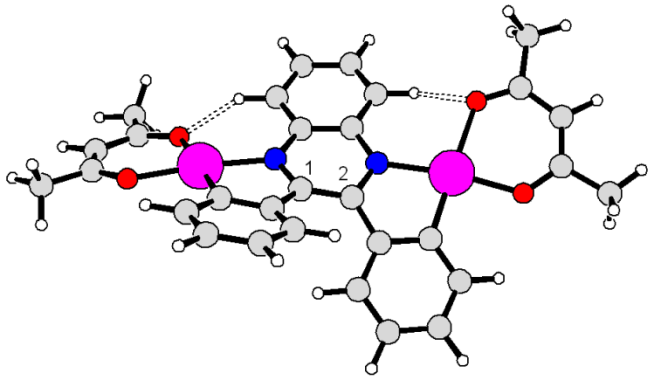

Figure 2.3 Calculated structure of 2.24, showing the steric distortion centred on the pyrazine ring. The dotted lines show the close contacts between the C–H groups and O atoms.

As expected, the ligands whose rings are linked by rotatable C–C bonds are non-planar in these complexes. In the mononuclear complexes of **2.3** and **2.5**, and all the complexes of the other ligands, the coordinated rings are essentially co-planar; however, some distortion is observed for the dinuclear complexes of **2.3** and **2.5**. This is greatest for **2.24**, as shown in Figure 2.3; the pyrazine ring is twisted, such that carbons 1 and 2 are displaced by 0.12 Å above and below the mean plane of the ring.

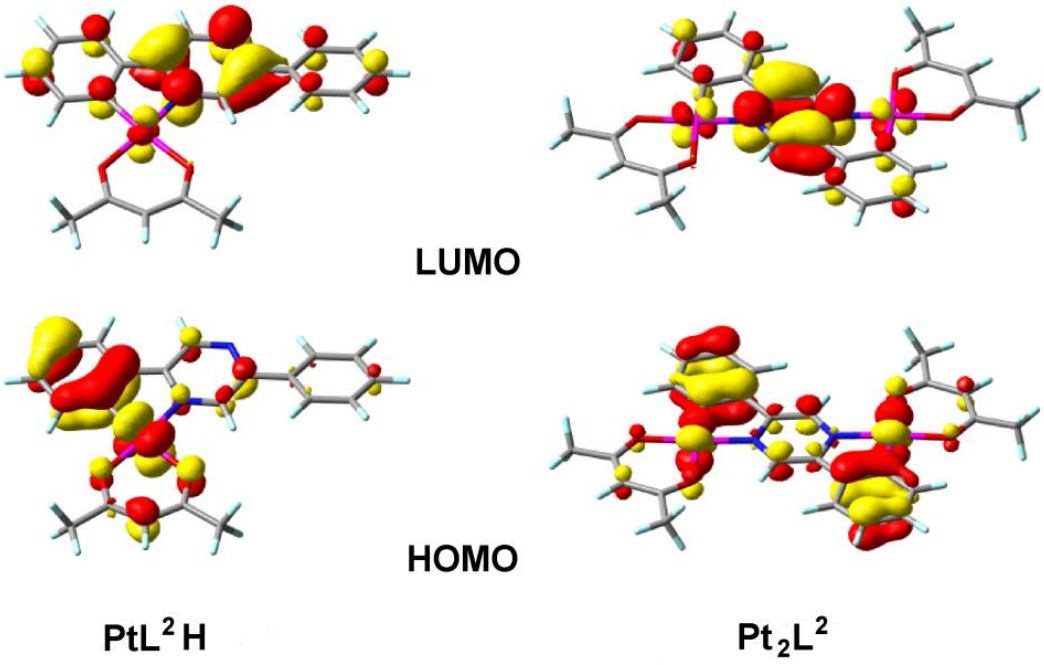

Figure 2.4 Frontier orbital diagrams for 2.15 (left) and 2.21 (right).

The frontier orbitals for the mono- and dinuclear complexes of L2, which are shown in Figure 2.4, are representative of all six pairs of complexes. For all 12 complexes, the HOMO's are derived mainly from combinations of platinum d-orbitals with π-orbitals of the surrounding ligands, with only small contributions from the pyrazine and pyrimidine rings. These heterocyclic rings are much more important components of the LUMO's. The frontier orbitals of the dinuclear complexes are all symmetrically distributed over both halves of the molecules. Frontier orbital diagrams for the remaining complexes can be found in the appendix.

There is a good correlation between the energy of the LUMO and energy of the lowest energy singlet transition in the calculated spectra (the data is shown in the appendices). The calculated absorption spectra are shown in Chart 2.9, and are in generally good agreement with the experimentally measured spectra. Calculations including the triplet excited states for **2.20**, **2.21** and **2.22** in dichloromethane placed the formally spin-forbidden S0→T1 transitions at 538, 622 and 591 nm respectively, in good agreement with the experimental phosphorescence data discussed previously.

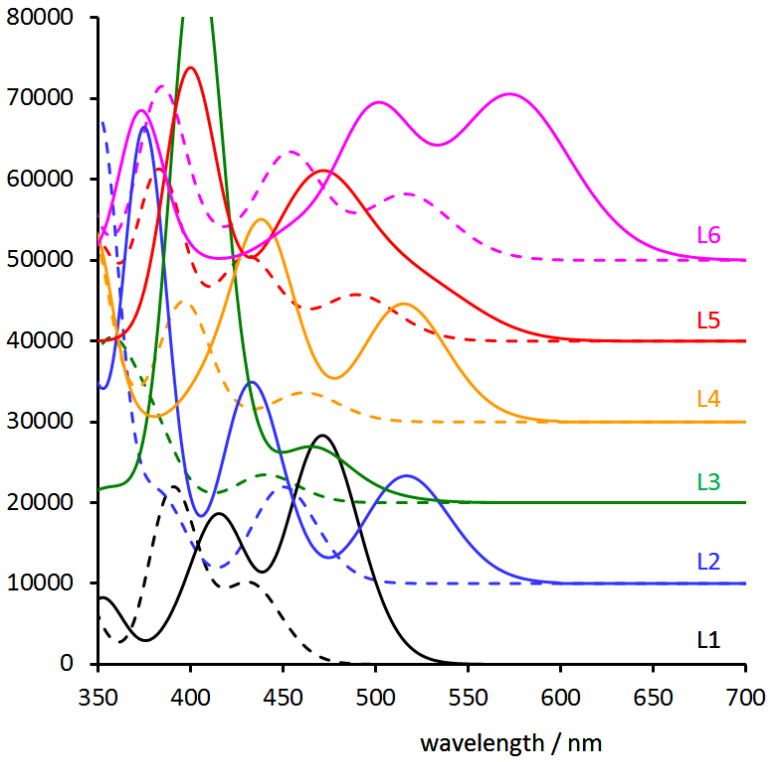

Chart 2.9 Simulated UV-visible absorption spectra of the complexes obtained by TD-DFT calculations with a CH_2Cl_2 implicit solvent model. Spectra are displaced vertically for clarity. Spectra of mononuclear complexes are represented by broken lines and dinuclear complexes are represented by solid lines.

2.6 Concluding Discussion

It has been previously shown how 4,6-diphenylpyrimidine can be used as a bridging ligand to prepare dinuclear cyclometallated platinum(II) complexes[43]. This study shows that diphenylpyrazines can likewise generate dinuclear platinum(II) complexes, through metallation of the two pendent phenyl rings and binding of the metal ions to the two nitrogen atoms of the central heterocycle. Both the 2,3- and 2,5-substituted isomers of diphenylpyrazine can be employed, along with diphenylquinoxaline and derivatives in which the phenyl rings are interlinked through their *ortho* positions. Mono- and di-nuclear complexes can be isolated from a single reaction by chromatographic separation.

The introduction of the second metal ion leads, for all six ligands investigated, to a significant stabilization of the LUMO of around 0.3 eV, according to TD-DFT calculations (data shown in appendices). In contrast, the HOMO energy seems to be influenced rather little. These contrasting effects are intuitively in line with the typical distribution of frontier orbitals in cyclometallated complexes of aryl-heterocycles, in that the ring to which *two* metal ions are bound is the heterocycle, on which the LUMO is predominantly localised. The decreased HOMO–LUMO gap that ensues leads to red-shifted absorption and emission spectra for the dinuclear complexes compared to their mononuclear analogues. Meanwhile, the increased conjugation within the heterocycle on going from a pyrazine through quinoxaline to a phenazine unit (as in **2.6**) has a much more significant effect on the LUMO, leading to the progressive shift towards the red region observed in the optical spectra.

Of particular interest is the effect of the second metal ion on the radiative rate constant k_r. For all of the systems in which this parameter can be estimated with confidence (Table 2.3), the value increases upon introduction of the second metal ion, despite the red shift.

In summary, dinuclear cyclometallated complexes are shown to offer interesting potential for obtaining phosphorescent materials that both absorb strongly and emit brightly at unusually low energies. Further derivatisation of the diarylpyrazine unit can be confidently expected to lead to further new compounds with opportunities for controlling excited states for contemporary applications, such as in imaging, solar energy conversion, and light-emitting displays.

Chapter 3: The effects of the Substitution Pattern in Bridging 2,5-diphenyl pyrazine ligands

3 The effects of the Substitution Pattern in Bridging 2,5-diphenyl pyrazine ligands

The aim of this section of work is to look at the effects of the substitution pattern in bridging 2,5-diphenyl pyrazine ligands on the photophysical properties of their cyclometallated platinum(II) complexes. In order to achieve this goal a series of substituted 2,5-diphenylpyrazines with electron withdrawing and donating groups were prepared. These proligands were then used to prepare the corresponding mono- and di-platinum(II) complexes. Their photophysical properties were investigated.

3.1 Synthesis

A range of ligands as well as their mono- and di-platinum (II) complexes are depicted in Figure 3.1 The substituents are added to the phenyl moiety of the proligand and are either electron donating (-OMe, -CH_3,) or electron withdrawing (-F). An unsubstituted (H) derivative was prepared earlier as part of the work in chapter 2.

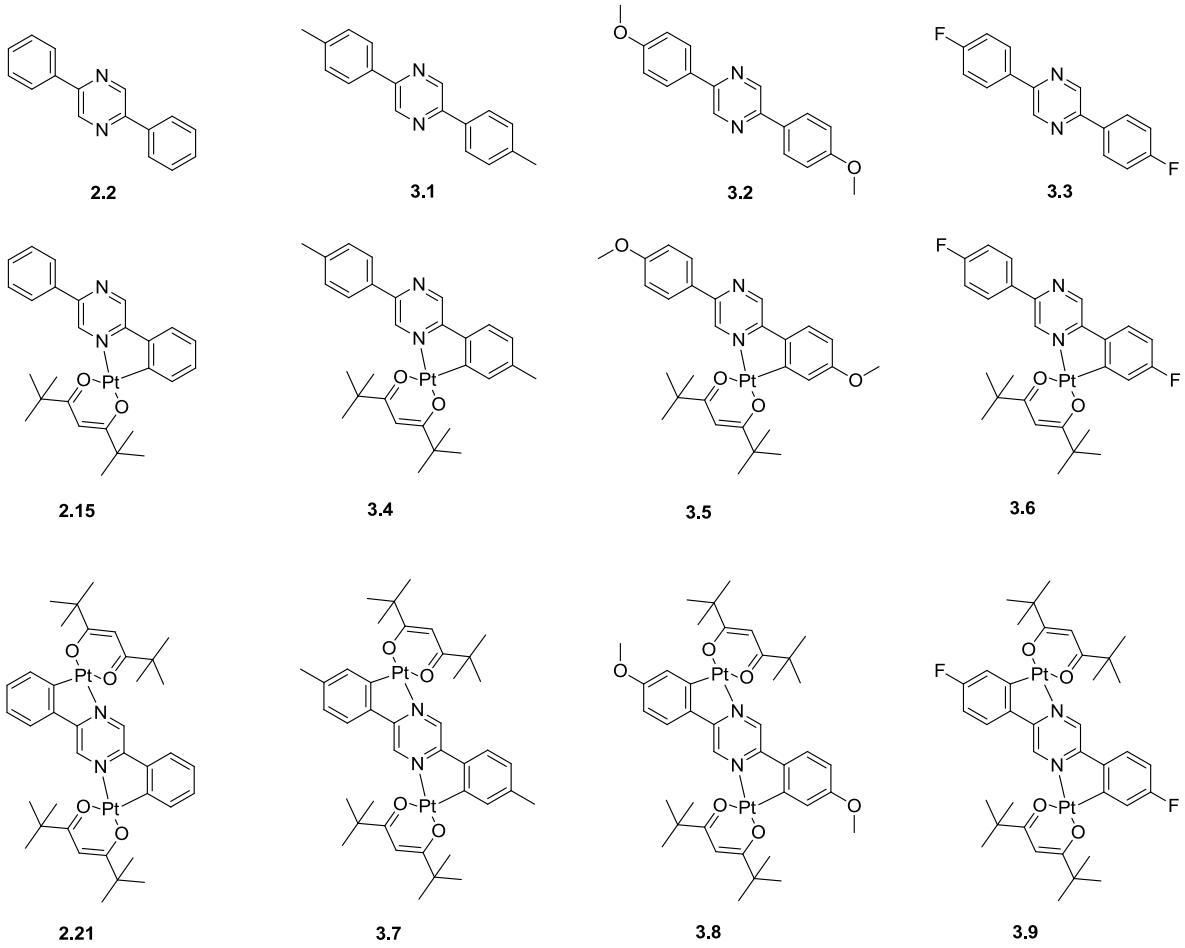

Figure 3.1 Structures of the proligands, mono-nuclear platinum(II) complexes, and dinuclear platinum(II) complexes

3.1.1 Proligand Synthesis

2.2 was synthesised via the Suzuki cross coupling reaction using commercially available 2,5-dibromopyrazine (**2.26**) and phenylboronic acid (**2.27**). The reaction was carried out by stirring at 95°C a deairated mixture of 1 equivalent of 2,5-diphenylpyrazine, 2.6 equivalents of phenylboronic acid, 5 equivalents of 2M aqueous K_2CO_3, 6 mol% of tetrakis(triphenylphosphine) palladium (0) as a catalyst and 1,4-dioxane as solvent. The isolated yield of the reaction was only 33% indicating that the reaction conditions should be further optimised. However, the big disadvantage of the reaction is the expensive starting materials, especially 2,5-dibromopyrazine.

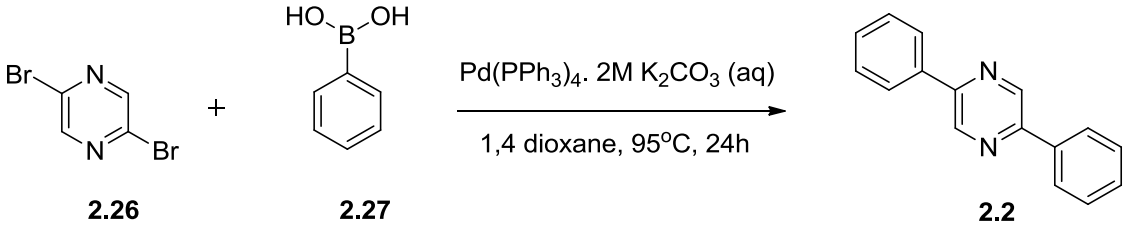

2.26 **2.27** **2.2**

Figure 3.2 Synthesis of 2. by Suzuki cross coupling reaction

For this reason, an alternative route to 2,5-diphenylpyrazines based on the formation of the central pyrazine ring was then tested[85,86]. Commercially available and cheap acetophenones were brominated in diethyl ether and then treated with ammonia in ethanol.

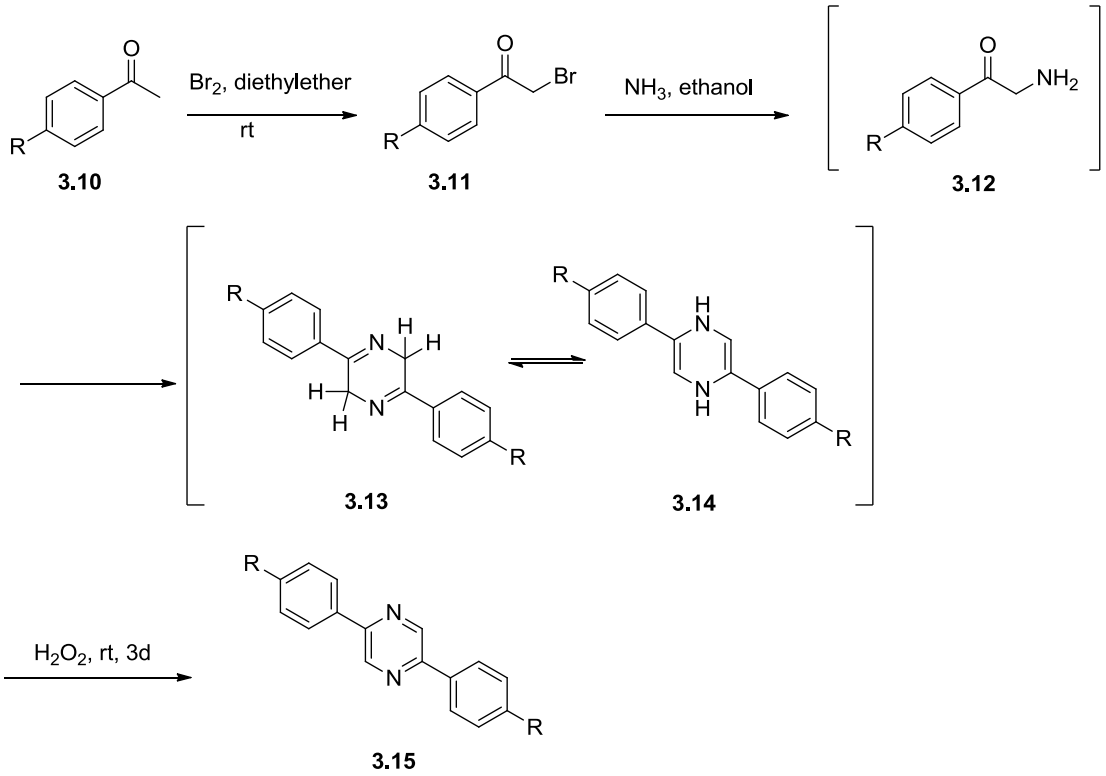

3.10 **3.11** **3.12** **3.13** **3.14** **3.15**

Scheme 3.1 General synthesis of the proligands using substituted acetophenones

Scheme 3.1 shows the general mechanism of the reaction. The bromoacetophenones (**3.11**) react with ammonia to give the corresponding aminoacetophenones (**3.12**). The latter spontaneously dimerise to form dihydropyrazines, which exist in two tautomeric forms (**3.13, 3.14**). If left stirring at room temperature, the dihydropyrazines are oxidised

by air to give pyrazines (**3.15**). The oxidation is, however, quite a slow process. In order to facilitate it, hydrogen peroxide was added leading to the targeted pyrazines. If oxidation was not complete, the crude product was redissolved in ethanol and more hydrogen peroxide was added. Figure 3.3 shows the NMR of the proligand **3.1** not quite at completion, as there are also peaks for the dihydropyrazine. After further oxidation overnight, Figure 3.4 shows that the reaction has gone to completion.

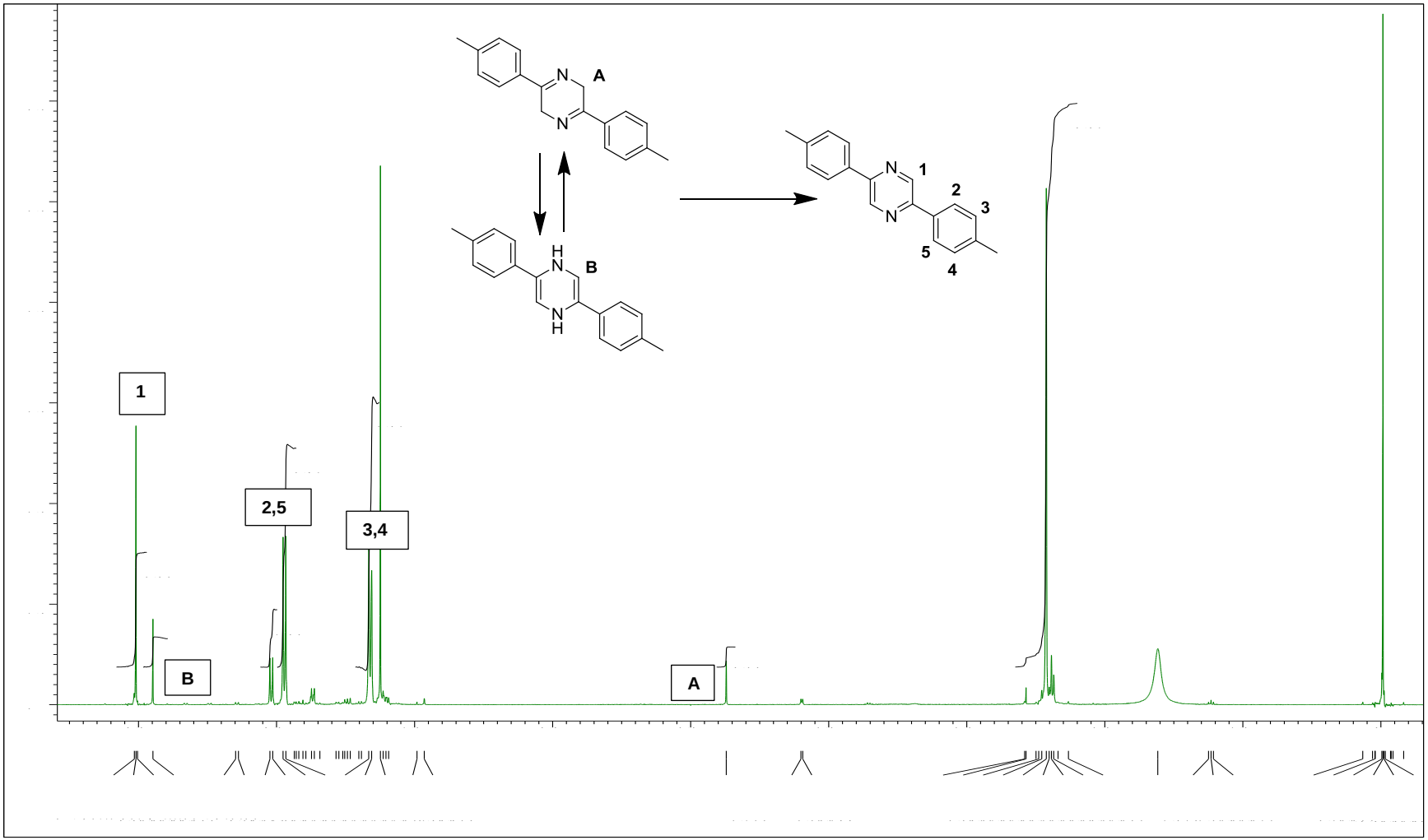

Figure 3.3 ^{1}H-NMR image showing the presence of dihydropyrazines

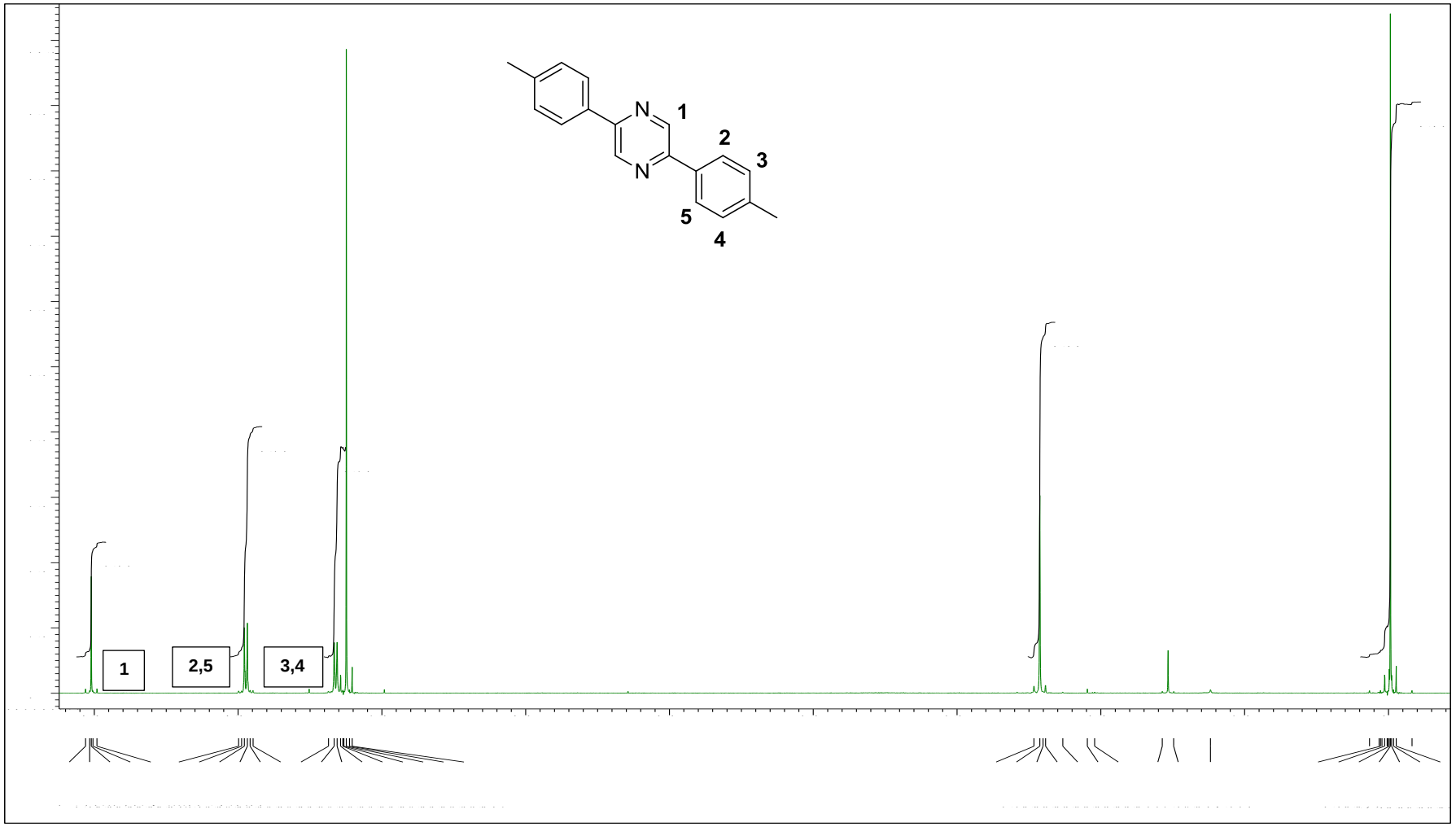

Figure 3.4 ^{1}H-NMR image showing the pure product after further oxidisation

This method of first bromination of acetophenones followed by treatment with aqueous ammonia has advantages over the Suzuki cross-coupling as the costs are lower and the reaction can be easily scaled up. We therefore used this method of synthesis to prepare the whole series of compounds.

3.1.2 Platinum(II) complex synthesis

The mono and dimetallic Platinum(II) complexes, were obtained by refluxing the ligand with 1.5 equivalents of K_2PtCl_4 in acetic acid for 1 day. The intermediate is then refluxed with 2 equivalents of DPM and 3 equivalents of potassium carbonate in acetone for 1 day. The mono- and dinuclear platinum complexes are readily separated by column chromatography (typically on silica gel eluting with dichloromethane) to give both products in one procedure (Scheme 3.2). Yields were 6-35% for monometallic complexes and 1-15% for dimetallic complexes.

3.1.2.1 Complexes 2.15 And 2.21

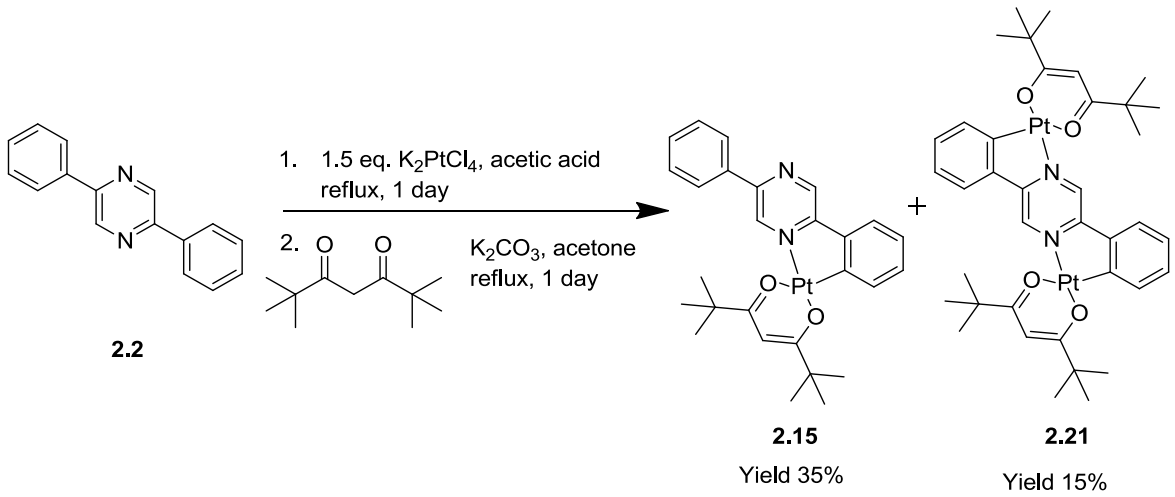

Scheme 3.2 One pot synthesis of 2.15 and 2.21

Scheme 3.2 shows the one pot synthesis of **2.15** and **2.21**. A yield of 35% for mono-Pt and 15% for di-Pt was achieved. Figure 3.5 shows the ^{1}H-NMR spectra of **2.2** (bottom spectrum), **2.15** (middle spectrum) and **2.21** (top spectrum).

It can be seen that the reaction has worked as signals for protons have shifted compared to the starting proligand and one proton disappears due to the formation of the C-Pt bond. Of the mono-Pt complex, protons 1 and 6 can be assigned by the Pt satellites (just seen on Figure 3.5). Proton 6 has satellites ($^{3}J_{H\text{-}Pt}$ 45.8 Hz) due to the close proximity to platinum whereas proton 1 does not. The difference between the mono-Pt and di-Pt complexes are also apparent as the di-Pt complex has equivalent protons from both phenyl moieties of the ligand, whereas the mono-Pt complex protons are not equivalent, the protons on both phenyl moieties are in different environments due to the presence of the platinum attached to one of them.

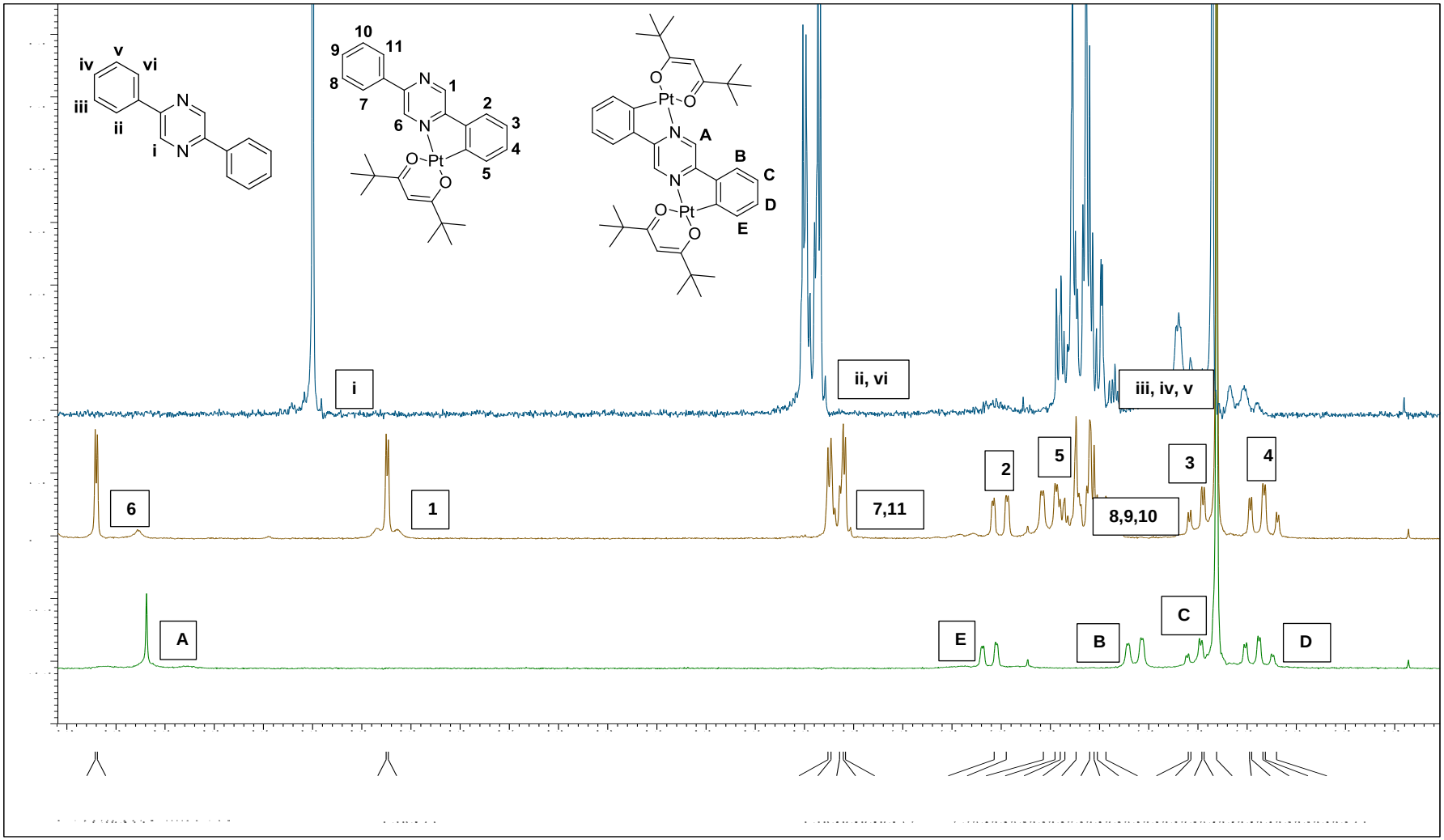

Figure 3.5 Expanded area of the ^{1}H-NMR spectra of 2.21 (bottom spectrum), 2.15 (middle spectrum) and 2.2 (top spectrum)

3.1.2.2 Complexes 3.4 and 3.7

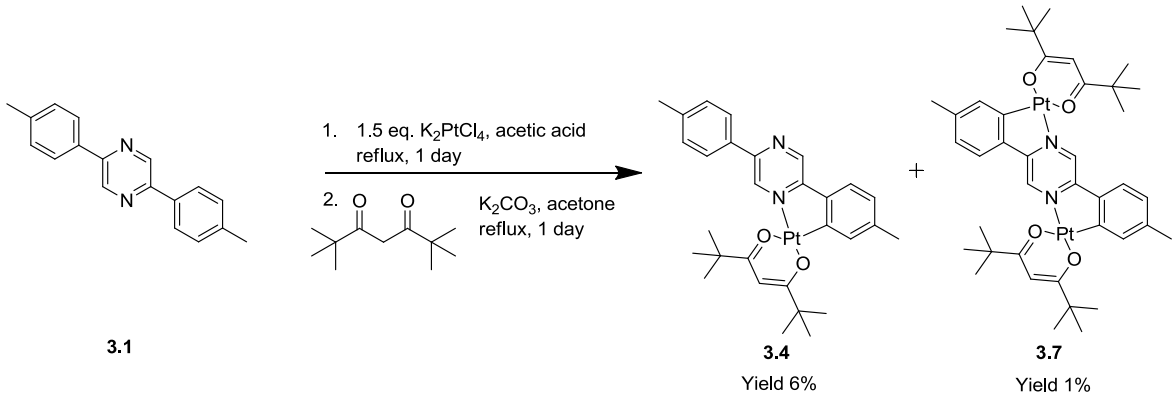

Scheme 3.3 One pot synthesis of 3.4 and 3.7

Scheme 3.3 shows the one pot synthesis of **3.4** and **3.7**. A yield of 6% for mono-Pt and 1% for di-Pt was achieved. Figure 3.6 shows the ^{1}H-NMR spectra of **3.7** (bottom spectrum), **3.4** (middle spectrum) and **3.1** (top spectrum). The complex is derived analogously to **2.2** and so the same conclusions can be drawn as to interpreting the 1H-NMR. Proton 5 of Figure 3.6 has platinum satellites ($^{3}J_{H\text{-}Pt}$ 34.8 Hz) and so can easily be assigned. In addition, there are also two singlets of integral three for the methyl groups attached to the pyridyl moiety on the mono-Pt spectrum. The di-Pt spectrum shows it as one singlet of integral six.

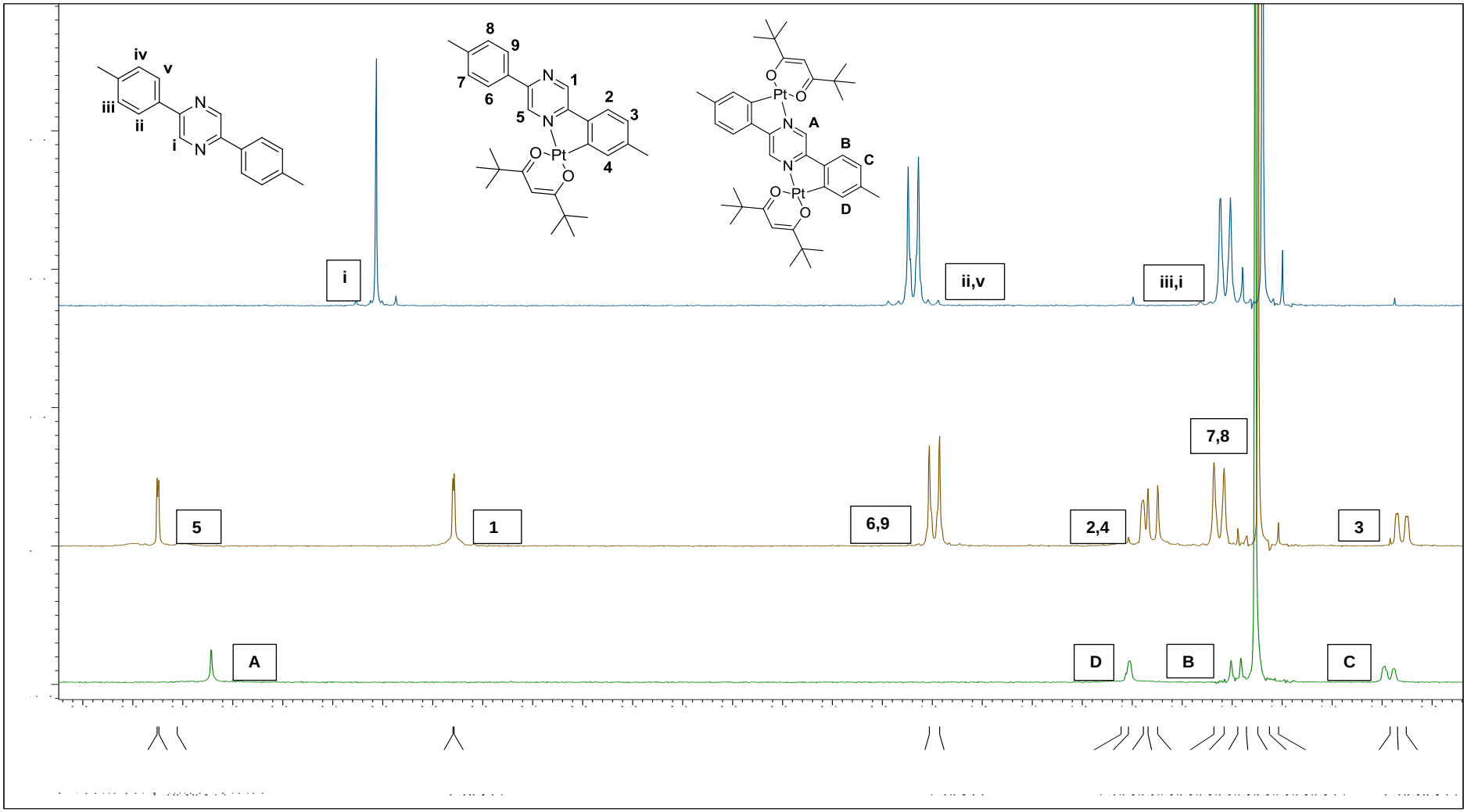

Figure 3.6 Expanded area of the ^{1}H-NMR spectra of 3.7 (bottom spectrum), 3.4 (middle spectrum) and 3.1 (top spectrum)

3.1.2.3 Complexes 3.5 and 3.8

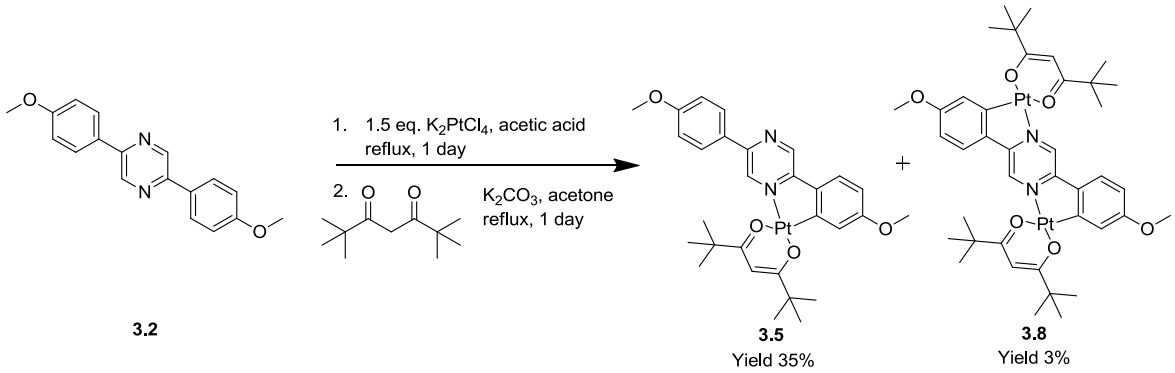

Scheme 3.4 One pot synthesis of 3.5 and 3.8

Scheme 3.4 shows the one pot synthesis of **3.5** and **3.8**. A yield of 35% for mono-Pt and 3% for di-Pt was achieved. Figure 3.7 shows the ^{1}H-NMR spectra of **3.8** (bottom spectrum), **3.5** (middle spectrum) and **3.2** (top spectrum). The complex is derived analogously to **2.2** and so the same conclusions can be drawn as to interpreting the ^{1}H-NMR. Proton 5 of Figure 3.7 has platinum satellites ($^{3}J_{H\text{-}Pt}$ 43.1 Hz) and so can easily be assigned. In addition, there are also two singlets of integral one for the methoxy groups attached to the pyridyl moiety on the mono-Pt spectrum. The di-Pt spectrum shows it as one singlet of integral two.

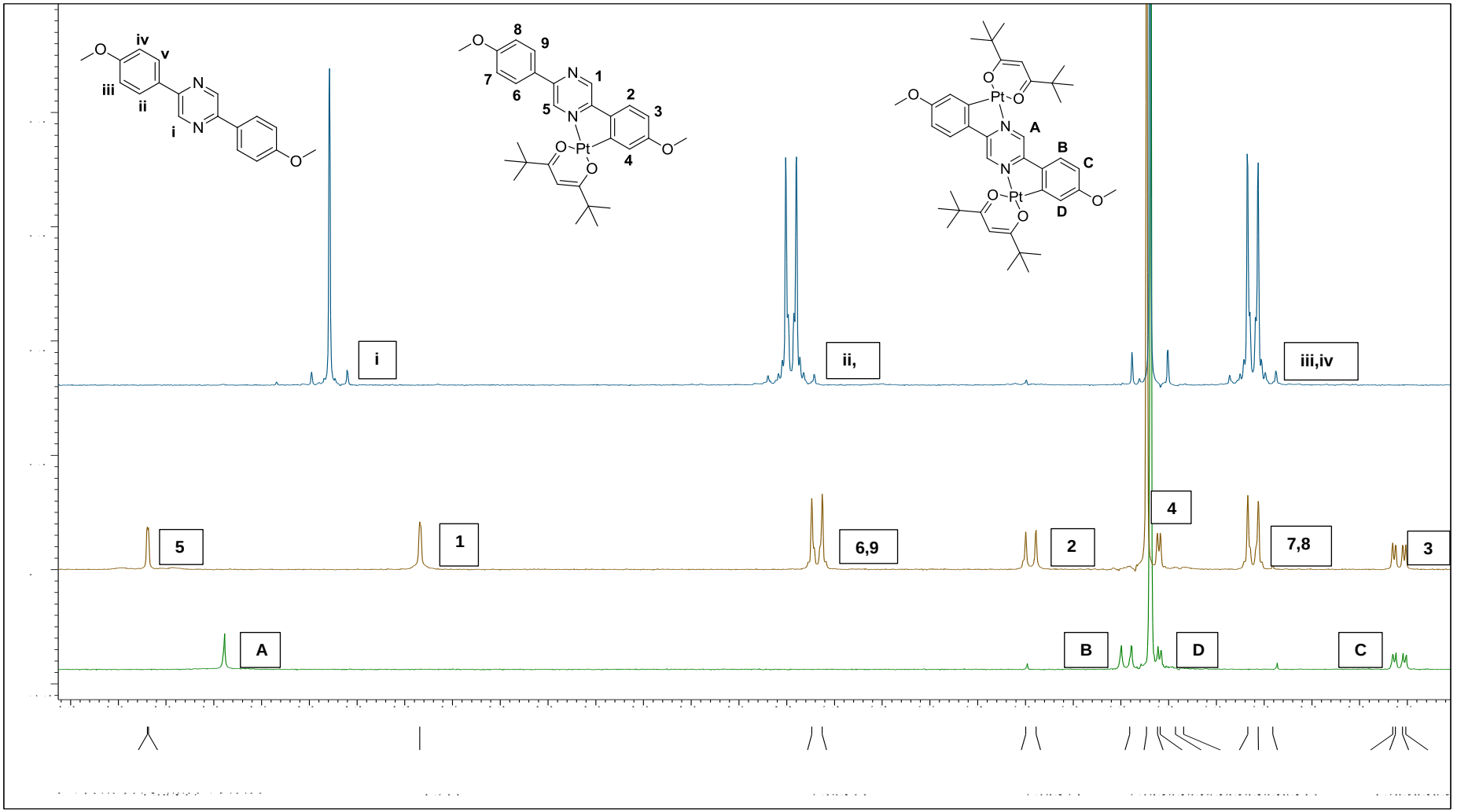

Figure 3.7 Expanded area of the ^{1}H-NMR spectra of 3.8 (bottom spectrum), 3.5 (middle spectrum) and 3.2 (top spectrum)

3.1.2.4 Complexes 3.6 and 3.9

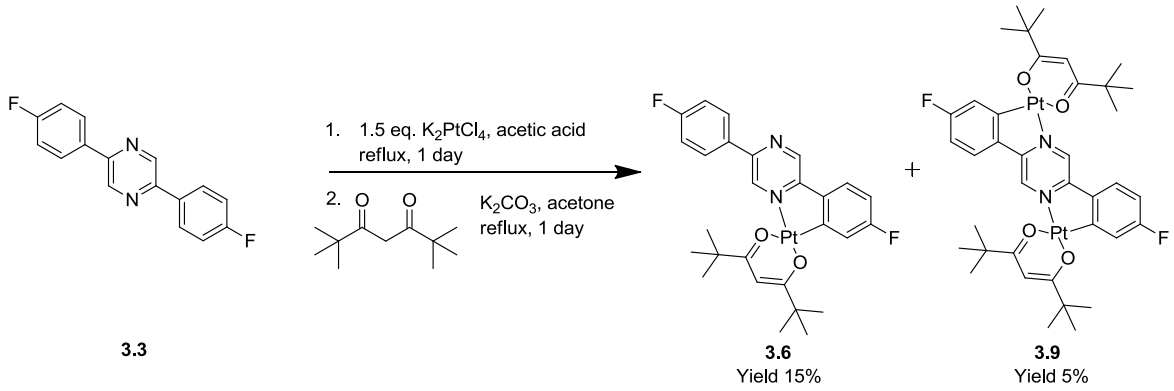

Scheme 3.5 One pot synthesis of 3.6 and 3.9

Scheme 3.5 shows the one pot synthesis of **3.6** and **3.9**. A yield of 15% for mono-Pt and 5% for di-Pt was achieved. Figure 3.8 shows the ^{1}H-NMR spectra of **3.9** (bottom spectrum), **3.6** (middle spectrum) and **3.3** (top spectrum). The complex is derived analogously to **2.2** and so the same conclusions can be drawn as to interpreting the ^{1}H-NMR. Proton 5 of Figure 3.8 has platinum satellites ($^{3}J_{H\text{-}Pt}$ 43.5 Hz) and so can easily be assigned. The additional splitting is due to the fluorine atoms.

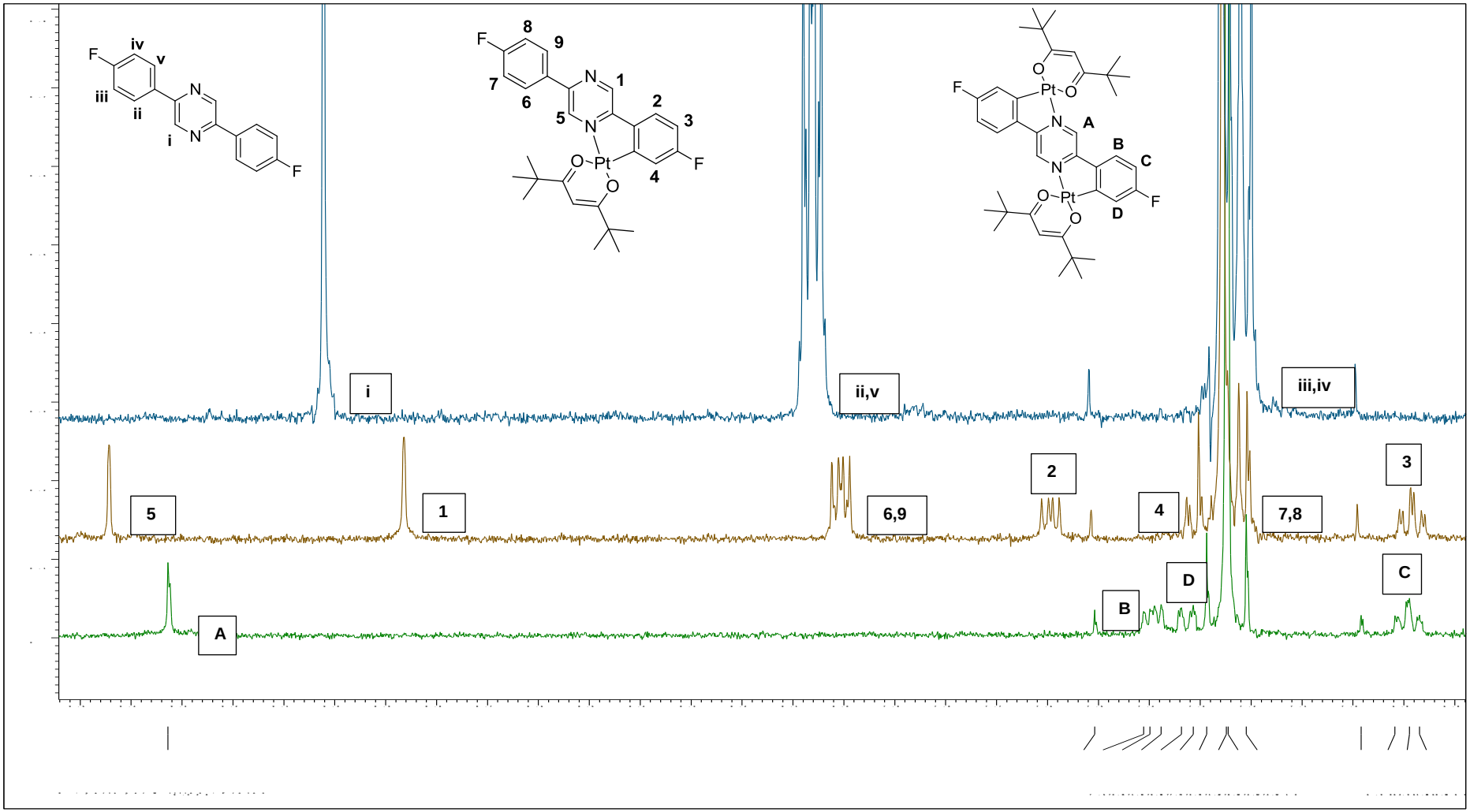

Figure 3.8 Expanded area of the ^{1}H-NMR spectra of 3.9 (bottom spectrum), 3.6 (middle spectrum) and 3.3 (top spectrum)

3.2 Absorption Spectroscopy

Table 3.1 UV-visible absorption data for the complexes

Complex	λ_{max} / nm (ε / $M^{-1}cm^{-1}$)
2.14 (-H)	341 (13435), 353 (12030), 398 (4996), 436 (4027)
3.4 (-Me)	307 (22588), 367 (14672), 388 (9266), 442 (5864)
3.5 (-OMe)	337 (20274), 367 (10288), 429 (8041), 452 (6877)
3.6 (-F)	358 (12759), 392 (7988), 429 (6124)
2.20 (-H)	336 (23380), 375 (17581), 453 (17044), 502 (7288), 521 (6264)
3.7 (-Me)	322 (24965), 339 (24026), 431 (12523), 448 (12895), 528 (6495)
3.8 (-OMe)	321 (21362), 370 (26295), 440 (12464), 504 (7762), 540 (8373)
3.9 (-F)	320 (6902), 363 (5634), 447 (5143), 515 (1938)

The absorption data for the complexes is shown in Table 3.1. Chart 3.1 shows the UV spectra of the mono-Pt complexes. The most red shifted are the complexes containing methoxy or methyl substituents. The complex containing the fluorine substituent is the most blue shifted. The same can be said of the di-Pt complexes, which are shown in Chart 3.2. The di-Pt complexes are significantly red shifted compared to the mono-Pt complexes.

There is trend in absorbance of F < H < CH_3 < OMe. This is due to the HOMO and LUMO orbitals being affected by the electron donating and withdrawing groups. Fluorine is an electron withdrawing group, so will therefore decrease the delocalised electron density in the aromatic ring. The HOMO, which is generally localised on the phenyl moiety, is reduced, increasing the HOMO-LUMO energy gap. Hence the compound containing the fluorine substituent has the lowest wavelength of absorption. Methoxy and methyl are electron donating groups and so destabilise the HOMO, with the methoxy group showing

the biggest effect. This too is reflected in the fact that the compounds containing these groups have the highest wavelength of absorption.

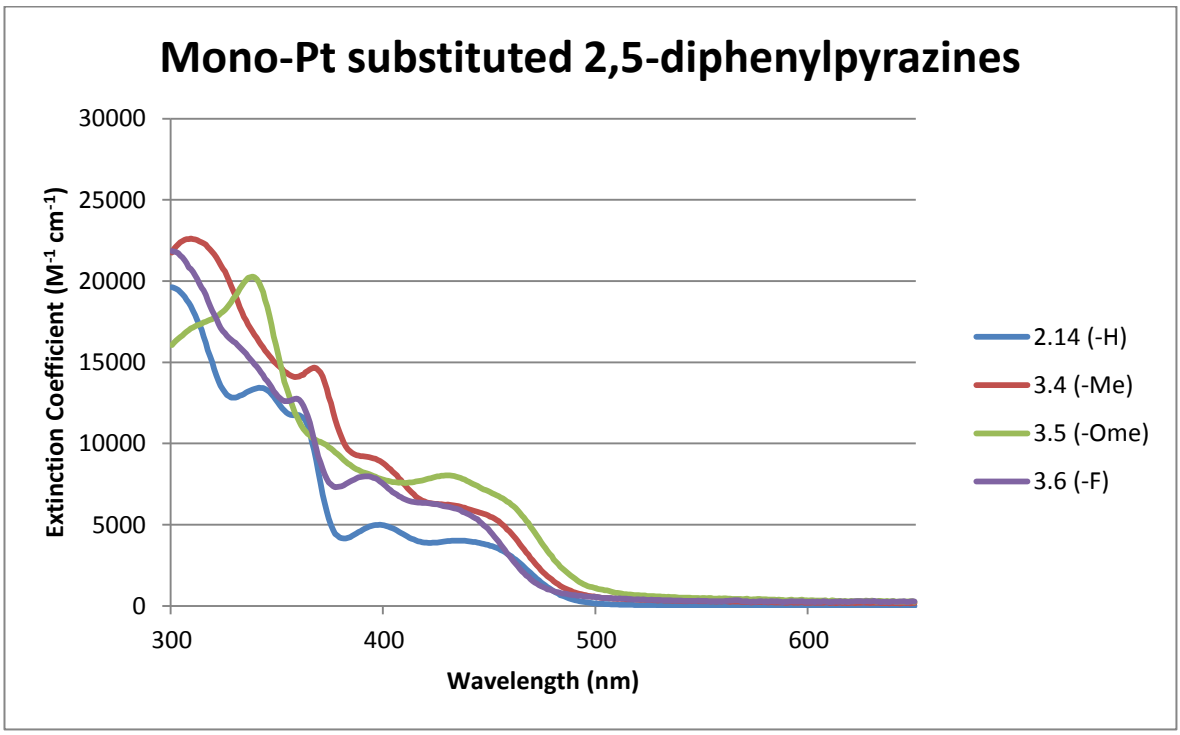

Chart 3.1 UV spectra of the mono-Pt complexes using substituted 2,5-diphenylpyrazines

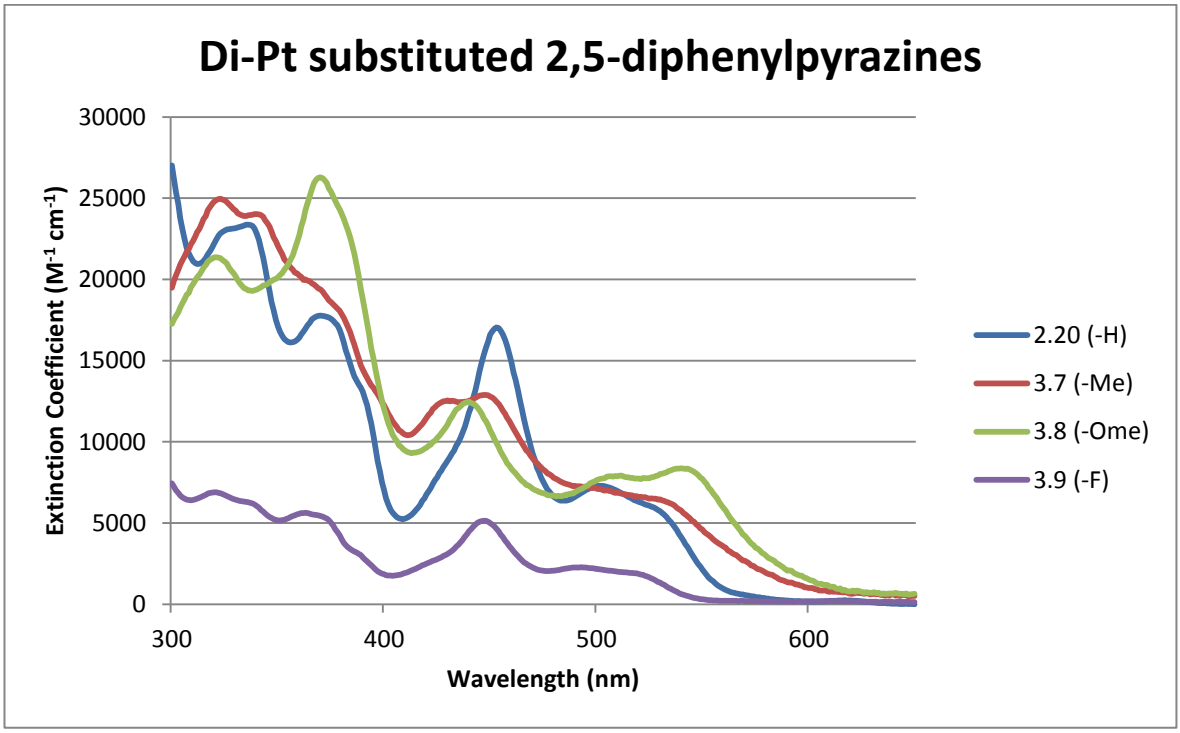

Chart 3.2 UV spectra of the di-Pt complexes using substituted 2,5-diphenylpyrazines

As mentioned previously, two metals in the complex cause a further red-shift. This is shown in Chart 3.3 which contains the UV data for the proligand **3.2** and its mono-Pt and di-Pt derivatives (Figure 3.9). The data shows a definite red-shift from the mono-Pt to the di-Pt complex. The extinction coefficients are higher for the di-Pt derivatives compared to their mono-Pt counterparts with the exception of **3.9** which is significantly reduced.

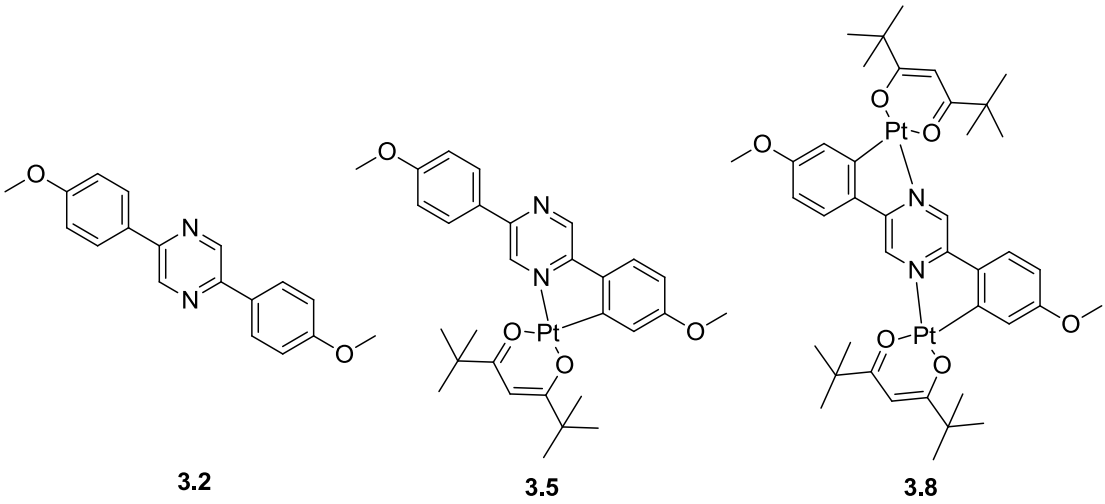

Figure 3.9 Proligand 3.2 and its mono-Pt (3.5) and di-Pt (3.8) derivatives

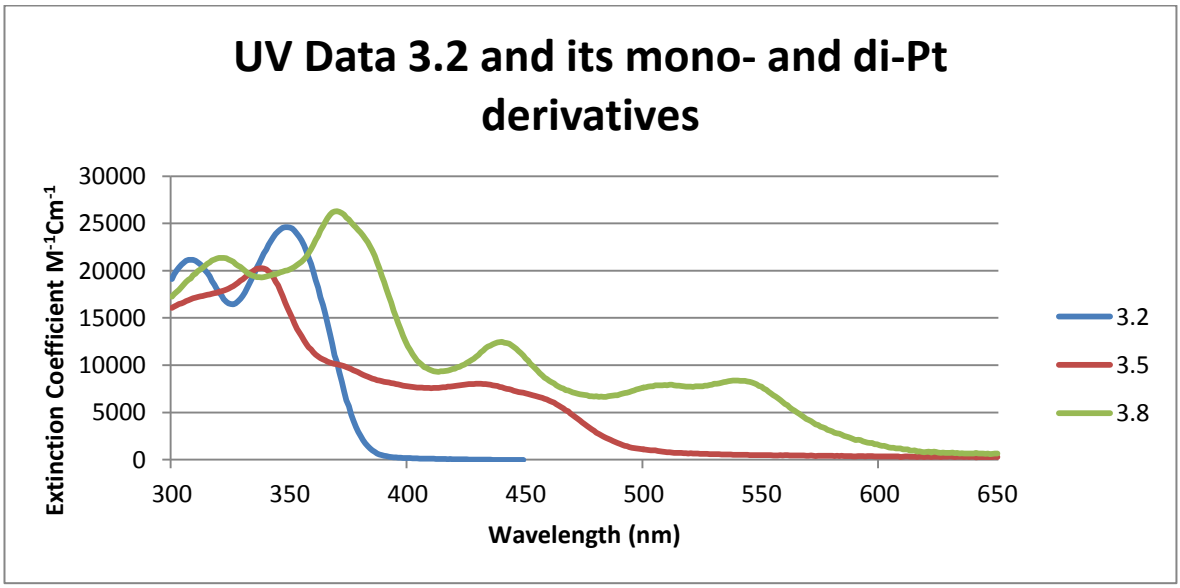

Chart 3.3 UV spectra for 3.2, 3.5 and 3.8

3.3 Photoluminescent properties

All eight complexes are luminescent in solution at room temperature. The complexes were unable to be degassed before measurements were taken and so comments on the intensity of the emission cannot be made as the quenching by oxygen will have an effect on the intensity. The emission data for the compounds are compiled in Table 3.2, and the spectra are shown in Chart 3.4 and Chart 3.5. The trends in emission maxima are quite similar to those observed in the absorption spectra. In particular, it may be immediately seen that, for a given ligand, the spectrum of the dinuclear complex is significantly red-shifted compared to that of the corresponding mononuclear complex, with a difference of around 65-80nm between the mono-Pt and di-Pt species.

Table 3.2 Emission data for the complexes

	Emission (nm)	
Complex	**Mono-Pt**	**Di-Pt**
2.14 & 2.20 (-H)	566	629
3.4 & 3.7 (-Me)	574	642
3.5 & 3.8 (-OMe)	590	667
3.6 & 3.9 (-F)	558	623

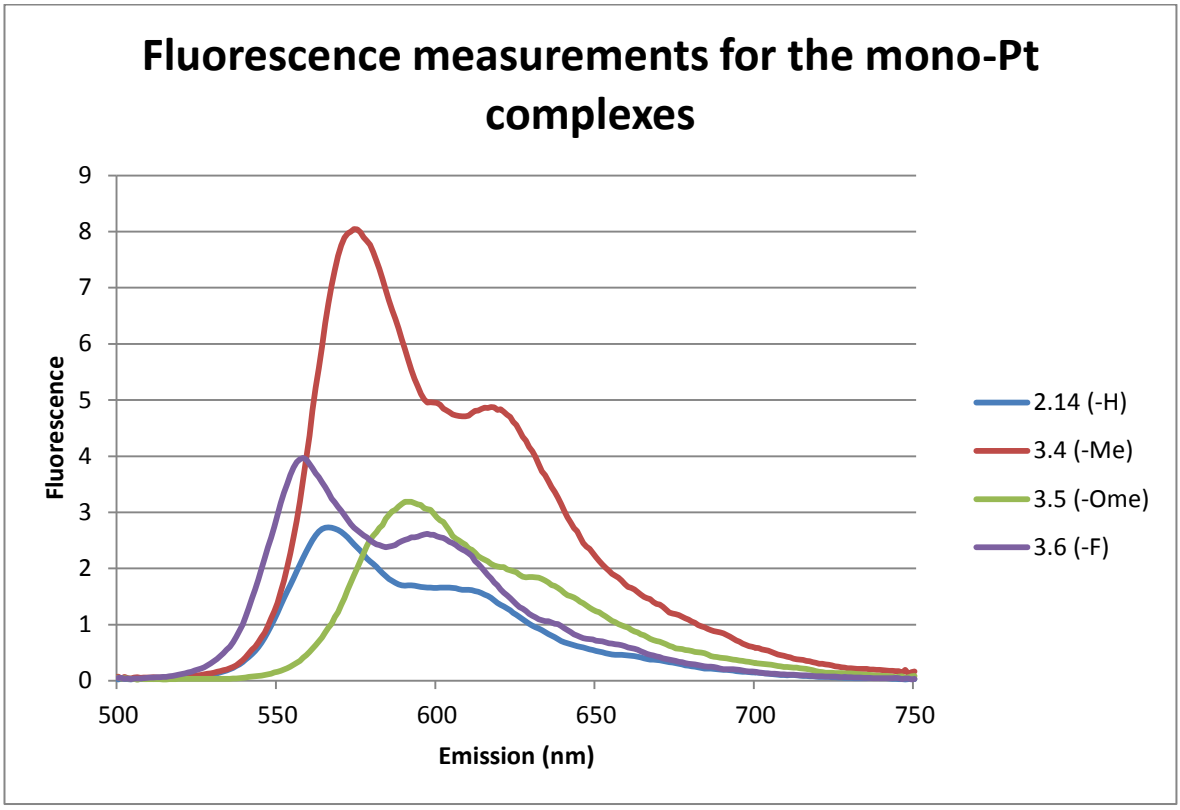

Chart 3.4 Emission spectra of the mono-Pt complexes using substituted 2,5-diphenylpyrazines

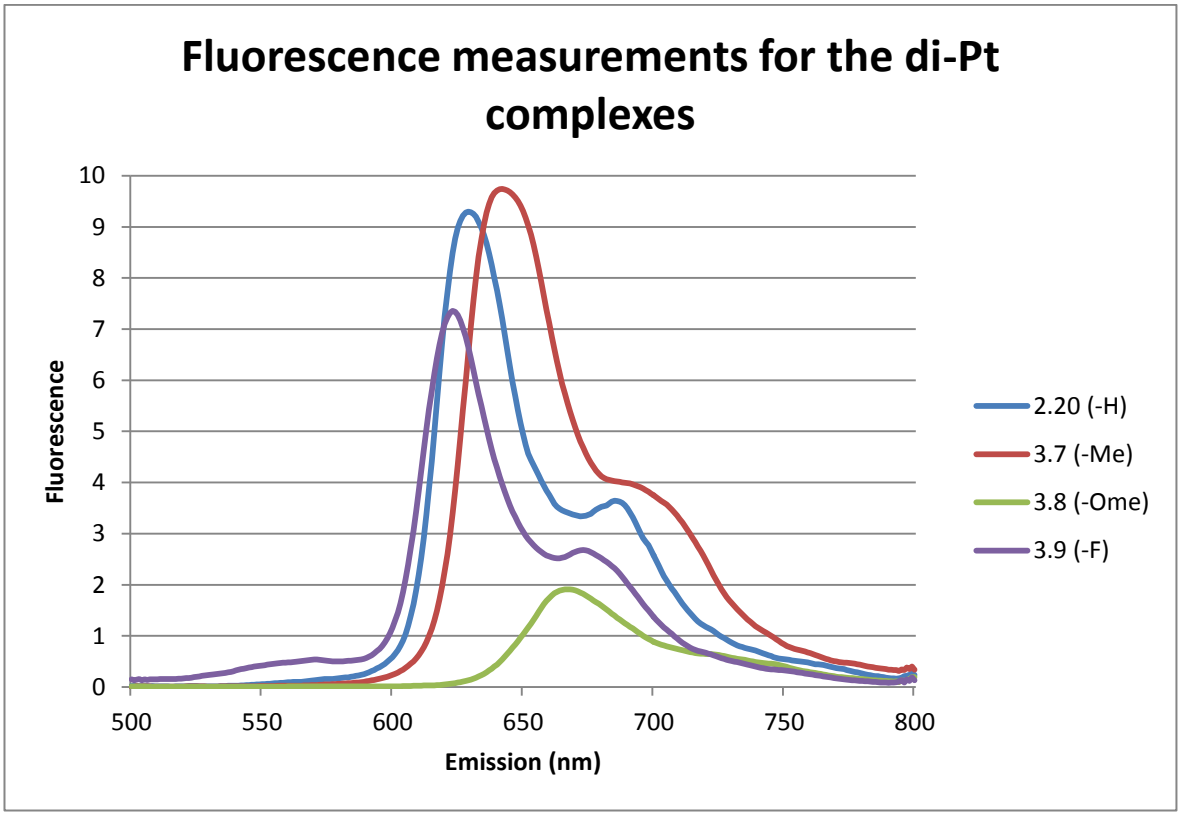

Chart 3.5 Emission spectra of the di-Pt complexes using substituted 2,5-diphenylpyrazines

3.4 Concluding Discussion

Four mono-Pt and four di-Pt complexes were prepared by a 'one pot' synthesis which yielded both the mono and di-Pt complexes in one synthesis. The complexes were separated by column chromatography. The UV data shows that changing the substituents on the proligand does affect the absorption and emission of the compound. By adding electron donating groups such as methoxy, there is a significant red-shift. Electron withdrawing groups such as fluorine cause a blue shift in the compound. Also an even greater red shift is achieved when there are two metals present in the compound in the order of 85-88 nm.

This trend was also shown by Laskar and co-workers[9]. They synthesised a series of 2-phenylbenzothiazolato substituted platinum(II) complexes with H (**3.16**), OMe (**3.17**), F (**3.18**) and CF_3 (**3.19**) substituents.

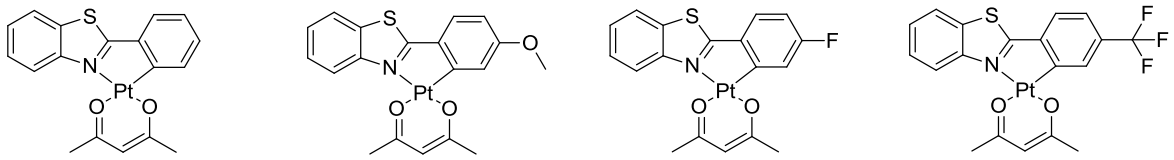

3.16 431 nm | **3.17** 423 nm | **3.18** 416 nm | **3.19** 398 nm

Figure 3.10 The series of 2-phenylbenzothiazolato substituted platinum(II) complexes

Complexes **3.18** and **3.19** are more blue shifted due to the electron withdrawing fluorines, compared to **3.16** and **3.17** which have electron donating substituents.

Chapter 4: Luminescent iridium(III) complexes incorporating cyclometallated N^C^N coordinating 1,3-di(2-pyridyl)benzene derivatives

4 Luminescent iridium(III) complexes incorporating cyclometallated N^C^N coordinating 1,3-di(2-pyridyl)benzene derivatives

The aim of this section is to synthesise a series of bis- Ir (III) complexes where metal centres are rigidly connected by a cyclometallating bridging ligand. Examples of such complexes are very rare in the literature[42,24,23,87]. This is probably due to the quite complex stereochemistry associated with the use of two or more metal centres. In this case, bidentate ligands are used. The synthesis is accompanied by the formation of a mixture of diasteromers making analysis and characterisation of the molecules difficult. For example, Tsuboyama and co-workers describe the synthesis of a red-phosphorescent dinuclear iridium complex[88](Figure 4.1). The desired di-iridium complex was isolated in only a 3% yield.

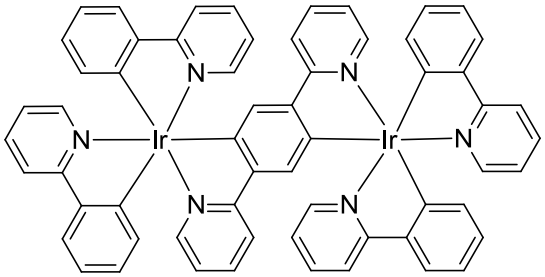

4.1
3 % Yield

Figure 4.1 $(ppy)_2Ir(\mu\text{-}BPB)Ir(ppy)_2$

One way to reduce this problem is by using *symmetrical terdentate proligands*. For example Figure 4.2 shows a variety of non-chiral mono Ir(III) complexes based on 1,5-bis(2-pyridyl)benzene that Brulatti and co-workers have recently reported[23]. This terdentate cyclometallating ligand is used in conjunction with bidentate cyclometallating unit as well as chloride ion yielding a neutral molecule. The complexes of this kind are highly luminescent with quantum yields in the region of 0.75.

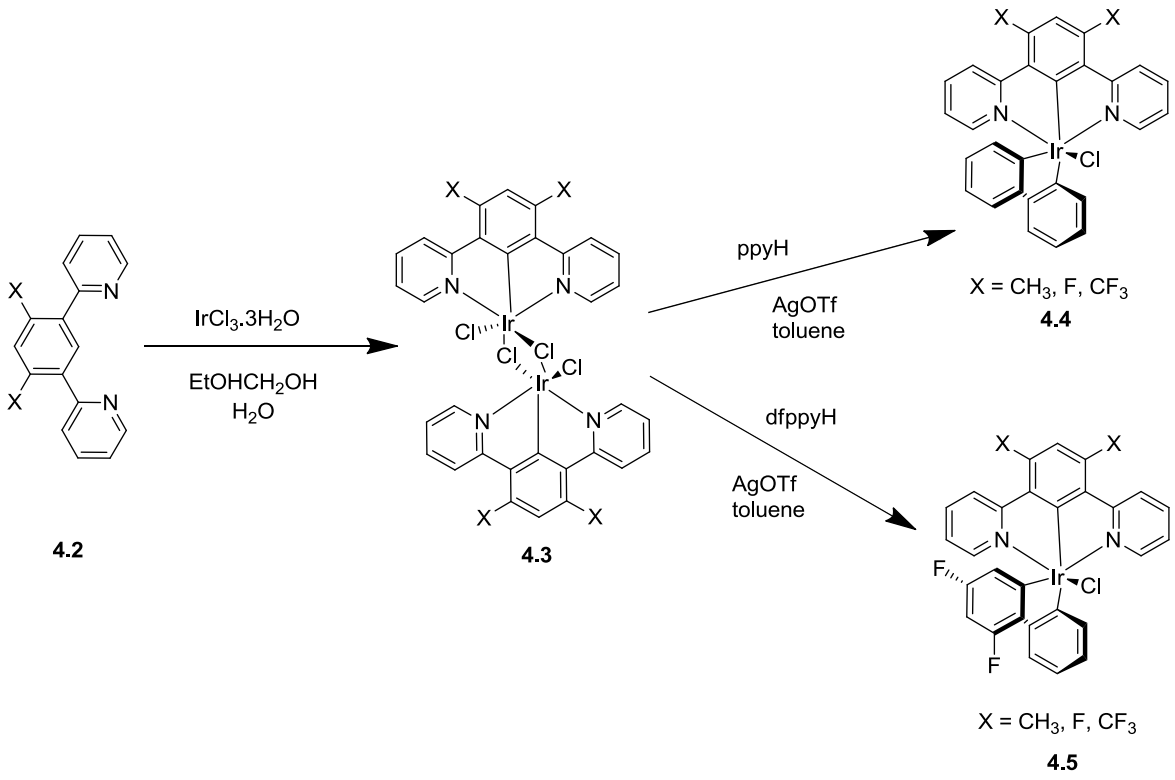

Figure 4.2 Mononuclear Iridium(III) complexes described by Brulatti and co-workers, and their preparation via the chloro-bridged dimers

We therefore decided to use this N^C^N motif and our bisbidentate bridging ligands to create rigid bimetallic complexes. It is important to mention that due to *trans*-effect of anionic carbon atoms in the ligands only *cis*-arrangement of these carbons takes place (Figure 4.3).

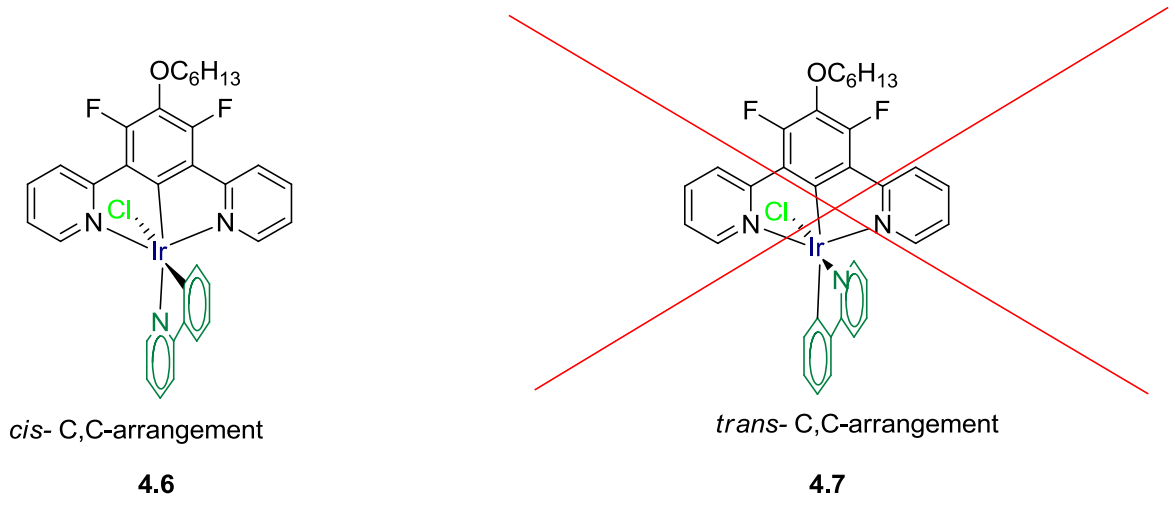

Figure 4.3 The trans effect only allows the *cis* arrangement

This is a unique feature which distinguishes these molecular systems from classical polypyridine-based architectures, known to produce mixtures of a variety of isomers. In

our targeted bis iridium (III) complexes (figure) the formation of only one stereoisomer is expected.

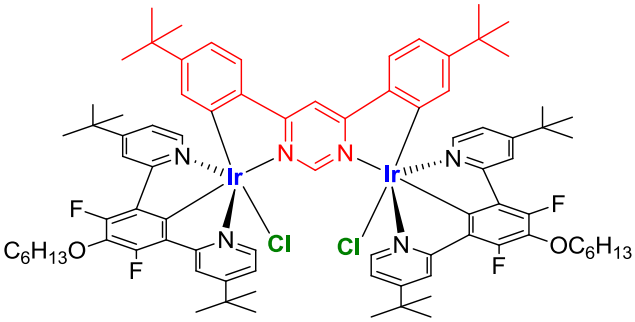

4.8

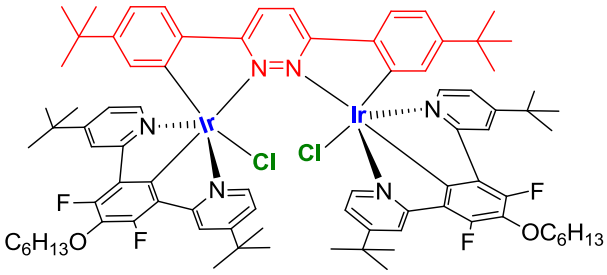

4.9

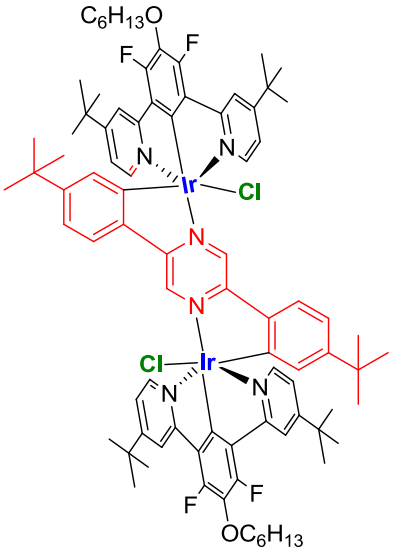

4.10

Figure 4.4 Targeted dinuclear iridium(III) complexes. Note that all coordinated carbon atoms are trans to each other.

In our systems we vary the central *bis*-bidentate cyclometallating bridging unit, while the symmetrical terdentate NCN proligand is the same for all systems. Aliphatic hexyl chains as well as *tert*-butyl groups are introduced in order to increase solubility and also to simplify the aromatic region of the ^{1}H-NMR spectra to aid characterisation. In this chapter we describe our attempts to synthesise these novel structures.

4.1 Synthesis

4.1.1 Proligand synthesis

4.1.1.1 Bis-bidentate cyclometallating proligands

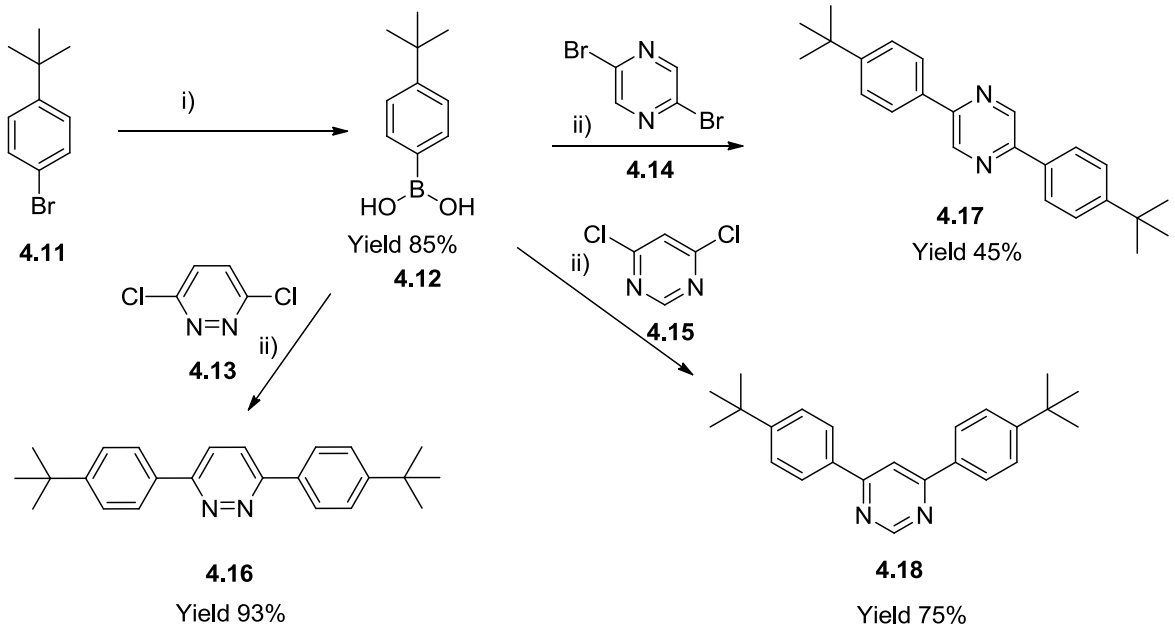

Figure 4.5 Synthesis of the starting proligands

Three ligands with linking pyrazine (**4.17**), pyrimidine (**4.18**) and pyridazine (**4.16**) heterocycles were prepared by Suzuki –Miyaura coupling of 4-*tert*-butylphenylboronic acid (**4.12**) and the corresponding dihilides (**4.13, 4.14, and 4.15**). Both the bromo and chloroderivatives of diazines can be used in this step. The starting 4-*tert*-butylphenylboronic acid (**4.12**) was prepared via lithium-halogen exchange followed by treatment with triisopropylborate and subsequent hydrolysis

4.1.1.2 Terdentate proligands

There are five synthetic steps involved to achieve the N^C^N proligand. Scheme 4.1 shows the steps involved to synthesise the terdentate proligand. The proligand contains fluorine groups at the C4 and C6 positions as competitive cyclometallation can then be avoided. The addition of the alkyl chain on the phenyl moiety, and the *tert*-butyl groups on the pyridine moieties is to improve the solubility of the resultant complex. In addition, the ^{1}H-NMR spectrum of the proligand is made easier to interpret as there are only 4 aromatic signals and less complicated spin-splitting patterns. The synthesis starts with 2,6-

difluorophenol (**4.18**) which is alkylated by 1-bromohexane in presence of potassium carbonate (step **A**) to give 1,3-difluoro-2-(hexyloxy)benzene (**4.19**).

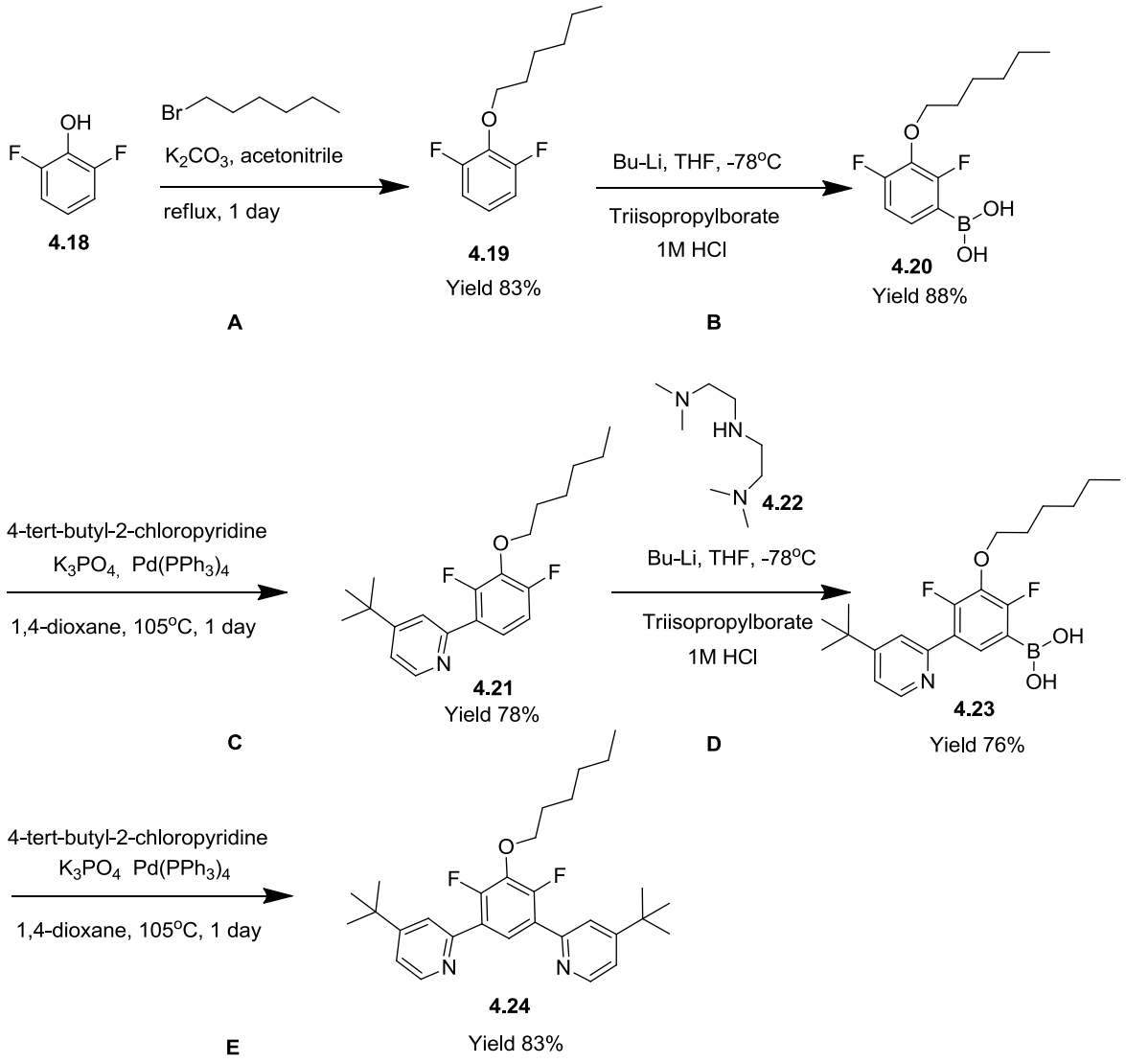

Scheme 4.1 Synthesis of the terdentate ligand

Step **B** is to synthesise the boronic acid **4.20** using n-butyllithium and triisopropyl borate. The fluorine groups are *ortho* directing ensuring that the synthesis takes place at the C1 or C3 position. Step **C** is a Suzuki reaction using 4-*tert*-butyl-2-chloropyridine, the boronic acid **4.20**, potassium phosphate and tetrakis(triphenylphosphine)palladium(0) in 1,4-dioxane, to attach one of the 4-*tert*-butylpyridine moieties (**4.21**). Step D is another boronic acid synthesis. We found that the addition of N,N,N',N'',N''-pentamethyldiethylenetriamine (**4.22**) is needed at this step. If the amine is not used a mixture of two boronic acids is formed. The undesired second boronic acid is a product of competitive *ortho*-lithiation directed by pyridine ring. The amine is used at this stage to

make the lithium more reactive. If the lithium is more reactive it will react quicker ortho to fluorine which is a stronger ortho director giving the desired boronic acid **4.23**. Step **E** is a final Suzuki synthesis to attach the second 4-*tert*-butylpyridine moiety, giving the terdentate proligand **4.24**.

4.1.2 Iridium(III) complex synthesis

4.1.2.1 Di-chloro-bridged intermediate

The chloride-bridged intermediate (**4.26**) was synthesised by reacting **4.25** with iridium chloride trihydrate[23] in a mixture of ethoxyethanol and water (3:1 ratio) and heating under reflux for 21 hours to give a yield of 84% (Scheme 4.2).

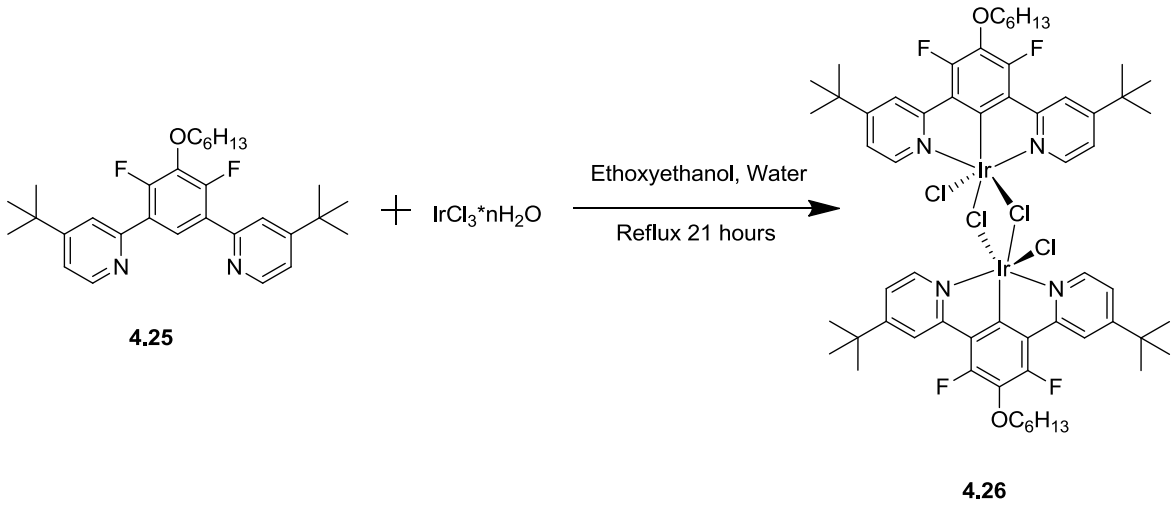

Scheme 4.2 Synthesis of dichloro-bridged intermediate

In contrast to previous reports that the chloride-bridged intermediate is too insoluble to obtain an ^{1}H-NMR[42], in our case the intermediate was found to be very soluble in $CDCl_3$ and allowed us to record ^{1}H, ^{19}F and ^{13}C-NMR spectra. Figure 4.6 shows the spectra of both the proligand (**4.25**, bottom spectra) and the chloride-bridged intermediate (**4.26**, top spectra). As can be seen clearly, the reaction took place as the triplet for the proton on the aromatic moiety is no longer present and the protons on the pyridine moiety have shifted. Protons **B** and **C** are more shielded and proton **A** is more deshielded compared to the chemical shifts of corresponding protons in the proligand.

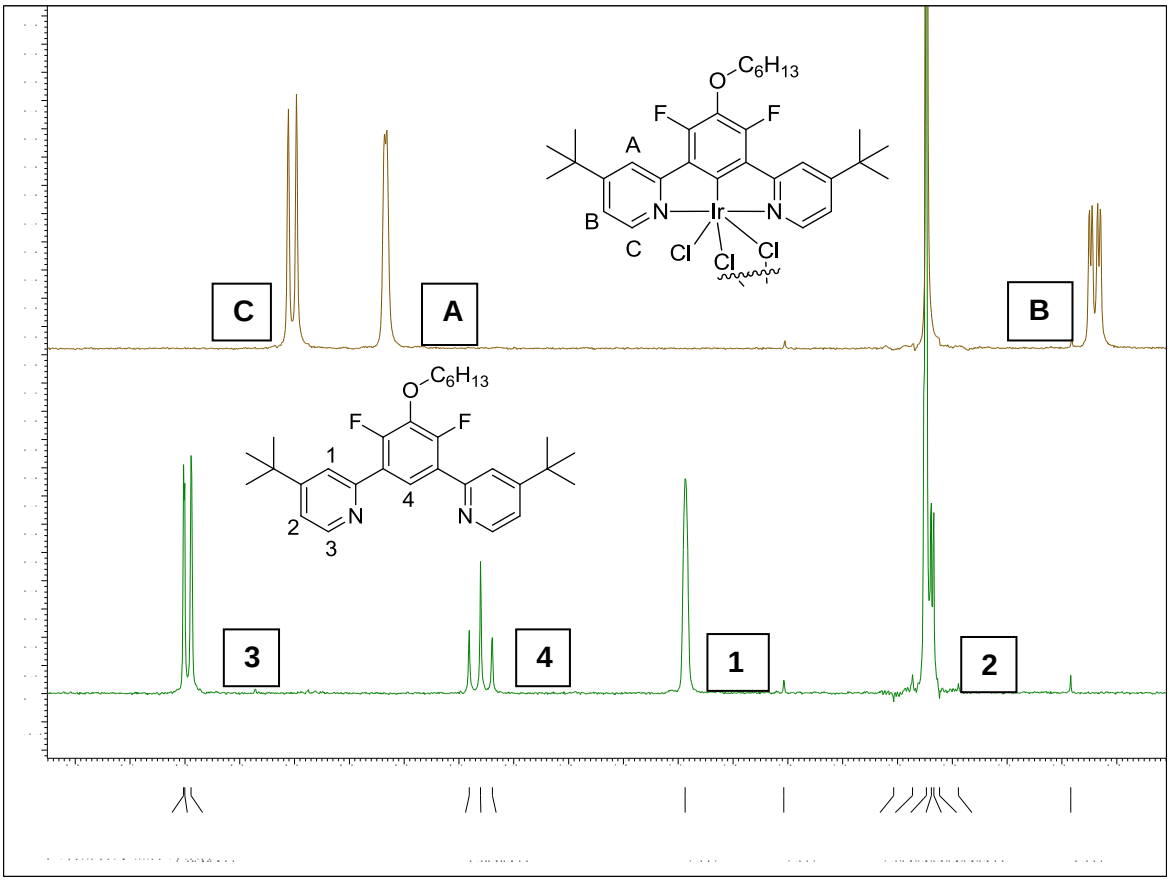

Figure 4.6 ^{1}H-NMR spectra of 4.25 (bottom spectra) and 4.26 (top spectra)

The ^{19}F spectra of the complex and the ligand also support the formation of cyclometallated complex. It can be seen (Figure 4.7) that the signal of F atoms in the ligand **4.25** is a doublet due to coupling with the proton 4. Upon coordination to Iridium (**4.26**) proton 4 is displaced by Ir and the signal becomes a singlet. The signal is also experiencing a large change in chemical shift value.

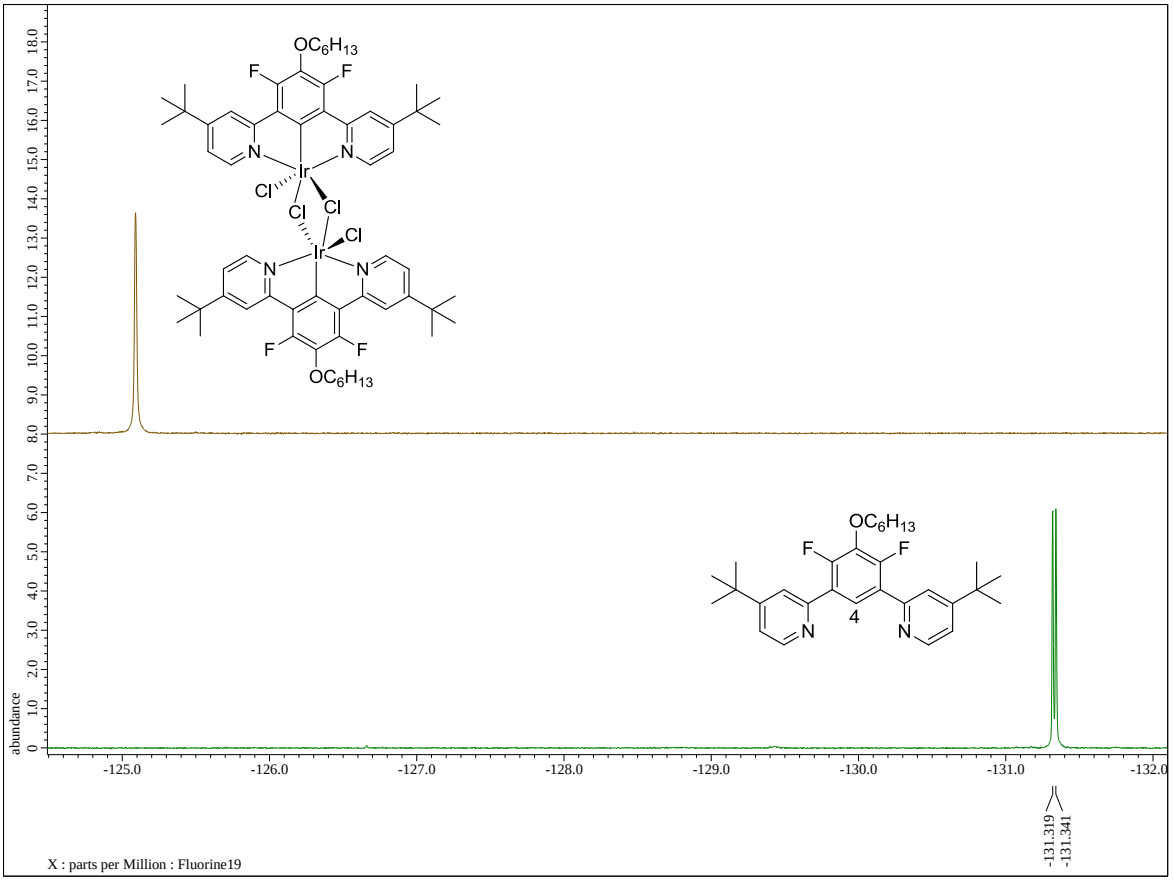

Figure 4.7 ^{19}F-NMR spectra of 4.25 (bottom spectra) and 4.26 (top spectra)

The NMR characterization of dichlorobridged Ir(III) complexes formed by NCN terdentate ligands was unprecedented in the literature. As a result of the work described above, we prepared and fully characterised key starting materials to be used in the following work.

4.1.2.2 Introduction of the central bridging unit

In our synthesis we adapted the methodology for mono Ir(III) complexes described by Brulatti and co-workers[23]. The method involves heating under reflux the mixture of dichlorobridged intermediate (**4.26**) with bidentate cyclometallating ligands in the presence of silver triflate as a chloride scavenger. Importantly, under these conditions, no scrambling of the ligands was registered. Below we describe the results of our attempts to synthesise bimetallic systems using three types of bridging ligands.

4.1.2.3 Pyrimidine-based system 4.27

Adapting known reaction conditions to our systems, the iridium(III) complexes were obtained by refluxing a mixture of **4.26** and a bis-bidentate proligand in the presence of

silver triflate in toluene. Initially the yields were quite low; but we optimised the conditions and achieved yields in the range of 50-80%. The optimised conditions are as follows- the ratio of dichloro-bridged intermediate and the bridging ligands was 1:1 which corresponds to one equivalent of bidentate coordinating unit per iridium atom. Three equivalents of silver triflate were used. The reaction time was in the range of 8-14 hours. After the reaction, the mixture was treated with excess of 2M hydrochloric acid. Column chromatography was found to reduce the yields and so best to be avoided.

Using the conditions described above, and 4,6-di(4-terbutylphenyl)pyrimidine (**4.18**) as a bridging ligand, the targeted complex **4.27** was obtained in 48% yield as a single isomer (Scheme 4.3 Synthesis of 4.27). The complex was characterised by ^{1}H, ^{19}F and ^{13}C NMR.

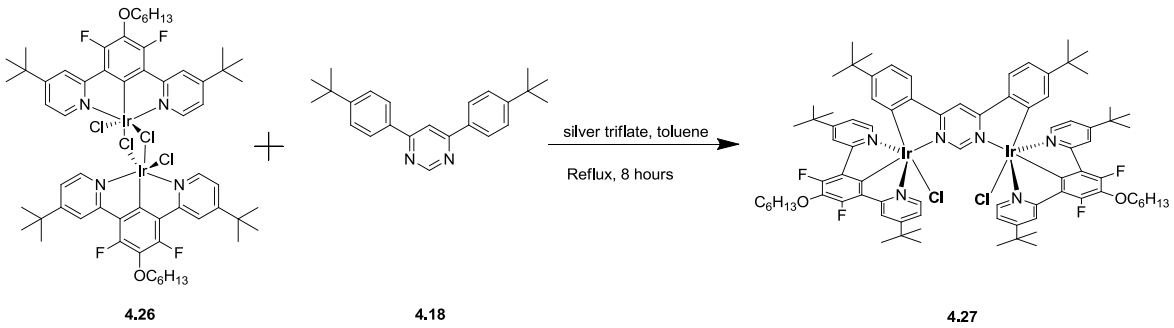

4.26 4.18 4.27

Scheme 4.3 Synthesis of 4.27

The ^{1}H NMR spectrum of the complex is depicted in Figure 4.8. The signals of all hydrogen environments can be found on the spectrum. The characteristic feature of the spectrum is that proton in the position two of the pyrimidine ring (labelled 5) has a very high chemical shift value of 11.8 ppm. This is due to the close proximity of the chlorides. Another characteristic signal at 6.3 ppm is assigned to proton which is in *ortho* position to iridium atom (labelled 1). The complex is stable at room temperature as a solid. For a solution of **4.27** in $CDCl_3$, no signs of isomerisation or degradation were registered after 1 day in day light.

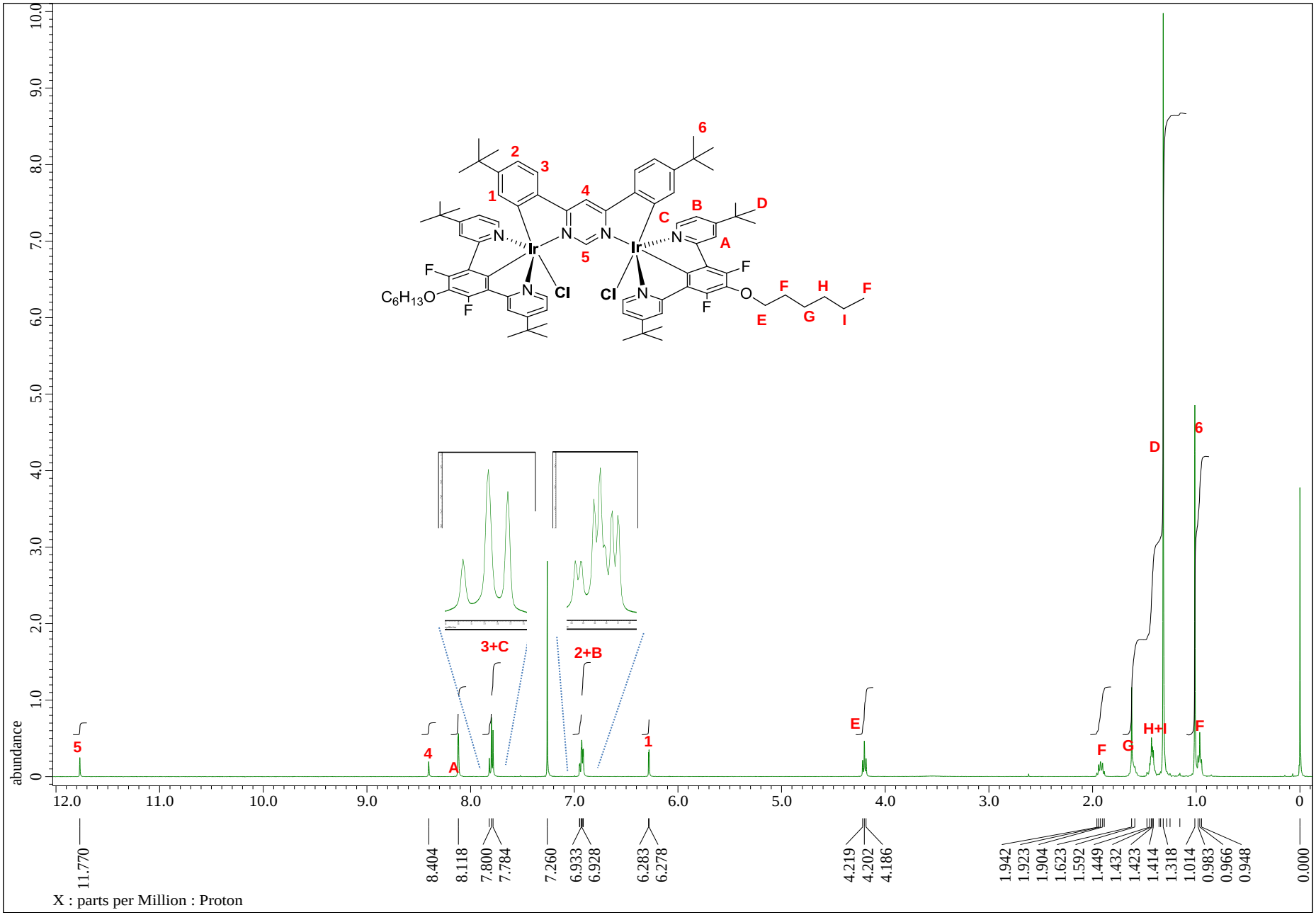

Figure 4.8 ^{1}H-NMR of complex 4.27

4.1.2.4 Pyridiazine based system 4.29

Identical conditions described for pyrimidine-based systems were applied to the pyridazine bridging ligand (**4.16**). We immediately realised that the solubility of the product was very different to pyrimidine-linked isomer **4.27**. We found for example that **4.29** is soluble in methanol while **4.27** is very insoluble in this solvent. This suggests that the product is ionic in character. One explanation would be that the iridium centres share one chloride ligand and this leads to an overall positively-charged complex. This behaviour was previously observed by Slater and co-workers[89] in corresponding Pd(II) complexes using the same bridging ligand. The counter ion in our reaction can be either chloride or triflate. To eliminate this ambiguity we decided to treat the product with excess of KPF_6 in order to prepare a uniform sample with hexafluorophosphate counter ion. The overall reaction is depicted in Scheme 4.4.

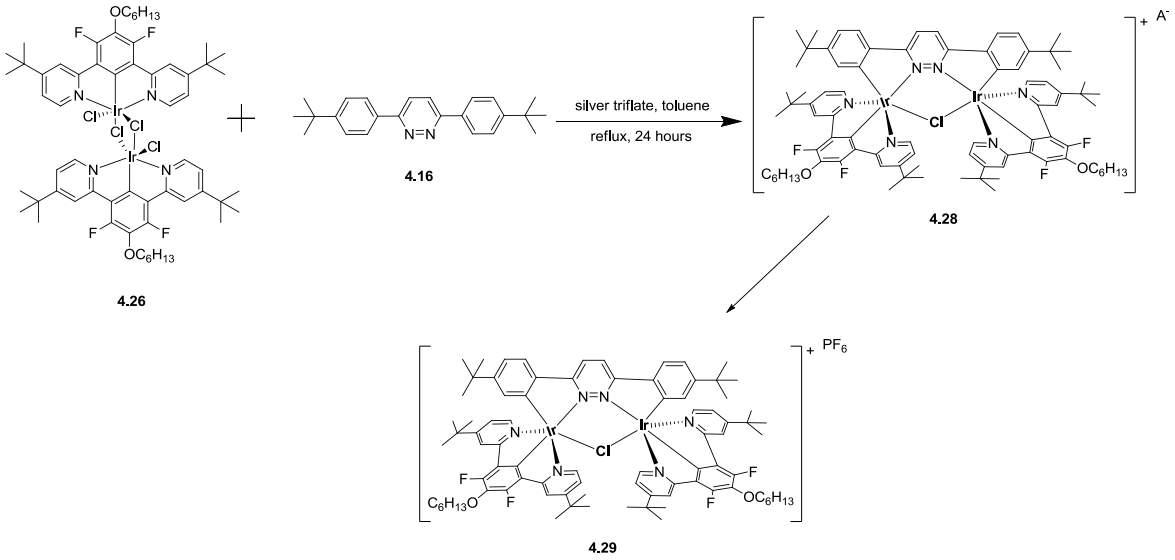

Scheme 4.4 Synthesis of complex 4.29

The yield of the reaction was very low, 3-7% for three attempts. At the moment we cannot comment why the yield is so low. Figure 4.9 and Figure 4.10 shows the ^{1}H-NMR spectra of **4.29**. As with previous case's, all signals can be assigned. ^{19}F NMR shows signals of fluoro groups in the NCN ligands as a singlet at – 125.8 ppm. There is also the signal of PF^{6} at -72.6 ppm, which is as a doublet $^{1}J_{F\text{-}P}$= 758 Hz.

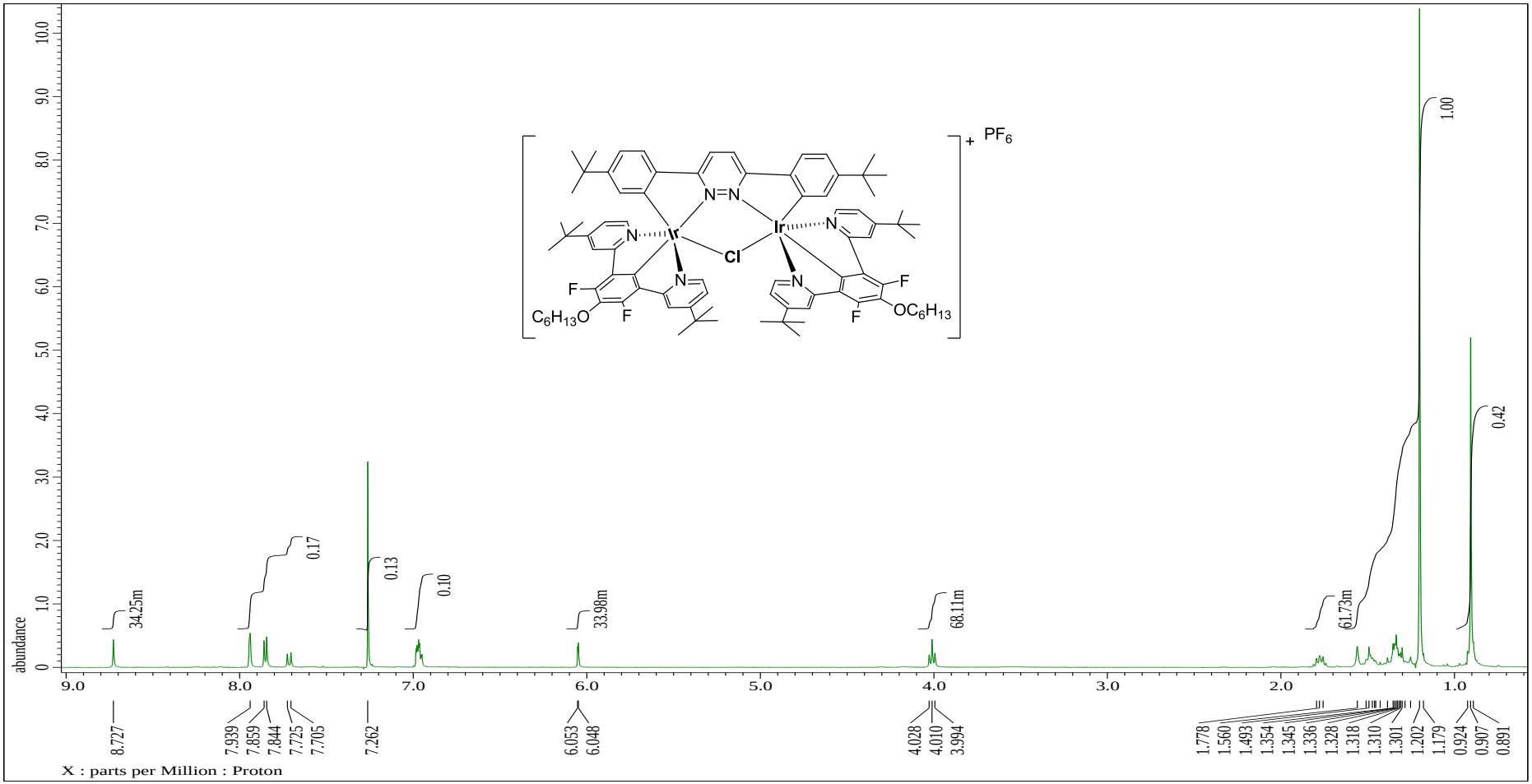

Figure 4.9 ^{1}H-NMR spectra of complex 4.29

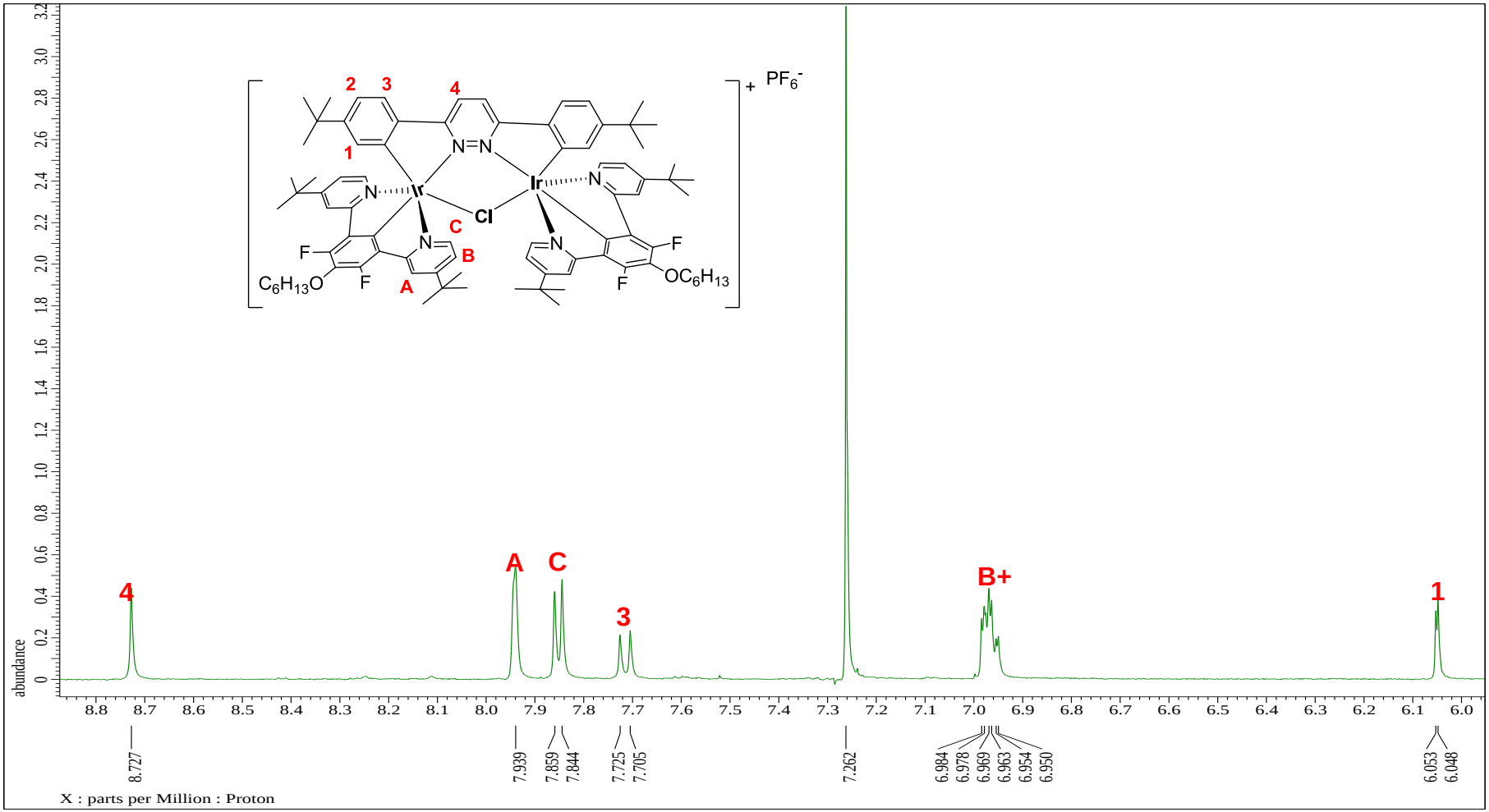

Figure 4.10 expanded aromatic region of the ^{1}H-NMR spectra for complex 4.29

The high resolution mass spec did confirm the correct mass for **4.29** of 1756 $gmol^{-1}$. Figure 4.11 shows the spectrum for the complex. It shows peaks at the correct mass for the complex but also a high abundance of a mass at 1721. This could be attributed to the presence of the complex with just one bridging chlorine atom as shown in Scheme 4.4.

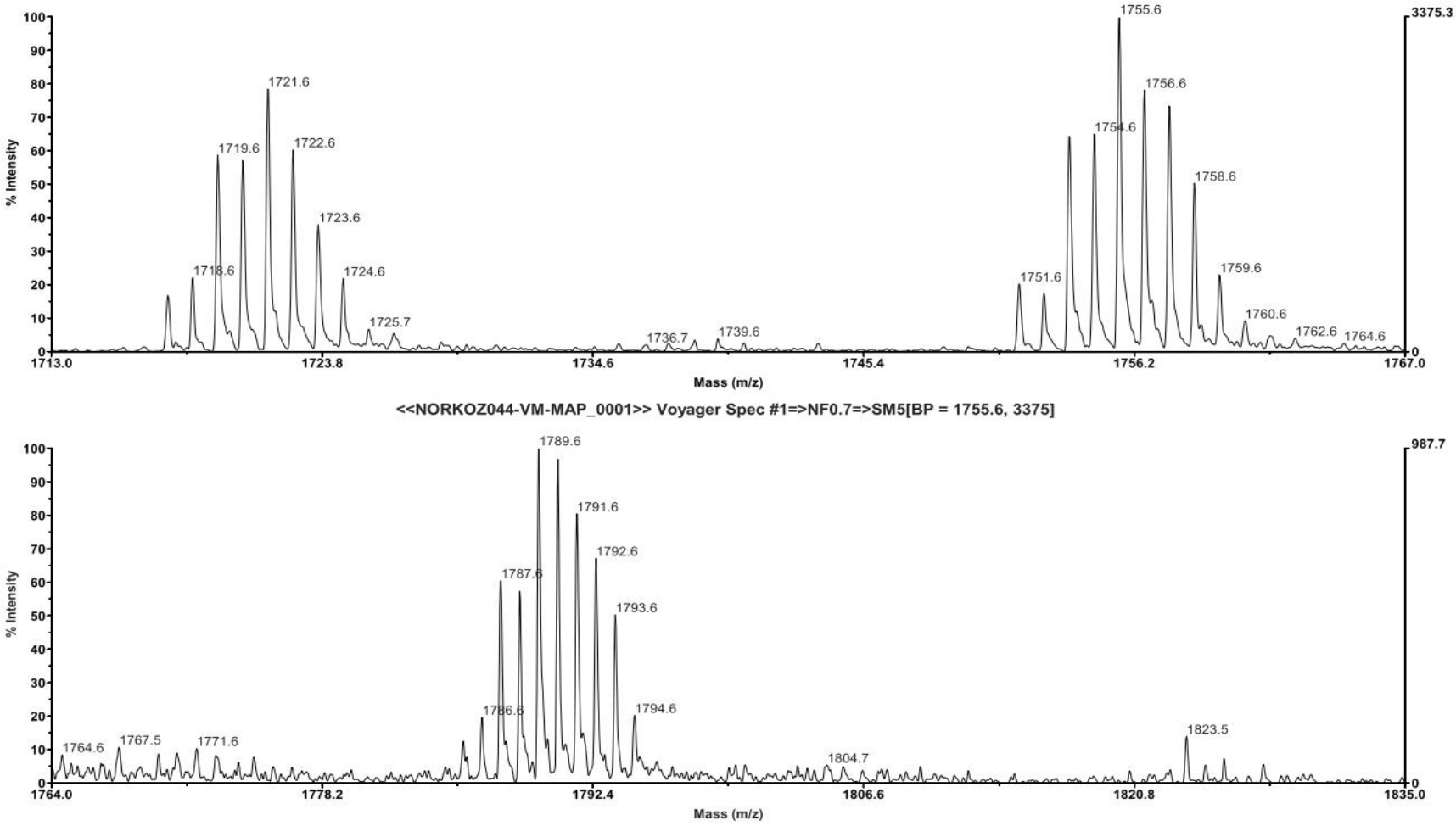

Figure 4.11 High resolution mass spec for compound 4.29

4.1.2.5 Pyrazine-based system 4.30

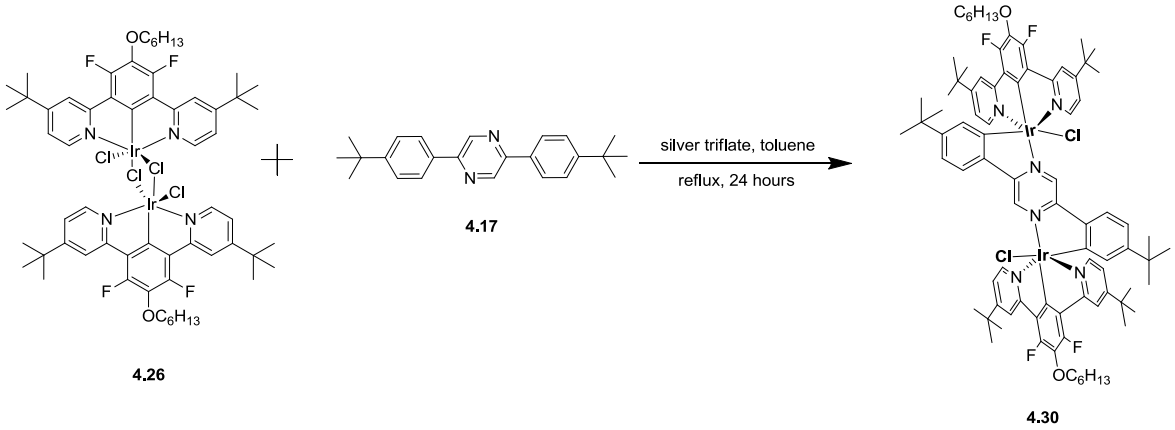

4.26 4.17 4.30

Scheme 4.5 Synthesis of complex 4.30

Scheme 4.5 shows the synthesis of the pyrazine-linked diiridium complex **4.30**. The first attempts to make this complex provided very low yields (5-10%). Based on the NMR data we can conclude that the complex did form as shown in Figure 4.12 and Figure 4.13.

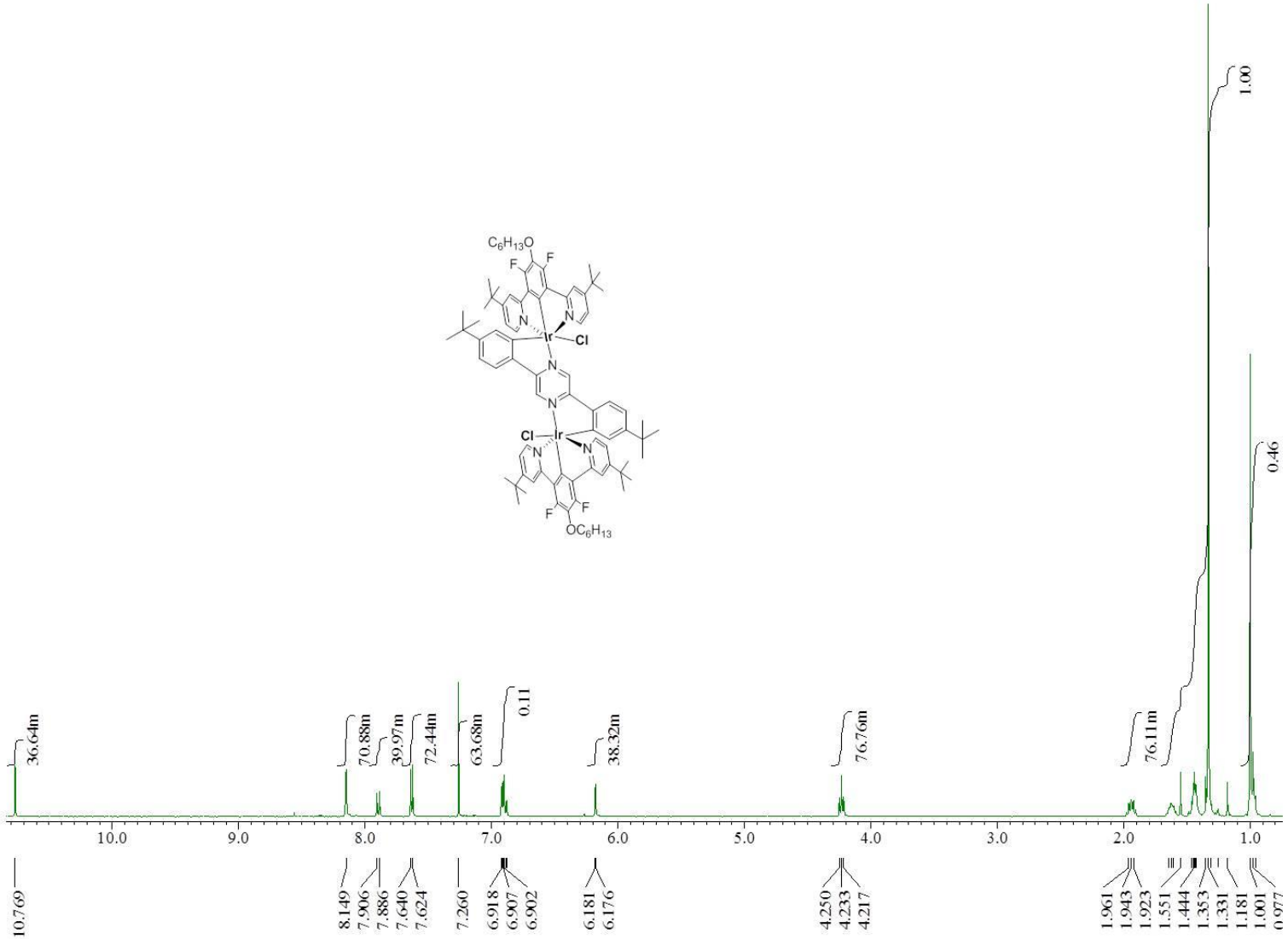

Figure 4.12 ^{1}H-NMR spectrum of pyrazine-bridged diiridium complex 4.30

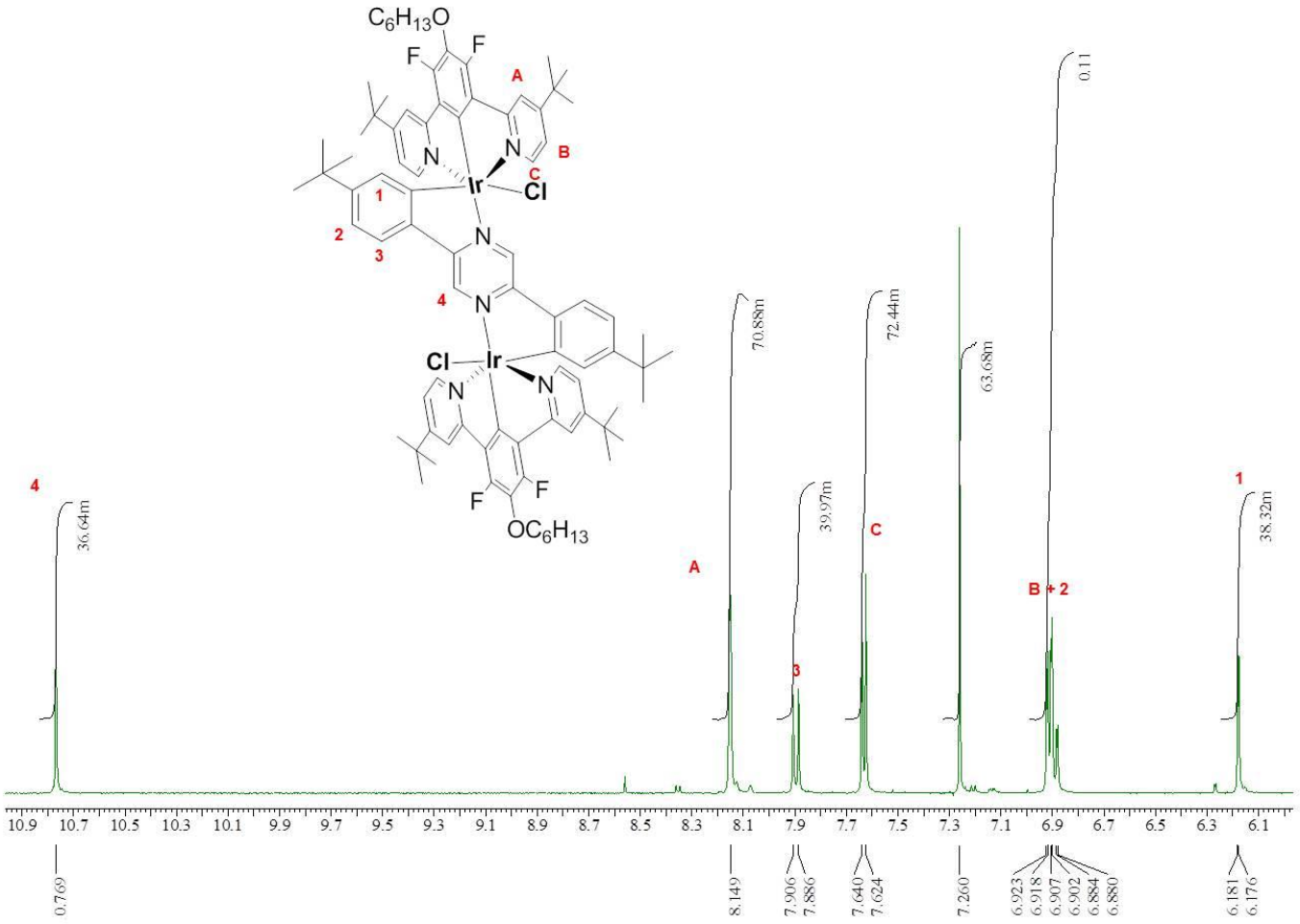

Figure 4.13 Aromatic region of ^{1}H-NMR spectrum of pyrazine-bridged diiridium complex 4.30

In order to try to establish if photodegradation was occurring, 2 identical samples were prepared by dissolving approximately 10-14 mg of the complex into 2 cm^3 of $CDCl_3$. This was then divided into two equal parts and placed into NMR tubes. One tube was wrapped in aluminium foil. Both tubes were placed on a windowsill between the hours of 10 am and 3 pm on quite a sunny day (we appreciate that we do not know exactly the spectral composition and intensity of the radiation experienced by the sample). The ^{1}H-NMR spectra were recorded at intervals (Figure 4.14). The NMR spectrum of the sample protected from the sun-light did not change over time. Conversely, the sample which was exposed to sun-light underwent a transformation. There is a formation of several species, but eventually, after approximately 15-24 hours the sample "stabilises" and is no longer changing. From this it is clear that the complex breaks down or isomerises when exposed to light. Similar behaviour was previously recorded for monometallic complexes [23]. Based on this data, the main degradation pathway is probably the loss of chloride atoms para to the cyclometallating carbon atoms. It is possible to exchange chlorides with neutral ligands such as acetonitrile to obtain dicationic complexes, which may be more stable. At the moment this is only a hypothesis. More detailed investigation is needed to determine the products and causes of photoisomerisation/transformation. Unfortunately, due to time constraints, we were not able to study this phenomena in more detail.

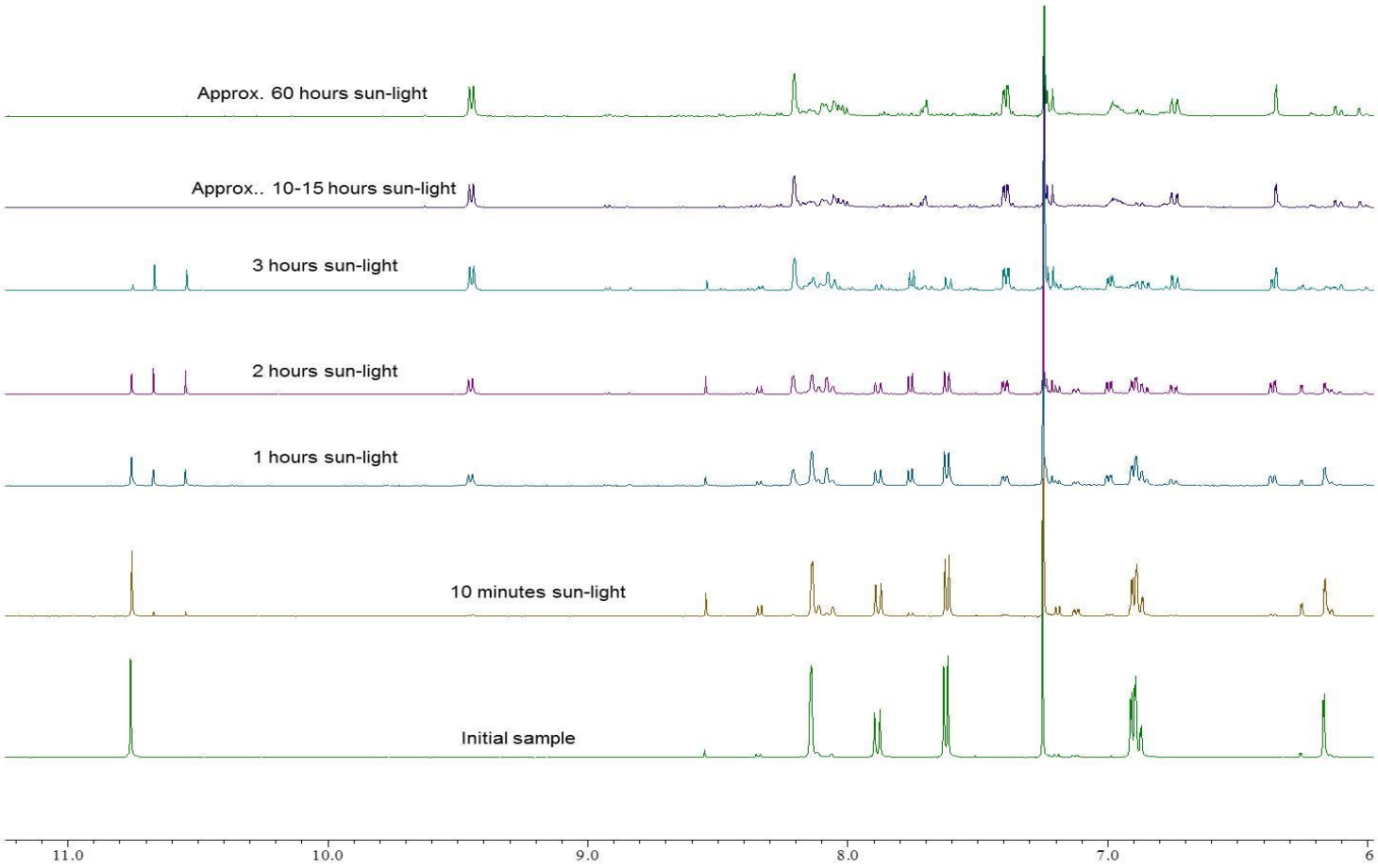

Figure 4.14 ^{1}H-NMR spectra of complex 4.30 after exposure to sun-light at various intervals

4.2 Concluding discussion

In this chapter we describe the synthesis of three unprecedented bimetallic Ir(III) complexes formed by ditopic cyclometallating C^NN^C bridging ligands and a terdentate NCN cyclometallating auxiliary ligand. The systems were carefully designed to produce a single isomer. Pyrimidine, pyrazine and pyridazines were tested as linking heterocycles and found to have a drastic influence on the outcome of the reaction.

The pyrimidine-linked complex gave the expected result with two metal centres connected by the linker and both metal centres include one terdentade, one bidentate and chloro ligands. This neutral complex is stable both in solid state and in solution and is intensely luminescent. The pyrazine-linked analogue was synthesised successfully, but was found to rapidly isomerise/decompose in $CDCl_3$ solution by the action of light leading to non-emissive products. The metal centres in the pyridazine-linked complex tend share a chloride ion to yield a positively charged ion.

These findings show that by using pyrimidine, pyrazine or pyridazine linkers, three *distinct families* of compounds rather than just structural isomers are obtained. The main result of this part of the work is that we collected valuable synthetic information, which will allow further, more detailed studies of these interesting complexes in the future.

Chapter 5: Summary

5 Summary

The purpose of this work was to synthesise and investigate the properties of a new class of cyclometallated Pt(II) and Ir(III) complexes with a rigid polymetallic assembly. The first part of the work was to investigate how the bridging ligand affects the luminescent properties of the mono-Pt and di-Pt systems. Using diphenylpyrazines to generate dinuclear platinum(II) complexes, through metallation of the two pendent phenyl rings and binding of the metal ions to the two nitrogen atoms of the central heterocycle. Both the 2,3- and 2,5-substituted isomers of diphenylpyrazine can be employed, along with diphenylquinoxaline and derivatives in which the phenyl rings are interlinked through their *ortho* positions. The introduction of the second metal ion leads, for all six ligands investigated, to a significant stabilization of the LUMO. In contrast, the HOMO energy seems to be influenced rather little. The decreased HOMO–LUMO gap that ensues leads to red-shifted absorption and emission spectra for the dinuclear complexes compared to their mononuclear analogues. Meanwhile, the increased conjugation within the heterocycle on going from a pyrazine through quinoxaline to a phenazine unit (as in L6) has a much more significant effect on the LUMO, leading to the progressive shift towards the red region observed in the optical spectra. Dinuclear cyclometallated complexes are shown to offer interesting potential for obtaining phosphorescent materials that both absorb strongly and emit brightly at unusually low energies. Further derivatisation of the diarylpyrazine unit can be confidently expected to lead to further new compounds with opportunities for controlling excited states for contemporary applications, such as in imaging and light-emitting displays.

In the second part of this work, four mono-Pt and four di-Pt complexes were prepared by a ‘one pot’ synthesis which yielded both the mono and di-Pt complexes in one synthesis. The complexes were separated by column chromatography. The study was to determine how much luminescence was affected by changing the substituents on the proligand. The UV data shows that changing the substituents on the proligand does affect the absorption

and emission of the compound. By adding electron donating groups such as methoxy, there is a significant red-shift. Electron withdrawing groups such as fluorine cause a blue shift in the compound. Also an even greater red shift is achieved when there are two metals present in the compound. This behaviour is an effective tool for the fine-tuning of luminescence properties.

In the final part of the work, we described the synthesis of three unprecedented bimetallic Ir(III) complexes formed by ditopic cyclometallating C^NN^C bridging ligands and a terdentate NCN cyclometallating auxiliary ligand. The systems were carefully designed to produce a single isomer. Pyrimidine, pyrazine and pyridazines were tested as linking heterocycles and found to have a drastic influence on the outcome of the reaction. These findings show that by using pyrimidine, pyrazine or pyridazine linkers, three *distinct families* of compounds rather than just structural isomers are obtained. The main result of this part of the work is that we collected valuable synthetic information, which will allow further, more detailed studies of these interesting complexes in the future.

Chapter 6: Experimental

6 Experimental

NMR spectra were recorded using a Jeol JNM Ex270 instrument at 270 MHz and 68 MHz or a Jeol JNM-ECS400 instrument at 400 MHz and 100 MHz, as specified, for ^{1}H- and ^{13}C- NMR respectively. ^{1}H NMR data are reported as follows: chemical shift (δ, ppm), multiplicity (s = singlet, d = doublet, t =triplet, q = quartet, m = multiplet), integration, coupling constants reported in Hz. Data for ^{13}C NMR are reported in terms of chemical shift (δ, ppm). UV/Visible spectra were run on a Varian Cary 50 UV-Visible spectrophotometer (range 600-200 nm), using a 10mm quartz cell at room temperature (18-22 °C). Infrared spectra were obtained using Durascope diamond ATR system on a Perkin Elmer RX1 FTIR spectrometer. Positive and negative electrospray ionisation mass spectrometry (ESI-MS) was conducted using a Thermo LCQ Advantage spectrometer by direct injection and high resolution mass spectrometry (HRMS) was performed by the EPSRC National Mass Spectrometry Service (Swansea, Wales) on a Thermofisher LTQ Orbitrap XL mass spectrometer low-resolution electrospray (ESI) or high-resolution nanoelectrospray (NSI) ionization techniques. Melting points were taken on a SRS DigiMelt MPA161 digital melting point apparatus (200 to 250 VAC 1/2AMP 50-60Hz). CHN analysis was performed by Richard Baron from the department of Advanced Materials and Chemical Analysis in the School of Chemistry, Newcastle University using a Carlo Erba 1108 Elemental Analyser controlled with CE Eager 200 software, run in accordance with the manufacturer's instructions and samples weighed using a certified Mettler MX5 Microbalance.

6.1 Ligand Synthesis

6.1.1 Compound 2.1

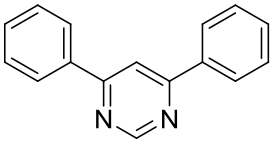

Phenylboronic acid (1 g, 8.20 mmol) and 4,6-dichloropyrimidine (469 mg, 3.15 mmol) were dissolved in 1,4-dioxane (25 cm^3) and the reaction mixture was then deairated by bubbling N_2 through the mixture for 10 minutes. Aqueous K_2CO_3 solution (2M, 9 cm^3, 18.8 mmol) and tetrakis(triphenylphosphine)palladium(0) (220 mg, 0.19 mmol) were added and the mixture deairated for a further 15 minutes. The reaction mixture was then stirred at 95°C under N_2 for 24 h. The solvents were removed under vacuum and DCM (35 cm^3) was added. The organic layer was separated, washed with water (3 × 35 cm^3), dried over $MgSO_4$, filtered and evaporated to dryness. The product was then purified by column chromatography using silica gel and ethyl acetate / DCM (1:4 ratio) as the eluent; yield 680 mg, 93%. ^{1}H NMR ($CDCl_3$, 270MHz) δ 9.31 (1H, d, *J* = 1.2 Hz), 8.16-8.12 (4H, m), 8.10 (1H, d, *J* = 1.5 Hz), 7.55-7.50 (6H, m). ^{13}C NMR ($CDCl_3$, 68 MHz) δ_C 164.8, 159.3, 137.1, 131.0, 129.1, 127.2, 112.9. IR = 2958.8, 2902.9, 2866.1, 1583.7, 831.6, 694.2 cm^{-1}. MS (ESI): *m/z* 233 $[M+H]^+$. Elemental analysis calcld for $C_{16}H_{12}N_2$: C 82.73, H 5.21, N 12.06 %; found C 82.85, H 5.33, N 11.92 %[90].

6.1.2 Compound 2.2

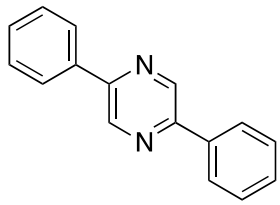

Method A. Suzuki synthesis: Phenylboronic acid (1 g, 8.20 mmol) and 2,5-dibromopyrazine (750 mg, 3.15 mmol) were dissolved in 1,4-dioxane (25 cm^3) and the reaction mixture then degassed by bubbling N_2 through it for 10 minutes. 2M aqueous K_2CO_3 solution (9 cm^3, 18.84 mmol) and tetrakis(triphenylphosphine)palladium(0) (6% mol, 220 mg, 0.19 mmol) was added and the reaction mixture degassed for a further 15 minutes. The reaction mixture was then stirred at 95°C for 24 hours under N_2. On cooling, water was added and the resulting precipitate was filtered and dried. The residue was then recrystallized from ethanol and activated charcoal. Yield 390 mg, 53%. Melting point 194-197°C (lit. 194°C). ^{1}H NMR ($CDCl_3$, 270 MHz) δ_H 9.07 (2H, d, *J* = 0.7 Hz), 8.08–8.03 (4H, m), 7.56-7.46 (6H, m). ^{13}C NMR ($CDCl_3$, 100 MHz) δ 150.8, 141.4, 136.4, 129.9, 129.2, 126.9.

Method B. Synthesis from 2-bromoacetophenones: 2-Bromoacetophenone (18 g, 0.09 mol) was dissolved in ethanol (150 cm^3) and aqueous ammonia (35 %, 100 cm^3) was added. The solution was left stirring at 50°C overnight. Hydrogen peroxide (30 cm^3) was then added and the mixture was left stirring at room temperature for 2 days. The precipitate was filtered off and recrystallized from acetic acid. Yield 2.6 g, 13 %. ^{1}H NMR ($CDCl_3$, 400MHz) δ 9.08 (2H, s), 8.07-8.05 (4H, m), 7.56-7.46 (6H, m). ^{13}C NMR ($CDCl_3$, 400MHz) δ150.8, 141.4, 136.37, 129.9, 129.2, 126.9[85,86].

6.1.3 Compound 2.4

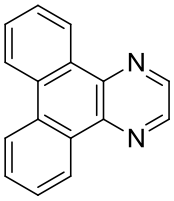

A solution of 9,10-phenanthenequinone (5.3 g, 25 mmol) and ethanol (100 cm^3) was refluxed for 5 minutes. Ethylenediamine (1.9 g, 32 mmol) was added and the solution heated under reflux for 1 hour. Acetic acid (200 cm^3) was added and the solution heated under reflux for 15 hours. The volume of the solution was then reduced to 150 cm^3 by rotary evaporation and again heated under reflux for 1 hour. The solution was then allowed to cool to room temperature and the precipitate solid was filtered. Yield 3.09 g, 46%. ^{1}H-NMR (270 MHz, $CDCl_3$) δ_H 9.22 (2H, dd, J = 7.92, 1.7 Hz), 8.90 (2H, s), 8.63 (2H, d, J = 7.42), 7.77 (4H, m). ^{13}C NMR ($CDCl_3$, 400MHz) δ_C 143.60, 141.55, 131.51, 129.97, 129.68, 127.79, 125.47, 122.85[74].

6.1.4 Compound 2.6

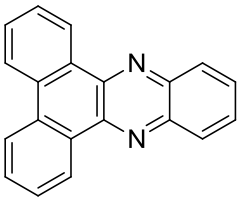

A solution of 9,10-phenanthenequinone (2.08 g, 0.01 mol) and ethanol (180 cm^3) was refluxed until dissolved. O-phenylenediamine (1.08 g, 0.01 mol) and ethanol (20 cm^3) was added and the solution heated under reflux for a further 10 minutes. A drop of conc. HCl was added and a precipitate is formed. The solution was then heated under reflux for 2 hours. The precipitate solid was filtered and washed with ethanol. Solid was then recrystallized from chloroform. Yield 1.97 g, 70 %. ^{1}H-NMR (400 MHz, $CDCl_3$) δ_H 9.41 (2H, dd, *J* = 7.79, 1.8 Hz), 8.57 (2H, d, *J* = 7.79 Hz), 8.35-8.31 (2H, m), 7.87-7.83 (1H, m), 7.82-7.73 (3H, m). ^{13}C NMR ($CDCl_3$, 400MHz) δ_C 142.52, 142.27, 132.13, 130.40, 129.84, 129.54, 128.02, 126.34, 123.00[75].

6.1.5 Compound 3.1

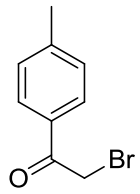

4'-methylacetophenone (27 g, 0.2 mol) was dissolved in diethyl ether (400 cm^3). Bromine (32 g, 0.2 mol) was added drop wise. The solution was then washed consecutively with water, sodium bicarbonate and water (50 cm^3 portions) and the diethyl ether evaporated. Yield 36 g, 84 %. ^{1}H NMR ($CDCl_3$, 400MHz) δ 7.88 (2H, d, *J* = 7.5 Hz), 7.28 (2H, d, *J* = 7.2 Hz), 4.56 (2H, s), 2.34 (3H, s)[91].

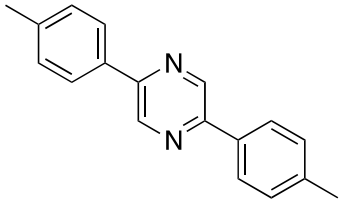

The 2-bromo-1-(*p*-tolyl)ethanone (36 g, 0.17 mol) was dissolved in ethanol (250 cm^3) and Aqueous ammonia (35 %, 140 mL) was added. The solution was left stirring at 50°C overnight. Hydrogen peroxide (20 cm^3) was then added and left stirring at room temperature for 2 days. The precipitate was recrystallized from acetic acid, washed with ethanol and dried. Yield 4.8 g, 11 %. Melting point 199-202°C. ^{1}H NMR ($CDCl_3$, 400MHz) δ 9.02 (2H, s), 7.95 (4H, d, *J* = 9.0 Hz), 7.32 (4H, d, *J* = 8.4 Hz), 2.43 (6H, s). ^{13}C NMR ($CDCl_3$, 400MHz) δ_C 157.9, 143.1, 141.6, 138.5, 129.1, 125.9, 106.8, 57.1, 44.0, 12.3[92].

6.1.6 Compound 3.2

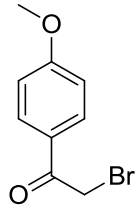

4’-methoxyacetophenone (30 g, 0.20 mol) was dissolved in diethyl ether (400 cm^3). Bromine (32 g, 0.20 mol) was added drop wise. The precipitated solid was then filtered and dried. Yield 30 g, 67 %. ^{1}H NMR ($CDCl_3$, 400MHz) δ 7.83 (2H, d, *J* = 8.2 Hz), 7.10 (2H, d, *J* = 8.7 Hz), 4.56 (2H, s), 3.83 (2H, s)[92].

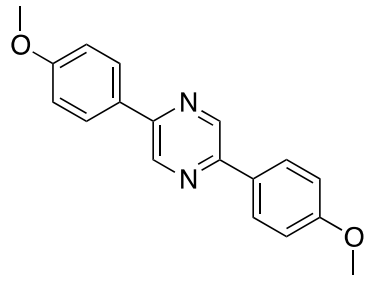

The 2-bromo-4’-methoxyacetophenone (10 g, 0.04 mol) was dissolved in ethanol (150 cm^3) and aqueous ammonia (35 %, 100 cm^3) was added. The solution was left stirring at 50°C overnight. Hydrogen peroxide (30 cm^3) was then added and left stirring at room temperature for 2 days. The precipitate was filtered off, washed with ethanol. The product was then purified by recrystallization from acetic acid. Yield 2.4 g, 21%. Melting point 226-228°C. ^{1}H NMR ($CDCl_3$, 400MHz) δ 8.96 (2H, s), 8.00 (4H, d, *J* = 10.4 Hz), 7.03 (4H, d, *J* = 10.9 Hz), 3.87 (6H, s). ^{13}C NMR ($CDCl_3$, 400MHz) δ_C 161.0, 149.7, 140.6, 129.1, 128.1, 114.6, 55.5[92].

6.1.7 Compound 3.3

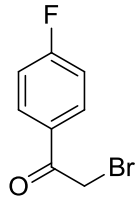

4'-fluoroacetophenone (25 g, 0.18 mol) was dissolved in diethyl ether (400 cm^3). Bromine (29 g, 0.18 mol) was added drop wise. The solution was then washed consecutively with water, sodium bicarbonate and water (50 cm^3 portions). 2-propanol (100 cm^3) was added and the flask was then placed into ice. The resulting precipitate was then filtered and dried. Yield 11.5 g, 30 %. ^{1}H NMR ($CDCl_3$, 400MHz) δ 8.12 (2H, m), 7.35 (2H, m), 4.56 (2H, s)[93].

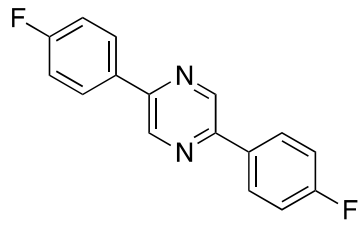

The 2-bromo-1-(4-fluorophenyl)ethanone (11.5 g, 0.05 mol) was dissolved in ethanol (150 cm^3) and aqueous ammonia (35 %, 100 mL) was added. The solution was left stirring at 50 ^{o}C overnight. Hydrogen peroxide (30 cm^3) was then added and left stirring at room temperature for 2 days. The precipitate was filtered and dried. Yield 1.26 g, 10 %. Melting point 229-232 °C. ^{1}H NMR ($CDCl_3$, 400MHz) δ 9.01 (2H, s), 8.07-8.03 (4H, m), 7.25-7.19 (4H, m). ^{13}C NMR ($CDCl_3$, 400MHz) δ_C 140.9, 128.8, 128.7, 116.4, 116.1

6.1.8 Compound 4.16

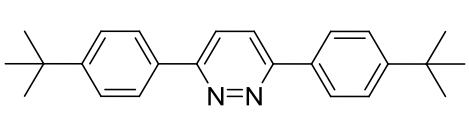

4-*tert*-butylphenylboronic acid (1 g, 5.65 mmol) and 3,6-dichloropyridazine (323 mg, 2.17 mmol) were dissolved in 1,4-dioxane (60 cm^3) and the solution then degassed by bubbling N_2 through it for 10 minutes. 2M aqueous K_2CO_3 solution (7 cm^3, 13 mmol) and tetrakis(triphenylphosphine) palladium (6% mol, 150 mg, 0.13 mmol) was added and the solution degassed for a further 15 minutes. The reaction mixture was then stirred at 95^{o}C for 24 hours under N_2. On cooling, product had crashed out. Filtered and washed with methanol. Yield 692 mg, 93%. ^{1}H-NMR (400 MHz, $CDCl_3$) δ 8.09 (d, 4H, *J* = 8.4), 7.89 (s, 2H), 7.55 (d, 4H, *J* = 6.4), 1.37 (s, 18H).

6.1.9 Compound 4.17

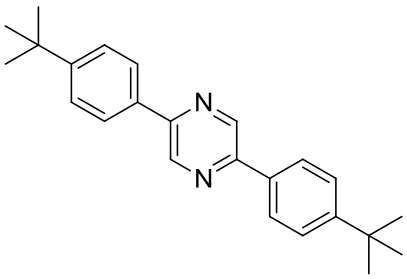

Potassium phosphate (2.6 g, 12.42 mmol) was dissolved in water (10 cm^3) and the solution was degassed by bubbling nitrogen through the mixture for 10 minutes. A mixture of (4-*tert*-butylphenyl)boronic acid (1.1 g, 6.21 mmol), 2,5-dibromopyrazine (985 mg, 4.14 mmol) and 1,4-dioxane (50 cm^3) was degassed for 10 minutes. Tetrakis triphosphine palladium(0) (289 mg, 0.25 mmol) and the solution of K_3PO_4 was then added and degassed for a further 15 minutes. The solution was then stirred under nitrogen at 105 ^oC for 24 hours. On cooling a precipitate started to form. Water was added and more precipitate was formed. The precipitate was filtered using Buchner filtration and was washed with water. The solid was recrystallized from acetic acid by hot filtration. Yield 623 g, 45 %. ^{1}H-NMR (400 MHz, $CDCl_3$) δ 9.04 (2H, d, *J* = 1.4 Hz), 7.99 (4H, d, *J* = 8.2 Hz), 7.54 (4H, d, *J* = 8.7 Hz), 1.36 (18H, s). ^{13}C NMR ($CDCl_3$, 400MHz) δ_C 153.10, 150.42, 141.13, 133.63, 126.56, 126.13, 34.90, 31.35.

6.1.10 Compound 4.18

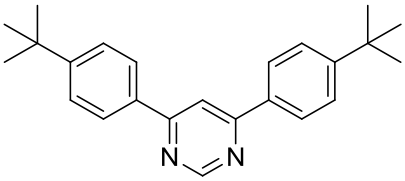

4-*tert*-butylphenylboronic acid (1 g, 5.65 mmol) and 4,6-dichloropyrimidine (323 mg, 2.17 mmol) were dissolved in 1,4-dioxane (25 cm^3) and the solution then degassed by bubbling N_2 through it for 10 minutes. 2M aqueous K_2CO_3 solution (7 cm^3, 13.02 mmol) and tetrakis(triphenylphosphine)palladium(0) (154 mg, 0.13 mmol) was added and the solution degassed for a further 15 minutes. The reaction mixture was then stirred at 95°C for 24 hours under N_2. 1,4-Dioxane was removed and the product dissolved in DCM (25 cm^3). The solution was washed with water (3 x 25 cm^3), dried over $MgSO_4$ and the solution was then evaporated to dryness. The residue was purified by column chromatography using silica gel and ethyl acetate/DCM (1:4 ratio) as the eluent. The column chromatography was then repeated using ethyl acetate/hexane (1:4 ratio) as the eluent. Yield 560 mg, 75%. Melting point 154-157°C. ^{1}H NMR ($CDCl_3$, 270MHz) δ 9.26 (1H, d, *J* = 1.2 Hz), 8.09-8.03 (5H, m), 7.54 (4H, d, *J* = 8.7 Hz), 1.35 (18H, s). ^{13}C NMR ($CDCl_3$, 68MHz) δ164.5, 159.2, 154.4, 134.3, 127.0, 126.1, 112.3, 34.9, 31.3. IR = 2958, 1583, 1505, 1464, 1362 cm^{-1}. MS (ESI): *m/z* 345 $[M+H]^+$. Elemental analysis calcld for $C_{24}H_{28}N_2$: C 83.68, H 8.19, N 8.13; found C 83.43, H 8.64, N 7.68[43].

6.1.11 Compound 4.19

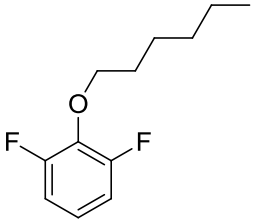

A mixture of K_2CO_3 (41.4 g, 300 mmol), acetonitrile (100 cm^3), 2,6-difluorophenol (13 g, 100 mmol) and 1-bromohexane (16.5 g, 100 mmol) was heated under reflux for 21 hours. Petroleum ether (100 cm^3), and water (100 cm^3) were added. The aqueous layer was then separated and washed with petrol ether (30 cm^3). All organic layers were combined, dried over $MgSO_4$, filtered and then volatiles evaporated under reduced pressure. The product was a colourless liquid. Yield 17.8 g, 83 %. ^{1}H-NMR (400 MHz, $CDCl_3$) δ 6.88 (m, 3H), 4.11 (t, 2H, *J* = 6.4 Hz), 1.75 (q, 2H, *J* = 6.9 Hz), 1.46 (m, 2H), 1.32 (m, 4H), 0.90 (t, 3H, *J* = 6.9 Hz). ^{13}C NMR ($CDCl_3$, 400MHz) δ_C 157.7, 155.2, 136.0, 122.5, 112.2, 112.1, 74.8, 31.8, 30.0, 25.4, 22.7, 14.0.

6.1.12 Compound 4.20

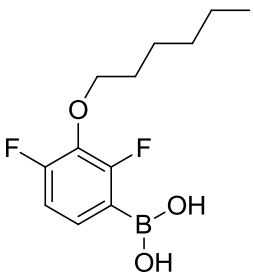

To a stirred solution of 2,4-difluor-3-n-hexyloxybenzene (9 g, 42 mmol) in dry THF (50 cm^3) at -78^{o}C, *n*-butyllithium (1.6 M solution in hexane, 31 cm^3, 50 mmol) was added slowly. The solution was stirred at -78^{o}C for 2 hours. Triisopropylborate (14 cm^3, 63 mmol) was added slowly and the mixture was stirred at -78^{o}C for 1 hour. The flask was then left to come up to room temperature whilst stirring for ~19 hours. The mixture was then acidified by the addition of 1M aqueous hydrochloric acid (50 cm^3). The mixture was separated and the organic layer was washed with brine (20 cm^3) then water (10 cm^3). All volatiles were then reduced by rotary evaporation under reduced pressure. The residue was then treated with petroleum ether (40 cm^3) and left standing at room temperature for 2 hours. The solid formed was then filtered off, washed with petroleum ether and dried. Yield 9.56 g, 89%. 1H-NMR (400 MHz, CDCl3) δ 7.47 (q, 1H, J = 6.9 Hz), 6.93 (ddd, 1H, J = 11.9, 1.8 Hz), 4.92 (d, 2H, J = 6.4 Hz), 4.09 (t, 2H, J = 6.4 Hz), 1.74 (q, 2H, J = 6.9 Hz), 1.49-1.42 (m, 2H), 1.33-1.30 (m, 4H), 0.91-0.88 (m, 3H). ^{13}C-NMR ($CDCl_3$, 400MHz) δ_C 157.4, 135.2, 129.9, 122.5, 112.9, 112.2, 31.6, 29.9, 26.6, 25.4, 22.6, 14.1.

6.1.13 Compound 4.21

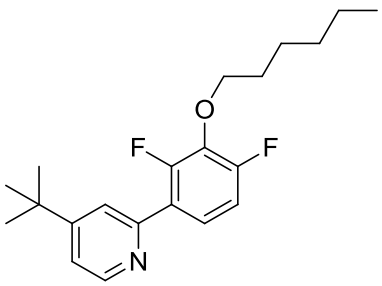

Potassium phosphate (8.2 g, 38.7 mmol) was dissolved in water (20 cm^3) and the solution was degassed by bubbling nitrogen through the mixture for 10 minutes. A mixture of [2,4-difluoro-3-(hexyloxy)phenyl]boronic acid (5 g, 19.4 mmol), 4-*tert*-butyl-2-chloropyridine (2.2 g, 12.9 mmol) and 1,4-dioxane (60 cm^3) was degassed for 10 minutes. Tetrakis(triphosphine)palladium(0) (889 mg, 0.77 mmol) and the solution of K_3PO_4 was then added and degassed for a further 15 minutes. The solution was then stirred under nitrogen at 105^oC for 24 hours. Toluene (10 cm^3) was added and the aqueous layer was removed. The organic layer was evaporated to dryness by rotary evaporation under reduced pressure. The product was then purified by column chromatography (silica gel, petroleum ether/ethyl acetate 5:1). Yield 3.54 g, 78%. ^{1}H-NMR (400 MHz, CDCl3) δ 8.57 (1H, d, *J* = 5.04 Hz), 7.69-7.67 (1H, s), 7.55 (1H, q, *J* = 8.70, 5.95, 2.75 Hz), 7.22 (1H, dd, *J* = 5.04, 1.83 Hz), 6.96 (1H, ddd, *J* = 10.07, 8.70, 1.83 Hz), 4.14 (2H, t, *J* = 6.87 Hz), 1.80-1.70 (2H, m), 1.50-1.41 (2H, m), 1.34-1.27 (13H, s), 0.89-0.84 (3H, m). ^{13}C NMR ($CDCl_3$, 400MHz) δ_C 157.71, 155.24, 136.37, 122.41, 112.09, 40.39, 30.23, 29.23, 23.59, 23.12, 14.07, 10.99.

6.1.14 Compound 4.23

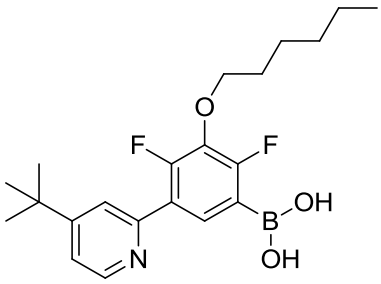

To a stirred solution of 4-*tert*-butyl-2-[2,4-difluoro-3-(hexyloxy)phenyl]pyridine (2.7 g, 7.8 mmol) and N, N, N', N'', N''-pentamethyldiethylenetriamine (1.4 g, 8.6 mmol) in dry THF (50 cm^3) at -78^oC, *n*-butyllithium (1.6 M solution in hexane, 5 cm^3, 8.6 mmol) was added slowly. The solution was stirred at -78^oC for 2 hours. Triisopropylborate (3 cm^3, 11.7 mmol) was added slowly and the mixture was stirred at -78^oC for 1 hour. The flask was then left to come up to room temperature whilst stirring for ~19 hours. The mixture was then neutralised by the addition of 1M aqueous hydrochloric acid (70 cm^3). The aqueous layer was separated and the organic layer was washed with brine (20 cm^3) then water (10 cm^3). Volatiles were then removed by rotary evaporation. The residue was then treated with petroleum ether and filtered. Yield 2.31 g, 76%. ^{1}H-NMR (400 MHz, CDCl3) δ 8.66 (1H, br.s), 7.99 (1H, t, *J* = 15.11, 7.79 Hz), 7.68 (1H, br.s), 7.64 (1H, br.s), 7.27 (1H, br.s), 4.09 (2H, t, *J* = 12.82, 6.41 Hz), 1.81-1.71 (2H, m), 1.51-1.40 (2H, m), 1.36-1.23 (13H, m), 0.92-0.80 (3H, m).

6.1.15 Compound 4.24

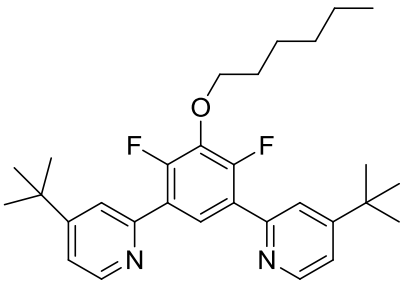

A mixture of the boronic acid derivative (1.0 g, 2.6 mmol), 2-chloro-4-*tert*-butylpyridine (0.44 g, 2.4 mmol) and toluene (30 mL) was deoxygenated by bubbling nitrogen through the mixture for 15 minutes. $Pd(PPh_3)_4$ (0.12 g, 0.12 mmol) was added and the mixture was additionally deoxygenated by bubbling nitrogen for 5 minutes. Aqueous solution of sodium carbonate (2 M, 3.6 mL, 7.2 mmol) was added and the mixture was additionally degassed for 5 minutes. The mixture was heated under reflux under nitrogen for 24 hours. Brine (30 mL) was added and layers were separated. The organic layer was separated, washed with brine, dried over anhydrous $MgSO_4$ and filtered. The solvent was removed by rotary evaporation under reduced pressure. The product was purified by column chromatography using silica gel and a mixture petroleum ether/ethyl acetate, 3/1 as eluent. Colorless solid. Yield: 43 %. ^{1}H NMR (400 MHz, $CDCl_3$) δ 8.60 (d, *J* = 5.4 Hz, 2H), 8.09 (t, *J* = 8.5 Hz, 1H), 7.69 (br.s, 2H), 7.20 (dd, *J* = 5.4, 2.1 Hz, 2H), 4.21 (t, *J* = 7.0 Hz, 2H), 1.57 (q, *J* = 7.2 Hz, 2H), 1.34 (m, 6H), 0.90 (t, *J* = 7.2 Hz, 3H); ^{13}C NMR (100 MHz, $CDCl_3$) δ 160.53, 154.25 (dd, *J* = 249.3, 5.6 Hz, C^4, C^6), 152.88, 149.72, 136.35 (t, *J* = 15.8 Hz, C^5), 125.76 (br.s), 125.35 (dd, *J* = 9.7, 5.7 Hz, C^1, C^3), 121.54 (t, *J* = 3.8 Hz, C^2), 75.39, 34.91, 31.65, 30.66, 30.14, 25.47, 22.68, 14.13; ^{19}F NMR (400 MHz): δ -131.3 (d, *J* = 21.5 Hz).

6.2 Platinum Complex Synthesis

6.2.1 Compound 2.7

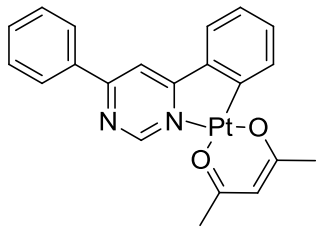

Method A: A solution of potassium tetrachloroplatinate (432 mg, 1.04 mmol) in water (2 cm^3) was added to a stirred solution of 4,6-diphenylpyrimidine (120 mg, 0.52 mmol) in acetic acid (40 cm^3). The mixture was heated under reflux and N_2 at 125^oC for 20 hours. The precipitate was filtered off and washed with acetic acid (10 cm^3) and ethanol (10 cm^3) and dried under vacuum. The dimer (345 mg, 0.25 mmol), sodium acetylacetonate (305 mg, 2.5 mmol) and acetone (50 cm^3) was heated under reflux and N_2 at 70^oC for 22 hours. The precipitate was filtered and acetone was removed from the filtrate by rotary evaporator. Water (70cm^3) was added and the yellow/orange solid was filtered. Yield 70 mg (26%). ^1H NMR ($CDCl_3$, 400 MHz) δ 9.59 (1H, d, *J* = 0.9 Hz), 8.17-8.11 (2H, m), 7.86 (1H, s), 7.66 (1H, d, *J* = 7.3), 7.6 (1H, d, *J* = 7.3 Hz), 7.57-7.50 (3H, m), 7.28 (1H, ddd, *J* = 7.3, 7.3, 0.9 Hz), 7.13 (1H, ddd, *J* = 7.9, 7.8, 1.3 Hz), 5.49 (1H, s), 2.01 (6H, s). ^{13}C NMR ($CDCl_3$, 400MHz) δ 186.12, 184.00, 174.56, 164.85, 156.07, 142.53, 135.91, 131.87, 129.17, 127.56, 123.79, 109.07, 102.56, 28.21, 27.19

Method B: A solution of potassium tetrachloroplatinate (200mg, 0.5 mmol) in water (10 cm^3) was added to a solution of tetrabutylammonium bromide (650 mg, 2.0 mmol) in DCM (20 cm^3). 4,6-diphenylpyrimidine (125 mg, 0.5 mmol) and ethoxyethanol (15 cm^3) was added and the solution was placed into an oil bath at 100 ^oC. The solution was purged with nitrogen until the DCM had evaporated. The solution was then left stirring at 100 ^oC for 17 hours. The precipitate was filtered off and washed with methanol (10 cm^3) and dried. The dimer (70 mg, 0.13 mmol), sodium acetylacetonate (159 mg, 1.3 mmol) and acetone (50 cm^3) was heated under reflux and N_2 at 95^oC for 24 hours. The precipitate was filtered and acetone was removed from the filtrate by rotary evaporator. Water (70cm^3) was added and the yellow solid was filtered. Yield 30 mg (11 %). ^1H NMR ($CDCl_3$, 270 MHz) δ 9.53 (1H, s), 8.14-8.03 (2H, m), 7.80 (1H, s), 7.61-7.45 (5H, m), 7.22 (1H, t, *J* = 15.1, 7.2 Hz), 7.07 (1H, t, *J* = 15.1, 7.7 Hz), 5.43 (1H, s), 1.95 (6H, s).

6.2.2 Compound 2.8

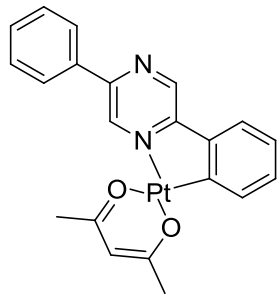

A solution of potassium tetrachloroplatinate (178mg, 0.43 mmol) in water (2 cm^3) was added to a stirred solution of SK51 (100 mg, 0.43 mmol) in acetic acid (60 cm^3). The mixture was heated under reflux and N_2 at 125°C for 48 hours. The precipitate was filtered off and washed with acetic acid (10 cm^3) and ethanol (10 cm^3) and dried under vacuum. The dimer (155 mg, 0.17 mmol), sodium acetylacetonate (208 mg, 1.7 mmol) and acetone (60 cm^3) was heated under reflux and N_2 at 95°C for 24 hours. The precipitate was filtered and acetone was removed from the filtrate by rotary evaporator. Water (70cm^3) was added and the yellow solid was filtered. Yield 121 mg, 54 %. ^{1}H NMR ($CDCl_3$, 270MHz) δ_H 9.41 (1H, s), 8.92 (1H, s), 8.04-7.98 (3H, m), 7.67-7.45 (4H, m), 7.18-7.09 (2H, m), 5.50 (1H, s), 1.55 (6H, s).

6.2.3 Compound 2.9

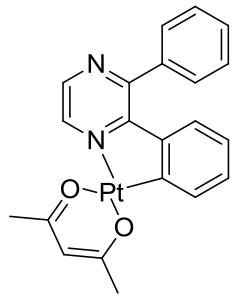

A solution of potassium tetrachloroplatinate (540mg, 1.3 mmol) in water (2 cm^3) was added to a stirred solution of 2,3-diphenylpyrazine (300 mg, 1.3 mmol) in acetic acid (60 cm^3). The mixture was heated under reflux and N_2 at 125°C for 15 hours. The precipitate was filtered off and washed with acetic acid (10 cm^3) and ethanol (10 cm^3) and dried under vacuum. The dimer (578 mg, 0.63 mmol), sodium acetylacetonate (769 mg, 6.3 mmol) and acetone (70 cm^3) was heated under reflux and N_2 at 70°C for 16 hours. The precipitate was filtered and acetone was removed from the filtrate by rotary evaporator. Water (70cm^3) was added and then residue was filtered and washed in acetone. Yield 590 mg, 78%. ^{1}H NMR ($CDCl_3$, 400MHz) δ_H 9.11 (1H, d, *J* = 3.2 Hz), 8.31 (1H, d, *J* = 3.2 Hz), 7.64 (1H, d, *J* = 7.8 Hz), 7.57-7.50 (5H, m), 7.11 (1H, t, *J* = 8.7 Hz), 6.71 (1H, t, *J* = 8.2 Hz), 6.64 (1H, d, *J* = 6.9 Hz), 5.50 (1H, s), 2.04 (6H, d, *J* = 4.1 Hz).

6.2.4 Compound 2.10

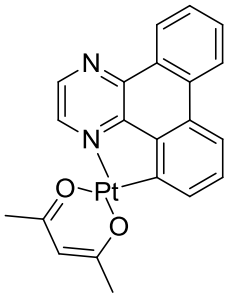

A solution of potassium tetrachloroplatinate (357mg, 0.86 mmol) in water (4 mL) was added to a stirred solution of SK44 (100 mg, 0.43 mmol) in acetic acid (60 mL). The mixture was heated under reflux and N_2 at 125°C for 20 hours. The precipitate was filtered off and washed with acetic acid (10 mL) and ethanol (10 mL) and dried under vacuum. The dimer (353 mg, 0.3 mmol), sodium acetylacetonate (183 mg, 1.5 mmol) and acetone (60 cm^3) was heated under reflux and N_2 at 95°C for 24 hours. The precipitate was filtered and acetone was removed from the filtrate by rotary evaporator. Water (70cm^3) was added and the yellow solid was filtered. Yield 56 mg, 27 %. ^{1}H NMR ($CDCl_3$, 270MHz) δ_H 8.63 (1H, d, *J* = 8.0 Hz), 8.98 (1H, d, *J* = 3.1 Hz), 8.64 (1H, d, *J* = 3.0 Hz), 8.5 (1H, d, *J* = 8.8 Hz), 8.09 (1H, d, *J* = 8.0 Hz), 7.63-7.52 (4H, m), 5.46 (1H, s). 2.00 (6H, d, *J* = 3.7).

6.2.5 Compound 2.11

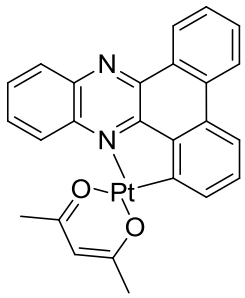

A solution of potassium tetrachloroplatinate (150mg, 0.36 mmol) in water (2 mL) was added to a stirred solution of SK45 (100 mg, 0.36 mmol) in acetic acid (60 mL). The mixture was heated under reflux and N_2 at 125°C for 24 hours. The precipitate was filtered off and washed with acetic acid (10 mL) and ethanol (10 mL) and dried under vacuum. The dimer (132 mg, 0.13 mmol), sodium acetylacetonate (159 mg, 1.3 mmol) and acetone (60 cm^3) was heated under reflux and N_2 at 95°C for 23 hours. The precipitate was filtered and acetone was removed from the filtrate by rotary evaporator. Water (70cm^3) was added and the yellow solid was filtered. Yield 40 mg (19 %). ^{1}H NMR ($CDCl_3$, 270MHz) δ_H 9.97 (1H, d, *J* = 8.9 Hz), 9.29 (1H, *J* = 8.4 Hz), 8.47 (1H, d, *J* = 8.1 Hz), 8.34 (1H, d, *J* = 8.3 Hz), 8.09 (1H, d, *J* = 8.3 Hz), 7.95-7.66 (5H, m), 7.56 (1H, t, *J* = 7.8 Hz), 5.62 (2H, s), 2.11 (6H, d, *J* = 11.1).

6.2.6 Compound 2.13

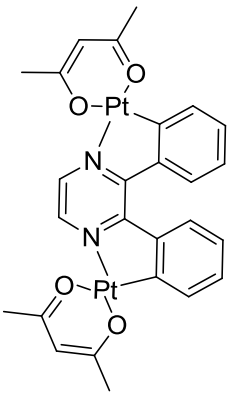

A solution of potassium tetrachloroplatinate (1.08 g, 2.6 mmol) in water (3 mL) was added to a stirred solution of 2,3-diphenylpyrazine (300 mg, 1.3 mmol) in acetic acid (60 mL). The mixture was heated under reflux and N_2 at 125^{o}C for 15 hours. The precipitate was filtered off and washed with acetic acid (10 mL) and ethanol (10 mL) and dried under vacuum. The dimer (500 mg, 0.36 mmol), sodium acetylacetonate (440 mg, 3.6 mmol) and acetone (70 cm^3) was heated under reflux and N_2 at 70^{o}C for 16 hours. Precipitate was filtered and washed with acetone. Water (70 cm^3) was added to residue and then filtered and rinsed with water then acetone. Yield 340 mg (32%). ^{1}H NMR ($CDCl_3$, 270MHz) δ_H 8.63 (2H, s), 8.03 (2H, d, *J* = 7.9 Hz), 7.67 (2H, d, *J* = 7.7 Hz), 7.26 (2H, t, *J* = 6.2 Hz), 7.00 (2H, t, *J* = 8.2 Hz), 5.48 (2H, s), 2.05 (6H, s), 2.00 (6H, s).

6.2.7 Compound 2.14 and 2.20

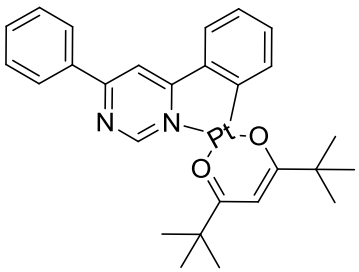
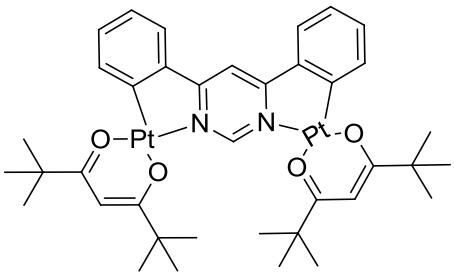

A solution of potassium tetrachloroplatinate (1 g, 2.42 mmol) in water (4 cm^3) was added to a stirred solution of L^1H_2 (375 mg, 1.61 mmol) in acetic acid (80 cm^3). The mixture was heated at reflux under a nitrogen atmosphere for 3 days. The precipitate was filtered off and washed successively with acetic acid (10 cm^3) and ethanol (10 cm^3) to give the dichlorobridged intermediate. A mixture of the intermediate (1.07 g, 1.29 mmol), 2,2,6,6-tetramethyl-3,5-heptanedione (949 mg, 5.16 mmol), aqueous K_2CO_3 solution (2M, 5 cm^3, 10.32 mmol) and acetone (80 cm^3) was heated at reflux under N_2 for 24 h. The solvent was removed by rotary evaporation, the residue was treated with DCM, filtered, and the filtrate was evaporated to dryness. The residue was then purified by column chromatography using silica gel and a mixture of dichloromethane/hexane, 1/2 as the eluent to give both the mononuclear and dinuclear products. **2.14** R_f = 0.1, yield 150 mg, 15 %. ^{1}H NMR ($CDCl_3$, 400 MHz) δ_H 9.62 (1H, d, *J* = 0.9 Hz), 8.17-8.14 (2H, m), 7.90 (1H, d, *J* = 0.9 Hz), 7.72 (1H, dd, *J* = 7.6, 0.8 Hz), 7.64 (1H, dd, *J* = 7.6, 1.0 Hz), 7.56–7.54 (3H, m), 7.31 (1H, ddd, *J* = 7.6, 7.6, 1.0 Hz), 7.15 (1H, ddd, *J* = 7.6, 7.6, 0.8 Hz), 5.84 (1H, s), 1.29 (9H, s), 1.28 (9H, s). HRMS (NSI): *m/z* 609.2003 $[M+H]^+$. calcld for $C_{27}H_{31}N_2O_2Pt$ *m/z* 609.2007. Elemental analysis calcld for $C_{27}H_{30}N_2O_2Pt$: C 53.20, H 4.96, N 4.60 %; found C 53.31, H 4.92, N 4.49 %. **2.20** R_f = 0.2, yield 29 mg, 1.8 %. ^{1}H NMR ($CDCl_3$, 400 MHz) δ_H 9.68 (1H, s), 7.71 (2H, br.d, *J* = 7.6 Hz), 7.70 (1H, s), 7.62 (2H, br.d, *J* = 7.6 Hz), 7.34 (2H, br.t, *J* = 7.6 Hz), 7.17 (2H, br.t, *J* = 7.6 Hz), 5.84 (2H, s), 1.28 (18H, s) 1.26 (18H, s). HRMS (NSI): *m/z* 985.2934 $[M+H]^+$. calcld for $C_{38}H_{48}N_2O_4Pt_2H$ *m/z* 985.2941. Elemental analysis calcld for $C_{38}H_{48}N_2O_4Pt_2$: C 46.24, H 4.90, N 2.84 %; found C 46.30, H 5.25, N 2.64%.

6.2.8 Compound 2.15 & 2.21

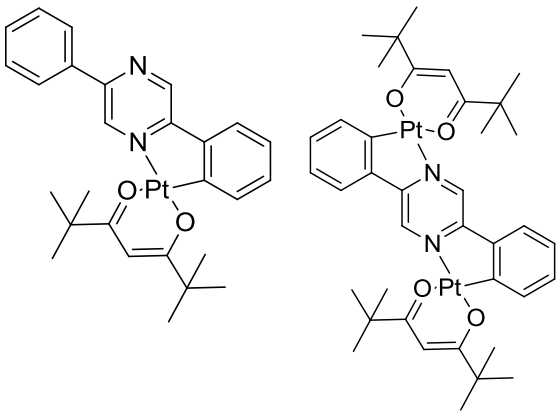

A solution of potassium tetrachloroplatinate (896 mg, 2.16 mmol) in water (4 cm^3) was added to a stirred solution of L^2H_2 (250 mg, 1.08 mmol) in acetic acid (80 cm^3). The mixture was heated at reflux under N_2 for 3 days. The precipitate was filtered off and washed consecutively with acetic acid (10 cm^3) and ethanol (10 cm^3) and dried to give the dichlorobridged dimer. A mixture of the dimer (680 mg, 1.32 mmol), 2,2,6,6-tetramethyl-3,5-heptanedione (972 mg, 5.28 mmol), aqueous K_2CO_3 solution (2M, 5 cm^3, 10.56 mmol) and acetone (80 cm^3) was heated at reflux under N_2 for 24 h. Acetone was removed by rotary evaporation and the residue was then washed with water, filtered and dried. The solid was purified by column chromatography using silica gel and dichloromethane as an eluent to give both the mononuclear and dinuclear products. For **PtL^2H**, R_f = 0.6, yield 230 mg, 35 %. ^{1}H NMR ($CDCl_3$, 400 MHz) δ_H 9.54 (1H, d, *J* = 1.2 Hz, $^3J_{H\text{-}Pt}$ = 46 Hz), 8.95 (1H, d, *J* = 1.2 Hz, $^4J_{H\text{-}Pt}$ = 13 Hz), 8.06–8.01 (2H, m), 7.70 (1H, dd, *J* = 7.8, 1.6 Hz), 7.60 (1H, dd, *J* = 7.8, 1.6 Hz), 7.58–7.48 (3H, m), 7.29 (1H, ddd, *J* = 7.4, 7.4, 1.2 Hz), 7.17 (1H, ddd, *J* = 7.4, 7.4, 1.2 Hz), 5.86 (1H, s), 1.34 (9H, s), 1.31 (9H, s). HRMS (NSI): *m/z* 609.2003 $[M+H]^+$. calcld for $C_{27}H_{31}N_2O_2PtH$ *m/z* 609.2007. Elemental analysis calcld for $C_{27}H_{30}N_2O_2Pt$: C 53.20, H 4.96, N 4.60 %; found C 52.52, H 4.47, N 4.15 %. For **Pt_2L_2**, R_f = 0.9, yield 150 mg, 15 %. ^{1}H NMR ($CDCl_3$, 400 MHz) δ_H 9.44 (2H, s), 7.72 (2H, dd, *J* = 6.7, 1.5 Hz), 7.43 (2H, dd, *J* = 6.7, 1.5 Hz), 7.29 (2H, ddd, *J* = 7.7, 7.7, 1.5 Hz), 7.17 (2H, ddd, *J* = 7.7, 7.7, 1.5 Hz), 5.88 (2H, s), 1.37 (18H, s), 1.30 (18H, s). HRMS (NSI): *m/z* 985.2940 $[M+H]^+$. calcld for $C_{38}H_{48}N_2O_4Pt_2H$ *m/z* 985.2941. Elemental analysis calcld for $C_{38}H_{48}N_2O_4Pt_2$: C 46.24, H 4.90, N 2.84 %; found C 46.36, H 5.27, N 2.60%.

6.2.9 Compound 3.4 & 3.7

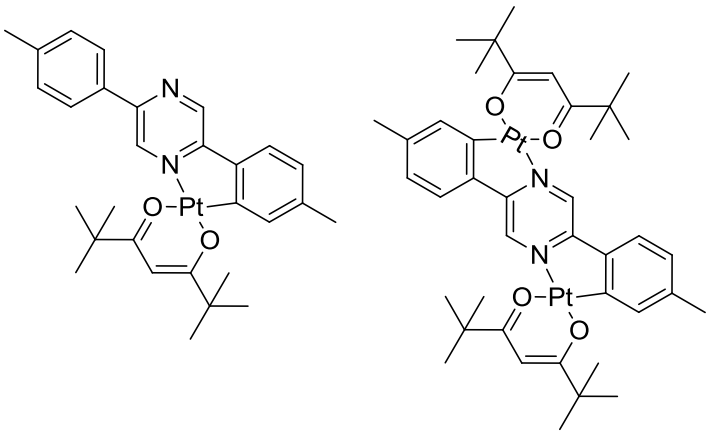

2,5-bis(4-methylphenyl)pyrazine (250 mg, 1.02 mmol) and potassium tetrachloroplatinate (635 mg, 1.53 mmol) were added to acetic acid (60 mL). The mixture was heated under reflux and N_2 at 125^{o}C for 1 day. The precipitate was filtered off rinsed with acetic acid (10 cm^3) dried to give the dichlorobridged intermediates. The dimer (560 mg), 2,2,6,6-tetramethylheptane-3,5-dione (405 mg, 2.2 mmol), and potassium carbonate (455 mg, 3.3 mmol) and acetone (70 cm^3) was heated under reflux and N_2 at 95^{o}C for 24 hours. Acetone was removed by rotary evaporator. Water (70cm^3) was added and the solid was filtered. The solid was purified by column chromatography using silica gel and DCM and Petroleum ether (2:1) as the eluent to give both the mono-Pt and di-Pt complexes. Mononuclear SK95 Rf 0.3. Yield 40 mg, 6 %. Melting point 233-235 °C. ^{1}H NMR ($CDCl_3$, 400 MHz) δ 9.45 (1H, d, *J* = 1.5 Hz), 8.86 (1H, d, *J* = 1.5 Hz), 7.90 (2H, d, *J* = 8.3 Hz), 7.48 (1H, s), 7.46 (1H, *d*, J = 8.1 Hz), 7.33 (2H, d, *J* = 8.5 Hz), 6.96, (1H, dd, *J* = 8.3, 1.8 Hz), 5.84 (1H, s), 2.43 (3H, s), 2.41 (3H, s), 1.32 (9H, s), 1.29 (9H, s). Dinuclear SK95 Rf 0.7. Yield 13 mg, 1 %. ^{1}H NMR ($CDCl_3$, 400 MHz) δ 9.34 (2H, s), 7.50 (2H, s), 7.29 (2H, d, *J* = 7.9 Hz), 6.98 (2H, d, *J* = 8.2 Hz), 5.86 (2H, s), 2.43 (6H, s), 1.35 (9H, s), 1.30 (9H, s)

6.2.10 Compound 3.5 & 3.8

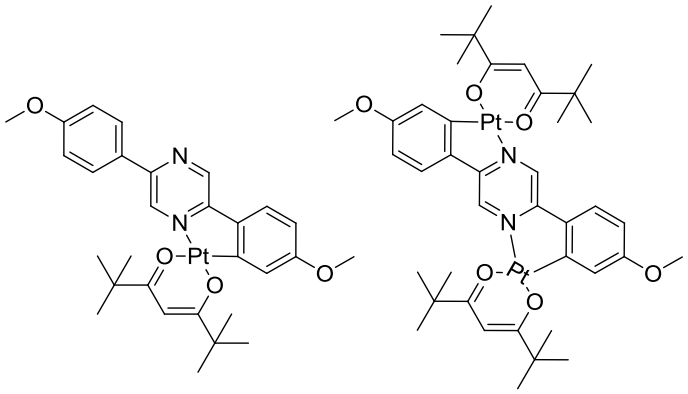

2,5-bis(4-methoxyphenyl)pyrazine (210 mg, 0.70 mmol) and potassium tetrachloroplatinate (290 mg, 0.70 mmol) were added to acetic acid (60 mL). The mixture was heated under reflux and N_2 at 125°C for 3 days. The precipitate was filtered off and dried to give the dichlorobridged dimer. The dimer (294 mg, 0.52 mmol), 2,2,6,6-tetramethylheptane-3,5-dione (287 mg, 1.56 mmol), potassium carbonate (2M, 1.5 cm^3) and acetone (70 cm^3) was heated under reflux and N_2 at 95°C for 24 hours. Acetone was removed by rotary evaporator. Water (70cm^3) was added and the solid was filtered. The solid was purified by column chromatography using silica gel and DCM as the eluent to give both the mono-Pt and di-Pt complexes. Mononuclear SK90 Rf 0.3. Yield 162 mg, 35 %. Melting point 238-239 °C. ^{1}H NMR ($CDCl_3$, 400 MHz) δ 9.33 (1H, d, *J* = 1.6 Hz), 8.77 (1H, s), 7.94 (2H, d, *J* = 8.9 Hz), 7.49 (1H, d, *J* = 8.6 Hz), 7.22 (1H, *d*, J = 2.7 Hz), 7.02 (2H, d, *J* = 9.1 Hz), 6.72, (1H, dd, *J* = 8.9, 2.8 Hz), 5.84 (1H, s), 3.88 (3H, s), 3.87 (3H, s), 1.32 (3H, s), 1.29 (3H, s). Dinuclear SK90 Rf 0.8. Yield 21 mg, 3 %. ^{1}H NMR ($CDCl_3$, 400 MHz) δ 9.19 (2H, s), 7.30 (2H, d, *J* = 8.6 Hz), 7.23 (2H, d, *J* = 2.9 Hz), 6.73 (2H, dd, *J* = 9.0, 2.8 Hz), 5.85 (2H, s), 3.88 (6H, s), 1.35 (3H, s), 1.29 (3H, s)

6.2.11 Compound 3.6 & 3.9

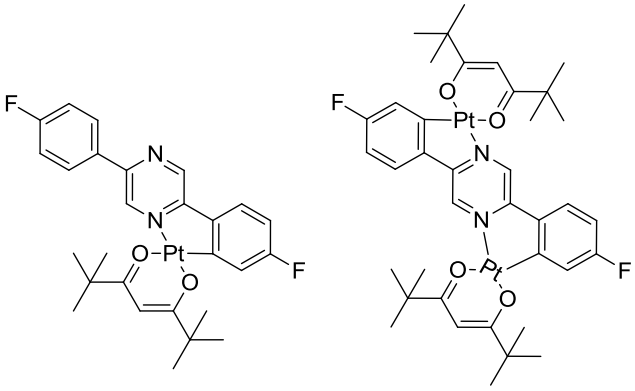

2,5-bis(4-fluorophenyl)pyrazine (250 mg, 1.00 mmol) and potassium tetrachloroplatinate (622 mg, 1.50 mmol) was added to acetic acid (60 mL). The mixture was heated under reflux and N_2 at 125^{o}C for 1 day. The acetic acid was evaporated and the solid was washed with water, filtered and dried to give the dichlorobridged dimer. The dimer (460 mg, 0.6 mmol), 2,2,6,6-tetramethylheptane-3,5-dione (221 mg, 1.2 mmol), and potassium carbonate (249 mg, 1.8 mmol) and acetone (70 cm^3) was heated under reflux and N_2 at 95^{o}C for 24 hours. Acetone was removed by rotary evaporator and the solid was washed with water, filtered and dried. The solid was purified by column chromatography using silica gel and DCM/Petroleum ether (2:1) as the eluent to give both the mono-Pt and di-Pt complexes. The mono-Pt complex had an Rf 0.5, yield 98 mg, 15 %. ^{1}H NMR ($CDCl_3$, 400 MHz) δ_H 9.44 (1H, s), 8.86 (1H, s), 8.02-7.97 (2H, m), 7.61-7.56 (2H, m), 7.33-7.18 (2H, m), 6.87 (1H, dd, *J* = 6.9, 2.3 Hz), 5.87 (1H, s), 1.32 (9H, s), 1.29 (9H, s). The di-Pt complex had an Rf 0.8, yield 47 mg, 5 %. ^{1}H NMR ($CDCl_3$, 400 MHz) δ_H 9.32 (2H, s), 7.40 (2H, t, *J* = 5.0 Hz), 7.33 (2H, d, *J* = 9.2 Hz), 6.89 (2H, t, *J* = 11.5 Hz), 5.88 (2H, s), 1.35 (18H, s), 1.29 (18H, s).

6.2.12 Compound 2.16

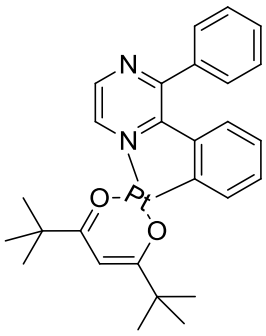

A solution of potassium tetrachloroplatinate (270 mg, 0.65 mmol) in water (2 cm^3) was added to a stirred solution of L^3H_2 (150 mg, 0.65 mmol) in acetic acid (60 cm^3). The mixture was heated at reflux under an argon atmosphere for 19 h. The precipitate was filtered off and washed successively with acetic acid (10 cm^3) and ethanol (10 cm^3) and dried to give the dichlorobridged dimer. A mixture of the dimer (150 mg, 0.30 mmol), 2,2,6,6-tetramethyl-3,5-heptanedione (166 mg, 0.90 mmol), aqueous K_2CO_3 solution (2M, 1 cm^3, 1.8 mmol) and ethoxyethanol (70 cm^3) was heated at reflux under argon for 15 h. The solvent was evaporated and the solid washed in water (70 cm^3). The solid was then filtered, dried, and purified by column chromatography using silica gel and dichloromethane as the eluent; R_f = 0.4 yield 140 mg, 35 %. ^{1}H NMR ($CDCl_3$, 400 MHz) δ_H 9.10 (1H, d, *J* = 3.4 Hz, $^3J_{H\text{-}Pt}$ = 47 Hz), 8.33 (1H, d, *J* = 4.5 Hz), 7.69 (1H, dd, *J* = 7.9, 1.4 Hz), 7.57–7.49 (5H, m), 7.13 (1H, ddd, *J* = 7.8, 7.2, 1.8 Hz), 6.75-6.23 (2H, m), 5.84 (1H, s), 1.29 (9H, s), 1.28 (9H, s). HRMS (ESI): *m/z* 609 $[M+H]^+$. Elemental analysis calcld for $C_{27}H_{30}N_2O_2Pt$: C 53.20, H 4.96, N 4.60 %; found C 53.64, H 5.18, N 4.52 %.

6.2.13 Compound 2.22

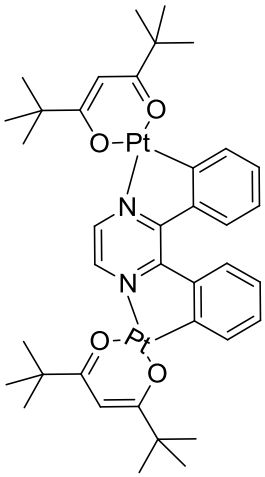

A solution of potassium tetrachloroplatinate (540 mg, 1.30 mmol) in water (4 cm^3) was added to a stirred solution of L^3H_2 (150 mg, 0.65 mmol) in acetic acid (60 cm^3). The mixture was heated at reflux under N_2 for 24 h. The precipitate was filtered off and washed successively with acetic acid (10 cm^3) and ethanol (10 cm^3) and dried to give the dichlorobridged dimer. A mixture of the dimer (200 mg, 0.26 mmol), 2,2,6,6-tetramethyl-3,5-heptanedione (144 mg, 0.78 mmol), aqueous K_2CO_3 solution (2M, 1 cm^3, 1.56 mmol) and ethoxyethanol (70 cm^3) was heated under reflux under nitrogen for 15 h. The solvent was evaporated and the solid washed with water (70 cm^3). The solid was then filtered off and dried. The product was purified by column chromatography using silica gel and dichloromethane as an eluent; R_f = 0.9 yield 60 mg, 9 %. ^{1}H NMR ($CDCl_3$, 400 MHz) δ_H 8.69 (2H, s), 8.03 (2H, dd, *J* = 8.5, 2.0 Hz), 7.73 (2H, dd, *J* = 8.5, 2.0 Hz), 7.31-7.25 (2H, m), 7.00 (2H, ddd, *J* = 7.6, 7.8, 1.8 Hz), 5.86 (1H, s), 1.31 (18H, s), 1.30 (18H, s). HRMS (ESI): *m/z* 985 $[M+H]^+$. Elemental analysis calcld for $C_{38}H_{48}N_2O_4Pt_2$: C 46.24, H 4.90, N 2.84 %; found C 46.31, H 5.05, N 2.79 %.

6.2.14 Compound 2.17 and 2.22

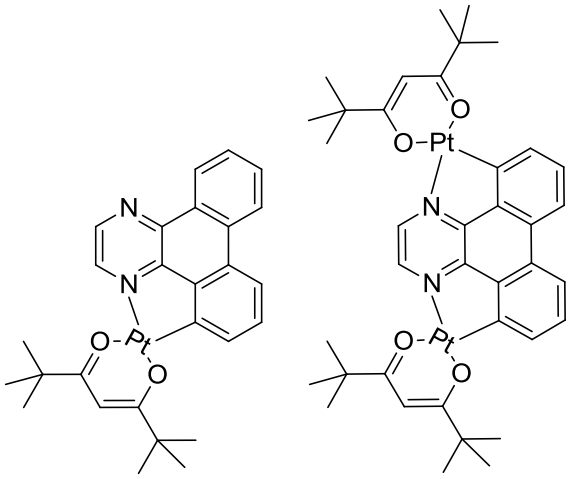

A solution of potassium tetrachloroplatinate (452 mg, 1.09 mmol) in water (2 cm^3) was added to a stirred solution of L^4H_2 (250 mg, 1.09 mmol) in acetic acid (75 cm^3). The mixture was heated at reflux under N_2 for 24 h. The precipitate was filtered off and washed successively with acetic acid (10 cm^3) and ethanol (10 cm^3) and dried to give the dichlorobridged dimer. A mixture of the dimer (270 mg, 0.55 mmol), 2,2,6,6-tetramethyl-3,5-heptanedione (304 mg, 1.65 mmol), aqueous K_2CO_3 solution (2M, 2 cm^3, 3.3 mmol) and acetone (70 cm^3) was heated under reflux, under N_2 for 23 h. The mixture was filtered and water (70 cm^3) was added to the filtrate. The precipitated solid was filtered off, washed with water and dried. The product was then purified by column chromatography using silica gel and dichloromethane as the eluent to give both the mononuclear and dinuclear products. For **PtL^4H**, Rf = 0.7, yield 100 mg, 15%. ^{1}H NMR ($CDCl_3$, 400 MHz) δ_H 9.13 (1H, dd, *J* = 7.7, 1.3 Hz), 9.09 (1H, d, *J* = 3.4 Hz), 8.75 (1H, d, *J* = 3.4 Hz), 8.60 (1H, dd, *J* = 8.2, 1.3 Hz), 8.19 (1H, dd, *J* = 8.2, 1.3 Hz), 7.86–7.63 (4H, m), 5.91 (1H, s), 1.18, (18H, s). HRMS (ESI): *m/z* 607 $[M^+ H]^+$. Elemental analysis calcld for $C_{27}H_{28}N_2O_2Pt$: C 53.37, H 4.64, N 4.61 %; found C 53.65, H 4.75, N 4.48 %. For **Pt_2L^4**, R_f = 0.9, yield 50 mg, 5 %. ^{1}H NMR ($CDCl_3$, 400 MHz) δ_H 8.69 (2H, s), 8.09 (2H, d, *J* = 7.6 Hz), 7.75 (2H, d, *J* = 8.4 Hz), 7.62 (2H, t, *J* = 8.0, 7.6 Hz), 5.91 (2H, s), 1.36 (18H, s), 1.35 (18H, s). HRMS (ESI): *m/z* 982 $[M+ H]^+$. Elemental analysis calcld for $C_{38}H_{46}N_2O_4Pt$: C 46.69, H 4.95, N 2.81 %; found C 46.86, H 4.87, N 2.82 %.

6.2.15 Compound 2.18

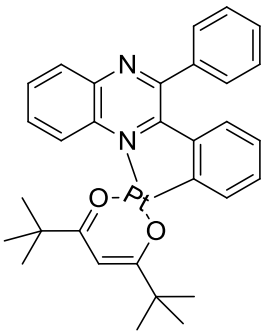

Under N2 atmosphere, L5H2 (220 mg, 0.78 mmol) and potassium tetrachloroplatinate (420 mg, 1.01 mmol) were dissolved in acetic acid (50 cm3) and the mixture was heated at reflux overnight. The mixture was cooled to room temperature and the black solid was filtered off, washed with ethanol (20 cm3) and air dried. The crude product was added to a solution of 2,2,6,6-tetramethyl-3,5-heptanedione (432 mg, 2.34 mmol) in acetone (60 cm3), followed by aqueous K2CO3 solution (2M, 5 cm3). The mixture was heated at reflux overnight. Acetone was removed under reduced pressure and the crude product was dissolved in DCM. The organic layer was washed with brine and dried with MgSO4. The solvent was removed under vacuum and the product was then purified by column chromatography using silica gel and CHCl3. Rf = 0.4, yield 231 mg, 45%. 1H NMR (CDCl3, 400 MHz) δH 9.42 (1H, dd, J = 8.7 Hz, J = 1.4 Hz), 8.08 (1H, dd, J = 7.2 Hz, J = 2.2 Hz), 7.85 (1H, dd, J = 7.6 Hz, J = 1.1 Hz), 7.74 (4H, m), 7.54 (3H, m), 7.15 (1H, ddd, J = 6.4 Hz, J = 2.3 Hz, J = 2.3 Hz), 6.76 (2H, m), 5.95 (1H, s), 1.33 (9H, s), 1.29 (9H, s). MS (ESI): m/z 659 [M+H]+. Elemental analysis calcld for C31H32N2O2Pt: C 56.44, H 4.89, N 4.25 %; found C 56.84, H 5.12, N 4.08 %.

6.2.16 Compound 2.24

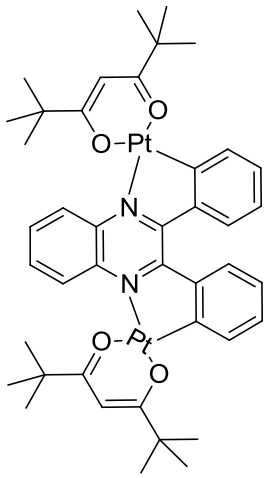

Under N_2 atmosphere, PtL^5H (200 mg, 0.3 mmol) and potassium tetrachloroplatinate (415 mg, 0.36 mmol) were dissolved in acetic acid (40 cm^3) and the mixture was heated at reflux 15 h. The mixture was cooled to room temperature and the black solid was filtered off, washed with ethanol (20 cm^3) and air dried. The crude product was added to a solution of 2,2,6,6-tetramethyl-3,5-heptanedione (74 mg, 0.4 mmol) in acetone (50 cm^3), followed by aqueous K_2CO_3 solution (2M, 5 cm^3). The mixture was heated at reflux for 16 h. Acetone was removed under reduced pressure and the crude product dissolved in DCM. The organic layer was washed with brine, dried over $MgSO_4$, filtered and evaporated to dryness. The residue was then purified by column chromatography using silica gel and CH_3Cl as the eluent to give the product; R_f = 0.8 yield 102 mg, 33%. ^1H NMR ($CDCl_3$, 400 MHz) δ_H 9.49 (2H, m), 8.00 (2H, br. d, *J* = 10 Hz), 7.85 (2H, dd, *J* = 12.0 Hz, *J* = 2.4 Hz), 7.64 (2H, m), 7.26 (2H, ddd, *J* = 12.0 Hz, *J* = 11.6 Hz, *J* = 1.6 Hz), 7.00 (2H, ddd, *J* = 11.6 Hz, *J* = 10.4 Hz, *J* = 2.4 Hz), 5.96 (2H, s), 1.34 (9H, s), 1.28 (9H, s). MS (ESI): *m/z* 1035 $[M+H]^+$. Elemental analysis calcld for $C_{42}H_{50}N_2O_4Pt_2$: C 48.64, H 4.86, N 2.70 %; found C 48.86, H 5.38, N 2.48 %

6.2.17 Compound 2.19 and 2.25

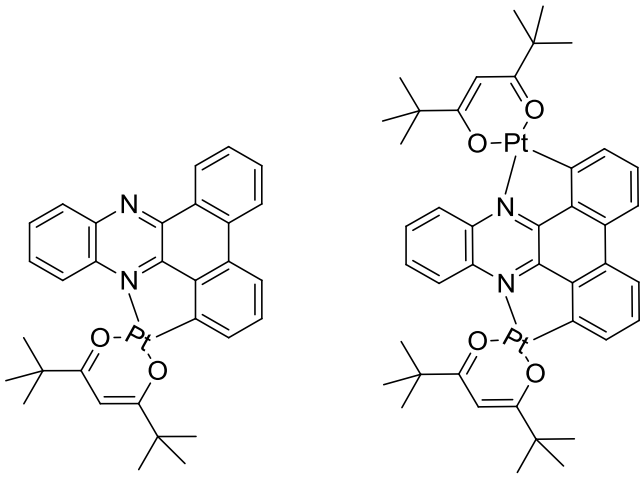

A mixture of L^6H_2 (93 mg, 0.33 mmol), potassium tetrachloroplatinate (150 mg, 0.4 mmol) and acetic acid (35 cm^3) were heated at reflux under nitrogen for 14 h. The mixture was allowed to cool to room temperature and the black solid was filtered off, washed with ethanol (20 cm^3) and air dried. The crude product was added to a solution of 2,2,6,6-tetramethyl-3,5-heptanedione (431 mg, 2.34 mmol) in acetone (60 cm^3), followed by aqueous K_2CO_3 solution (2M, 5 cm^3). The mixture was heated at reflux for 14 h. Acetone was removed under reduced pressure, and DCM (30 cm^3) and brine (15 cm^3) were added. The organic layer was dried over $MgSO_4$ and filtered. The solvent was removed by rotary evaporation and the residue was then purified by column chromatography using silica gel and $CHCl_3$ / hexane, 7/3 v/v, as the eluent to give both the mononuclear and dinuclear products. For **2.9** R_f = 0.7, yield 24 mg, 11%. ^{1}H NMR ($CDCl_3$, 400 MHz) δ_H 10.07 (1H, dd, *J* = 8.7 Hz, *J* = 1.4 Hz), 9.31 (1H, dd, *J* = 9.2 Hz, *J* = 1.4 Hz), 8.50 (1H, d, *J* = 7.8 Hz), 8.36 (1H, dd, *J* = 8.7 Hz, *J* = 1.4 Hz), 8.12 (1H, d, J = 7.8 Hz), 7.99 (1H, d, *J* = 6.9 Hz), 7.69-7.92 (4H, m), 7.62 (1H, t, *J* = 7.8 Hz), 5.99 (1H, s), 1.38 (9H, s), 1.37 (9H, s). HRMS (ESI): *m/z* 657 $[M^+ H]^+$. Elemental analysis calcld for $C_{31}H_{30}N_2O_2Pt$: C 56.61, H 4.60, N 4.26 %; found C 56.59, H 4.63, N 4.18 %. For **2.25** R_f = 0.8, yield 2 mg, 0.6%. ^{1}H NMR ($CDCl_3$, 400 MHz) δ_H 10.15 (2H, m), 8.06 (2H, d, *J* = 7.8 Hz), 7.96 (2H, d, *J* = 7.3 Hz), 7.87 (2H, m), 7.61 (2H, t, *J* = 7.8 Hz), 5.99 (2H, s), 1.38 (18H, s), 1.37 (18H, s). HRMS (ESI): *m/z* 1033 $[M+ H]^+$.

6.3 Iridium Complex Synthesis

6.3.1 Compound 4.26

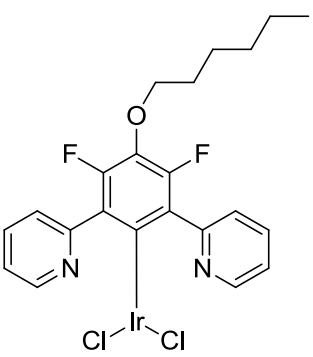

A mixture of 4-*tert*-butyl-2-[3-(4-*tert*-butylpyridin-2-yl)-5-(hexyloxy)phenyl]pyridine (2.1 g, 4.38 mmol), iridium chloride trihydrate (1.59 g, 4.38 mmol), ethoxyethanol (90 cm^3) and water (30 cm^3) was heated under reflux for 14 hours. The solid was filtered off washed with water and ethanol to give, after drying, an orange solid. Yield 2.6 g, 80%. ^{1}H NMR (400 MHz, $CDCl_3$) δ 8.43 (d, *J* = 5.9 Hz, 2H), 8.25 (br.s, 2H), 6.96 (dd, *J* = 5.9, 1.9 Hz, 2H), 4.18 (t, *J* = 6.5 Hz, 2H), 1.89 (m, 2H), 1.58 (m, 2H), 1.49 (s, 18H), 1.42 (m, 4H), 0.95 (t, *J* = 6.9 Hz, 3H); ^{19}F NMR (400 MHz): δ -125.1; ^{13}C NMR DEPT135 (100 MHz, $CDCl_3$) δ 153.5(CH), 120.5 (t, *J* = 5.6 Hz, CH), 119.9(CH), 75.9(CH_2), 31.7(CH_2), 30.8 (CH_3), 30.1(CH_2), 25.5(CH_2), 22.7(CH_2), 14.1(CH_3)

6.3.2 Compound 4.27

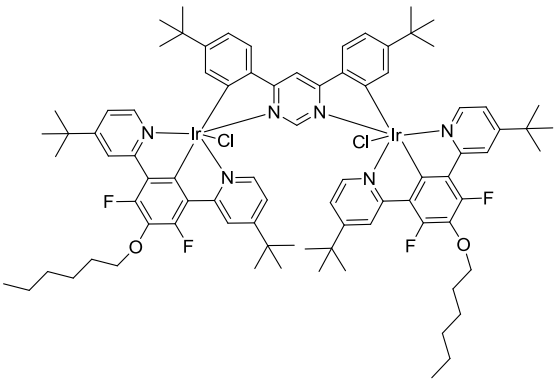

To a mixture of Ir complex **4.26** (370 mg, 0.5 mmol), the bis NC ligand **4.18** (90 mg, 0.26 mmol) and toluene (60 mL), silver triflate (191 mg, 0.74 mmol, 1.49 eq) was added and the reaction mixture was heated under reflux for 8 hours. The heating was removed and 10 cm^3 of 3M HCl was added to a still warm mixture. After stirring for 5 minutes the mixture was separated. Organic phase was evaporated and the residue was treated with methanol (40 cm^3). The solid was filtered off and washed with on filter with methanol. The solid was then dissolved in DCM (20 cm^3) and gravity filtered through paper filter. To the filtrate methanol (40 cm^3) was added the volume of the mixture was reduced to approximately 10 cm^3 using rotary evaporator. The orange solid was filtered off, washed with little amount of methanol. Yield 210 mg, 48%. ^{1}H NMR (400 MHz, $CDCl_3$) δ 11.77 (s, 1H), 8.40 (s,1H), 8.12 (s, 4H), 7.81 (d, *J* = 8.0 Hz, 2H), 7.79 (d, *J* = 5.9 Hz, 4H), 6.95 (dd, *J* = 8.0, 1.6 Hz, 2H), 6.92 (dd, *J* = 5.9, 1.6 Hz, 4H), 6.28 (d, *J* = 1.6 Hz, 2H), 4.20 (t, *J* = 6.5 Hz, 4H), 1.92 (m, 4H), 1.62 (m, 4H), 1.44 (m, 8H), 1.32 (s, 36H), 1.01 (s, 18H), 0.97 (t, *J* = 6.9 Hz, 6H); ^{19}F NMR (400 MHz): δ -126.9; ^{13}C NMR DEPT135 (100 MHz, $CDCl_3$) δ 160.3(CH), 150.6(CH), 133.1(CH), 125.8(CH), 120.3(CH), 120.0(CH), 119.2(CH), 105.8(CH), 77.2(CH_2), 31.7(CH_2), 30.9 (CH_3), 30.5(CH_3), 30.2(CH_2), 25.6(CH_2), 22.7(CH_2), 14.1(CH_3)

6.3.3 Compound 4.28

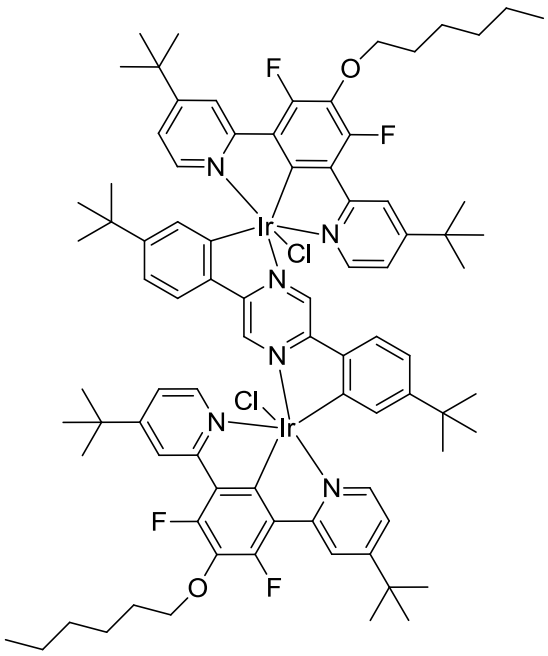

To a mixture of Ir complex **4.26** (148 mg, 0.2 mmol), the bis NC ligand **4.17** (34 mg, 0.1 mmol) and toluene (25 cm^3), silver triflate (77 mg, 0.3 mmol, 3 eq) was added and the reaction mixture was heated under reflux for 17 hours. The reaction flask was protected from light by aluminium foil. The heating was removed and 5 cm^3 of 2M HCl was added to a still warm mixture. Toluene was evaporated leaving a suspension of the product in aqueous medial. The solid was separated, triturated with methanol and filtered. The solid was then dissolved in DCM (20 cm^3) and filtered through celite. To the filtrate methanol (40 cm^3) was added the volume of the mixture was reduced to approximately 10 cm^3 using rotary evaporator. The red solid was filtered off, washed with little amount of methanol. Yield 112 mg, 64%. The product is light sensitive in solution. δ^1H NMR (400 MHz, $CDCl_3$) δ 10.77 (s, 2H), 8.40 (s,1H), 8.15 (s, 4H), 7.89 (d, *J* = 8.0 Hz, 2H), 7.63 (d, *J* = 5.9 Hz, 4H), 6.90 (m,6H), 6.18 (d, *J* = 1.6 Hz, 2H), 4.23 (t, *J* = 6.5 Hz, 4H), 1.94 (m, 4H), 1.62 (m, 4H), 1.44 (m, 8H), 1.33 (s, 36H), 1.00 (s, 18H), 0.97 (t, *J* = 6.9 Hz, 6H); ^{19}F NMR (400 MHz): δ -126.5

6.3.4 Compound 4.29

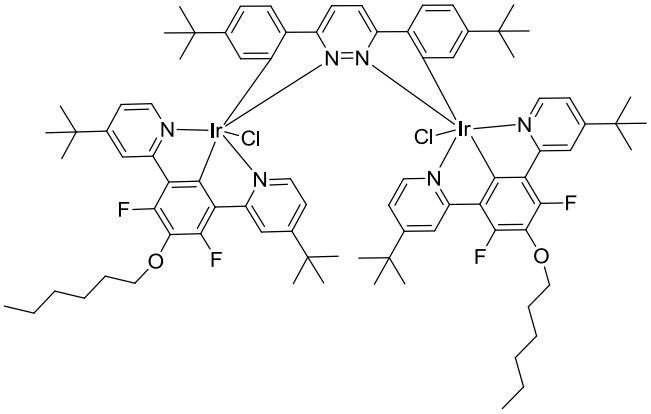

To a mixture of Ir complex **4.26** (148 mg, 0.1 mmol), the bis NC ligand **4.16** (34 mg, 0.1 mmol) and toluene (30 cm^3), silver triflate (77 mg, 0.3 mmol, 3 eq) was added and the reaction mixture was heated under reflux for 8 hours. The heating was removed and 10 cm^3 of 2M HCl was added to a still warm mixture. The mixture was stirred for 5 minutes. Toluene was evaporated using rotary evaporator leaving behind around 5 cm^3 of aqueous solution and amorphous solid on sides of the flask. The aqueous solution was decanted. To the residue 30 cm^3 of methanol was added. The mixture was heated to reflux and filtered. To the filtrate, 5 cm^3 of saturated solution of KPF_6 was added, followed by 20 cm^3 of water leading to fine precipitate. The mixture was heated to boil then stirred at Rt for 10 min. The solid was filtered off, washed with water to give yellow solid. The solid was dried in oven at 100 ^oC for 2 hours. Yield 100 mg. NMR shows that this is a mixture of the desired product and unreacted dichlorobridged complex. The product was then purified by column chromatography using silicagel as a stationary phase. The column was eluted firstly with DCM, followed by a mixture of DCM/MeOH 20/1. Yield 18 mg (10%) ^{1}H-NMR (400 MHz, $CDCl_3$) δ 8.74 (2H, s), 7.96 (4H, d, *J* = 5.95 Hz), 7.92 (4H, s), 7.65 (2H, d, *J* = 8.70 Hz), 7.02 (4H, dd, *J* = 6.41, 2.29 Hz), 6.91 (2H, dd, *J* = 8.24, 1.83 Hz), 6.03 (2H, d, *J* = 1.83 Hz), 4.00 (4H, t, *J* = 13.28, 6.87 Hz), 1.79-1.71 (4H, m), 1.53-1.42 (4H, m), 1.37-1.27 (8H, m), 1.18 (36H, s), 0.93-0.83 (24H, m). ^{13}C-NMR (101 MHz, $CDCl_3$) δ 169.95, 164.68, 163.57, 162.60, 155.95, 154.33, 153.29, 152.60, 141.65, 139.95, 131.11, 127.26, 127.00, 124.04, 120.68, 120.58, 120.42, 75.49, 35.05, 34.58, 31.64, 30.84, 30.44, 30.02, 29.78, 25.49, 22.66, 14.10. ^{19}F NMR (400 MHz): δ -125.75.

6.4 Miscellaneous

6.4.1 (4-*tert*-butylphenyl)boronic acid

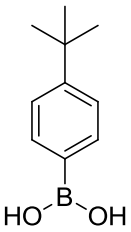

To a stirred solution of 1-bromo-4-*tert* butylbenzene (9.7 g, 45.7 mmol) in dry THF (80 cm^3) at -78°C, *n*-butyllithium (1.6 M solution in hexane, 30 cm^3, 48 mmol) was added slowly. The solution was stirred at -78°C for 2 hours. Triisopropylborate (16 cm^3, 70.5 mmol) was added slowly and the mixture was stirred at -78°C for 1 hour. The flask was then left to come up to room temperature whilst stirring for ~19 hours. The mixture was then acidified by the addition of 1M aqueous hydrochloric acid (50 cm^3). Ethyl acetate was added and the mixture was separated. The organic layer was washed with brine (20 cm^3) then water (10 cm^3). All volatiles were then reduced by rotary evaporation under reduced pressure. Yield 6.9 g, 85%. ^{1}H-NMR (400 MHz, CDCl3) δ_H 8.16 (2H, d, *J* = 8.24 Hz), 7.53 (2H, d, *J* = 8.24 Hz), 1.37 (9H, s)[94].

6.4.2 Tetrakis(triphenylphosphine) palladium (o)

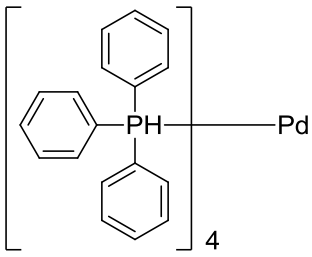

Palladium dichloride (1 g, 5.6 mmol), triphenylphosphine (7.4 g, 28.2 mmol) and dimethyl sulfoxide (68 mL) were heated to 140 °C until the solid dissolved. The solution was then removed from the oil bath and left stirring for a further 10 minutes. Hydrazine hydrate (1.1 mL) was then rapidly added and the solution cooled to ~120°C where crystallisation occurs. The solution was then removed from the water bath and left to cool to room temperature. The solution was then filtered and washed with absolute ethanol (2 x 10 mL) and diethyl ether (2 x 10 mL). The resulting yellow solid was then left to dry for 2 hours. Yield 6.4 g[95].

6.4.3 Sodium acetylacetonate

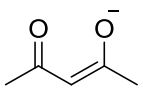

Metallic sodium (2.1 g, 90 mmol) was dissolved in ethanol (50 cm^3). Acetylacetone (9 g, 90 mmol) was then added drop wise whilst stirring. The solution was then left stirring for 1 hour. The resulting precipitate was then filtered off. Yield 7.2 g. ^{1}H-NMR (270 MHz, CDCl3) δ_H 5.51 (1H, s), 2.05 (6H, s).

6.4.4 Sodium dipivaloylmethane

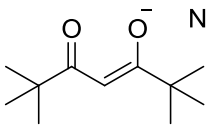

Metallic sodium (750 mg, 32.6 mmol) was dissolved in ethanol (50 cm^3). Dipivaloylmethane (6 g, 32.6 mmol) was then added drop wise whilst stirring. The solution was then left stirring for 2 hours. The resulting precipitate was then filtered off. Yield 6.97 g. Not soluble for NMR.

Appendices

7 Appendices

7.1 TD DFT Data

7.1.1 Complex 2.14 and 2.20

Table 7.1 Selected calculated excitation energies (ΔE), oscillator strengths (f), and main orbital components for the proligand 2.1 and its mono- and dinuclear complexes[a]

	vacuum			dichloromethane		
	ΔE, nm	f	transition (coefficient)	ΔE, nm	f	transition (coefficient)
L^1H_2	295	0.398	HOMO → LUMO (0.67) HOMO-1 → LUMO+1 (0.19)	302	0.609	HOMO → LUMO (0.69) HOMO-1 → LUMO+1 (0.11)
PtL^1H	443	0.050	HOMO → LUMO (0.65) HOMO-1 → LUMO (-0.27)	432	0.091	HOMO → LUMO (0.65) HOMO-1 → LUMO (-0.27)
	394	0.136	HOMO-1 → LUMO (0.63) HOMO → LUMO (0.27)	390	0.198	HOMO-1 → LUMO (0.64) HOMO → LUMO (0.27)
	357	0.033	HOMO → LUMO+1 (0.69)	347	0.031	HOMO → LUMO+1 (0.69)
	336	0.029	HOMO-1 → LUMO+1 (0.52) HOMO-3 → LUMO (0.44)	331	0.145	HOMO-3 → LUMO (0.55) HOMO-1 → LUMO+1 (-0.41)
	324	0.025	HOMO → LUMO+2 (0.69)	317	0.382	HOMO-5 → LUMO (0.43) HOMO-1 → LUMO+1 (-0.41)
	316	0.285	HOMO-3 → LUMO (0.47) HOMO-1 → LUMO+1 (-0.38)	316	0.260	HOMO-5 → LUMO (0.53) HOMO-1 → LUMO+1 (0.34)
	313	0.284	HOMO-4 → LUMO (0.59) HOMO-1 → LUMO+2 (0.22)	309	0.033	HOMO-4 → LUMO (0.67) HOMO-1 → LUMO+1 (0.11)
Pt_2L^1	470	0.177	HOMO → LUMO (0.69) HOMO-5 → LUMO (0.13)	471	0.260	HOMO → LUMO (0.69) HOMO-5 → LUMO (0.12)
	416	0.109	HOMO-2 → LUMO (0.60) HOMO-1 → LUMO (-0.36)	417	0.155	HOMO-2 → LUMO (0.59) HOMO-1 → LUMO (0.38)
	396	0.023	HOMO-5 → LUMO (0.67) HOMO-2 → LUMO+1 (-0.12)	394	0.037	HOMO-5 → LUMO (0.67) HOMO-8 → LUMO (-0.11)
	365	0.026	HOMO-1 → LUMO+1 (0.64) HOMO-2 → LUMO+1 (0.19)	360	0.020	HOMO-1 → LUMO+1 (0.60) HOMO-2 → LUMO+1 (-0.26)
				350	0.061	HOMO-6 → LUMO (0.43) HOMO-2 → LUMO+1 (0.40)

[a] For brevity, only transitions with f >0.01 and/or ΔE > 290 nm have been included, and only the two largest components of each transition are listed.

7.1.2 Complex 2.15 and 2.21

Table 7.2 Selected calculated excitation energies (ΔE), oscillator strengths (f), and main orbital components for the proligand 2.2 and its mono- and dinuclear complexes[a]

	vacuum			dichloromethane		
	ΔE, nm	f	transition (coefficient)	ΔE, nm	f	transition (coefficient)
L^2H_2	279	0.909	HOMO → LUMO (0.64) HOMO → LUMO+10 (-0.12)	287	1.057	HOMO → LUMO (0.64) HOMO-3 → LUMO+7 (-0.11)
	241	0.025	HOMO → LUMO+3 (0.55) HOMO-4 → LUMO+3 (0.17)	243	0.041	HOMO → LUMO+2 (0.55) HOMO-4 → LUMO+2 (-0.17)
PtL^2H	456	0.068	HOMO → LUMO (0.68) HOMO-3 → LUMO (0.12)	450	0.110	HOMO → LUMO (0.68) HOMO-3 → LUMO (0.11)
	384	0.065	HOMO-1 → LUMO (0.65) HOMO-3 → LUMO (0.16)	384	0.095	HOMO-1 → LUMO (0.66) HOMO-3 → LUMO (0.15)
	364	0.042	HOMO → LUMO+1 (0.66) HOMO-1 → LUMO (0.17)	356	0.035	HOMO → LUMO+1 (0.62) HOMO-3 → LUMO (-0.28)
	349	0.269	HOMO-3 → LUMO (0.61) HOMO-1 → LUMO+1 (-0.26)	350	0.496	HOMO-3 → LUMO (0.59) HOMO → LUMO+1 (0.30)
	328	0.019	HOMO → LUMO+2 (0.69)	324	0.019	HOMO → LUMO+2 (0.68)
	322	0.057	HOMO-2 → LUMO+1 (0.61) HOMO-1 → LUMO+1 (0.30)	320	0.019	HOMO-2 → LUMO+1 (0.66) HOMO-1 → LUMO+1 (0.18)
	322	0.201	HOMO-1 → LUMO+1 (0.55) HOMO-2 → LUMO+1 (-0.33)	320	0.241	HOMO-1 → LUMO+1 (0.64) HOMO-2 → LUMO+1 (-0.20)
	307	0.064	HOMO-4 → LUMO (0.63) HOMO-1 → LUMO+2 (-0.21)	307	0.056	HOMO-4 → LUMO (0.65) HOMO-1 → LUMO+2 (-0.18)
Pt_2L^2	522	0.075	HOMO → LUMO (0.69) HOMO-6 → LUMO (0.11)	517	0.123	HOMO → LUMO (0.69) HOMO-2 → LUMO (-0.11)
	429	0.156	HOMO-2 → LUMO (0.67) HOMO → LUMO+1 (-0.15)	433	0.225	HOMO-2 → LUMO (0.68) HOMO → LUMO (0.12)
	385	0.042	HOMO-6 → LUMO (0.48) HOMO → LUMO+1 (0.47)	380	0.061	HOMO → LUMO+1 (0.49) HOMO-6 → LUMO (0.46)
	374	0.340	HOMO → LUMO+1 (0.49) HOMO-6 → LUMO (-0.44)	374	0.461	HOMO → LUMO+1 (0.49) HOMO-6 → LUMO (-0.47)
	342	0.171	HOMO-2 → LUMO+1 (0.62) HOMO-7 → LUMO (0.22)	343	0.237	HOMO-2 → LUMO+1 (0.65) HOMO-6 → LUMO (0.19)

[a] For brevity, only transitions with f >0.01 and/or ΔE > 200 nm have been included, and only the two largest components of each transition are listed.

7.1.3 Complex 2.16 and 2.22

Table 7.3 Selected calculated excitation energies (ΔE), oscillator strengths (f), and main orbital components for the proligand 2.3 and its mono- and dinuclear complexes[a]

	vacuum			dichloromethane		
	ΔE, nm	f	transition (coefficient)	ΔE, nm	f	transition (coefficient)
L^3H_2	308	0.116	HOMO → LUMO (0.69)	312	0.173	HOMO → LUMO (0.70)
	295	0.230	HOMO → LUMO+1 (0.70)	298	0.299	HOMO → LUMO+1 (0.30)
PtL^3H	450	0.019	HOMO → LUMO (0.68) HOMO-1 → LUMO (-0.16)	441	0.032	HOMO → LUMO (0.67) HOMO-1 → LUMO (0.17)
	381	0.039	HOMO-1 → LUMO (0.60) HOMO → LUMO+1 (0.31)	379	0.084	HOMO-1 → LUMO (0.64) HOMO → LUMO+1 (0.18)
	365	0.131	HOMO → LUMO+1 (0.61) HOMO-1 → LUMO (-0.32)	359	0.145	HOMO → LUMO+1 (0.66) HOMO-1 → LUMO (-0.19)
	344	0.046	HOMO-3 → LUMO (0.60) HOMO-1 → LUMO+1 (0.33)	342	0.090	HOMO-3 → LUMO (0.63) HOMO-1 → LUMO+1 (0.25)
	329	0.025	HOMO → LUMO+2 (0.69)	324	0.026	HOMO → LUMO+2 (0.67) HOMO-2 → LUMO+1 (0.19)
	322	0.077	HOMO-1 → LUMO+1 (0.57) HOMO-3 → LUMO (-0.31)	319	0.111	HOMO-1 → LUMO+1 (0.59) HOMO-3 → LUMO (-0.25)
	318	0.013	HOMO-5 → LUMO (0.52) HOMO-6 → LUMO (0.38)			
Pt_2L^3	475[b]	0.033	HOMO-1 → LUMO (0.62) HOMO-2 → LUMO (0.32)	467[c]	0.059	HOMO-1 → LUMO (0.60) HOMO-2 → LUMO (0.35)
	410	0.060	HOMO-3 → LUMO (0.66) HOMO-1 → LUMO+1 (0.21)	433	0.013	HOMO-2 → LUMO (0.39) HOMO-4 → LUMO (0.37)
	399	0.413	HOMO → LUMO+1 (0.52) HOMO-2 → LUMO (-0.43)	406	0.075	HOMO-3 → LUMO (0.65) HOMO-1 → LUMO+1 (0.23)
	390	0.025	HOMO-1 → LUMO+1 (0.60) HOMO-2 → LUMO+1 (0.24)	403	0.534	HOMO → LUMO+1 (0.54) HOMO-2 → LUMO (0.41)
	356	0.013	HOMO-6 → LUMO (0.50) HOMO-2 → LUMO+1 (0.46)	389	0.046	HOMO-1 → LUMO+1 (0.61) HOMO-3 → LUMO (-0.24)
				356	0.017	HOMO-6 → LUMO (0.44) HOMO-4 → LUMO+1 (0.42)

[a] For brevity, only transitions with f >0.01 and/or ΔE > 290 nm have been included, and only the two largest components of each transition are listed. [b]Additional very weak transition at 511 nm (f = 0.004); character HOMO → LUMO (0.69). [c]Additional very weak transition at 501 nm (f = 0.006); character HOMO → LUMO (0.69).

7.1.4 Complex 2.17 and 2.23

Table 7.4 Selected calculated excitation energies (ΔE), oscillator strengths (f), and main orbital components for the proligand 2.4 and its mono- and dinuclear complexes[a]

	vacuum			dichloromethane		
	ΔE, nm	f	transition (coefficient)	ΔE, nm	f	transition (coefficient)
L^4H_2	327	0.094	HOMO-1 → LUMO (0.63) HOMO → LUMO+1 (0.28)	338	0.021	HOMO-1 → LUMO (0.69) HOMO → LUMO+1 (-0.11)
	297	0.088	HOMO → LUMO+1 (0.50) HOMO-1 → LUMO+2 (0.42)	331	0.161	HOMO → LUMO (0.66) HOMO-1 → LUMO+1 (0.22)
				299	0.115	HOMO-1 → LUMO+1 (0.53) HOMO → LUMO+2 (-0.40)
				290	0.070	HOMO → LUMO+1 (0.58) HOMO-1 → LUMO+2 (0.33)
PtL^4H	470	0.021	HOMO → LUMO (0.68) HOMO-1 → LUMO (-0.13)	462	0.033	HOMO → LUMO (0.68) HOMO-1 → LUMO (-0.14)
	398	0.089	HOMO-1 → LUMO (0.66) HOMO → LUMO+1 (0.17)	396	0.135	HOMO-1 → LUMO (0.66) HOMO → LUMO (0.15)
	350	0.135	HOMO → LUMO+1 (0.67) HOMO-1 → LUMO (-0.16)	347	0.194	HOMO → LUMO+1 (0.68) HOMO-1 → LUMO (-0.14)
	335	0.038	HOMO-4 → LUMO (0.55) HOMO-1 → LUMO+1 (-0.28)	335	0.060	HOMO-4 → LUMO (0.60) HOMO-1 → LUMO+1 (-0.26)
	329	0.013	HOMO → LUMO+2 (0.65) HOMO-4 → LUMO (-0.21)	325	0.018	HOMO → LUMO+2 (0.68) HOMO-4 → LUMO (-0.13)
Pt_2L^4	531	0.064	HOMO → LUMO (0.68) HOMO-2 → LUMO (0.18)	516	0.104	HOMO → LUMO (0.68) HOMO-2 → LUMO (0.19)
	521	0.021	HOMO-1 → LUMO (0.69) HOMO-7 → LUMO (0.11)	513	0.030	HOMO-1 → LUMO (0.69) HOMO-7 → LUMO (0.10)
	435	0.171	HOMO-2 → LUMO (0.66) HOMO → LUMO (-0.18)	439	0.218	HOMO-2 → LUMO (0.66) HOMO → LUMO (-0.20)
	411	0.035	HOMO-3 → LUMO (0.70)	412	0.045	HOMO-3 → LUMO (0.69)
	348	0.155	HOMO-1 → LUMO+1 (0.64) HOMO-8 → LUMO (-0.24)	347	0.213	HOMO-1 → LUMO+1 (0.65) HOMO-8 → LUMO (-0.22)

[a] For brevity, only transitions with f >0.02 and/or ΔE > 290 nm have been included, and only the two largest components of each transition are listed.

7.1.5 Complex 2.18 and 2.24

Table 7.5 Selected calculated excitation energies (ΔE), oscillator strengths (f), and main orbital components for the proligand 2.5 and its mono- and dinuclear complexes[a]

	vacuum			dichloromethane		
	ΔE, nm	f	transition (coefficient)	ΔE, nm	f	transition (coefficient)
L^5H_2	345	0.223	HOMO → LUMO (0.68) HOMO-1 → LUMO+1 (0.15)	351	0.329	HOMO → LUMO (0.69) HOMO-1 → LUMO+1 (0.12)
PtL^5H	494	0.032	HOMO → LUMO (0.68) HOMO-1 → LUMO (-0.15)	490	0.052	HOMO → LUMO (0.67) HOMO-1 → LUMO (-0.17)
	428	0.068	HOMO-1 → LUMO (0.66) HOMO → LUMO (0.17)	430	0.094	HOMO-1 → LUMO (0.66) HOMO → LUMO (0.19)
	380	0.124	HOMO-3 → LUMO (0.65) HOMO-1 → LUMO+1 (-0.16)	383	0.194	HOMO-3 → LUMO (0.67) HOMO-1 → LUMO+1 (-0.13)
	352	0.080	HOMO → LUMO+1 (0.66) HOMO-4 → LUMO (-0.15)	348	0.107	HOMO → LUMO+1 (0.68)
	328	0.031	HOMO → LUMO+2 (0.52) HOMO-1 → LUMO+1 (-0.32)	326	0.032	HOMO-1 → LUMO+1 (0.50) HOMO-7 → LUMO (-0.38)
	327	0.017	HOMO → LUMO+2 (0.44) HOMO-1 → LUMO+1 (0.39)	323	0.023	HOMO → LUMO+2 (0.65) HOMO-1 → LUMO+1 (0.14)
	322	0.011	HOMO-6 → LUMO (0.47) HOMO-10 → LUMO (-0.32)			
Pt_2L^5	539	0.023	HOMO → LUMO (0.69) HOMO-6 → LUMO (-0.11)	538	0.038	HOMO → LUMO (0.69)
	507	0.032	HOMO-1 → LUMO (0.58) HOMO-2 → LUMO (-0.39)	506	0.055	HOMO-1 → LUMO (0.55) HOMO-2 → LUMO (-0.43)
	468	0.099	HOMO-2 → LUMO (0.52) HOMO-1 → LUMO (0.37)	477	0.100	HOMO-2 → LUMO (0.46) HOMO-4 → LUMO (0.38)
	456	0.020	HOMO-4 → LUMO (0.65) HOMO-2 → LUMO (-0.19)	467	0.057	HOMO-4 → LUMO (0.58) HOMO-2 → LUMO (-0.28)
	444	0.059	HOMO-3 → LUMO (0.68) HOMO-5 → LUMO (0.12)	447	0.074	HOMO-3 → LUMO (0.69)
	408	0.029	HOMO-6 → LUMO (0.63) HOMO-2 → LUMO+1 (-0.27)	409	0.057	HOMO-6 → LUMO (0.63) HOMO-2 → LUMO+1 (0.27)
	395	0.203	HOMO → LUMO+1 (0.68) HOMO-2 → LUMO (-0.14)	399	0.258	HOMO → LUMO+1 (0.68) HOMO-2 → LUMO (0.13)
				384	0.015	HOMO-7 → LUMO (0.67) HOMO-9 → LUMO (0.13)

[a] For brevity, only transitions with f >0.02 and/or ΔE > 290 nm have been included, and only the two largest components of each transition are listed.

7.1.6 Complex 2.19 and 2.25

Table 7.6 Selected calculated excitation energies (ΔE), oscillator strengths (f), and main orbital components for the proligand 2.6 and its mono- and dinuclear complexes[a]

	vacuum			dichloromethane		
	ΔE, nm	f	transition (coefficient)	ΔE, nm	f	transition (coefficient)
L^6H_2	362	0.239	HOMO-1 → LUMO (0.67) HOMO → LUMO+1 (0.21)	391	0.029	HOMO → LUMO (0.69)
	294	0.174	HOMO → LUMO+1 (0.50) HOMO-1 → LUMO+2 (-0.42)	369	0.377	HOMO-1 → LUMO (0.68) HOMO → LUMO+1 (0.17)
				296	0.316	HOMO → LUMO+1 (0.57) HOMO-1 → LUMO+2 (-0.37)
PtL^6H	518	0.049	HOMO → LUMO (0.67) HOMO-1 → LUMO (0.16)	517	0.075	HOMO → LUMO (0.67) HOMO-1 → LUMO (0.18)
	451	0.084	HOMO-1 → LUMO (0.67) HOMO → LUMO (-0.17)	454	0.120	HOMO-1 → LUMO (0.67) HOMO → LUMO (-0.19)
	418	0.013	HOMO-2 → LUMO (0.69)	419	0.019	HOMO-3 → LUMO (0.70)
	378	0.126	HOMO-4 → LUMO (0.68) HOMO-1 → LUMO+1 (-0.15)	384	0.197	HOMO-4 → LUMO (0.69) HOMO-1 → LUMO+1 (-0.11)
	335	0.071	HOMO → LUMO+1 (0.58) HOMO-6 → LUMO (-0.23)	343	0.020	HOMO-6 → LUMO (0.65) HOMO → LUMO+1 (0.16)
	331	0.017	HOMO → LUMO+2 (0.68) HOMO-7 → LUMO (-0.11)	334	0.090	HOMO → LUMO+1 (0.63) HOMO-7 → LUMO (0.25)
				327	0.100	HOMO-7 → LUMO (0.59) HOMO → LUMO+2 (-0.22)
Pt_2L^6	589	0.078	HOMO → LUMO (0.68) HOMO-2 → LUMO (-0.20)	582	0.124	HOMO → LUMO (0.67) HOMO-2 → LUMO (-0.22)
	557	0.053	HOMO-1 → LUMO (0.69) HOMO-7 → LUMO (0.12)	559	0.079	HOMO-1 → LUMO (0.69) HOMO-7 → LUMO (0.11)
	492	0.112	HOMO-2 → LUMO (0.66) HOMO → LUMO (0.19)	501	0.170	HOMO-2 → LUMO (0.66) HOMO → LUMO (0.22)
	459	0.047	HOMO-4 → LUMO (0.69) HOMO-2 → LUMO (-0.11)	459	0.013	HOMO-3 → LUMO (0.69) HOMO-1 → LUMO (0.11)
	450	0.011	HOMO-3 → LUMO (0.69)	456	0.020	HOMO-6 → LUMO (0.70)
	371	0.093	HOMO-7 → LUMO (0.65) HOMO-2 → LUMO+1 (0.14)	373	0.171	HOMO-7 → LUMO (0.66) HOMO-2 → LUMO+1 (0.13)

[a] For brevity, only transitions with f >0.02 and/or ΔE > 290 nm have been included, and only the two largest components of each transition are listed.

7.2 Calculated frontier orbital energies

Table 7.7 Calculated Frontier Orbital Energies (eV, *in vacuo*) for the Complexes

Complex	**2.14**	**2.20**	**2.15**	**2.21**	**2.16**	**2.22**	**2.17**	**2.23**	**2.18**	**2.24**	**2.19**	**2.24**
LUMO+2	-1.296	-1.416	-1.380	-1.471	-1.359	-1.447	-1.399	-1.451	-1.357	-1.420	-1.415	-1.461
LUMO+1	-1.714	-1.926	-1.791	-1.953	-1.799	-2.186	-1.651	-1.672	-1.708	-2.085	-1.512	-1.500
LUMO	-2.396	-2.633	-2.426	-2.764	-2.311	-2.684	-2.515	-2.854	-2.629	-2.889	-2.834	-3.095
HOMO	-5.816	-5.828	-5.824	-5.789	-5.801	-5.793	-5.807	-5.794	-5.817	-5.822	-5.809	-5.751
HOMO-1	-6.133	-6.005	-6.194	-6.036	-6.194	-5.971	-6.239	-5.871	-6.093	-5.968	-6.145	-5.897
HOMO-2	-6.301	-6.114	-6.415	-6.159	-6.388	-6.247	-6.412	-6.268	-6.352	-6.139	-6.378	-6.179
HOMO-LUMO gap	3.420	3.196	3.397	3.025	3.490	3.109	3.292	2.940	3.188	2.933	2.976	2.65

7.3 Frontier orbital plots

7.3.1 Complex 2.14 and 2.20

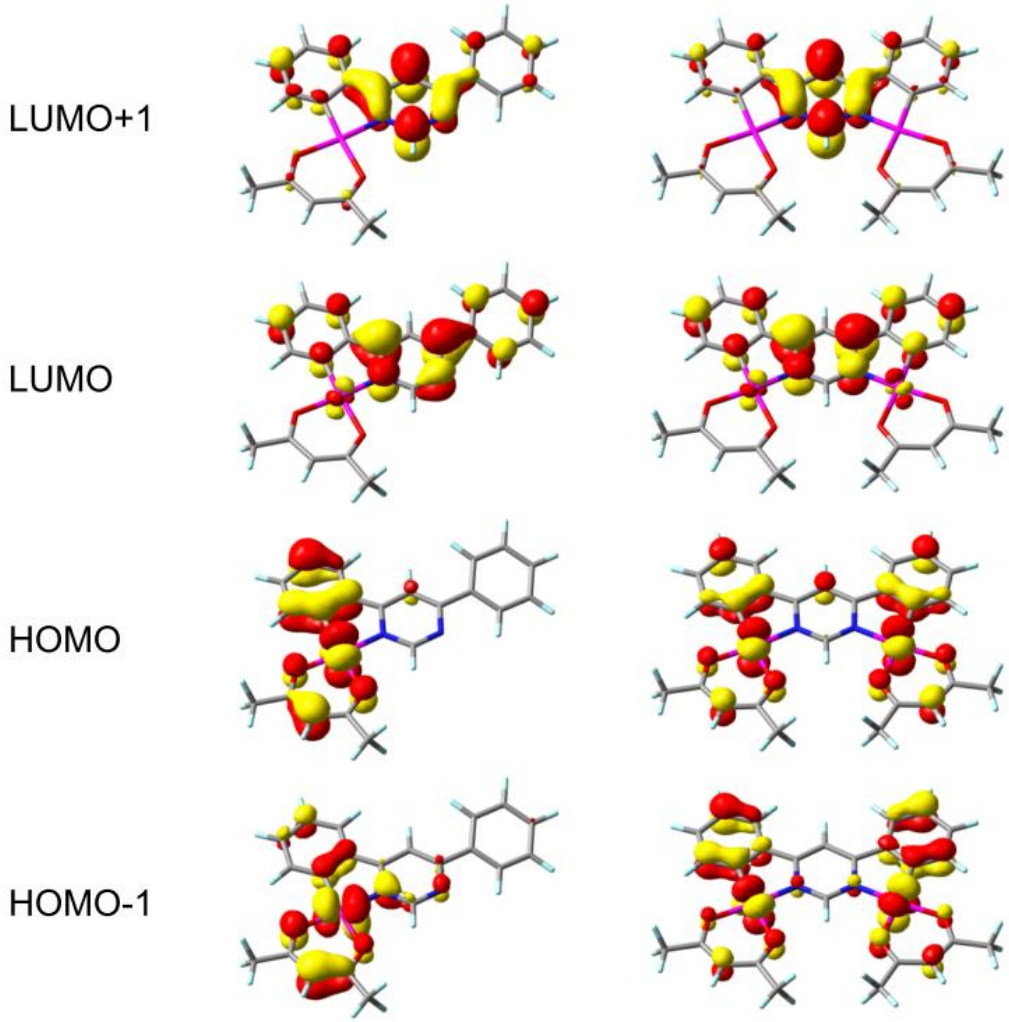

7.3.2 Complex 2.15 and 2.21

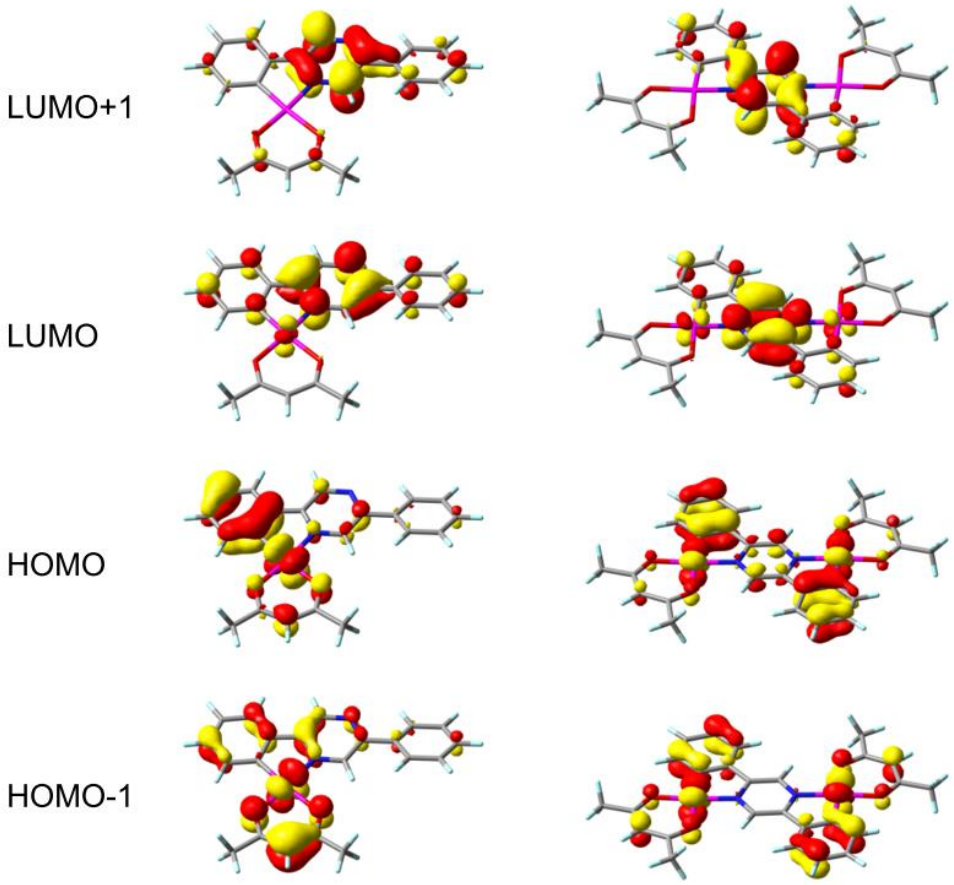

7.3.3 Complex 2.16 and 2.22

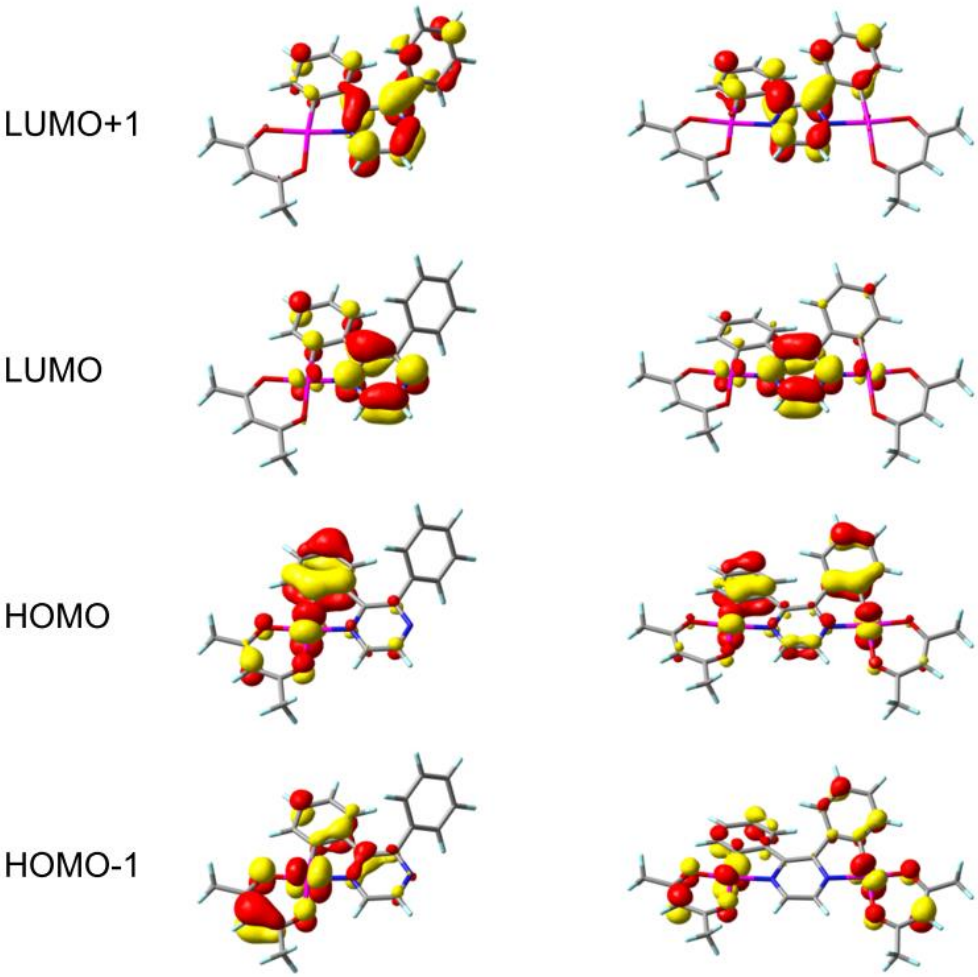

7.3.4 Complex 2.17 and 2.23

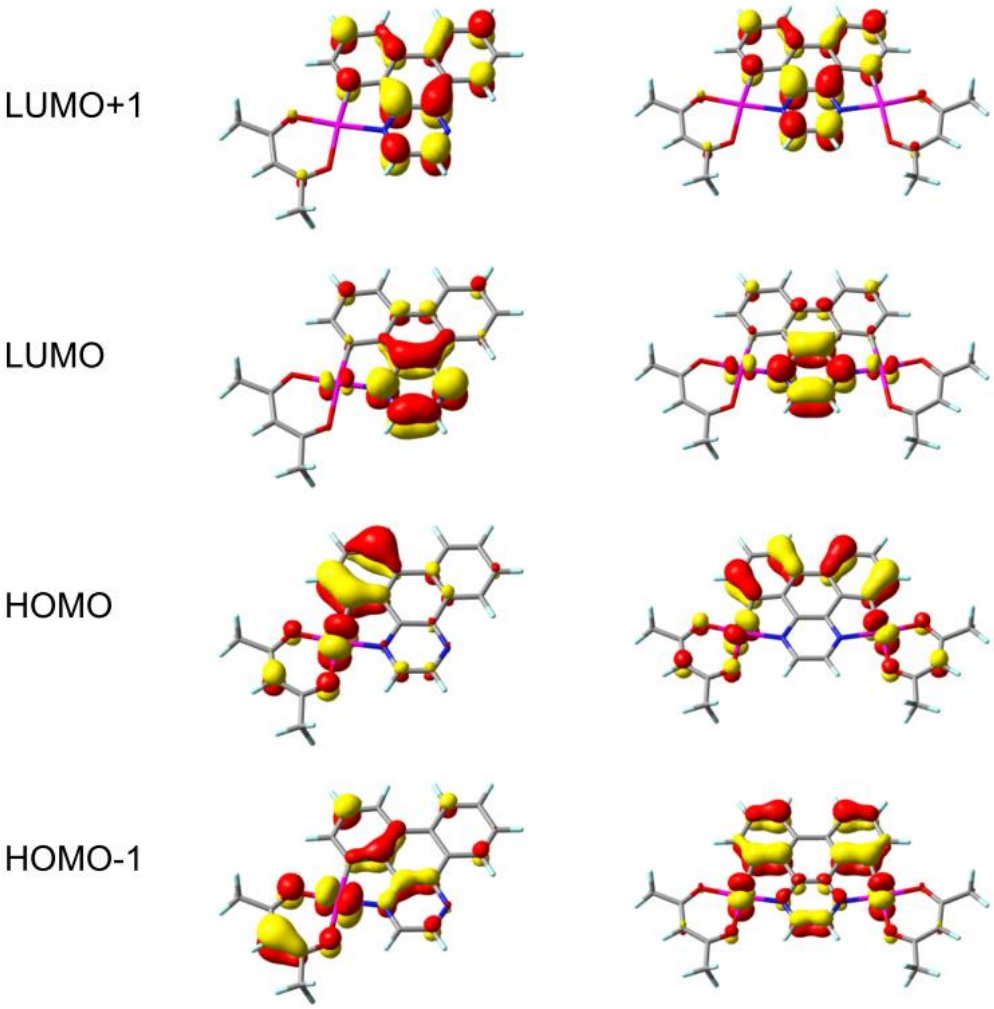

7.3.5 Complex 2.18 and 2.24

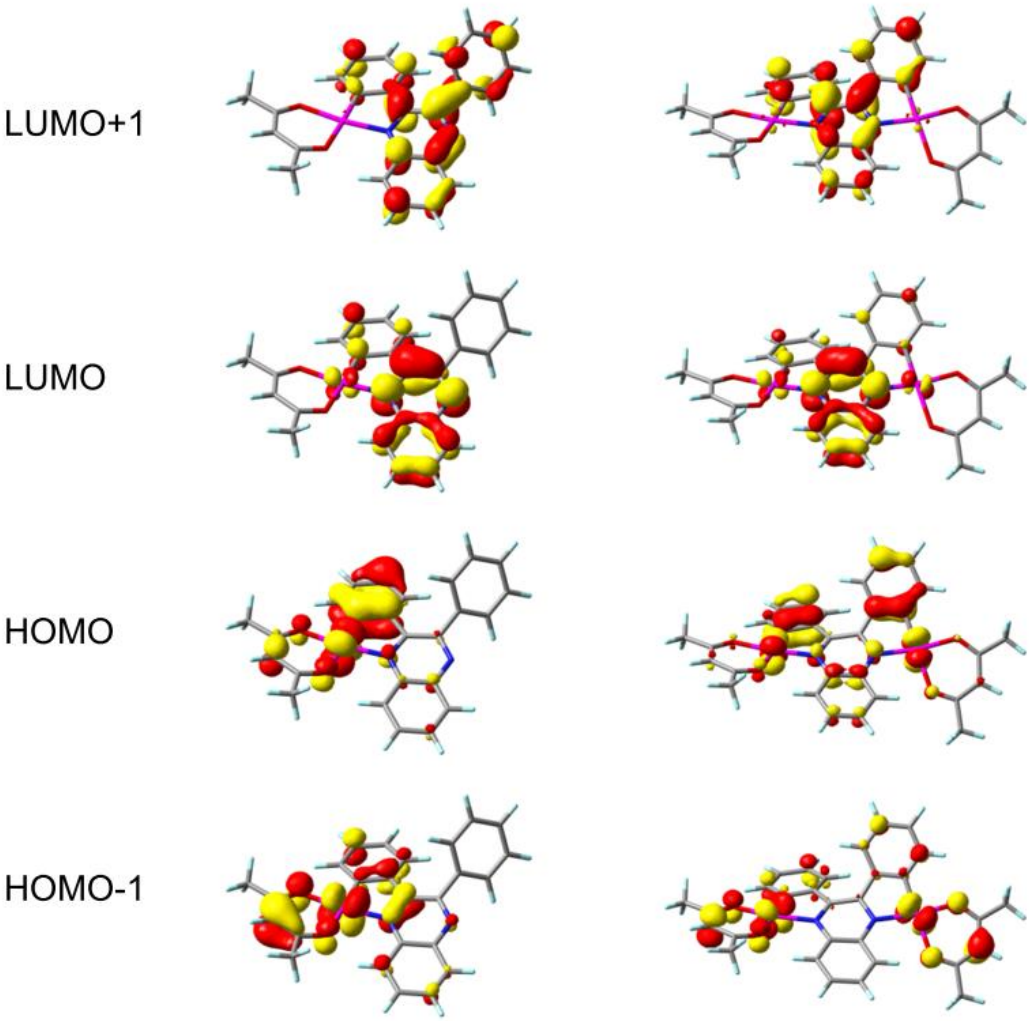

7.3.6 Complex 2.19 and 2.25

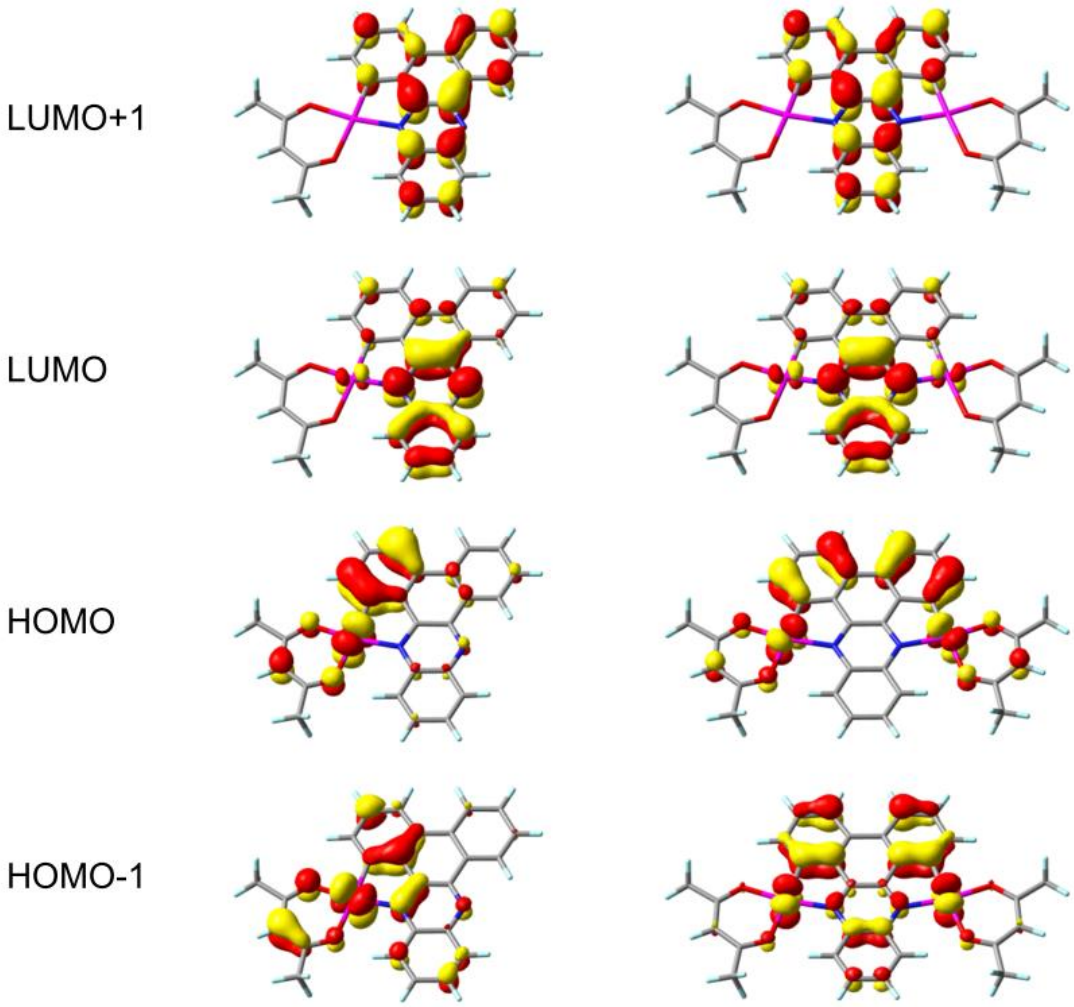

References

References

(1) Qiao, J.; Duan, L.; Tang, L.; He, L.; Wang, L.; Qiu, Y. *J. Mater. Chem.* **2009**, *19*, 6573.

(2) Thorp-Greenwood, F.; Balasingham, R. G. *J. Organomet. Chem.* **2012**, *714*, 12–21.

(3) Zhao, Q.; Huang, C.; Li, F. *Chem. Soc. Rev.* **2011**, *40*, 2508–2524.

(4) Li, C.; Lin, J.; Yang, X.; Wan, J. *J. Organomet. Chem.* **2011**, *696*, 2445–2450.

(5) Anthopoulos, T. D.; Frampton, M. J.; Namdas, E. B.; Burn, P. L.; Samuel, I. D. W. *Adv. Mater.* **2004**, *16*, 557–560.

(6) Williams, J. A. G. *Top. Curr. Chem.* **2007**, *281*, 205–268.

(7) Kozhevnikov, D. N.; Kozhevnikov, V. N.; Ustinova, M. M.; Santoro, A.; Bruce, D. W.; Koenig, B.; Czerwieniec, R.; Fischer, T.; Zabel, M.; Yersin, H. *Inorg. Chem.* **2009**, *48*, 4179–4189.

(8) Brooks, J.; Babayan, Y.; Lamansky, S.; Djurovich, P. I.; Tsyba, I.; Bau, R.; Thompson, M. E. *Inorg. Chem.* **2002**, *41*, 3055–3066.

(9) Laskar, I. R.; Hsu, S.-F.; Chen, T.-M. *Polyhedron* **2005**, *24*, 881–888.

(10) Borisov, S. M.; Klimant, I. *Dye. Pigment.* **2009**, *83*, 312–316.

(11) Duan, J.-P.; Sun, P.-P.; Cheng, C.-H. *Adv. Mater.* **2003**, *15*, 224–228.

(12) Nazeeruddin, K.; Humphry-Baker, R.; Berner, D.; Rivier, S.; Zuppiroli, L.; Graetzel, M. *J. Am. Chem. Soc.* **2003**, *125*, 8790–8797.

(13) Nonoyama, M. *Bull. Chem. Soc. Jpn.* **1974**, *47*, 767–768.

(14) Hwang, F.-M.; Chen, H.-Y.; Chen, P.-S.; Liu, C.-S.; Chi, Y.; Shu, C.-F.; Wu, F.-I.; Chou, P.-T.; Peng, S.-M.; Lee, G.-H. *Inorg. Chem.* **2005**, *44*, 1344–1353.

(15) Li, M.; Zeng, H.; Meng, Y.; Sun, H.; Liu, S.; Lu, Z.; Huang, Y.; Pu, X. *Dalt. Trans.* **2011**, *40*, 7153–7164.

(16) King, K. A.; Spellane, P. J.; Watts, R. J. *J. Am. Chem. Soc.* **1985**, 1431–1432.

(17) Sprouse, S.; King, K. A.; Spellane, P. J.; Watts, R. J. *J. Am. Chem. Soc.* **1984**, *106*, 6647–6653.

(18) Tsuboyama, A.; Iwawaki, H.; Furugori, M.; Mukaide, T.; Kamatani, J.; Igawa, S.; Moriyama, T.; Miura, S.; Takiguchi, T.; Okada, S.; Hoshino, M.; Ueno, K. *J. Am. Chem. Soc.* **2003**, *125*, 12971–12979.

(19) Dedeian, K.; Djurovich, P. I.; Garces, F. O.; Carlson, G.; Watts, R. J. *Inorg. Chem.* **1991**, 1685–1687.

(20) Williams, J. A. G.; Beeby, A.; Davies, E. S.; Weinstein, J. A.; Wilson, C. *Inorg. Chem.* **2003**, *42*, 8609–8611.

(21) Williams, J. A. G.; Beeby, A.; Davies, E. S.; Weinstein, J. A.; Wilson, C. *Inorg. Chem.* **2003**, *42*, 8609–8611.

(22) Cardenas, D. J.; Echavarren, A. M.; Ramırez de Arellano, M. C. *Organometallics* **1999**, *18*, 3337–3341.

(23) Brulatti, P.; Gildea, R. J.; Howard, J. A. K.; Fattori, V.; Cocchi, M.; Williams, J. A. G. *Inorg. Chem.* **2012**, *51*, 3813–3826.

(24) Wilkinson, A. J.; Puschmann, H.; Howard, J. A. K.; Foster, C. E.; Williams, J. A. G. *Inorg. Chem.* **2006**, *45*, 8685–8699.

(25) Flynn, C. M.; Demas, J. N. *J. Am. Chem. Soc.* **1973**, *96*, 1959–1960.

(26) Collin, J. P.; Dixon, I. M.; Sauvage, J. P.; Williams, J. A. G.; Barigelletti, F.; Flamigni, L. *J. Am. Chem. Soc.* **1999**, *121*, 5009–5016.

(27) Hay, P. J. *J. Phys. Chem. A* **2002**, *106*, 1634–1641.

(28) Kang, H. J.; Lee, K. H.; Lee, S. J.; Seo, J. H.; Kim, Y. K.; Yoon, S. S. *Thin Solid Films* **2011**, *519*, 6544–6549.

(29) Lu, W.; Mi, B.-X.; Chan, M. C. W.; Hui, Z.; Che, C.-M.; Zhu, N.; Lee, S.-T. *J. Am. Chem. Soc.* **2004**, *126*, 4958–4971.

(30) Lamansky, S.; Djurovich, P.; Murphy, D.; Abdel-Razzaq, F.; Kwong, R.; Tsyba, I.; Bortz, M.; Mui, B.; Bau, R.; Thompson, M. E. *Inorg. Chem.* **2001**, *40*, 1704–1711.

(31) Laskar, I. R.; Chen, T.-M. *Chem. Mater.* **2004**, *16*, 111–117.

(32) Lee, K. H.; Kang, H. J.; Lee, S. J.; Seo, J. H.; Kim, Y. K.; Yoon, S. S. *Synth. Met.* **2011**, *161*, 1113–1121.

(33) Lee, K. H.; Kang, H. J.; Lee, S. J.; Kim, Y. K.; Yoon, S. S. *Synth. Met.* **2012**, *162*, 715–721.

(34) Zhou, G.; Ho, C.-L.; Wong, W.-Y.; Wang, Q.; Ma, D.; Wang, L.; Lin, Z.; Marder, T. B.; Beeby, A. *Adv. Funct. Mater.* **2008**, *18*, 499–511.

(35) Lepeltier, M.; Dumur, F.; Wantz, G.; Vila, N.; Mbomekallé, I.; Bertin, D.; Gigmes, D.; Mayer, C. R. *J. Lumin.* **2013**, *143*, 145–149.

(36) Dahule, H. K.; Dhoble, S. J.; Ahn, J.-S.; Pode, R. *J. Phys. Chem. Solids* **2011**, *72*, 1524–1528.

(37) Kim, K. H.; Lee, J. Y.; Park, T. J.; Jeon, W. S.; Kennedy, G. P.; Kwon, J. H. *Synth. Met.* **2010**, *160*, 631–635.

(38) Yang, C.-H.; Tai, C.-C.; Sun, I.-W. *J. Mater. Chem.* **2004**, *14*, 947.

(39) Tao, R.; Qiao, J.; Zhang, G.; Duan, L.; Wang, L.; Qiu, Y. *J. Phys. Chem. C* **2012**, *116*, 11658–11664.

(40) Jiang, J.; Jiang, C.; Yang, W.; Zhen, H.; Huang, F.; Cao, Y. *Macromolecules* **2005**, *38*, 4072–4080.

(41) Kozhevnikov, D. N.; Kozhevnikov, V. N.; Shafikov, M. Z.; Prokhorov, A. M.; Bruce, D. W.; Williams, J. A. G. *Inorg. Chem.* **2011**, *50*, 3804–3815.

(42) Obara, S.; Itabashi, M.; Okuda, F.; Tamaki, S.; Tanabe, Y.; Ishii, Y.; Nozaki, K.; Haga, M.-A. *Inorg. Chem.* **2006**, *45*, 8907–8921.

(43) Kozhevnikov, V. N.; Durrant, M. C.; Williams, J. A. G. *Inorg. Chem.* **2011**, *50*, 6304–6313.

(44) Tsujimoto, H.; Yagi, S.; Asuka, H.; Inui, Y.; Ikawa, S.; Maeda, T.; Nakazumi, H.; Sakurai, Y. *J. Organomet. Chem.* **2010**, *695*, 1972–1978.

(45) Campbell, N. A.; Reece, J. B. *Biology*; 7th ed.; Pearson Benjamin Cummings: San Fransisco, 2005; pp. 94–123.

(46) Fernández-Moreira, V.; Thorp-Greenwood, F. L.; Coogan, M. P. *Chem. Commun. (Camb).* **2010**, *46*, 186–202.

(47) *Molecular Probes Handbook, A Guide to Fluorescent Probes and Labelling Techniques*; Johnson, I.; Spence, M. T. Z., Eds.; 11th ed.; Invitrogen Molecular Probes.

(48) Elmes, R. B. P.; Orange, K. N.; Cloonan, S. M.; Williams, D. C.; Gunnlaugsson, T. *J. Am. Chem. Soc.* **2011**, *133*, 15862–15865.

(49) Kobayashi, H.; Ogawa, M.; Alford, R.; Choyke, P. L.; Urano, Y. *Chem. Rev.* **2010**, *110*, 2620–2640.

(50) *Photochemistry and Photophysics of Coordination Compounds*; Balzani, V.; Campagna, S., Eds.; Springer, 2007; p. 1.

(51) Botchway, S. W.; Charnley, M.; Haycock, J. W.; Parker, A. W.; Rochester, D. L.; Weinstein, J. a; Williams, J. a G. *Proc. Natl. Acad. Sci. U. S. A.* **2008**, *105*, 16071–16076.

(52) Zipfel, W. R.; Williams, R. M.; Webb, W. W. *Nat. Biotechnol.* **2003**, *21*, 1369–1377.

(53) Zhao, Q.; Yu, M.; Shi, L.; Liu, S.; Li, C.; Shi, M.; Zhou, Z.; Huang, C.; Li, F. *Organometallics* **2010**, *29*, 1085–1091.

(54) Jiang, W.; Gao, Y.; Sun, Y.; Ding, F.; Xu, Y.; Bian, Z.; Li, F.; Bian, J.; Huang, C. *Inorg. Chem.* **2010**, *49*, 3252–3260.

(55) Lo, K.; Lee, P. *Organometallics* **2008**, 2998–3006.

(56) Wu, P.; Wong, E. L.-M.; Ma, D.-L.; Tong, G. S.-M.; Ng, K.-M.; Che, C.-M. *Chemistry* **2009**, *15*, 3652–3656.

(57) Eryazici, I.; Moorefield, C. N.; Newkome, G. R. *Chem. Rev.* **2008**, *108*, 1834–1895.

(58) Koo, C.-K.; Wong, K.-L.; Man, C. W.-Y.; Lam, Y.-W.; So, L. K.-Y.; Tam, H.-L.; Tsao, S.-W.; Cheah, K.-W.; Lau, K.-C.; Yang, Y.-Y.; Chen, J.-C.; Lam, M. H.-W. *Inorg. Chem.* **2009**, *48*, 872–878.

(59) Koo, C.-K.; So, L. K.-Y.; Wong, K.-L.; Ho, Y.-M.; Lam, Y.-W.; Lam, M. H.-W.; Cheah, K.-W.; Cheng, C. C.-W.; Kwok, W.-M. *Chemistry* **2010**, *16*, 3942–3950.

(60) Lo, K. K.-W.; Louie, M.-W.; Zhang, K. Y. *Coord. Chem. Rev.* **2010**, *254*, 2603–2622.

(61) Chen, H.; Zhao, Q.; Wu, Y.; Li, F.; Yang, H.; Yi, T.; Huang, C. *Inorg. Chem.* **2007**, *46*, 11075–11081.

(62) Yu, M.; Zhao, Q.; Shi, L.; Li, F.; Zhou, Z.; Yang, H.; Yi, T.; Huang, C. *Chem. Commun.* **2008**, 2115–2117.

(63) Quick guide to HeLa cells http://www.wellcome.ac.uk/Education-resources/Education-and-learning/Big-Picture/All-issues/The-Cell/WTDV030785.htm (accessed Sep 19, 2013).

(64) Zhang, K. Y.; Li, S. P.-Y.; Zhu, N.; Or, I. W.-S.; Cheung, M. S.-H.; Lam, Y.-W.; Lo, K. K.-W. *Inorg. Chem.* **2010**, *49*, 2530–2540.

(65) Li, S. P.-Y.; Liu, H.-W.; Zhang, K. Y.; Lo, K. K.-W. *Chemistry* **2010**, *16*, 8329–8339.

(66) Murphy, L.; Congreve, A.; Pålsson, L.-O.; Williams, J. A. G. *Chem. Commun.* **2010**, *46*, 8743–8745.

(67) Zhang, K. Y.; Liu, H.-W.; Fong, T. T.-H.; Chen, X.-G.; Lo, K. K.-W. *Inorg. Chem.* **2010**, *49*, 5432–5443.

(68) Moromizato, S.; Hisamatsu, Y.; Suzuki, T.; Matsuo, Y.; Abe, R.; Aoki, S. *Inorg. Chem.* **2012**, *51*, 12697–12706.

(69) Aoki, S.; Matsuo, Y.; Ogura, S.; Ohwada, H.; Hisamatsu, Y.; Moromizato, S.; Shiro, M.; Kitamura, M. *Inorg. Chem.* **2011**, *50*, 806–818.

(70) Kalinowski, J.; Fattori, V.; Cocchi, M.; Williams, J. A. G. *Coord. Chem. Rev.* **2011**, *255*, 2401–2425.

(71) Ortmans, I.; Didier, P.; Kirsch-De Mesmaeker, a. *Inorg. Chem.* **1995**, *34*, 3695–3704.

(72) Liu, Z. W.; Guan, M.; Bian, Z. Q.; Nie, D. B.; Gong, Z. L.; Li, Z. B.; Huang, C. H. *Adv. Funct. Mater.* **2006**, *16*, 1441–1448.

(73) Hudson, Z. M.; Blight, B. A.; Wang, S. *Org. Lett.* **2012**, *14*, 1700–1703.

(74) Mason, A. T. *Berichte der Dtsch. Chem. Gesellschaft* **1886**, *19*, 112–113.

(75) Minsky, A.; Cohen, Y.; Rabinovitz, M. *J. Am. Chem. Soc.* **1985**, *107*, 1501–1505.

(76) Tsujimoto, H.; Yagi, S.; Asuka, H.; Inui, Y.; Ikawa, S.; Maeda, T.; Nakazumi, H.; Sakurai, Y. *J. Organomet. Chem.* **2010**, *695*, 1972–1978.

(77) Wong, W.-Y.; Ho, C.-L. *J. Mater. Chem.* **2009**, *19*, 4457.

(78) Balashev, K. P.; Puzyk, M. V; Kotlyar, V. S.; Kulikova, M. V. *Coord. Chem. Rev.* **1997**, *159*, 109–120.

(79) Yin, B.; Niemeyer, F.; Williams, J. A. G.; Jiang, J.; Boucekkine, A.; Toupet, L.; Le Bozec, H.; Guerchais, V. *Inorg. Chem.* **2006**, *45*, 8584–8596.

(80) Lamansky, S.; Djurovich, P.; Murphy, D.; Abdel-Razzaq, F.; Lee, H. E.; Adachi, C.; Burrows, P. E.; Forrest, S. R.; Thompson, M. E. *J. Am. Chem. Soc.* **2001**, *123*, 4304–4312.

(81) Bronstein, H. A.; Finlayson, C. E.; Kirov, K. R.; Friend, R. H.; Williams, C. K. *Organometallics* **2008**, *27*, 2980–2989.

(82) Becke, A. D. *J. Chem. Phys.* **1993**, *98*, 5648–5652.

(83) Hay, P. J.; Watt, W. R. *J. Chem. Phys.* **1985**, *82*, 270–284.

(84) Cossi, M.; Scalmani, G.; Rega, N.; Barone, V. *J. Chem. Phys.* **2002**, *117*, 43–55.

(85) Gabriel, S. *Berichte der Dtsch. Chem. Gesellschaft* **1908**, *41*, 1127–1156.

(86) Gabriel, S. *Berichte der Dtsch. Chem. Gesellschaft* **1913**, *46*, 3859–3861.

(87) Gildea, L. F.; Batsanov, A. S.; Williams, J. A. G. *Dalt. Trans.* **2013**, *42*, 10388–10393.

(88) Tsuboyama, A.; Takiguchi, T.; Okada, S.; Osawa, M.; Hoshino, M.; Ueno, K. *Dalt. Trans.* **2004**, 1115–1116.

(89) Slater, J.; Rourke, J. P. *J. Organomet. Chem.* **2003**, *688*, 112–120.

(90) Qing, F.; Ruowen Wang; Li, B.; Zheng, X.; Meng, W. *J. Fluor. Chem.* **2003**, *120*, 21–24.

(91) Patil, R. D.; Joshi, G.; Adimurthy, S.; Ranu, B. C. *Tetrahedron Lett.* **2009**, *50*, 2529–2532.

(92) Utsukihara, T.; Nakamura, H.; Watanabe, M.; Akira Horiuchi, C. *Tetrahedron Lett.* **2006**, *47*, 9359–9364.

(93) Macharla, A. K.; Chozhiyath Nappunni, R.; Marri, M. R.; Peraka, S.; Nama, N. *Tetrahedron Lett.* **2012**, *53*, 191–195.

(94) Balaganesan, B.; Shen, W.; Chen, C. H. *Tetrahedron Lett.* **2003**, *44*, 5747–5750.

(95) Coulson, D. R.; Satek, L. C.; Grim, S. O. *Inorg. Synth.* **1972**, *13*, 121.